DEVELOPMENT OF A MICROFLUIDIC IMMUNOASSAY FOR DETERMINATION OF KINASE PHOSPHORYLATION

Joseph Carl Gaiteri

A dissertation submitted to the faculty of the University of North Carolina at Chapel Hill in partial fulfillment of the requirements for the degree of Doctor of Philosophy in the Department of Chemistry.

Chapel Hill
2014

Approved by:

J. Michael Ramsey

Nancy L. Allbritton

James W. Jorgenson

Linda L. Spremulli

Eric M. Brustad

ABSTRACT

Joseph Carl Gaiteri: Development of a Microfluidic Immunoassay
for Determination of Kinase Phosphorylation
(Under the direction of J. Michael Ramsey)

Extracellular signal-related kinases 1 and 2 (ERK1/2) are signaling proteins involved in cell survival and proliferation and are overactive/phosphorylated (forming pERK1/2) in approximately 1/3 of human cancers. Measuring pERK1/2:ERK1/2 is therefore common in cancer-related research, but conventional methods are some combination of slow, expensive, and labor-intensive, and large samples are often required. Microfluidic devices offer the possibility of determining pERK1/2:ERK1/2 rapidly, with lower costs, and with substantially reduced labor and reagent requirements compared to conventional methods. This would facilitate more expedient medical decisions and increase experimental throughput in research that requires determining pERK1/2:ERK1/2, such as that related to tumor cell signaling and anti-cancer drug development. This dissertation describes the development of a microfluidic immunoassay for determining the ratio of pERK1/2:ERK1/2 in human cell lysate.

Early experiments used antibody-coated beads loaded into chips with poly(dimethylsiloxane) (PDMS) microwell arrays. The fluorophore, assay buffer, incubation protocol, and capture antibody used in all subsequent experiments were chosen here, but these experiments suffered from high (>10%) coefficients of variance. To improve the sensitivity and clinical relevance of the pERK1/2:ERK1/2 assay, the assay was systematically examined until it

was determined that the process of loading beads into the PDMS arrays was mechanically damaging their capture antibodies.

The next chapter introduced a new chip design for performing pERK1/2:ERK1/2 assays without harsh mechanical loading. These chips were used to optimize assay conditions and determine pERK1/2:ERK1/2 in human Jurkat cell lysate at physiologically relevant concentrations. Further improvement of the assay called for automation to minimize labor/user interaction during experiments, and this required valves to control fluid flow on-chip. The next chapter therefore focused on developing computer-controlled, Peltier-based freeze-thaw valves for microfluidic chips. In the final chapter, these valves were coupled with a chip design for assaying up to 8 samples simultaneously. These chips could be used to perform multiple replicate measurements of a sample or to produce a calibration curve on the same device used to measure samples. Finally, the 8-sample chips were used with the freeze-thaw valves to determine pERK1/2:ERK1/2 in cell lysate with automated fluid control, marking a significant advance toward the realization of automated kinase assays.

For my family

ACKNOWLEDGEMENTS

I'd first like to thank my advisor, Professor J. Michael Ramsey, for providing funding, laboratory space, guidance, and support during my time at UNC. I'd also like to thank all the other members of the Ramsey group for their assistance over the years and for making the lab a fun and friendly place to be. A few members of the group especially stand out here. Hamp Henley has been an astonishingly capable and indefatigable source of ideas, guidance, and technical wizardry. J.P. Alarie has been extremely helpful over the years with providing advice, technical expertise, and more recently, editing my dissertation. Amy Hargis Ellefsen, Josh Herr, and especially Patty Dennis were generous with their time in helping me get started when I was a first-year student. I'd also like to thank Derek Wolfe for his assistance with the electronics for the freeze-thaw valves and John Perry for some helpful discussions on fabricating the wafer molds for the freeze-thaw valve chips. In the Allbritton lab, thanks to Doug Ornoff for teaching me the basics of cell culture and to Professor Nancy Allbritton herself for some insightful discussions on cancer biology. Finally, thanks to my friends and family for their loving support and for helping to keep me (relatively) sane and grounded for the past few years.

TABLE OF CONTENTS

LIST OF TABLES

LIST OF FIGURES

LIST OF ABBREVIATIONS AND SYMBOLS

A	Ampere
Ab	Antibody
AF488	Alexa Fluor® 488, streptavidin conjugate
BOE	Buffered oxide etchant
BP	Base Peltier
BSA	Bovine serum albumin
CAb	Capture antibody
CCD	Charge-coupled device
CE	Capillary electrophoresis
cm	Centimeter
CML	Chronic myelogenous leukemia
CV	Coefficient of variance
dAb	Detection antibody
DC	Direct current
d_f	Depth of field
DI	Deionized
DRIE	Deep reactive-ion etching
EDAC	1-ethyl-3-(-3-dimethylaminopropyl) carbodiimide hydrochloride
EDTA	Ethylene diamine tetraacetic acid
EGFR	Epidermal growth factor receptor
ELISA	Enzyme-linked immunosorbent assay
EM-CCD	Electron-multiplying charge-coupled device

ERK1	Extracellular signal-related kinase 1 (refers to both phospho-forms of ERK1)
ERK2	Extracellular signal-related kinase 2 (refers to both phospho-forms of ERK2)
FIB	Focused ion beam
FTV	Freeze-thaw valve
g	Gram
h	Hour
Hz	Hertz
IgG	Immunoglobulin-G
IR	Infrared
IU	International unit
λ_{em}	Emission wavelength
λ_{ex}	Excitation wavelength
LC	Liquid chromatography
LOC	Lab-on-a-chip
LOD	Limit of detection
M	Molar
mAb	Monoclonal antibody
MAPK	Mitogen-activated protein kinase
MEK1/2	Mitogen-activated protein kinase kinases 1 and 2
MES	2-(N-morpholino)ethanesulfonic acid
µg	Microgram
µL	Microliter
µm	Micrometer

µM	Micromolar
mg	Milligram
mJ	Millijoule
mL	Milliliter
mm	Millimeter
mM	Millimolar
min	Minute
µTAS	Micro total chemical analysis system
NA	Numerical aperture
NaCl	Sodium chloride
ng	Nanogram
nm	Nanometer
nM	Nanomolar
nERK1	Non-phosphorylated ERK1
nERK2	Non-phosphorylated ERK2
Ω	Ohm
pAb	Polyclonal antibody
PBS	Phosphate-buffered saline
PCR	Polymerase chain reaction
PDMS	Poly(dimethylsiloxane)
PEG	Polyethylene glycol
pERK1	Phospho-ERK1
pERK2	Phospho-ERK2

PF-127	Pluronic F-127
PMA	Phorbol 12-myristate 13-acetate
pg	Picogram
pM	Picomolar
PMSF	Phenylmethanesulfonyl fluoride
POC	Point-of-care
PWM	Pulse-width modulation
rcf	Relative centrifugal force, 1 x gravity
rpm	Revolutions per minute
%RSD	Percent relative standard deviation
s	Second
S1813	Shipley 1813 photoresist
SA-PE	Streptavidin-B-phycoerythrin
SA-QD	Streptavidin-quantum dot
S/N	Signal-to-noise ratio
Si	Silicon
Sulfo-NHS	N-hydroxysulfosuccinimide
TBS	Tris-buffered saline
tERK1	Total ERK1
tERK2	Total ERK2
UV	Ultraviolet
V	Volt
VEGF	Vascular endothelial growth factor

VP	Valve Peltier
W	Watt

CHAPTER 1

INTRODUCTION

1.1 Background

Benchtop assays that yield accurate, reproducible results now exist for a vast range of medical and research purposes. However, these conventional assays can be slow and labor-intensive. In research terms, this leads to lower experimental throughput, while in medical terms, this often increases the time required to make healthcare decisions. These delays are exacerbated by the fact that medical tests are often performed at centralized facilities, requiring the samples to be packaged and shipped with the results communicated back to the healthcare provider and then the patient. In recent decades, these considerations have led to a trend towards miniaturizing conventional benchtop assays. Ideally, these miniaturized devices would meet or exceed the performance of their conventional counterparts in terms of accuracy, reproducibility, and sensitivity. They should also offer further advantages including portability, reduced reagent/sample consumption and lower cost in general, and greater speed due to the reduced incubation/migration times that come with the small dimensions of the miniature devices.[1–7]

A well-known example of miniaturized medical testing is the self-monitoring of blood glucose, where a patient places a drop of blood on a test strip and their blood glucose level is determined by a portable meter.[8] Even more simply, home pregnancy tests utilize the lateral-flow immunoassay technique, are accurate and rapid, and do not require any power.[9] Useful miniature devices exist in laboratory settings as well. One such example is Millipore's handheld Scepter™ hemocytometer, which determines the concentration and size distribution of cells in a

sample in approximately thirty seconds, much faster than conventional microscope-based hemocytometers.[10]

The speed and accuracy of miniaturized assays make them well-suited to the domain of cancer research and medicine, where time – in terms of discovering treatments and making medical decisions related to a patient's ongoing therapy – is of the utmost concern. One of the fundamental characteristics of cancer is the dysregulation of the cell signaling process on multiple fronts such that cancer cells have overcome the normal processes that tightly regulate tissue growth.[11,12] In approximately one-third of human cancers, the extracellular signal-related kinase 1 and 2 (ERK1/2) signaling cascade is involved in this dysregulation.[13] ERK1 and ERK2 are proteins involved in regulating fundamental processes such as apoptosis and growth and are activated by dual phosphorylation. Upon becoming phospho-ERK1/2 (pERK1/2), they migrate to the cell nucleus and activate transcription factors and genes related to growth and proliferation.[13–17] Cancer-related mutations in the ERK1/2 pathway often lead to excessive ERK1/2 phosphorylation and activity.[13–16,18–21] It is therefore a pathway whose activity is commonly monitored in cancer research. Also, many drugs have been and are being designed to inhibit mutationally activated proteins in the ERK1/2 cascade.[21] The most successful of these is imatinib (Gleevec®), a drug that inhibits the kinase domain in the mutant BCR-ABL kinase (upstream from ERK1/2) in patients with chronic myelogenous leukemia (CML). Prior to the invention of imatinib and related drugs in its class, the prognosis for CML was extremely poor; it is now considered highly treatable.[22]

However, these mutant proteins sometimes acquire further mutations that prevent their inhibitory drugs from binding.[21,23] Monitoring the extent of ERK1/2 phosphorylation is, therefore, desirable to assess the efficacy of an ongoing treatment plan or to determine a patient's

response to a new one. Various methods[24–28] currently exist for determining pERK1/2 and/or total ERK1/2 in cell lysate. These include the Western Blot, enzyme-linked immunosorbent assay (ELISA), and AlphaScreen™, Li-Cor®, and Meso-Scale Discovery® systems. These methods are effective, but each has one or more of the following drawbacks: being labor-intensive, requiring large samples (hundreds of thousands to millions of cells in some cases), requiring long incubation times (up to overnight), and being difficult to automate or not being automatable at all. A miniaturized or microfluidic device for determining pERK1/2:ERK1/2 in a sample can potentially solve many of these issues. This is desirable from a medical standpoint, as the time required to make a crucial medical decision may be reduced. It is also desirable from a scientific standpoint, as it can increase experimental throughput in studies that involve determining cellular pERK1/2 expression. Such research includes examining cell signaling in tumors under various circumstances or studying the effects of kinase inhibitor drugs on the ERK1/2 pathway.[16,20,21,29] The remainder of this chapter will provide a general overview of the field of microfluidics and explain why it is well-suited for addressing this problem. Immunoassays, the central technique in the device, will then be reviewed. Finally, the ERK1/2 signaling pathway will be explained in greater detail and the research goals for the project outlined.

1.2 General microfluidics, point-of-care devices, and poly(dimethylsiloxane)

Microfluidics is an interdisciplinary science concerned with using micrometer-scale systems for manipulating and studying liquids in nanoliter to attoliter volumes.[1] The field of microfluidics has multiple progenitors. For molecular biology, analytical chemistry, and biodefense, the possibility of conducting high-throughput, high-resolution analysis with miniature, portable devices was a major driver of the field's development.[1,2] Technologies

developed in the microelectronics industry also contributed to the growth of microfluidics, as photolithography and other techniques were adapted to fabricate microfluidic devices. These techniques make it possible to create micrometer- or nanometer-scale features in silicon and glass. It was in these materials[1,2] that much of the early work in microfluidics was conducted using such techniques as liquid chromatography (LC) and capillary electrophoresis (CE).[2,30–33]

In 1990, Manz and co-workers[30] proposed the possibility of constructing a micro total chemical analysis system (μTAS), also called a lab-on-a-chip (LOC).[2,3,30,34] A LOC would incorporate all the steps from a conventional benchtop technique into a single miniaturized device. These steps could include sample pretreatment,[31,35] analysis through techniques such as immunoassays,[36,37] the polymerase chain reaction,[35,38] or CE,[31,39–41] and detection of the results through optical,[2,31,37] electrochemical,[4,42,43] mass spectrometric,[39,40] or other means.[1,2,5,6] Ideally, all this would be possible while maintaining or exceeding the performance of the corresponding conventional technique. In addition,[1,2,5,6] the high surface area-to-volume ratio reduces incubation or reaction times due to the reduced time required for molecules to diffuse across the dimensions of the device, thus reducing analysis times.[4] Microfluidic devices also have the advantage of requiring significantly lower volumes of sample and reagent than conventional techniques.[1–3,7] This reduces costs given the lowered consumption of expensive reagents such as enzymes and monoclonal antibodies, and it enables the analysis of samples of which only micro-quantities are available, as is the case with many biological samples.[44,45]

Since Manz and co-workers' proposal, many examples of LOC devices have been demonstrated, aided by developments in technology for such components as pumps, valves, mixers, and detectors.[1,2,6,46] The integration of these techniques into a single chip have also made it possible to automate the devices,[1,7] thus allowing a user to input a sample and receive a

result with minimal or no additional interaction with the system.[1,2,47] These devices are ideal for point-of-care (POC) diagnostics, where a test is performed at or near the site of patient care.[48,49] Performing analyses at the POC instead of a separate testing facility can reduce the results' turnaround time from days or weeks to minutes or hours.[7,48–50] Devices such as these have the potential to improve a patient's outcome in time-critical decisions as well as reduce costs associated with labor and shipping/handling the samples.[49,50] A recent example of POC devices is the microfluidic paper-based class of devices developed by the Whitesides group, which are usable in a low- or zero-resource setting.[51] As the results of these devices can be captured with a cell phone camera and transmitted anywhere in the world for diagnosis, these devices can bring healthcare to places where there are no physicians or other medical professionals.[52]

Since the early years of microfluidics, polymers such as poly(dimethylsiloxane) (PDMS) have become extremely popular as the base material.[1,2,6] PDMS is widely used because it is optically transparent from 240 nm to 1100 nm, impermeable to water, and compatible with biological molecules.[53,54] Unlike glass and silicon, it is flexible, making it compatible with useful components like mixers, pumps, and valves that are mechanically or pneumatically actuated.[1,55–57] It is gas-permeable, permitting microfluidic cell culture.[1] PDMS is also favored in research because it is possible to rapidly create prototype devices in PDMS to test new ideas.[1,54,58] Master molds for PDMS can be fabricated with a variety of materials and methods and used to make an indefinite number of castings/chips.[4,54,59] Molds with low aspect-ratio features may be fabricated with isotropic wet etching techniques such as the buffered hydrogen fluoride etching of glass,[36] whereas molds with high-aspect-ratio features and vertical sidewalls may be fabricated with focused ion beam (FIB) milling[36] or dry etching techniques such as deep reactive-ion etching (DRIE).[2,37,43,60] Simpler chips that require no etching may also be fabricated

directly from molds consisting of photoresist patterned on a substrate such as a silicon wafer.[61–63] After a device is fabricated in PDMS, access holes (vias) to the channels can be cut from the bulk material and the channels irreversibly sealed by bonding the PDMS to glass following plasma treatment.[36,53,54] The bonded device may then be used in an experiment or its surface modified[64,65] if necessary prior to use.

1.3 Microfluidic valving

In LOC devices, multiple solutions are typically used simultaneously, so valves play an important role in controlling the fluid flow throughout the chip by opening/closing channels or otherwise modulating the flow direction. Some valves are closed until intentionally opened and are referred to as "normally-closed," while others are generally open and are referred to as "normally-open." Many valving strategies have been demonstrated, one of the earliest of which was the electrokinetic valve.[31,41,66–68] These are normally-closed valves in which voltages applied to channels are used to dispense plugs of sample through electrokinetic flow. Major types of electrokinetic valves include the double-T valve,[33,69] pinched valve,[67,70,71] and gated valve.[31,41,68] The volume of sample delivered through each injection will primarily be a function of either the spatial dimensions of the chip (for pinched and double-T valves) or the field strength and duration of the injection (for gated valves).[67] Depending on the chip design, electrokinetic valves may require only a single voltage source while exhibiting excellent reproducibility (<0.5% RSD) in the sample volumes delivered.[41]

Hydrogel valves are another means of controlling flow in microfluidic chips.[72–75] These consist of posts or other shapes that are fabricated *in situ* on a chip through photopolymerization. The volume of the posts varies greatly depending on an environmental stimulus, most commonly pH, although electrical control of hydrogels has also been demonstrated.[75] This expansion is

reversible given a change in the stimulus. Generally, valving is accomplished when the posts swell to occlude the channel they occupy, but if fluidic isolation of the analysis channels is a requirement, it is also possible for an expanding post to deflect an impermeable PDMS layer to close an adjacent channel.[73,74]

The final hydrogel example above is also an example of a larger class of valves known as pinch valves.[37,55–57,61,62,76,77] These consist of a membrane made from an elastomeric material such as PDMS that is deflected to open or close a channel. Several primary means of controlling the valve exist. Pneumatic actuation is used in one of the most well-known types of microfluidic valves, the Quake-style valve.[55–57] These are normally-open valves in which a thin (~30 μm) membrane of PDMS separates a fluidic channel and a pneumatic channel in a multilayer chip. Pressure is applied through the pneumatic channel to deflect the PDMS membrane into the fluidic channel, closing it. A similar design adds a post on the fluidic side of the PDMS membrane to make the valve normally-closed, and negative pressure is used to pull the membrane into the pneumatic channel and open the valve.[77] Quake-style valves can be actuated at approximately 100 Hz, enabling them to act as a peristaltic pump when multiple valves are arranged sequentially in the same channel.[55] Pinch valves can also be actuated through mechanical rather than pneumatic pressure. The Whitesides group has demonstrated numerous examples of this, include manually-actuated screw valves and computer-driven solenoid valves.[61,62] A recent device developed by the Ramsey group in collaboration with the Walt group also utilizes computer-controlled normally-closed pinch valves.[37]

Thermal actuation is another means of controlling fluid flow in microfluidic channels. The use of paraffin wax is one such method of thermally-driven valving.[78–80] Paraffin is immiscible with water and expands from 10-30% upon melting,[78] and this has been exploited to

close normally-open channels by melting the wax in both reversible and irreversible configurations.[78,79] Paraffin can also be used in a normally-closed configuration if a solid plug initially seals a channel but opens the channel upon heating.[80] Finally, a type of thermal valve that does not require extra material inside the device is the freeze-thaw valve.[63,81–84] This strategy uses an external cooling source to freeze a segment of a microfluidic channel, thus stopping flow. Early examples of freeze-thaw valves used low-temperature fluids such as liquid nitrogen[81] or carbon dioxide[82,83] to induce freezing, while thawing was initiated by removal of the coolant. A freeze-thaw strategy that is recently emerging in the literature utilizes Peltier devices to effect freezing and thawing.[63,84] Peltiers consist of alternating semiconductor pellets sandwiched between two insulating layers.[85] The application of voltage creates a temperature gradient across the device, and the use of multiple Peltiers stacked on top of one another can generate successively lower temperatures that are sufficiently cold to rapidly freeze aqueous solutions in microfluidic channels. They can also generate heat for thawing/opening a channel if their voltage is reversed. Peltiers are easily computer-controlled, indefinitely reusable, inexpensive, compatible with a wide range of materials, and do not require the manipulation of high-pressure gases.[63]

1.4 Immunoassays

Immunoassays are a widely-used analytical technique whose defining characteristic is the utilization of capture antibodies (CAbs) to bind molecules of interest ("antigens") with high specificity and affinity.[86] Antigens range in size from <1000 daltons ("haptens") up to large proteins. In addition to their specificity, immunoassays are highly sensitive and relatively easy to perform.[87] While all immunoassays utilize CAbs, two major classes of immunoassays – competitive and non-competitive – differ in their measurement methods.[88,89] In competitive

immunoassays, sample analytes are incubated along with labeled antigens (most commonly more analyte molecules) such that the unlabeled antigens compete with the labeled antigens for binding sites on the CAbs. Measurements are therefore made of sites unoccupied by the sample analytes and the signal is inversely proportional to the sample concentration.

The other major type is non-competitive immunoassays, which usually takes the form of a "sandwich assay" because the analyte molecules are sandwiched between two antibodies. Here, analyte molecules are bound by CAbs before a second detection antibody (dAb) is incubated that completes the sandwich by binding to another epitope (binding site). These dAbs are labeled, or are themselves detected with a third labeled antibody following a third incubation, and after excess dAb is washed away, the occupied sites are measured.[88,89] These assays have the disadvantage of requiring two antibodies with specificity for two epitopes on the analyte. This two-antibody characteristic means that sandwich assays are rarely suitable for haptens, as immunoglobulin-G (IgG) antibodies are more than two orders of magnitude larger than haptens and steric effects generally preclude sandwich formation.[90] However, use of sandwich immunoassays for proteins is specific enough that it is possible to distinguish between otherwise identical proteins with different post-translational modifications, such as phosphorylation states. Also, sandwich assays tend to be more sensitive than non-competitive assays because the signal is directly proportional to the analyte concentration.[42]

Several broad types of detection labels have been used in immunoassays. The first immunoassay technique, described in 1959, was a competitive radioimmunoassay for human insulin.[91] The competitive antigen in this case was ^{131}I-labeled human insulin. Assays with radiometric labels are extremely sensitive due to the ease of detection of decay events, but their use has been largely displaced in favor of techniques that do not require radioactive labels.[87,89]

In particular, fluorescent labels have become extremely popular,[42,86] especially in microfluidic systems.[92] A wide range of fluorescent labels with varying spectral profiles exist, ranging from small organic molecules to quantum dots. Enzyme labels on dAbs are also used in immunoassays in enzyme-linked immunosorbent assays (ELISAs).[93] In ELISAs, following the washing away of unbound dAb, a substrate for the enzyme is introduced to the system and the enzyme-substrate reaction products are detected. It is also common to utilize detection antibodies labeled with biotin.[42] Biotin binds rapidly and strongly to streptavidin,[94] and while the use of biotin has the drawback of requiring an additional incubation step for the detection label, it has several advantages. First, biotin is small (molecular mass = 244 daltons) and can generally be conjugated to antibodies without reducing their activity. Any label that can be conjugated to streptavidin may then be used, and streptavidin may be conjugated to multiple detection labels for further signal amplification.[95]

There are two types of antibodies used in immunoassays: polyclonal antibodies (pAb) and monoclonal antibodies (mAb). Polyclonal antibodies are a mixture of antibodies that target many epitopes on an antigen.[96] Compared to mAbs, they are relatively easy to produce, but they lack the mono-specificity of mAbs. The single-epitope specificity of mAbs enables them to target and discriminate between extremely similar molecules, such as differing phosphorylation states of the same protein. Developing mAbs for highly specific sequences, e.g. a particular peptide sequence on a protein, is often accomplished by using the peptide itself rather than the intact protein. The injected peptide sequence may be unfolded or otherwise not have the same shape as the epitope on the target native molecule.[96,97] During an assay, therefore, it may be necessary to unfold the analyte protein so that its target epitope resembles the shape of the

peptide used in generating the mAb. Multiple means of accomplishing this are possible, but adding a denaturing agent such as urea[98] to the assay buffer may be the simplest.

1.5 ERK1/2 signaling pathway

Profound dysregulation of the cell signaling process is one of the defining characteristics of cancer. In order to become cancerous, cells must acquire characteristics dubbed "hallmarks" by Hanahan & Weinberg.[11,12] Among these hallmarks is the ability to continue to survive and proliferate in spite of contrary signals from other cells in their environment. Cancers utilize many strategies[11,12] to accomplish this, one of which is the deregulation of the extracellular signal-related kinase 1 and 2 (ERK1 and ERK2, or ERK1/2 collectively) signaling cascade. This pathway is involved in regulating cellular processes such as apoptosis, proliferation, and growth in response to extracellular signals, and its dysregulation presents in approximately 33% of human cancers.[13] The ERK1/2 cascade begins with epidermal growth factor receptors (EGFR) at the cell membrane. Signals from EGFR are sent through other membrane proteins to Ras. Signals then travel from Ras to Raf, then to mitogen-activated protein kinase kinases 1 and 2 (MEK1/2). ERK1/2 are themselves activated by MEK1/2. The activation of ERK1/2 consists of dual phosphorylation at one serine and one threonine residue each,[14,15] leading to a conformation change and 1,000-fold increase in activity.[15] Activated ERK1/2 translocate to the cell nucleus, where they activate transcription factors and genes related to cell survival and proliferation.[13,16,17]

In this signaling cascade, cancer-related mutations have been documented in EGFR, Ras, and Raf. Notably, Raf is mutationally active in 70% of melanomas and 50% of papillary thyroid cancers, Ras is mutationally active in 90% of pancreatic cancers, 60% of papillary thyroid cancers, and 50% of colon cancers, while overexpression or mutations in EGFR are present in up to 80% of lung cancers, up to 91% of non-small cell lung cancers, up to 77% of colorectal

cancers, over 50% of carcinomas, up to 50% of pancreatic cancers, and 20% of glioblastomas.[13,16] These mutational activations upstream from ERK1/2 often lead to excessive activation of ERK1/2 to the extent that some tumors are dependent upon ERK1/2 for survival and are "ERK-addicted."[18] Excessive ERK1/2 activation is also seen because of downstream signal amplification, wherein relatively few molecules are needed to activate a relatively large number of molecules further down the signaling cascade.[14,99] For example, activation of just 5% of a cell's Ras molecules has been estimated to be sufficient for fully activating that cell's ERK1/2.[100]

Several factors call for the development of assays for determining the phosphorylation extent (pERK1/2:ERK1/2) of ERK1/2. Because of the commonality of mutations in the ERK1/2 cascade leading to elevated ERK1/2 activity, the pERK1/2:ERK1/2 ratio is a useful biomarker in many cases.[14,16,19–21] Drugs have been and continue to be developed to inhibit mutationally activated proteins in the pathway by binding to and antagonizing their kinase domains. However, the mutated proteins sometimes acquire further mutations that prevent the drugs from binding. The pERK1/2:ERK1/2 ratio in these cells is thus a useful diagnostic here as well, as it changes in response to the specific drug and mutation[21] and can be used in the monitoring of treatment efficacy. Finally, because they are present at approximately micromolar concentrations,[21] ERK1 and ERK2 are among the most abundant proteins in their signaling cascade, making them an attractive analytical target. They also possess a sequence homology of approximately 83-85% and share many structural features.[14,17] A single antibody can therefore capture ERK1 and ERK2 by targeting an epitope common to both. Monoclonal antibodies specific for the phosphorylation loop (in pERK1/2) and a second common site on all forms of

ERK1/2 can then be used to determine pERK1/2 and ERK1/2 and thus the pERK1/2:ERK1/2 ratio in cells.[29]

These strategies and considerations open the door for developing a microfluidic device for determining pERK1/2:ERK1/2 in a sample. Current methods of pERK1/2:ERK1/2 determination (namely the Western Blot) are time- and labor-intensive and can require millions of cells. A device with the advantages of microfluidics – relatively small sample size and reagent consumption, fast incubation times, high sensitivity, and the potential for automation – can provide a substantial improvement over these methods in terms of time and cost.

1.6 Research goals

The goal of this project is to develop a bead-based microfluidic immunoassay device for determining pERK1/2:ERK1/2 in human cell lysate. The microfluidic device would be automated such that once sample and reagents were added to vias on the microfluidic device, no other user interaction would be needed. Early efforts centering on the selection of fluorophores, optimizing incubation times, determining suitable antibody pairs for a pERK1/2 and ERK2 sandwich immunoassay, and the development of a general on-chip assay protocol are described in Chapter 2. Based on these early results, troubleshooting efforts to improve the reproducibility of the assay to clinically relevant standards are the subject of Chapter 3. The results of Chapter 3 led to an improved chip design investigated in Chapter 4, wherein an on-chip assay for determining pERK1/2:ERK1/2 in human cell lysate is demonstrated. Chapter 5 focused on automating the assay using a computer-controllable valving method (freeze-thaw valves, FTVs). Finally, a chip design where fluid flow is controlled by automatable FTVs is described in Chapter 6, and the utility of it for the pERK1/2:ERK1/2 assay is demonstrated. The final device

represents a significant advance toward a microfluidic pERK1/2:ERK1/2 assay that is automated and requires relatively few cells compared to conventional methods.

1.7 References

(1) Whitesides, G. M. The Origins and the Future of Microfluidics. *Nature* **2006**, *442*, 368–373.

(2) Reyes, D. R.; Iossifidis, D.; Auroux, P.-A.; Manz, A. Micro Total Analysis Systems. 1. Introduction, Theory, and Technology. *Anal. Chem.* **2002**, *74*, 2623–2636.

(3) Janasek, D.; Franzke, J.; Manz, A. Scaling and the Design of Miniaturized Chemical-Analysis Systems. *Nature* **2006**, *442*, 374–380.

(4) Bange, A.; Halsall, H. B.; Heineman, W. R. Microfluidic Immunosensor Systems. *Biosens. Bioelectron.* **2005**, *20*, 2488–2503.

(5) Arora, A.; Simone, G.; Salieb-Beugelaar, G. B.; Kim, J. T.; Manz, A. Latest Developments in Micro Total Analysis Systems. *Anal. Chem.* **2010**, *82*, 4830–4847.

(6) Dittrich, P. S.; Tachikawa, K.; Manz, A. Micro Total Analysis Systems. Latest Advancements and Trends. *Anal. Chem.* **2006**, *78*, 3887–3908.

(7) Weigl, B.; Domingo, G.; Labarre, P.; Gerlach, J. Towards Non- and Minimally Instrumented, Microfluidics-Based Diagnostic Devices. *Lab Chip* **2008**, *8*, 1999–2014.

(8) Olansky, L.; Kennedy, L. Finger-Stick Glucose Monitoring: Issues of Accuracy and Specificity. *Diabetes Care* **2010**, *33*, 948–949.

(9) Posthuma-Trumpie, G. A.; Korf, J.; van Amerongen, A. Lateral Flow (immuno)assay: Its Strengths, Weaknesses, Opportunities and Threats. A Literature Survey. *Anal. Bioanal. Chem.* **2009**, *393*, 569–582.

(10) Scepter ™ Handheld Automated Cell Counter User Guide http://qb3.berkeley.edu/qb3/sscf-htsf/docs/Scepter User Guide _RevE.pdf.

(11) Hanahan, D.; Weinberg, R. A. Hallmarks of Cancer: The Next Generation. *Cell* **2011**, *144*, 646–674.

(12) Hanahan, D.; Weinberg, R. A. The Hallmarks of Cancer. *Cell* **2000**, *100*, 57–70.

(13) Dhillon, A. S.; Hagan, S.; Rath, O.; Kolch, W. MAP Kinase Signalling Pathways in Cancer. *Oncogene* **2007**, *26*, 3279–3290.

(14) Roux, P.; Blenis, J. ERK and p38 MAPK-Activated Protein Kinases: A Family of Protein Kinases with Diverse Biological Functions. *Microbiol. Mol. Biol. Rev.* **2004**, *68*, 320–344.

(15) Canagarajah, B. J.; Khokhlatchev, A.; Cobb, M. H.; Goldsmith, E. J. Activation Mechanism of the MAP Kinase ERK2 by Dual Phosphorylation. *Cell* **1997**, *90*, 859–869.

(16) Roberts, P. J.; Der, C. J. Targeting the Raf-MEK-ERK Mitogen-Activated Protein Kinase Cascade for the Treatment of Cancer. *Oncogene* **2007**, *26*, 3291–3310.

(17) Seger, R.; Krebs, E. The MAPK Signaling Cascade. *FASEB J.* **1995**, *9*, 726–735.

(18) Balmanno, K.; Cook, S. J. Tumour Cell Survival Signalling by the ERK1/2 Pathway. *Cell Death Differ.* **2009**, *16*, 368–377.

(19) Lee Jr., J. T.; McCubrey, J. A. The Raf/MEK/ERK Signal Transduction Cascade as a Target for Chemotherapeutic Intervention in Leukemia. *Leukemia* **2002**, *16*, 486–507.

(20) Kohno, M.; Pouyssegur, J. Targeting the ERK Signaling Pathway in Cancer Therapy. *Ann. Med.* **2006**, *38*, 200–211.

(21) Roskoski, R. ERK1/2 MAP Kinases: Structure, Function, and Regulation. *Pharmacol. Res.* **2012**, *66*, 105–143.

(22) Hernández-Boluda, J. C.; Cervantes, F. Prognostic Factors in Chronic Myeloid Leukaemia. *Best Pract. Res. Clin. Haematol.* **2009**, *22*, 343–353.

(23) Wu, D.; Nair-Gill, E.; Sher, D. A.; Parker, L. L.; Campbell, J. M.; Siddiqui, M.; Stock, W.; Kron, S. J. Assaying Bcr-Abl Kinase Activity and Inhibition in Whole Cell Extracts by Phosphorylation of Substrates Immobilized on Agarose Beads. *Anal. Biochem.* **2005**, *347*, 67–76.

(24) Garbison, K. E.; Heinz, B. A.; Lajiness, M. E.; Weidner, J. R.; Sittampalam, G. S. Phospho-ERK Assays. In *Assay Guidance Manual [Internet]*; Eli Lilly & Company and the National Center for Advancing Translational Sciences: Bethesda (MD), 2012.

(25) Phospho-ERK1 (T202/Y204)/ERK2 (T185/Y187) DuoSet IC http://www.rndsystems.com/pdf/DYC1018B.pdf.

(26) Seljeset, S.; Siehler, S. Receptor-Specific Regulation of ERK1/2 Activation by Members of the "Free Fatty Acid Receptor" Family. *J. Recept. Signal Transduct. Res.* **2012**, *32*, 196–201.

(27) Complete Sample Protocol for PMA-Induced ERK Activation in Suspension Cell Lines http://biosupport.licor.com/docs/ICW_Susp_11460.pdf.

(28) Phospho-ERK1/2 (Thr202/Tyr204; Thr185/Tyr187) Assay Whole Cell Lysate Kit http://www.meso-scale.com/CatalogSystemWeb/Documents/Phospho_ERK_1_2_WCL.pdf.

(29) Yeh, J. J.; Routh, E. D.; Rubinas, T.; Peacock, J.; Martin, T. D.; Shen, X. J.; Sandler, R. S.; Kim, H. J.; Keku, T. O.; Der, C. J. KRAS/BRAF Mutation Status and ERK1/2 Activation as Biomarkers for MEK1/2 Inhibitor Therapy in Colorectal Cancer. *Mol. Cancer Ther.* **2009**, *8*, 834–843.

(30) Manz, A.; Graber, N.; Widmer, H. M. Miniaturized Total Chemical Analysis Systems: A Novel Concept for Chemical Sensing. *Sensors Actuators B Chem.* **1990**, *1*, 244–248.

(31) Jacobson, S. C.; Hergenruder, R.; Moore, A. W.; Ramsey, J. M. Precolumn Reactions with Electrophoretic Analysis Integrated on a Microchip. *Anal. Chem.* **1994**, *66*, 4127–4132.

(32) Jacobson, S.; Culbertson, C.; Daler, J. E.; Ramsey, J. M. Microchip Structures for Submillisecond Electrophoresis. *Anal. Chem.* **1998**, *70*, 3476–3480.

(33) Effenhauser, C. S.; Manz, A.; Widmer, H. M. Glass Chips for High-Speed Capillary Electrophoresis Separations with Submicrometer Plate Heights. *Anal. Chem.* **1993**, *65*, 2637–2642.

(34) West, J.; Becker, M.; Tombrink, S.; Manz, A. Micro Total Analysis Systems: Latest Achievements. *Anal. Chem.* **2008**, *80*, 4403–4419.

(35) Oblath, E. A.; Henley, W. H.; Alarie, J. P.; Ramsey, J. M. A Microfluidic Chip Integrating DNA Extraction and Real-Time PCR for the Detection of Bacteria in Saliva. *Lab Chip* **2013**, *13*, 1325–1332.

(36) Henley, W. H.; Dennis, P. J.; Ramsey, J. M. Fabrication of Microfluidic Devices Containing Patterned Microwell Arrays. *Anal. Chem.* **2012**, *84*, 1776–1780.

(37) Nie, S.; Henley, W. H.; Miller, S. E.; Zhang, H.; Mayer, K. M.; Dennis, P. J.; Oblath, E. A.; Alarie, J. P.; Wu, Y.; Oppenheim, F. G.; et al. An Automated Integrated Platform for Rapid and Sensitive Multiplexed Protein Profiling Using Human Saliva Samples. *Lab Chip* **2014**, *14*, 1087–1098.

(38) Kricka, L. J.; Wilding, P. Microchip PCR. *Anal. Bioanal. Chem.* **2003**, *377*, 820–825.

(39) Batz, N. G.; Mellors, J. S.; Alarie, J. P.; Ramsey, J. M. Chemical Vapor Deposition of Aminopropyl Silanes in Microfluidic Channels for Highly Efficient Microchip Capillary Electrophoresis-Electrospray Ionization-Mass Spectrometry. *Anal. Chem.* **2014**, *86*, 3493–3500.

(40) Mellors, J. S.; Black, W. A.; Chambers, A. G.; Starkey, J. A.; Lacher, N. A.; Ramsey, J. M. Hybrid Capillary/Microfluidic System for Comprehensive Online Liquid Chromatography-Capillary Electrophoresis-Electrospray Ionization-Mass Spectrometry. *Anal. Chem.* **2013**, *85*, 4100–4106.

(41) Jacobson, S. C.; Ermakov, S. V; Ramsey, J. M. Minimizing the Number of Voltage Sources and Fluid Reservoirs for Electrokinetic Valving in Microfluidic Devices. *Anal. Chem.* **1999**, *71*, 3273–3276.

(42) Bilitewski, U. Protein-Sensing Assay Formats and Devices. *Anal. Chim. Acta* **2006**, *568*, 232–247.

(43) Lillehoj, P. B.; Wei, F.; Ho, C.-M. A Self-Pumping Lab-on-a-Chip for Rapid Detection of Botulinum Toxin. *Lab Chip* **2010**, *10*, 2265–2270.

(44) Su, C.; Sun, Y.; Tzeng, S.; Yang, C.; Wang, C.; Yang, M. In Vivo Monitoring of the Transfer Kinetics of Trace Elements in Animal Brains With Hyphenated Inductively Coupled Plasma Mass Spectrometry Techniques. *Mass Spectrom. Rev.* **2010**, *29*, 392–424.

(45) Takasaki, Y.; Inagaki, K.; Sabarudin, A.; Fujii, S.; Iwahata, D. Multielement Analysis of Micro-Volume Biological Samples by ICP-MS with Highly Efficient Sample Introduction System. *Talanta* **2011**, *87*, 24–29.

(46) Auroux, P.-A.; Iossifidis, D.; Reyes, D. R.; Manz, A. Micro Total Analysis Systems. 2. Analytical Standard Operations and Applications. *Anal. Chem.* **2002**, *74*, 2637–2652.

(47) Walt, D. R. Miniature Analytical Methods for Medical Diagnostics. *Science (80-.).* **2005**, *308*, 217–219.

(48) Mascini, M.; Tombelli, S. Biosensors for Biomarkers in Medical Diagnostics. *Biomarkers* **2008**, *13*, 637–657.

(49) Hart, R. W.; Mauk, M. G.; Liu, C.; Qiu, X.; Thompson, J. a; Chen, D.; Malamud, D.; Abrams, W. R.; Bau, H. H. Point-of-Care Oral-Based Diagnostics. *Oral Dis.* **2011**, *17*, 745–752.

(50) Lee-Lewandrowski, E.; Lewandrowski, K. Perspectives on Cost and Outcomes for Point-of-Care Testing. *Clin. Lab. Med.* **2009**, *29*, 479–489.

(51) Martinez, A. W.; Phillips, S. T.; Whitesides, G. M.; Carrilho, E. Diagnostics for the Developing World: Microfluidic Paper-Based Analytical Devices. *Anal. Chem.* **2010**, *82*, 3–10.

(52) Martinez, A. W.; Phillips, S. T.; Carrilho, E.; Thomas, S. W.; Sindi, H.; Whitesides, G. M. Simple Telemedicine for Developing Regions: Camera Phones and Paper-Based Microfluidic Devices for Real-Time, off-Site Diagnosis. *Anal. Chem.* **2008**, *80*, 3699–3707.

(53) McDonald, J. C.; Duffy, D. C.; Anderson, J. R.; Chiu, D. T.; Wu, H.; Schueller, O. J. A.; Whitesides, G. M. Fabrication of Microfluidic Systems in Poly (dimethylsiloxane). *Electrophoresis* **2000**, *21*, 27–40.

(54) Sia, S. K.; Whitesides, G. M. Microfluidic Devices Fabricated in Poly(dimethylsiloxane) for Biological Studies. *Electrophoresis* **2003**, *24*, 3563–3576.

(55) Unger, M. A.; Chou, H.-P.; Thorsen, T.; Scherer, A.; Quake, S. R. Monolithic Microfabricated Valves and Pumps by Multilayer Soft Lithography. *Science (80-.).* **2000**, *288*, 113–116.

(56) Thorsen, T.; Maerkl, S. J.; Quake, S. R. Microfluidic Large-Scale Integration. *Science* **2002**, *298*, 580–584.

(57) Studer, V.; Hang, G.; Pandolfi, A.; Ortiz, M.; Anderson, W. F.; Quake, S. R. Scaling Properties of a Low-Actuation Pressure Microfluidic Valve. *J. Appl. Phys.* **2004**, *95*, 393–398.

(58) McDonald, J. C.; Whitesides, G. M. Poly(dimethylsiloxane) as a Material for Fabricating Microfluidic Devices. *Acc. Chem. Res.* **2002**, *35*, 491–499.

(59) Henares, T. G.; Mizutani, F.; Hisamoto, H. Current Development in Microfluidic Immunosensing Chip. *Anal. Chim. Acta* **2008**, *611*, 17–30.

(60) Vilkner, T.; Janasek, D.; Manz, A. Micro Total Analysis Systems. Recent Developments. *Anal. Chem.* **2004**, *76*, 3373–3385.

(61) Hulme, S. E.; Shevkoplyas, S. S.; Whitesides, G. M. Incorporation of Prefabricated Screw, Pneumatic, and Solenoid Valves into Microfluidic Devices. *Lab Chip* **2009**, *9*, 79–86.

(62) Weibel, D.; Kruithof, M.; Potenta, S.; Sia, S. K.; Lee, A.; Whitesides, G. M. Torque-Actuated Valves for Microfluidics. *Anal. Chem.* **2005**, *77*, 4726–4733.

(63) Gui, L.; Yu, B. Y.; Ren, C. L.; Huissoon, J. P. Microfluidic Phase Change Valve with a Two-Level Cooling/heating System. *Microfluid. Nanofluidics* **2011**, *10*, 435–445.

(64) Séguin, C.; McLachlan, J. M.; Norton, P. R.; Lagugné-Labarthet, F. Surface Modification of Poly(dimethylsiloxane) for Microfluidic Assay Applications. *Appl. Surf. Sci.* **2010**, *256*, 2524–2531.

(65) Zhou, J.; Ellis, A. V.; Voelcker, N. H. Recent Developments in PDMS Surface Modification for Microfluidic Devices. *Electrophoresis* **2010**, *31*, 2–16.

(66) Jacobson, S. C.; Ramsey, J. M. Electrokinetic Focusing in Microfabricated Channel Structures. *Anal. Chem.* **1997**, *69*, 3212–3217.

(67) Alarie, J. P.; Jacobson, S. C.; Ramsey, J. M. Electrophoretic Injection Bias in a Microchip Valving Scheme. *Electrophoresis* **2001**, 312–317.

(68) Zhang, G.; Du, W.; Liu, B.-F.; Hisamoto, H.; Terabe, S. Characterization of Electrokinetic Gating Valve in Microfluidic Channels. *Anal. Chim. Acta* **2007**, *584*, 129–135.

(69) Koutny, L. B.; Schmalzing, D.; Taylor, T. A.; Fuchs, M. Microchip Electrophoretic Immunoassay for Serum Cortisol. *Anal. Chem.* **1996**, *68*, 18–22.

(70) Ermakov, S. V.; Jacobson, S. C.; Ramsey, J. M. Computer Simulations of Electrokinetic Injection Techniques in Microfluidic Devices. *Anal. Chem.* **2000**, *72*, 3512–3517.

(71) Ermakov, S. V.; Jacobson, S. C.; Ramsey, J. M. Computer Simulations of Electrokinetic Transport in Microfabricated Channel Structures. *Anal. Chem.* **1998**, *70*, 4494–4504.

(72) Beebe, D. J.; Moore, J. S.; Bauer, J. M.; Yu, Q.; Liu, R. H.; Devadoss, C.; Jo, B.-H. Functional Hydrogel Structures for Autonomous Flow Control inside Microfluidic Channels. *Nature* **2000**, *404*, 588–590.

(73) Eddington, D. T.; Beebe, D. J. Flow Control with Hydrogels. *Adv. Drug Deliv. Rev.* **2004**, *56*, 199–210.

(74) Liu, R. H.; Beebe, D. J. Fabrication and Characterization of Hydrogel-Based Microvalves. *J. Microelectromechanical Syst.* **2002**, *11*, 45–53.

(75) Bassetti, M. J.; Beebe, D. J. Demonstration of Hydrogel Volume Control Using Pulse Width Modulation. In *Micro Total Analysis Systems*; Nara, Japan, 2002; pp. 718–720.

(76) Ismagilov, R. F.; Rosmarin, T. D.; Kenis, J. A.; Chiu, D. T.; Zhang, W.; Stone, H. A.; Whitesides, G. M. Pressure-Driven Laminar Flow in Tangential Microchannels: An Elastomeric Microfluidic Switch. *Anal. Chem.* **2001**, *73*, 4682–4687.

(77) Mohan, R.; Schudel, B. R.; Desai, A. V.; Yearsley, J. D.; Apblett, C. A.; Kenis, P. J. A. Design Considerations for Elastomeric Normally Closed Microfluidic Valves. *Sensors Actuators B Chem.* **2011**, *160*, 1216–1223.

(78) Selvaganapathy, P.; Carlen, E. T.; Mastrangelo, C. H. Electrothermally Actuated Inline Microfluidic Valve. *Sensors Actuators A Phys.* **2003**, *104*, 275–282.

(79) Klintberg, L.; Svedberg, M.; Nikolajefff, F.; Thornell, G. Fabrication of a Paraffin Actuator Using Hot Embossing of Polycarbonate. *Sensors Actuators A Phys.* **2003**, *103*, 307–316.

(80) Liu, R. H.; Bonanno, J.; Yang, J.; Lenigk, R.; Grodzinski, P. Single-Use, Thermally Actuated Paraffin Valves for Microfluidic Applications. *Sensors Actuators B Chem.* **2004**, *98*, 328–336.

(81) Tan, H.; Yeung, E. S. Automation and Integration of Multiplexed On-Line Sample Preparation with Capillary Electrophoresis for High-Throughput DNA Sequencing. *Anal. Chem.* **1998**, *70*, 4044–4053.

(82) Bevan, C. D.; Mutton, I. M. Freeze-Thaw Flow Management: A Novel Concept for High-Performance Liquid Chromatography, Capillary Electrophoresis, Electrochromatography and Associated Techniques. *J. Chromatogr. A* **1995**, *697*, 541–548.

(83) Bevan, C. D.; Mutton, I. M. Use of Freeze-Thaw Flow Management for Controlling and Switching Fluid Flow in Capillary Tubes. *Anal. Chem.* **1995**, *67*, 1470–1473.

(84) He, Y.; Zhang, Y. H.; Yeung, E. S. Capillary-Based Fully Integrated and Automated System for Nanoliter Polymerase Chain Reaction Analysis Directly from Cheek Cells. *J. Chromatogr. A* **2001**, *924*, 271–284.

(85) Tellurex. Frequently Asked Questions About Our Cooling And Heating Technology http://tellurex.com/wp-content/uploads/2014/04/peltier-faq.pdf.

(86) Luppa, P. B.; Sokoll, L. J.; Chan, D. W. Immunosensors--Principles and Applications to Clinical Chemistry. *Clin. Chim. Acta* **2001**, *314*, 1–26.

(87) Gosling, J. P. A Decade of Development in Immunoassay Methodology. *Clin. Chem.* **1990**, *36*, 1408–1427.

(88) Ekins, R. P. Ligand Assays: From Electrophoresis to Miniaturized Microarrays. *Clin. Chem.* **1998**, *44*, 2015–2030.

(89) Ekins, R.; Chu, F.; Biggart, E. Development of Microspot Multi-Analyte Ratiometric Immunoassay Using Dual Fluorescent-Labelled Antibodies. *Anal. Chim. Acta* **1989**, *227*, 73–96.

(90) Wei, T. Q.; Zheng, Y. F.; Dubowy, M.; Sharma, M. Sandwich Assay for Tacrolimus Using 2 Antitacrolimus Antibodies. *Clin. Chem.* **2014**, *60*, 621–630.

(91) Yalow, R. S.; Berson, S. A. Assay of Plasma Insulin in Human Subjects by Immunological Methods. *Nature* **1959**, *48*, 1648–1649.

(92) Bilitewski, U.; Genrich, M.; Kadow, S.; Mersal, G. Biochemical Analysis with Microfluidic Systems. *Anal. Bioanal. Chem.* **2003**, *377*, 556–569.

(93) Ngo, T. T. Developments in Immunoassay Technology. *Methods* **2000**, *22*, 1–3.

(94) Srisa-Art, M.; Dyson, E. C.; deMello, A. J.; Edel, J. B. Monitoring of Real-Time Streptavidin-Biotin Binding Kinetics Using Droplet Microfluidics. *Anal. Chem.* **2008**, *80*, 7063–7067.

(95) Kricka, L. J.; Wild, D. Signal Generation and Detection Systems (Excluding Homogenous Assays). In *The Immunoassay Handbook*; Wild, D., Ed.; Nature Publishing Group: New York, NY, 2001; pp. 159–176.

(96) Trier, N. H.; Hansen, P. R.; Houen, G. Production and Characterization of Peptide Antibodies. *Methods* **2012**, *56*, 136–144.

(97) Rubinstein, N. D.; Mayrose, I.; Halperin, D.; Yekutieli, D.; Gershoni, J. M.; Pupko, T. Computational Characterization of B-Cell Epitopes. *Mol. Immunol.* **2008**, *45*, 3477–3489.

(98) Zangi, R.; Zhou, R.; Berne, B. J. Urea's Action on Hydrophobic Interactions. *J. Am. Chem. Soc.* **2009**, *131*, 1535–1541.

(99) Jr, J. F. Tripping the Switch Fantastic: How a Protein Kinase Cascade Can Convert Graded Inputs into Switch-like Outputs. *Trends Biochem. Sci.* **1996**, *0004*, 460–466.

(100) Hallberg, B.; Rayter, S. I.; Downward, J. Interaction of Ras and Raf in Intact Mammalian Cells upon Extracellular Stimulation. *J. Biol. Chem.* **1994**, *269*, 3913–3916.

CHAPTER 2

BEAD-BASED SANDWICH IMMUNOASSAY FOR pERK1/2 AND TOTAL ERK2

2.1 Introduction

This work builds on a microfluidic device previously designed and reported on by the Ramsey group and collaborators (Figure 2.1).[1,2] The device incorporated an array of antibody-coated microspheres (beads) and used multiplex sandwich immunoassays to determine the concentrations of cytokines in human saliva. Four reagent inlets/vias introduced sample, biotinylated detection antibody (dAb), a streptavidin-conjugated fluorescent complex, and wash buffer to the chip. Fluid flow from the reagent inlets was controlled by pinch valves. While the device was designed to be used in a single experiment with an automated reader,[2] its experimental parameters were developed through use of a simpler version of the chip that facilitated running many assays simultaneously. The simplified device (Figure 2.2A) featured eight single straight channels with bead arrays at their center, vias for introducing beads/reagent to the chip, and vias for applying waste/vacuum. A 1,024-microwell array and its corresponding location on one of the straight channels is shown in Figure 2.2B. With this simple design, 8 assays/chip can be run simultaneously in addition to running multiple chips as well. With the large throughput capability, the device was used to develop the immunoassay by testing different experimental conditions. This included the testing of antibody pairs for sandwich immunoassays, the optimization of reagent concentrations and incubation times, and the lengths of wash steps between each incubation.

Several aspects of this simple array chip are applicable for determining

pERK1/2:ERK1/2 in human samples. The first is its utilization of the sandwich immunoassay. Figure 2.3 shows the steps of a sandwich immunoassay with the first step involving an antibody capturing a target analyte during a sample incubation period (Figure 2.3A). After a wash step, a dAb is introduced to bind to a second epitope site on any captured target analyte (Figure 2.3B). The dAb in these particular assays has been conjugated with multiple molecules of biotin. After the dAb incubation, a streptavidin-conjugated fluorescent label is introduced and incubated with the beads (Figure 2.3C). Streptavidin and biotin bind together rapidly with extremely high affinity,[3] and the fluorescent label thus becomes bound to the antibody-analyte complex. Unbound streptavidin-fluorescence complex is washed away and a fluorescence image of the beads taken (Figure 2.3D). The amount of fluorescent label present corresponds directly to the amount of analyte captured.

This two-antibody feature of sandwich immunoassays can be applied for determining the phosphorylation ratio of ERK1/2. Due to the ~83-85% sequence homology of ERK1 and ERK2,[4] they share many epitopes, making it possible to capture all phosphorylation states of ERK1 and ERK2 with one monoclonal capture antibody. As phosphorylation considerably changes the shape of ERK1 and ERK2,[5] a monoclonal dAb that recognizes only pERK1 and pERK2 can be used to distinguish them from non-phosphorylated ERK1 and ERK2 (nERK1 and nERK2). Two assay strategies are possible based on this.

In the first strategy (Figure 2.4), a single dAb for pERK1/2 is used to determine both pERK1/2 and nERK1/2. For this assay, two successive pERK1/2 dAb incubations are used with a phosphorylation step in between to convert captured nERK1/2 to pERK1/2. The assay begins by capturing both pERK1/2 and nERK1/2 and determining the pERK1/2 concentration using the sandwich immunoassay steps shown in Figure 2.4A-D. After quantifying the pERK1/2,

mitogen-activated protein kinase kinases 1 and 2 (MEK1/2), the enzymes responsible for phosphorylating ERK1/2 *in vivo*,[4] are then incubated with the necessary cofactors in order to convert all captured nERK1/2 to pERK1/2 (Figure 2.4E). The pERK1/2 dAb is incubated a second time (Figure 2.4F) in tandem with the fluorescent streptavidin complex (Figure 2.4G) and the captured complex's fluorescence is measured (Figure 2.4H). The ratio of the fluorescence from the initial pERK1/2 measurement and the second pERK1/2 measurement corresponds to the sample's ratio of pERK1/2 to total ERK1.2 (pERK1/2:ERK1/2). An initially highly phosphorylated sample would yield a relatively high fluorescence ratio between the two measurements. In a clinical sample, this would be seen in many cancers due to overexpression of the ERK1/2 pathway, though the extent of overexpression varies by patient, disease, and disease stage.[6] A sample from a healthy patient would have a low proportion of pERK1/2 and would experience a greater degree of phosphorylation during the MEK1/2 incubation. The fluorescence from the second measurement would thus be greater than from the first.

The second assay strategy for determining pERK1/2:ERK1/2 utilizes two distinct dAbs (Figure 2.5). In addition to the pERK1/2 dAb, a dAb that recognizes all phosphorylation states of ERK1/2 is used to determine the total amount of ERK1/2 captured. A standard immunoassay as in Figure 2.3 would be performed with a pERK1/2 dAb, followed by introduction of the total ERK1/2 dAb and subsequent measurement of the total ERK1/2. It is also possible to reverse the dAb incubation steps, first using the total ERK1/2 dAb and then the pERK1/2 dAb.

The approach as proposed in Figure 2.3 and Figure 2.4 has the advantage of requiring only a single dAb as only one analyte (pERK1/2) is targeted. The disadvantages lie with using the MEK1/2 enzyme to convert the nERK to pERK. The MEK1/2 enzymes are expensive, and they may require the nERK1 and nERK2 to be in their native conformation. This is a potential

issue because target epitopes for many monoclonal antibodies may be poorly accessible in the native protein, requiring the protein to be unfolded with a denaturing agent like urea[7] to expose the binding site. The two-dAb approach has the advantage of not requiring nERK1/2 to be in their native conformations in order for dAb recognition. The cost may also be lower since MEK1/2 is not required. A disadvantage is the need for a total ERK1/2 dAb in addition to the pERK1/2 dAb. Ideally, the total ERK1/2 dAb would be capable of binding to ERK1/2 molecules captured by the pERK1/2 capture antibody, as only one capture bead type would then be needed. The use of a total ERK1/2 dAb not capable of such binding would require at least two bead types, further complicating experimental procedures and data analysis.

While capture antibodies for sandwich immunoassays can be affixed to many surfaces, including microtiter plate wells[8] and microfluidic channels,[9] covalently binding antibodies to beads has several advantages over these approaches. A single coupling reaction can produce enough antibody-coated beads for months or even years of experiments, while other approaches often require a long incubation step to immobilize the capture antibody on the surface prior to sample introduction for each experiment. The use of beads from a single antibody-bead reaction for many assays improves interexperimental reproducibility as well as experimental throughput. Beads can be spatially placed within a device without the need for such steps as photoinitiated or passive antibody-surface binding, and through the use of internal encoding dyes, beads coated with different capture antibodies can be distinguished to assay numerous analytes simultaneously.[1,2] The arrays used in our devices facilitate this by placing up to 1,024 beads in a single fluorescence microscope image. The chips are fabricated from poly(dimethylsiloxane) (PDMS), an elastic material where the beads can be easily loaded by pressing on the PDMS to force the beads into the microwells.

This chapter covers efforts in developing a microfluidic bead-based immunoassay for determining pERK2 and nERK2 using the simple array device shown in Figure 2.2. Several assay parameters including the detection fluorophore and the reagent incubation times are examined, and different capture and dAbs are also tested. The two assay strategies (single-dAb and dual-dAb) for determining pERK1/2:ERK1/2 are developed and compared in terms of their sensitivity and the signal levels they yield for various pERK2 and nERK2-containing samples.

2.2 Materials and methods

2.2.1 Materials and reagents

Dow Corning's Sylgard 184 PDMS was purchased from Ellsworth Adhesives (Germantown, WI) and was prepared according to the manufacturer's instructions at a 10:1 elastomer/cross-linker ratio. Tris-buffered saline with 0.05% Tween-20 (TBS-Tween), 1-ethyl-3-(-3-dimethylaminopropyl) carbodiimide hydrochloride (EDAC), N-hydroxysulfosuccinimide (sulfo-NHS), octyltrichlorosilane, sodium fluoride, ethylene diamine tetraacetic acid (EDTA), urea, and Triton X-100 were purchased from Sigma-Aldrich (St. Louis, MO). Sodium phosphate monobasic, 2-(N-morpholino)ethanesulfonic acid (MES), 10x phosphate-buffered saline (PBS, pH = 7.4), 10% bovine serum albumin (BSA) in PBS, sodium azide, optically clear polypropylene plate-sealing tape (PCR tape), Contrad 70 detergent, and microscope slides (75 mm x 25 mm x 0.99 mm) were purchased from Thermo Fisher Scientific (Waltham, MA). Purified recombinant human vascular endothelial growth factor (VEGF), phosphorylated and non-phosphorylated extracellular signal-related kinase 2 (pERK2 and nERK2), biotinylated detection antibodies for VEGF, pERK1/2, and ERK2, capture antibodies for pERK1/2, VEGF, ERK2, and a control capture antibody were purchased from R&D Systems (Minneapolis, MN). All proteins and antibodies were reconstituted according to the manufacturer’s instructions.

Tween-20 and MagPlex Luminex beads were purchased from Bio-Rad Laboratories (Hercules, CA). Non-magnetic Luminex beads were purchased from Luminex Corporation (Austin, TX). Polyethylene glycol (PEG) with an average molar mass of 10,000 g (PEG10k) was purchased from Alfa Aesar (Ward Hill, MA). MF-319 photoresist developer, KMPR 1010 photoresist, and SU-8 thinner were purchased from MicroChem (Newton, MA); the SU-8 thinner was mixed with KMPR 1010 to prepare 35% (w/w) KMPR solutions. P-type 6" crystalline Si wafers were purchased from University Wafer (Boston, MA). Streptavidin-B-phycoerythrin (SA-PE) and streptavidin-Alexa Fluor 488 (AF488) were purchased from Invitrogen (Carlsbad, CA). All aqueous solutions were prepared with deionized (DI) water from a NANOpure Diamond system (Barnstead International, Dubuque, IA).

Several different blocking buffers are used during immunoassay experiments, all of which are prepared in 1x PBS buffer. PBS-PEG contains 0.1% PEG-10k. PBS-B contains 0.1% BSA and 0.05% Tween-20. PBS-BTBL contains 1% BSA and 0.05% Tween-20. ERK buffer contains 5 mM sodium fluoride, 1 mM EDTA, 1 M urea, and 0.5% Triton X-100. A variant of ERK buffer without 1 M urea is also used in one experiment.

2.2.2 Bead-antibody coupling

Luminex beads are carboxyl-terminated polystyrene microspheres available with or without a superparamagnetic core. The magnetic beads are 6.5 μm in diameter while the non-magnetic beads are 5.6 μm in diameter.[10,11] Early work described in Chapter 2 used non-magnetic beads, while all subsequent experiments used magnetic beads. The beads are impregnated with two different fluorescent dyes. By varying the concentration ratio of both dyes, Luminex produces 100 unique bead types (called "regions") suitable for up to 100-plex assays.[12] A custom optical filter cube (632 nm/22 nm excitation, 685 nm dichroic, 677 nm/50

nm emission) purchased from Semrock (Lake Forest, IL) was used for distinguishing between beads containing different concentrations of Luminex's infrared-emitting dye.

Through use of the carboxyl groups covering the beads' surfaces, antibodies and other ligands of interest can be covalently bound to the beads. Antibody linkage to the beads was done via the carbodiimide chemistry of EDAC and sulfo-NHS. EDAC is a heterobifunctional cross-linker, one end binding to the carboxyl groups on the beads, and the other binding to surface amine groups on amino acid residues in immunoglobulin-G (IgG) antibodies. Sulfo-NHS is used in conjunction with EDAC to yield a less labile chemical intermediate, which allows for a much longer bead-antibody coupling period and thus greater coupling efficiency.[13]

2.2.2.1 Coupling procedure for non-magnetic beads

The procedure for coupling antibodies to beads was provided by the vendor[14] and is summarized here. It utilizes four buffers that are prepared prior to each bead coupling. The activation buffer is 100 mM sodium phosphate monobasic at a pH of 6.2. The coupling buffer is 50 mM MES at a pH of 5.0. Sodium hydroxide and hydrochloric acid were used to adjust buffer pH. The wash buffer is PBS + 0.05% Tween-20. The storage/blocking buffer is PBS + 0.1% (BSA) + 0.02% Tween-20 with 0.05% sodium azide as a preservative. The stock beads are at a concentration of 12.5 million beads/mL. All buffers and beads were brought to room temperature prior to use. Region 1 beads were used with the control antibody and region 50 beads were used with the VEGF capture antibody.

Stock beads were vortexed at 3000 rpm for 30 s and sonicated for 15 s. 5 million beads (400 µL bead stock) were transferred to a 500-µL LoBind microcentrifuge tube (Eppendorf, Hauppauge, New York) and pelleted by centrifuging them at 8,000 rcf for 3 min. The supernatant was removed and replaced with 100 µL of wash buffer. The beads were

resuspended by vortexing them for 30 s at 3000 rpm, then pelleted. The supernatant was removed and replaced with 80 µL of activation buffer. 10 µL of 50 mg/mL sulfo-NHS and 10 µL of 50 mg/mL EDAC (both prepared in activation buffer) were added and the beads were vortexed at 3000 rpm for several seconds. The beads were activated by placing them on a plate shaker (MS1 S7, Fisher Scientific) at 1000 rpm for 20 min at room temperature. The activated beads were pelleted and the supernatant was replaced with 250 µL of coupling buffer. The beads were resuspended and then pelleted. The supernatant was removed and replaced with 250 µL of coupling buffer. 16 µg capture antibody (prepared in PBS) was added and the total volume of the mixture was brought to 500 µL with coupling buffer. The bead tube was covered with foil, gently vortexed, and placed on a 25 rpm rotator (H5500; Labnet International Inc., Edison, NJ) for 2 h at room temperature to couple the beads to the antibodies.

Coupled beads were pelleted and resuspended in 500 µL storage/wash buffer. They were then pelleted, resuspended in 1 mL storage/wash buffer, and this step was repeated once more. The beads were finally resuspended in 250 µL storage/wash buffer and stored at 4 ºC until use.

2.2.2.2 Coupling procedure for magnetic beads

The procedure for coupling antibodies to beads was provided by Bio-Rad.[15] The buffers used for coupling antibodies to magnetic beads are the same as those for the non-magnetic beads, except the coupling buffer is PBS at a pH of 7.4. The stock beads are at a concentration of 12.5 million beads/mL. All buffers and beads were brought to room temperature prior to use.

Stock beads were vortexed at 3000 rpm for 30 s and then sonicated for 15 s. 100 µL of stock beads were transferred to a 500-µL LoBind microcentrifuge tube and pelleted on the bottom of the tube with a large rare-earth magnet. The supernatant liquid was removed and replaced with 100 µL of wash buffer. The beads were resuspended in the wash buffer by

vortexing at 3000 rpm for 30 s and then pelleted with the magnet. With the bead tube still on the magnet, the wash buffer was removed and replaced with 80 μL of activation buffer, then the beads were vortexed at 3000 rpm for 30 s. 10 μL of 50 mg/mL sulfo-NHS and 10 μL of 50 mg/mL EDAC (both prepared in activation buffer) were added and the beads were vortexed at 3000 rpm for several seconds. The beads were then placed on a plate shaker (MS1 S7, Fisher Scientific) at 1000 rpm for 20 min at room temperature. 150 μL of coupling buffer was added and the beads were pelleted on the magnet. The supernatant liquid was removed and then 150 μL of coupling buffer was added. The beads were resuspended by vortexing at 3000 rpm and pelleted again. The supernatant was removed and replaced with 100 μL of coupling buffer. 9 μg of capture antibody (prepared in PBS) was added and the total volume of the solution was brought to 500 μL with coupling buffer. The beads were vortexed and then incubated on a 25 rpm rotator for 2 h at room temperature to couple them to the antibody.

The coupled beads were pelleted from solution and the supernatant was removed. 250 μL of storage/blocking buffer was added and the beads were vortexed at 1500 rpm for 15 s. The beads were pelleted, the supernatant was removed, and 500 μL of storage/blocking buffer was added. The beads were vortexed for 20 s at 1500 rpm and pelleted again. The supernatant was removed and 100 μL storage/blocking buffer was added. The antibody-coupled beads were stored at 4 ºC when not in use.

2.2.3 Fabrication of master molds and assay chips

The chips used to determine appropriate antibodies/incubation buffers/wash buffers consisted of eight linear channels with a microarray centered in each (Figure 2.2). With the 8 channels, replicate measurement can be made simultaneously. The linear channel is approximately 1.5 cm long, 100 μm wide, and the array chamber is 400 μm wide. Each channel

is spaced 5.6 mm apart. Once fabricated, a 3-mm hole is made at each end of the channel for sample/reagent delivery and waste/vacuum. The chips are filled with a blocking buffer (varied by experiment) by pipetting buffer into the reagent inlet and pulling vacuum on the opposite end. The bead array consists of 1,024 circular wells with 11 μm center-to-center spacing; as the beads have an average diameter of 6.5 μm, the 11-micron well spacing corresponds to slightly less than two bead diameters. This spacing was previously found to prevent the problem of fluorescence overlap between the beads when imaging. The wells are approximately 5.2 μm in lateral diameter with a depth of approximately 5 μm.

Designs for the straight-channel chips were created in TurboCAD Professional 14 drafting software (IMSI/Design, Novato, CA) and the corresponding photolithography mask received from Infinite Graphics (Minneapolis, MN). This mask was divided into two halves, one with the microwell array features and the other with the channels.

2.2.3.1 Fabrication of silicon masters

In a clean room, 35% (w/w) KMPR photoresist was poured on a P-type 6" crystalline Si wafer (University Wafer, Boston, MA) and spin-coated at 500 rpm for 10 s, then 3000 rpm for 30 s to produce a 3-μm-thick layer of photoresist. The coated wafer was pre-baked at 100 °C for 4 min on a level hot plate. Once cool, the wafer was photolithographically exposed to the array features using a mask aligner (MA6/BA6; SUSS MicroTec, Garching, Germany). Exposures were performed for 30 s (approximately 300 mJ/cm^2 exposure energy) in hard contact mode. The exposed wafer was baked at 100 °C for 2 min, air cooled, developed in MF-319, and baked again at 100 °C for 5 min. The microwell array features were then etched via the Bosch process into the wafer to a depth of approximately 5 μm using deep reactive-ion etching (DRIE) (Alcatel AMS-100). Remaining photoresist was stripped from the wafer with a 2800 W oxygen plasma

in the DRIE and the etched feature sizes were determined with profilometry (P-15; KLA-Tencor, San Jose, CA).

The procedure to fabricate the channel layer was the same as that used for the microwell arrays except for the following details. 55% (w/w) KMPR was used instead of 35% to produce a 9-µm-thick layer in order to protect the microwell array. Exposure of the channel layer features required topside alignment of the mask's and mold's fiducials in the mask aligner. Channels were etched to a depth of approximately 20 µm. The completed master mold was silanized in a vacuum desiccator for 1 h with 500 µL of octyltrichlorosilane.

2.2.3.2 PDMS chip fabrication

To make chips, 10:1 PDMS was mixed and degassed. Approximately 13 g of PDMS were poured onto the center of the silicon master and spun in a two-step process at 150 rpm for 10 s followed by 200 rpm for 30 s. The coated wafer was degassed under vacuum then cured on a hot plate at 150 °C for 3 min. Two additional PDMS layers were cast and cured in the same manner, although air bubbles were removed with a nitrogen gun or via the spin-coating process, not with vacuum, as vacuum could delaminate the first PDMS layer. The PDMS was peeled from the wafer and laid upon glass cleaned with 5% Contrad and deionized water. Reagent/bead and waste/vacuum vias were created in the channels with a 3 mm biopsy punch (Sklar Instruments, West Chester, PA) and individual chips were cut from the bulk PDMS with a razor blade. Microscope slides were cleaned with 5% Contrad, rinsed with water, and dried with nitrogen. The PDMS chips were placed channel-side up in an oxygen plasma cleaner (PDC-32G; Harrick Plasma, Ithaca, NY) along with the cleaned slides and activated for 12 s at 18 W. The chips were irreversibly bonded by pressing the activated sides of the glass and PDMS together. Bonded chips were placed in a 95 °C oven for at least 1 h prior to use in order to

stabilize the PDMS.[16]

2.2.4 Loading beads into microarrays

To load antibody-coupled beads into the arrays, the chips are first filled with a blocking buffer consisting of PBS + 1% BSA + 0.05% Tween-20 (PBS-BTBL). A bead slurry containing a 1:1 mix of both target and control beads was then pipetted into the sample inlet and vacuum applied on the outlet to pull the beads into the channel (Figure 2.6A). As the beads flow into the microarray chamber, the PDMS above the array is pressed down to force beads into the wells (Figure 2.6B). As the diameter of an unloaded microwell is smaller than the bead diameter, the microwell stretches to accommodate the bead, which is held in place by the elastic force of the PDMS attempting to relax to its native state (Figure 2.6C). The extent of the microarray's loading is monitored using an epifluorescent microscope, and the loading process stopped when approximately 90%+ of the microwells are loaded (Figure 2.6D). Remaining bead slurry is removed from the inlet and the chips are filled with fresh PBS-BTBL (Figure 2.6E). The inlet/outlet are sealed with PCR tape and stored at 4 ºC for at least 24 h prior to use (Figure 2.6F).

Storing the chips under blocking buffer results in the surfaces of the glass and PDMS being dynamically coated with molecules of protein and surfactant from the buffer.[17,18] This prevents nonspecific adsorption from proteins and other biomolecules present in the sample, which is critical for reducing background and ensuring that the chips are biocompatible with assay reagents and samples. PDMS is especially prone to this nonspecific adsorption as its surface is hydrophobic.[18–21] While it is possible to functionalize the surface of PDMS,[22] the use of a dynamic coating from a blocking buffer is preferable because it is simpler to implement and has proven effective.

2.2.5 Data collection

All assay data was collected on an Eclipse Ti-U inverted microscope with an Intensilight C-HGFIE mercury lamp (Nikon, Melville, NY) and an electron-multiplying charge-coupled device (EM-CCD) camera (Cascade II-512; Photometrics, Tucson, AZ). Custom optical filter cubes for the encoding dye (632 nm/22 nm excitation, 685 nm dichroic, 677 nm/50 nm emission) and B-phycoerythrin (531 nm/40 nm excitation, 562 nm dichroic, 593 nm/40 nm emission) were purchased from Semrock (Lake Forest, IL). A Nikon B-2E/C filter cube (465 nm/30 nm excitation, 505 nm dichroic, 515 nm/40 nm emission) was used for AF-488. The beads were brought into focus by imaging the encoding beads with 100 ms exposure times. Assay images were taken at either 531 nm (for B-phycoerythrin) or 465 nm (for AF-488) for a total of 8 s. Micro-Manager[23] was used to control the camera and images were analyzed with ImageJ[24] (National Institutes of Health, USA) and Excel (Microsoft, Inc., Redmond, WA). The methods of analysis evolved with the project and will be discussed as necessary.

2.2.6 Data analysis

Micro-Manager[23] was used to collect two images for each assay: an encoding image and an assay image. The encoding image, taken at 632 nm, collected fluorescence from the internal dyes in the beads. The assay image, taken immediately after the encoding image at 531 nm (SA-PE) or 465 nm (AF-488), collected fluorescence from the dye in the antibody-analyte complex on the bead surfaces. As the control beads contained significantly less dye than the assay beads, the two types could be easily distinguished. The encoding images were decoded by selecting each bead in ImageJ.[24] A sample encoding image with three different bead types selected is shown in Figure 2.7A. Control beads are within the blue boxes, total ERK2 beads are in the yellow pentagons, and pERK1/2 beads are in the red circles. These selections were overlaid on

the assay image (Figure 2.7B) to extract the corresponding fluorescence data from each bead. The raw average signal and standard deviation are obtained from the fluorescence from each bead's brightest pixel. Outliers are removed[25] by rejecting fluorescence values not within 2.2 standard deviations of the raw mean, and the corrected signal is calculated from the remaining values. The net signal is finally calculated by subtracting the fluorescence of the control beads from the fluorescence of the assay beads.

2.2.7 Sandwich assay procedure

The sandwich immunoassay procedure used was adapted from one previously developed and recently described elsewhere.[1,2] A schematic of the process is provided in Figure 2.3. All chips used in assays were loaded with beads and passivated with blocking buffer. Solutions are introduced to the chips by using vacuum to remove the fluid in the chip inlets, filling the inlets with 10 μL of liquid, and pulling vacuum on the vacuum/waste via for 10 s to fill the chip with the new reagent. Washing is performed by introducing the appropriate buffer to the chip inlet vias and pulling vacuum for the time specified.

Two incubation protocols – short and long – were used in early experiments. In the short protocol, incubations were performed at 37 °C. Sample was introduced to the chips and incubated for 20 min. Detection antibody at 3 μg/mL was incubated for 15 min. Fluorescent dye was incubated for 10 min. The reagent vias were filled with TBS-Tween, washed for 10 min, and then imaged.

In the long protocol, incubations were performed at room temperature. Sample was introduced to the chips and incubated for 1 h. Detection antibody at 3 μg/mL was incubated for 30 min. SA-PE at either 2 μg/mL or 20 μg/mL was incubated for 20 min. The chips were filled with TBS-Tween, washed for 10 min and imaged.

2.3 Results and discussion

2.3.1 Fluorophore selection

Early sandwich immunoassays in the group[1] utilized AF-488 as the detection fluorophore. AF-488 was used because of its high fluorescence quantum efficiency and excitation/emission spectra that do not overlap with the encoding dye. However, different beads were used in those experiments and AF-488 was untested in conjunction with the Luminex beads. SA-PE is recommended as the fluorophore for Luminex beads by the vendor so a comparison between the two fluorophores was made. B-phycoerythrin[26] is an exceptionally bright multi-chromophore protein with a quantum yield of 0.98 and a molar extinction coefficient of 2.41×10^6 cm^{-1} M^{-1}; it was thus hypothesized to yield substantially more fluorescent signal than AF-488,[27,28] which possesses a quantum yield of 0.92 and an extinction coefficient of 73,000 cm^{-1} M^{-1}.

VEGF was used as a model analyte at 0, 300, 600, and 900 pg/mL in two separate chip sets (consisting of 3 arrays per sample) loaded with non-magnetic VEGF and control beads. Anti-VEGF at 3 µg/mL was used as the dAb. The assay was run according to the short assay protocol and AF-488 at 20 µg/mL was used as the detection fluorophore in one chip set while SA-PE at 20 µg/mL was used in the other. All reagent solutions were prepared in PBS-PEG buffer. The results in Figure 2.8 show that the arrays imaged with SA-PE produced over 10 times greater signal than AF-488 arrays at the tested concentrations of VEGF. SA-PE was therefore used as the detection fluorophore in all future experiments.

2.3.2 Reagent incubation time and concentration

The short assay protocol was originally developed in an attempt to minimize the total assay time while trying to maintain sensitivity. This is desirable for a point-of-care (POC)

device as a rapid assay is preferable for a situation in which a patient waits at a clinic for results.[29,30] The protocol used a higher incubation temperature to overcome the limitations of shorter incubation times,[2] as immunoassay analyte capture is diffusion-limited[31] and the reagent diffusion rate is directly proportional to the incubation temperature.[32] A disadvantage of using the elevated temperature to increase reagent capture is that it requires a heating source. A second strategy for increasing reagent capture in a diffusion-limited situation is to simply perform incubations for longer time periods. As the pERK1/2:ERK1/2 assay does not have the same stringent time demands as a POC device, the second strategy was pursued in order to increase the sensitivity.

VEGF was again used as a model analyte at concentrations of 0, 300, 600, and 900 pg/mL in two separate chip sets (consisting of 3 replicate arrays per VEGF concentration per incubation protocol) loaded with non-magnetic VEGF and control beads. The long assay protocol (1 h sample incubation, 30 min dAb incubation, 20 min SA-PE incubation at room temperature) was followed in one chipset and the short assay protocol (20 min sample incubation, 15 min dAb incubation, 10 min SA-PE incubation at 37 °C) was used in the second chipset. 2 µg/mL SA-PE was used as the detection fluorophore in both, and all solutions were prepared in PBS-PEG buffer.

The long assay protocol yielded over 3 times the signal as the short protocol for each concentration tested (Figure 2.9) while using the lower SA-PE concentration. Besides improving the signal, the reduction in non-specific adsorption of the SA-PE is another important consideration. Figure 2.10 shows that there is a reduction in non-specific binding to the control beads with 2 µg/mL SA-PE compared to using a 20 µg/mL SA-PE, in spite of the fact that the incubation times are much longer. Based on these results, the long assay format and the lower

SA-PE concentration were used in all future experiments.

2.3.3 Development of pERK1/2 assay

The assay buffers used in the pERK1/2 experiments differed from those used in the VEGF experiments. Rather than PBS-PEG buffer, sample incubations were performed in ERK buffer, while dAb and SA-PE incubations were performed in PBS-B buffer. These changes were made in accordance with the recommendation of the pERK1/2 Ab's manufacturer. Chips were loaded with magnetic pERK1/2 and control beads. Assays were performed with and without urea to determine the effect on sensitivity. This was investigated because synthetic peptides are often used to create antibodies for specific epitopes, and these peptides do not necessarily have the same shape as the epitope in the native protein.[33] The epitope may also become more sterically accessible if the protein is denatured. Urea is used to unfold the protein without disrupting other components of the assay. Figure 2.11 shows the results of both assays where the undenatured pERK2 is detectable but with poorer sensitivity compared to the denatured state. Adding urea to the ERK incubation buffer results in more than a six-fold improvement in sensitivity.

These results suggest that the single-dAb strategy using the MEK1/2 phosphorylation step (Figure 2.4) would only be feasible if a suitable dAb for nERK1/2 was unavailable. MEK1/2 would likely be incapable of phosphorylating denatured ERK1/2, and given the poor sensitivity of the assay with native pERK1/2, a protocol in which both pERK1/2 and nERK1/2 are assayed in their denatured state would be preferable if it considerably improves the sensitivity. That is because an improvement in sensitivity translates to an improvement in the range of ERK1/2 phosphorylation ratios distinguishable by the assay.

2.3.4 Protocol development for dual-dAb pERK2:ERK2 assay

The successful detection of pERK2 was followed by the development of the nERK2 portion of the assay. Once both forms of ERK2 are detectable, a general method for determining the pERK2:ERK2 ratio could be developed. If that could be extended to include pERK1 and nERK1 as well, the assay would be capable of determining pERK1/2:ERK1/2. A total ERK2 (tERK2) detection kit (DYC1230-C; R&D Systems) was purchased that included capture antibody, nERK2 standards, and a biotinylated dAb that recognizes both pERK2 and nERK2. Total ERK2 beads were prepared by coupling the kit's capture antibody to magnetic beads. Multiplex assays were then run with both pERK1/2 and tERK2 beads in the same arrays to determine whether the tERK2 dAb would bind to ERK2 molecules captured by pERK1/2 beads, as well as whether the pERK1/2 dAb would bind to pERK2 molecules captured by the tERK2 beads. The fluorescence signal obtained from the beads would be reflective of the degree of binding. Ideally, the tERK2 and pERK1/2 dAbs would identify their respective antigens using one capture antibody, as future assays could then be run using only one bead type. The dual-dAb pERK2:ERK2 assay was developed by incubating some of the chips with the pERK1/2 dAb first (as shown in Figure 2.5) and other chips with the tERK2 dAb first to see if the incubation order mattered.

Chips were loaded in triplicates with an equal-parts mixture of pERK1/2 beads, tERK2 beads, and control beads. Assays were performed with five sample solutions consisting of various combinations and concentrations of stock pERK2 and nERK2: 5 ng/mL pERK2, 10 ng/mL pERK2, 5 ng/mL nERK2, 10 ng/mL nERK2, and a mixture of 5 ng/mL each pERK2 and nERK2 (total ERK2 = 10 ng/mL). Half of the chips were incubated with the pERK1/2 dAb for 30 min, and the other half were incubated with the tERK2 dAb for 30 min. The chips were then

washed for 1 min, incubated with SA-PE, washed for 1 min, and imaged. Following this, the chips that were initially incubated with the pERK1/2 dAb were incubated with the tERK2 dAb, and vice versa. They were then washed, incubated with SA-PE, washed, and imaged a second time.

A comparison of the signals from the pERK1/2 beads and tERK2 beads after the first dAb incubation showed the pERK1/2 beads with up to 5X the signal of the tERK2 beads. Since the pERK1/2 beads were more responsive than the tERK2 beads, further studies relied solely on the pERK1/2 beads. Figure 2.12A shows the results for the pERK1/2 beads first incubated with the pERK1/2 dAb. The first incubation/imaging step with the pERK1/2 dAb (gray bars) only showed fluorescence signals with samples containing pERK2. The nERK2 samples and blank signals were indistinguishable. The fluorescence increased with pERK2 concentration while the signals for the mixed sample were similar to those of the low-concentration pERK2 sample. This is in accordance with the pERK1/2 dAb only recognizing the pERK2 in the mixed sample. After these beads were incubated with the total ERK2 dAb (red bars), they showed an increase in fluorescence signal in samples containing nERK2. The fluorescence again increases as the nERK2 concentration increases; this includes the mixed sample, which contained equal parts pERK2 and nERK2. This opens the possibility of using the dual dAb assay strategy. There also appears to be a slight increase in signal with the pERK2 samples, suggesting that the tERK2 dAb recognizes pERK2 molecules captured by the pERK1/2 beads and is capable of specifically binding to them. This signal increase, however, may not be statistically significant due to overlapping error bars between the signals from the two imaging steps.

The beads first incubated with the tERK2 dAb showed somewhat different trends (Figure 2.12B). Between the two dAb/imaging cycles (represented by the white bars for the tERK2 dAb

and blue bars for both dAbs), they showed a small increase in fluorescence for the pERK2 samples, a small increase for the mixed pERK2 and nERK2 sample, and a large reduction in fluorescence for the nERK2 samples. The large decrease in signal for the nERK2-only samples follows from the fact that the first dAb recognizes nERK2 while the second does not, so the fluorescence seen on the beads is from the SA-PE complex formed in the first dAb/dye cycle. Many of those tags had photobleached during the first imaging step, and imaging the same complexes a second time yielded less signal as no additional tags were specifically added during the second incubation. The fluorescence increase for the pERK2 samples between steps is not nearly as drastic as was the signal increase for the nERK2 samples in the other chip set, suggesting that the tERK2 dAb has sterically interfered with the binding of the pERK1/2 dAb here.

These results show that the pERK1/2 beads can be used in the capture and detection of pERK1, pERK2, and nERK2. They also suggest that the pERK1/2 dAb should be used before the tERK2 dAb as the results obtained from the former protocol are much more straightforward to interpret; the signal from the first imaging step corresponds to the amount of pERK1/2 present, while the second step is indicative of total ERK2. In the tERK2 dAb-first protocol, the first imaging step's signal is dependent upon total ERK2, while the second imaging step shows a sharp reduction in signal from the nERK samples and a slight increase from the pERK samples.

2.4 Conclusions

In this chapter, several experimental parameters were optimized for the on-chip sandwich immunoassay. The cytokine-based assay protocol was considerably improved upon through the use of a new fluorophore (SA-PE) and longer reagent incubation times. The addition of urea to the assay incubation buffer was shown to improve the sensitivity of the pERK2 assay more than

six-fold compared to the same assay with no urea. A detection antibody for total ERK2 suitable for use with the pERK1/2 beads was identified and tested. Finally, the dual-dAb approach with the pERK1/2 dAb incubated first was shown to be appropriate for determining both pERK2 and nERK2 in a sample. One unresolved problem with the assays was that the percent relative standard deviations (%RSDs) are too high to be clinically useful. The chip-to-chip %RSD was often in the 20-30% range or more, while most clinically-accepted assays have %RSDs below 10%.[34] As this high variance impacts the assay's ability to distinguish differing phosphorylation levels of ERK1/2, as well as its clinical relevance, the next chapter covers efforts to discover the source of this variation and remedy it.

2.5 Figures

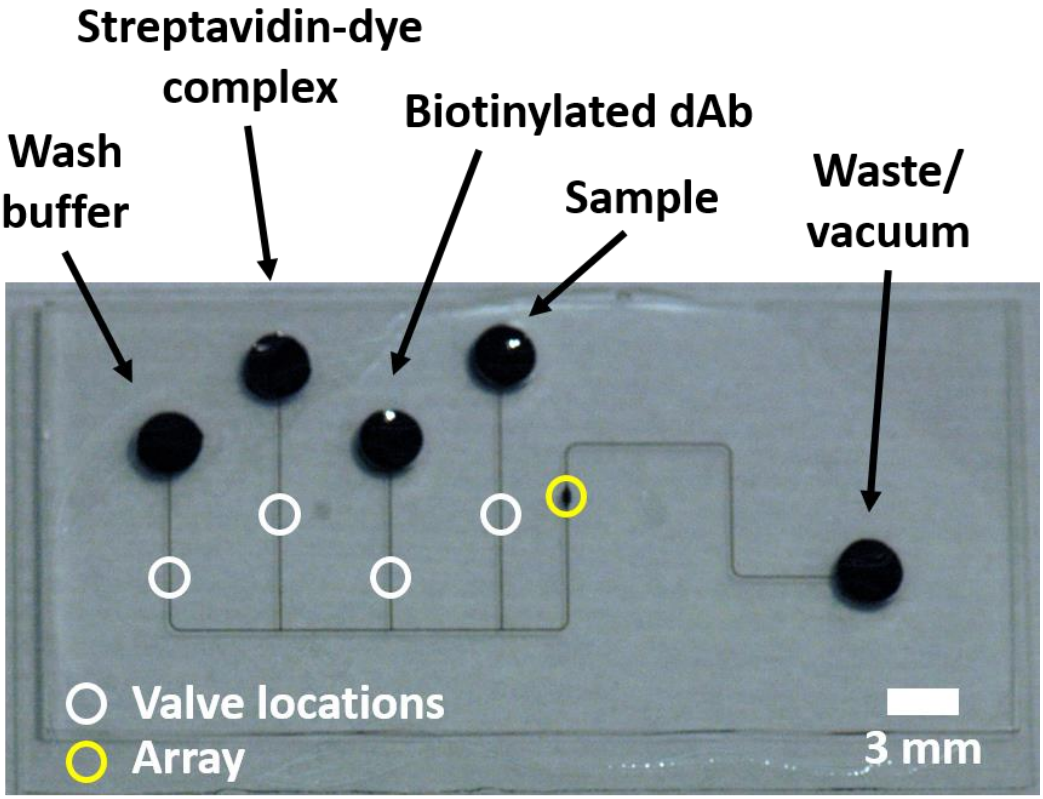

Figure 2.1. Photograph of saliva cytokine chip filled with ink for visualization. Each inlet via is labeled to indicate its corresponding reagent, as is the waste/vacuum via. The locations at which the inlet vias/inlets are valved are circled in white. The location of the array on the chip is indicated with a yellow circle.

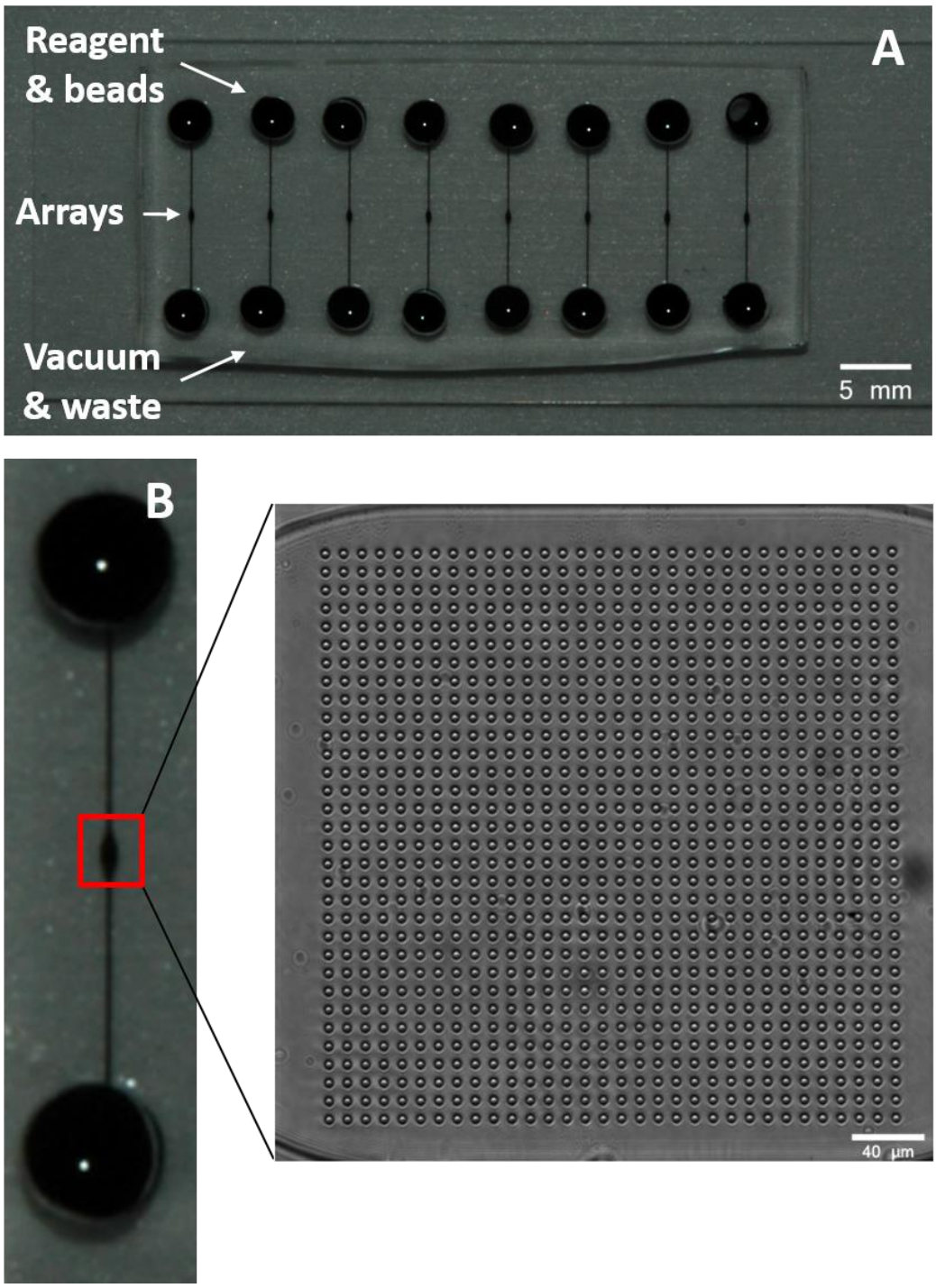

Figure 2.2. Schematic of 8-channel chip with array. (A) Photograph of 8-channel chip filled with ink for visualization. One set of vias is used for introducing reagents and beads while the other is used for waste and applying vacuum. (B) Bead array location with white light image of 1,024 unloaded microwells.

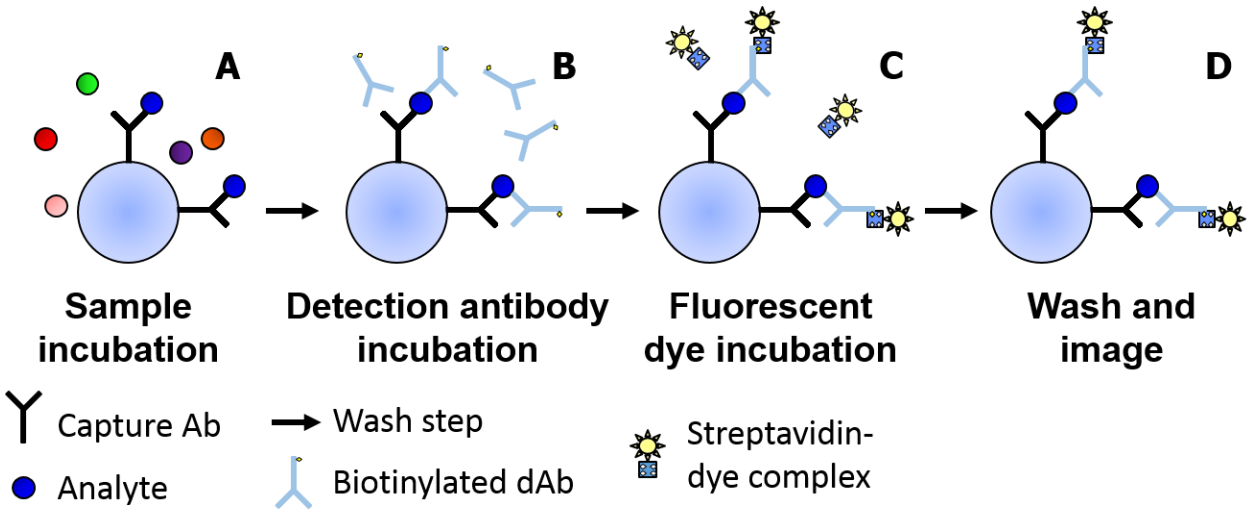

Figure 2.3. Schematic of single-analyte sandwich immunoassay. (A) Sample containing analyte molecules (and often other molecules) are incubated with and specifically captured by antibody-conjugated beads. (B) A biotinylated dAb is incubated and binds to a second epitope on the captured analyte. (C) A fluorescent dye conjugated to streptavidin is incubated, and the streptavidin binds to a biotin molecule on the dAb. (D) Unbound fluorophores are washed away and the beads are imaged with a fluorescence microscope.

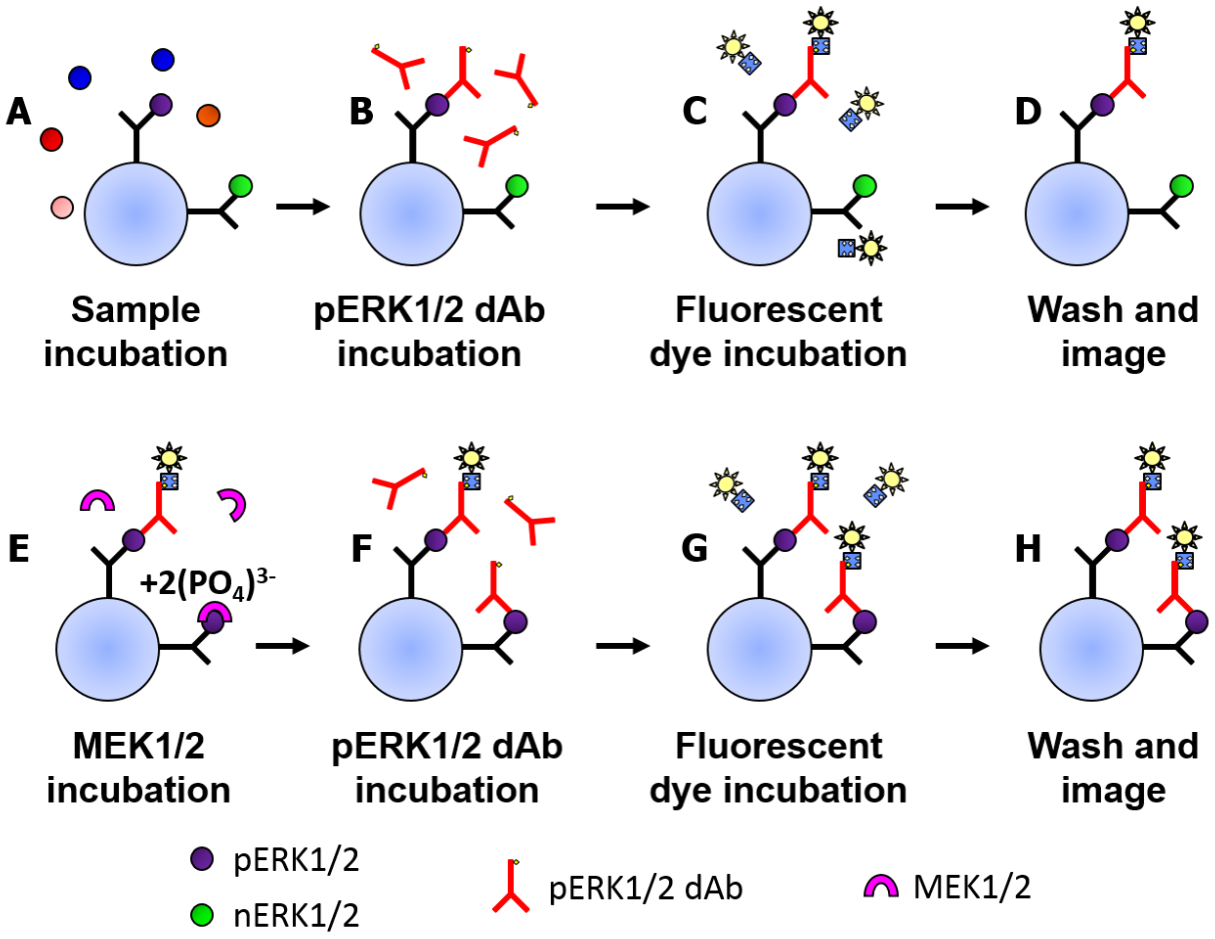

Figure 2.4. Schematic of single-dAb strategy for determining pERK1/2:ERK1/2. (A) Sample containing ERK1/2 is incubated with the beads, and all phosphorylation states of pERK1/2 are captured. (B) pERK1/2 is then determined through use of a biotinylated monoclonal antibody specific for pERK1/2, (C) a streptavidin-conjugated fluorescent dye complex, and (D) an imaging step. (E) The beads are then incubated with a cocktail containing MEK1/2 and its cofactors, which dually phosphorylates nERK1/2 to produce pERK1/2. (F) The pERK1/2 dAb, (G) dye complex, and (H) imaging steps are repeated to determine ERK1/2.

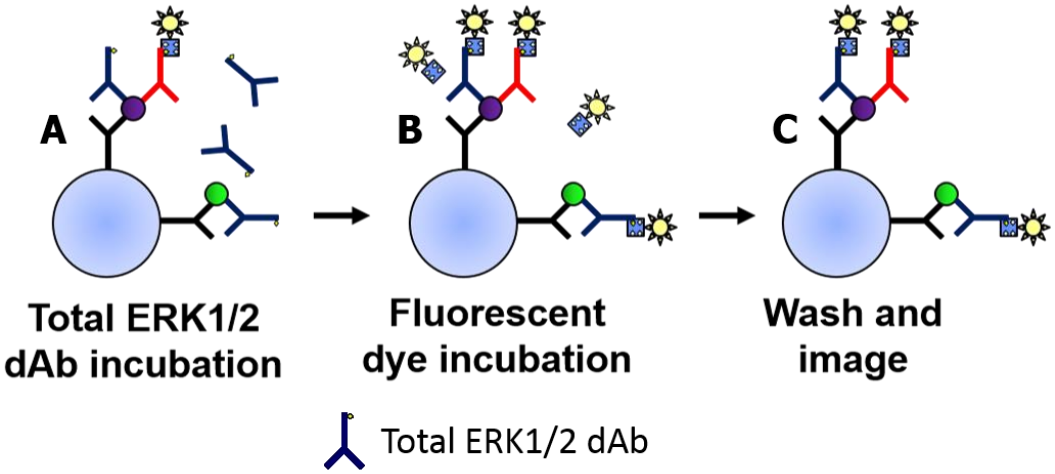

Figure 2.5. Dual-dAb strategy for determining pERK1/2:ERK1/2 in which pERK1/2 is determined first. The assay begins with steps (A)-(D) from Figure 2.4. (A) A total ERK1/2 dAb is used after the first imaging step with (B) the fluorescent dye complex in order to (C) determine ERK1/2.

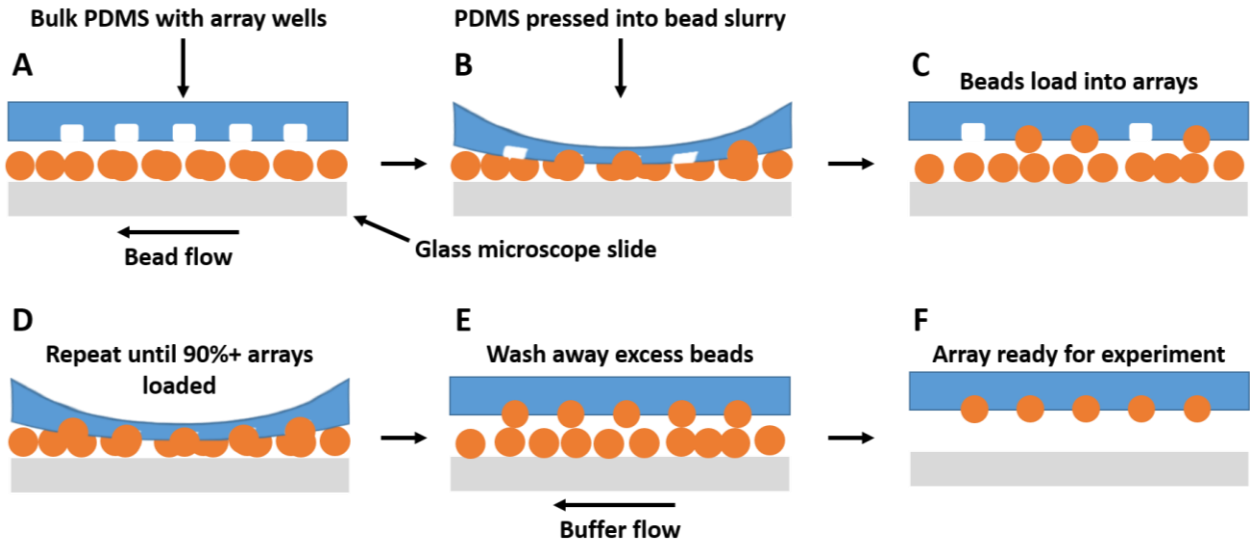

Figure 2.6. Schematic of loading process for PDMS arrays. (A) Bead-containing slurry is pulled through the chips and under the arrays. (B) The PDMS is pressed down into the beads and some beads are forced into the wells. (C) The wells are smaller than the diameter of the beads, and loaded beads are held in place by the elasticity of the PDMS. (D) The process is repeated until approximately 90% of arrays are loaded. (E) The bead slurry is removed from the bead via on the chip, replaced with blocking buffer, and excess beads are washed away. (F) The array is ready for an assay following passivation with blocking buffer.

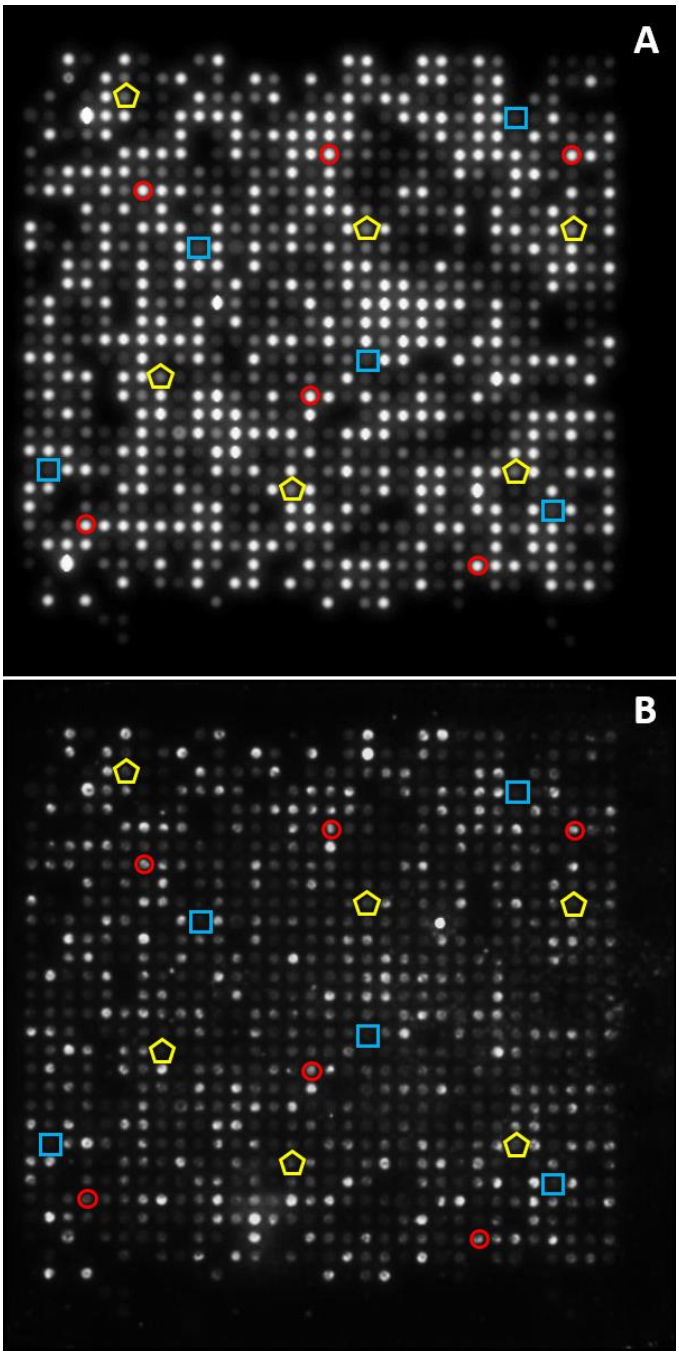

Figure 2.7. Encoding image and corresponding assay image from a 3-bead assay. Control beads are the dimmest in encoding image (A) and are enclosed in blue boxes. Total ERK2 beads are medium brightness in assay image (B) and are in yellow boxes. The brightest beads are in red boxes and correspond to pERK1/2 beads. Control beads are within blue boxes, total ERK2 beads are within the yellow pentagons, and pERK1/2 beads are within the red circles.

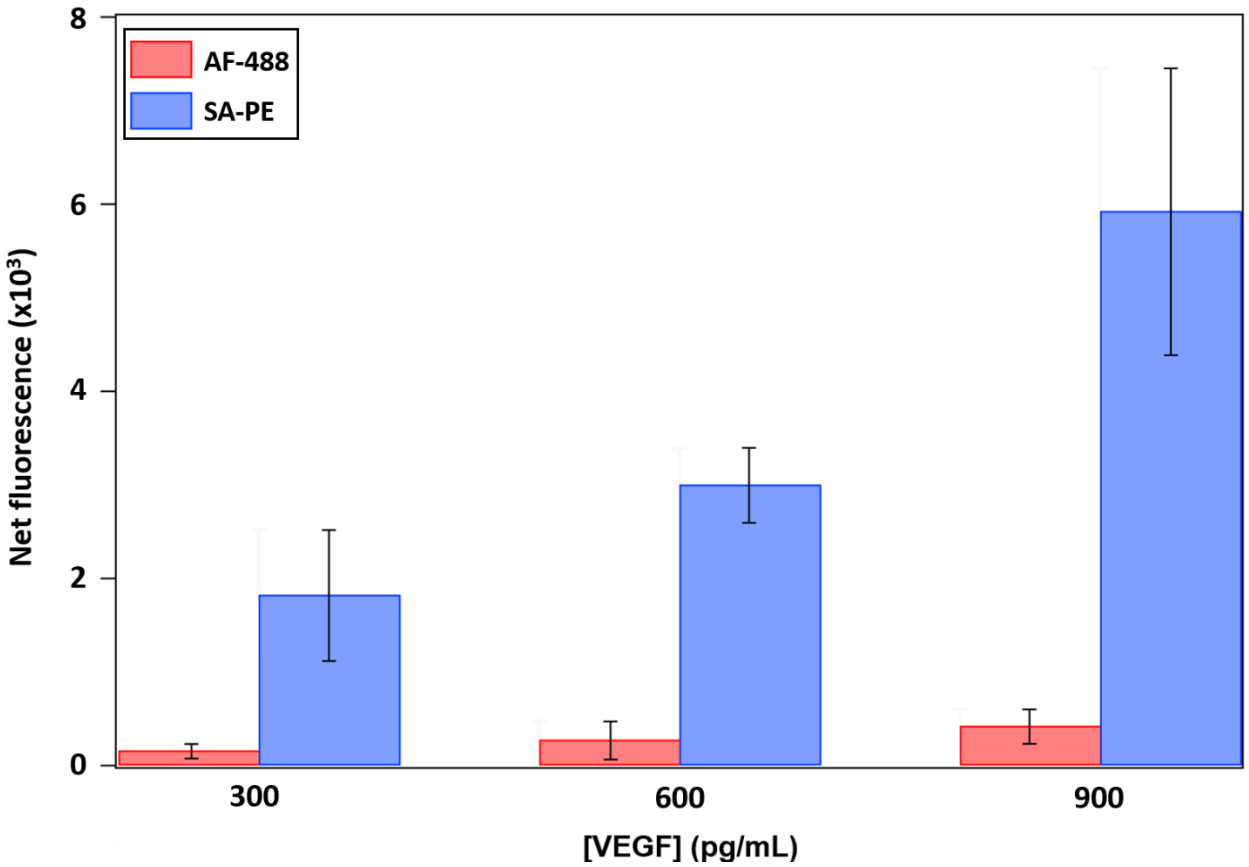

Figure 2.8. Comparison of reporter dye complexes used for detection in VEGF assay. Streptavidin-B-phycoerythrin far outperforms streptavidin-AlexaFluor 488 in terms of signal at each VEGF concentration. Error bars represent the standard deviation of three arrays.

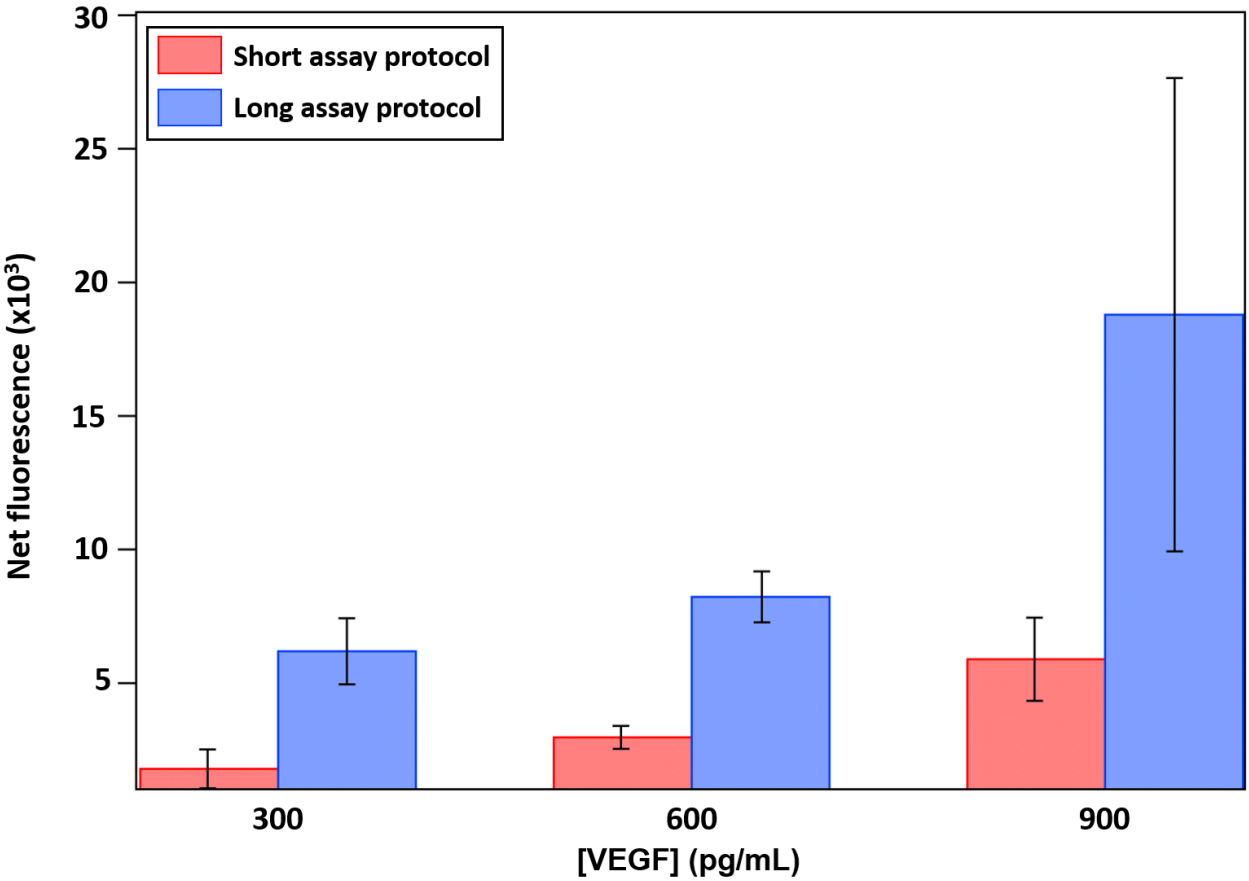

Figure 2.9. Comparison of reagent incubation strategies. In the short incubation protocol, sample, dAb, and SA-PE were incubated at 37 °C for 20 min, 15 min, and 10 min, respectively. Long incubations were performed at room temperature for 1 h, 30 min, and 20 min, respectively. The longer incubations resulted in significantly more fluorescence despite the difference in incubation temperature.

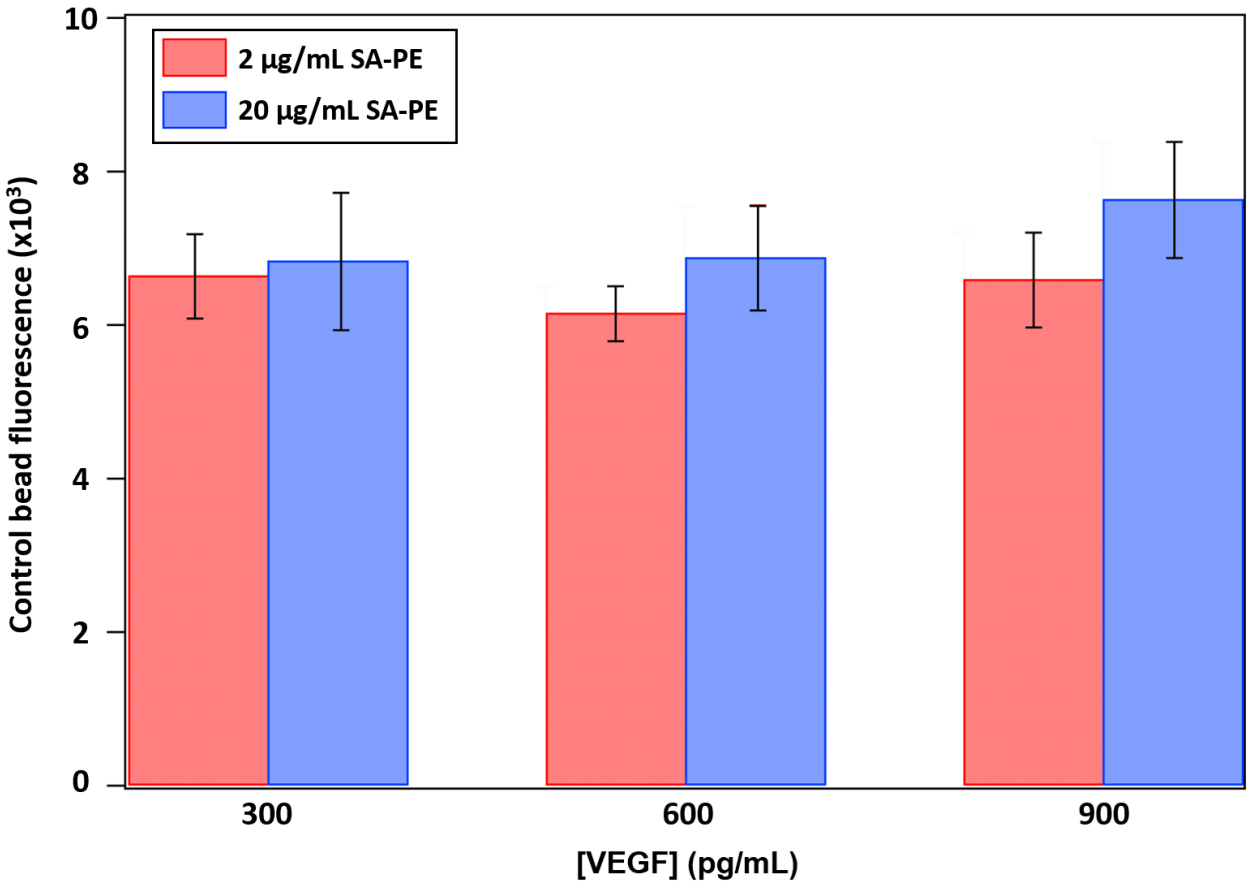

Figure 2.10. Comparison of non-specific binding on control beads from two different concentrations of fluorescent dye. Reducing the SA-PE concentration to 2 µg/mL results in less non-specific binding, but does not result in less signal from VEGF beads.

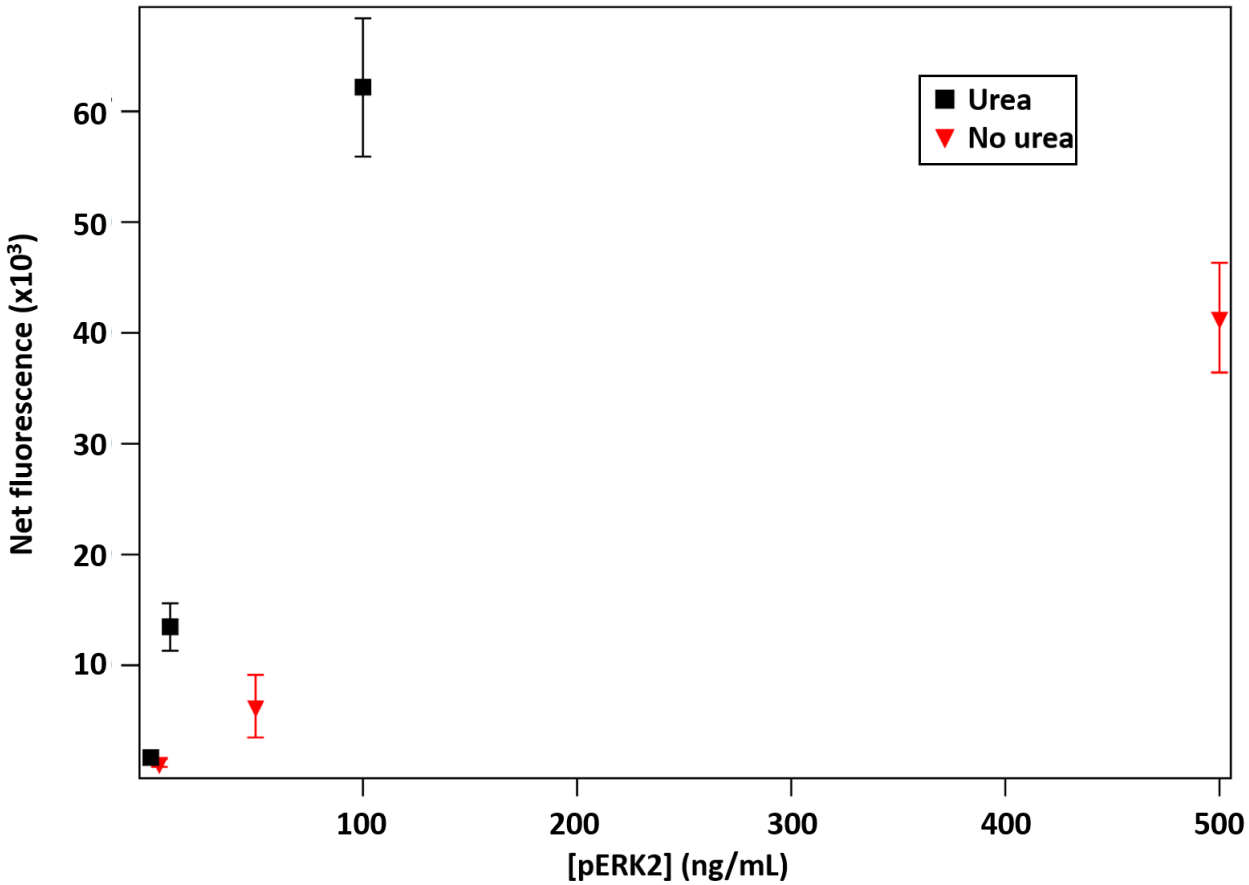

Figure 2.11. Comparison of pERK2 assay results with and without urea in the assay buffer. Urea results are indicated by black squares and the no-urea results with red triangles. The sensitivity of the assay is improved more than sixfold with the use of urea due to the denaturation of the analyte.

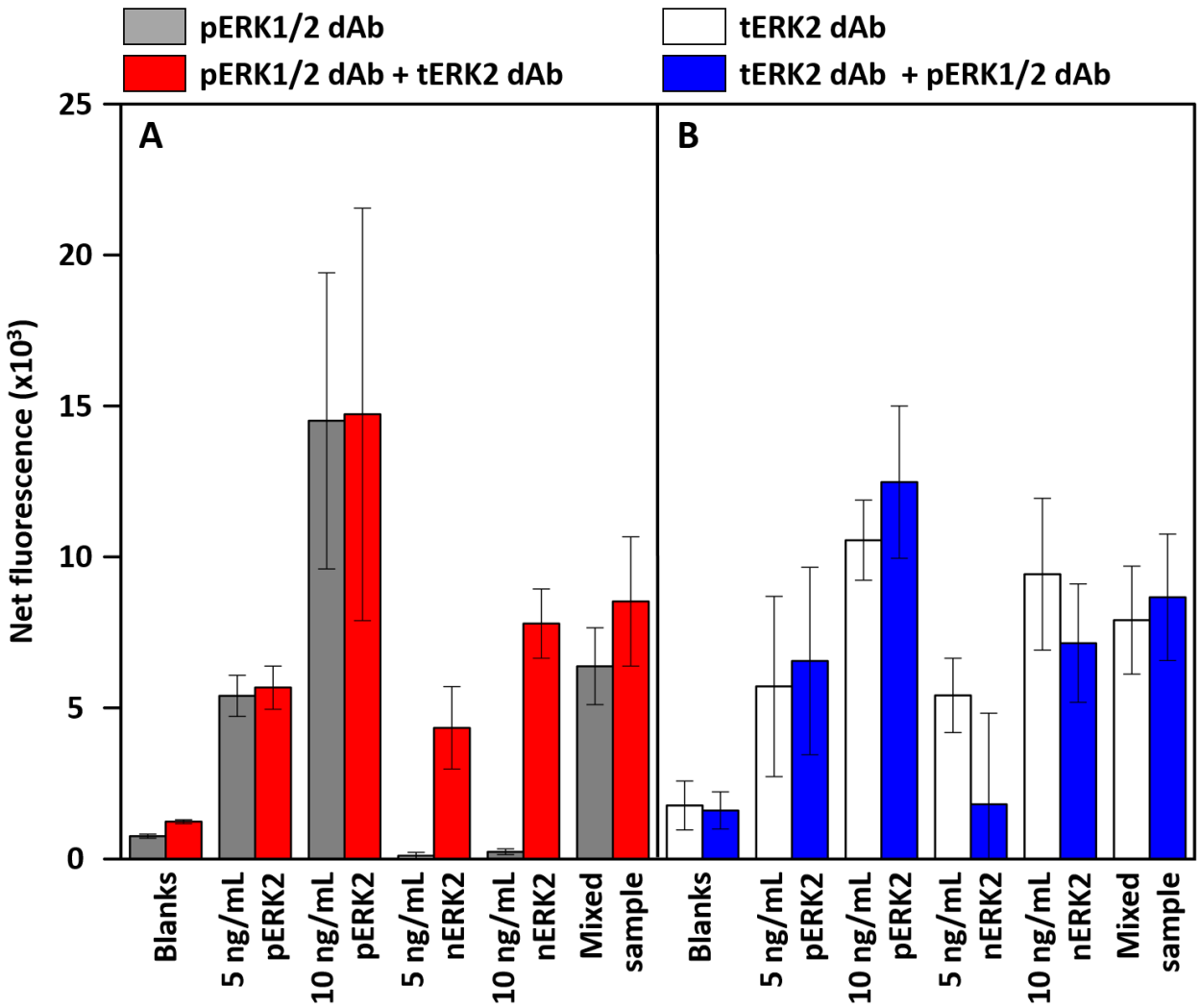

Figure 2.12. Results from pERK2:ERK2 protocol development experiment. (A) Results from pERK1/2 dAb-first beads. Incubation with pERK1/2 dAb (gray bars) produces relatively high signal for pERK2 and mixed samples and zero signal from nERK2 samples. Subsequent incubation with the tERK2 dAb (red bars) produces mild (though statistically insignificant) signal increases for the pERK2 and mixed samples and substantial signal increases for the nERK2 samples. This is consistent with the pERK1/2 dAb recognizing only pERK2 and the tERK2 dAb recognizing all the samples. (B) Results from tERK2 dAb-first experiment. Following incubation with the tERK2 dAb (white bars) and subsequent incubation with the pERK1/2 dAb (blue bars), the trends for the pERK2 samples and mixed sample are similar to those from the pERK1/2 dAb-fist experiment. However, the nERK2 samples show signal loss instead of gain after the pERK1/2 dAb incubation and imaging. This is also consistent with the tERK2 dAb binding to all the samples and the pERK1/2 dAb only binding to pERK2.

2.6 References

(1) Henley, W. H.; Dennis, P. J.; Ramsey, J. M. Fabrication of Microfluidic Devices Containing Patterned Microwell Arrays. *Anal. Chem.* **2012**, *84*, 1776–1780.

(2) Nie, S.; Henley, W. H.; Miller, S. E.; Zhang, H.; Mayer, K. M.; Dennis, P. J.; Oblath, E. A.; Alarie, J. P.; Wu, Y.; Oppenheim, F. G.; et al. An Automated Integrated Platform for Rapid and Sensitive Multiplexed Protein Profiling Using Human Saliva Samples. *Lab Chip* **2014**, *14*, 1087–1098.

(3) Srisa-Art, M.; Dyson, E. C.; deMello, A. J.; Edel, J. B. Monitoring of Real-Time Streptavidin-Biotin Binding Kinetics Using Droplet Microfluidics. *Anal. Chem.* **2008**, *80*, 7063–7067.

(4) Seger, R.; Krebs, E. The MAPK Signaling Cascade. *FASEB J.* **1995**, *9*, 726–735.

(5) Canagarajah, B. J.; Khokhlatchev, A.; Cobb, M. H.; Goldsmith, E. J. Activation Mechanism of the MAP Kinase ERK2 by Dual Phosphorylation. *Cell* **1997**, *90*, 859–869.

(6) Roberts, P. J.; Der, C. J. Targeting the Raf-MEK-ERK Mitogen-Activated Protein Kinase Cascade for the Treatment of Cancer. *Oncogene* **2007**, *26*, 3291–3310.

(7) Zangi, R.; Zhou, R.; Berne, B. J. Urea's Action on Hydrophobic Interactions. *J. Am. Chem. Soc.* **2009**, *131*, 1535–1541.

(8) Phospho-ERK1 (T202/Y204)/ERK2 (T185/Y187) DuoSet IC http://www.rndsystems.com/pdf/DYC1018B.pdf.

(9) Li, P.; Abolmaaty, A.; D'Amore, C.; Demming, S.; Anagnostopoulos, C.; Faghri, M. Development of an Ultrafast Quantitative Heterogeneous Immunoassay on Pre-Functionalized Poly(dimethylsiloxane) Microfluidic Chips for the next-Generation Immunosensors. *Microfluid. Nanofluidics* **2009**, *7*, 593–598.

(10) MagPlex® Microspheres http://www.luminexcorp.com/Products/ReagentsMicrospheres/MagPlex_Microspheres/ (accessed May 6, 2014).

(11) MicroPlex® Microspheres http://www.luminexcorp.com/Products/ReagentsMicrospheres/MicroPlex_Microspheres/ (accessed May 6, 2014).

(12) Bio-Rad. Bio-Plex System Bead Coupling http://www.bio-rad.com/webroot/web/pdf/lsr/literature/Bulletin_2904.pdf.

(13) Sehgal, D.; Vijay, I. A Method for the High Efficiency of Water-Soluble Carbodiimide-Mediated Amidation. *Anal. Biochem.* **1994**, *218*, 87–91.

(14) xMAP Antibody Coupling Kit User Manual http://www.luminexcorp.com/prod/groups/public/documents/lmnxcorp/89-00002-00-319.pdf.

(15) Bio-Rad. Bio-Plex Amine Coupling Kit http://www.bio-rad.com/webroot/web/pdf/WWMSDS/LSGC/USA/USA_USA_171406001.pdf (accessed May 6, 2014).

(16) Vickers, J. A.; Caulum, M. M.; Henry, C. S. Generation of Hydrophilic Poly(dimethylsiloxane) for High-Performance Microchip Electrophoresis. *Anal. Chem.* **2006**, *78*, 7446–7452.

(17) Kricka, L. J.; Wilding, P. Microchip PCR. *Anal. Bioanal. Chem.* **2003**, *377*, 820–825.

(18) Zhou, J.; Ellis, A. V.; Voelcker, N. H. Recent Developments in PDMS Surface Modification for Microfluidic Devices. *Electrophoresis* **2010**, *31*, 2–16.

(19) Sia, S. K.; Whitesides, G. M. Microfluidic Devices Fabricated in Poly(dimethylsiloxane) for Biological Studies. *Electrophoresis* **2003**, *24*, 3563–3576.

(20) Brunner, C.; Ernst, K.-H.; Hess, H.; Vogel, V. Lifetime of Biomolecules in Polymer-Based Hybrid Nanodevices. *Nanotechnology* **2004**, *15*, S540–S548.

(21) Séguin, C.; McLachlan, J. M.; Norton, P. R.; Lagugné-Labarthet, F. Surface Modification of Poly(dimethylsiloxane) for Microfluidic Assay Applications. *Appl. Surf. Sci.* **2010**, *256*, 2524–2531.

(22) Sui, G.; Wang, J.; Lee, C.-C.; Lu, W.; Lee, S. P.; Leyton, J. V; Wu, A. M.; Tseng, H.-R. Solution-Phase Surface Modification in Intact Poly(dimethylsiloxane) Microfluidic Channels. *Anal. Chem.* **2006**, *78*, 5543–5551.

(23) Edelstein, A.; Amodaj, N.; Hoover, K.; Vale, R.; Stuurman, N. Computer Control of Microscopes Using μManager. *Curr. Protoc. Mol. Biol.* **2010**, *Chapter 14*, Unit14.20.

(24) Rasband, W. S. ImageJ http://imagej.nih.gov/ij/.

(25) Healy, M. J. Outliers in Clinical Chemistry Quality-Control Schemes. *Clin. Chem.* **1979**, *25*, 675–677.

(26) Medintz, I. L.; Pons, T.; Delehanty, J. B.; Susumu, K.; Brunel, F. M.; Dawson, P. E.; Mattoussi, H. Intracellular Delivery of Quantum Dot-Protein Cargos Mediated by Cell Penetrating Peptides. *Bioconjug. Chem.* **2008**, *19*, 1785–1795.

(27) The Alexa Fluor Dye Series—Note 1.1 http://www.lifetechnologies.com/us/en/home/references/molecular-probes-the-handbook/technical-notes-and-product-highlights/the-alexa-fluor-dye-series.html.

(28) Fluorescence Quantum Yields (QY) and Lifetimes (τ) for Alexa Fluor Dyes http://www.lifetechnologies.com/us/en/home/references/molecular-probes-the-handbook/tables/fluorescence-quantum-yields-and-lifetimes-for-alexa-fluor-dyes.html.

(29) Mascini, M.; Tombelli, S. Biosensors for Biomarkers in Medical Diagnostics. *Biomarkers* **2008**, *13*, 637–657.

(30) Park, S.; Zhang, Y.; Lin, S.; Wang, T.-H.; Yang, S. Advances in Microfluidic PCR for Point-of-Care Infectious Disease Diagnostics. *Biotechnol. Adv.* **2011**, *29*, 830–839.

(31) Kusnezow, W.; Syagailo, Y. V; Rüffer, S.; Baudenstiel, N.; Gauer, C.; Hoheisel, J. D.; Wild, D.; Goychuk, I. Optimal Design of Microarray Immunoassays to Compensate for Kinetic Limitations: Theory and Experiment. *Mol. Cell. Proteomics* **2006**, *5*, 1681–1696.

(32) Berg, O.; Hippel, P. von. Diffusion-Controlled Macromolecular Interactions. *Annu. Rev. Biophys. Biophys. Chem.* **1985**, *14*, 131–158.

(33) Trier, N. H.; Hansen, P. R.; Houen, G. Production and Characterization of Peptide Antibodies. *Methods* **2012**, *56*, 136–144.

(34) Wians, F. H. Clinical Laboratory Tests: Which, Why, and What Do The Results Mean? *Lab. Med.* **2009**, *40*, 105–113.

CHAPTER 3

INVESTIGATING SOURCES OF ERROR IN MICROBEAD ARRAY ASSAYS

3.1 Introduction

This chapter covers efforts to reduce the array-to-array variance in the assay signal to less than 10% relative standard deviation (%RSD), as most accepted clinical assays meet or exceed this level of precision.[1] The high standard deviations shown by the microbead array assays negatively impacts their ability to distinguish between different pERK1/2:ERK1/2 ratios. While the development of a pERK1/2:ERK1/2 assay is the goal, experiments in this chapter primarily used vascular endothelial growth factor (VEGF) as a model analyte in place of ERK1/2. This was done because an optimized assay for VEGF had previously been developed, it is easier to work with than ERK1/2, and the principles being explored apply to any analyte that might be assayed by the microbead array chips.

Major determinants of sandwich immunoassay sensitivity include the antibodies' affinity for their target epitopes,[2] instrumental noise, the signal of the blank, non-specific binding of reagent or analyte proteins to the beads,[3] and mass transport rates throughout the chips.[4,5] Some of these factors, such as instrumental noise and non-specific binding, are expected to be constant from chip to chip. This is because the same equipment and software are used for all experiments, and the chips were fabricated from the same materials and passivated with the same buffers prior to use. These factors were thus hypothesized to not be significant contributors to the high variance.

Mass transport rates were one candidate due to the possibility of varied flow rates from

chip to chip. This may be caused by differences in sample volume, or by fabrication issues leading to differences in channel properties. While antibody affinity should nominally be the same from chip to chip due to the same bead stock and reagents being used in all experiments, the possibility that capture antibody affinity varied significantly from array to array was another candidate cause of the variance. This may stem from the bead surfaces – either the beads themselves or the bound antibodies – being damaged by the mechanical loading process. The mechanical loading process involves pressing PDMS, a hydrophobic material, onto hydrophobic polystyrene beads coated with monoclonal antibodies. As more than 90% of monoclonal antibody activity can be lost due to denaturation when passively adsorbed onto a hydrophobic surface,[6,7] it is possible that higher losses occur during the repeated hydrophobic contact from loading. Differences in the contact time with the PDMS experienced by beads may lead to varied abilities to capture analyte molecules, and thus, differences in their fluorescent signal.

To explore the contribution of mass transfer rates to the high variance, two types of experiments were run. In the first, a chip featuring four arrays that share common reagent and waste/vacuum vias was designed (Figure 3.1). These chips were symmetrical relative to both the vias and the arrays, thus ensuring equalized reagent flux through all channels. The use of an internal standard to account for differences in sample delivery to the beads[8] was also investigated. At the same time, to speed up data analysis times and experimental throughput, chips featuring 100-bead arrays instead of 1,024-bead arrays were used for some experiments.

To systematically test whether any particular reagent incubation step was the cause of the variance, incubations were performed by using a vortexer to suspend the beads in solution. This ensured uniform delivery of reagent to the bead surfaces, and as the Walt group at Tufts has performed highly sensitive immunoassays involving suspension incubations,[9,10] the possibility of

high variance stemming from this incubation technique was not a concern. While initial experiments in this vein imaged the beads after loading them into arrays, chip designs that did not require mechanical loading were used to assess the assay's performance in the absence of potentially harsh loading conditions. Finally, experiments were run with the single-array chips in which the extent and type of mechanical manipulation of the beads during their loading was quantified.

3.2 Materials and methods

3.2.1 Materials and reagents

Sylgard 184 PDMS was purchased from Ellsworth Adhesives (Germantown, WI) and prepared at a 10:1 elastomer/cross-linker ratio. Tween-20 and MagPlex Luminex beads were purchased from Bio-Rad Laboratories (Hercules, CA). Non-magnetic Luminex beads were purchase from Luminex (Austin, TX). Purified recombinant human vascular endothelial growth factor (VEGF), phosphorylated and non-phosphorylated extracellular signal-related kinase 2 (pERK2 and nERK2), biotinylated detection antibodies for VEGF, pERK1/2, and ERK2, capture antibodies for pERK1/2, VEGF, and a control capture antibody were purchased from R&D Systems (Minneapolis, MN). All proteins and antibodies were reconstituted according to the manufacturer's instructions. Glass photolithography substrates (4" x 4" B270, 5" x 5" soda lime) were purchased from Telic Corp. (Valencia, CA). Nano-Strip was purchased from KMG Chemicals (Fremont, CA). Octyltrichlorosilane, sodium fluoride, ethylene diamine tetraacetic acid (EDTA), urea, and Triton X-100 were purchased from Sigma-Aldrich (St. Louis, MO). AZ-400K (3:1 developer) was purchased from AZ Electronic Materials USA (Somerville, NJ). Chromium etchant 1020 and 10:1 buffered oxide etch (BOE) were purchased from Transene Co. Inc. (Danvers, MA). Acetone, 10x phosphate-buffered saline (PBS, pH = 7.4), 10% bovine

serum albumin (BSA) in PBS, optically clear polypropylene plate-sealing tape (PCR tape), Contrad 70 detergent and microscope slides (75 mm x 25 mm x 0.99 mm) were purchased from Thermo Fisher Scientific (Waltham, MA). Shipley S1813 photoresist (S1813), MF-319 photoresist developer, KMPR 1010 photoresist, and SU-8 thinner were purchased from MicroChem Corp. (Newton, MA); the SU-8 thinner was mixed with KMPR 1010 to prepare 35% (w/w) KMPR solutions. P-type 6" crystalline Si wafers were purchased from University Wafer (Boston, MA). Streptavidin-B-phycoerythrin (SA-PE) was purchased from Invitrogen (Carlsbad, CA).

All aqueous solutions were prepared with deionized (DI) water from a NANOpure Diamond system (Barnstead International, Dubuque, IA), including PBS-T (PBS + 0.05% Tween-20), PBS-BB (PBS + 1% BSA), ERK diluent (PBS + 5 mM sodium fluoride + 1 mM EDTA + 0.5% Triton X-100), and ERK buffer (ERK diluent + 1 M urea).

3.2.2 Fabrication of multi-array chips and 100-bead arrays

The experiment in Section 3.3.1 used a multi-array chip (Figure 3.1) in place of the single-array chip. The multi-array mask was designed for use with the 1,024-bead array mask used in Chapter 2. Later experiments used the single-array, 8-channel chips from Chapter 2 with 100-bead arrays in place of the 1,024-bead arrays.

Designs for the multi-array chips and 100-bead arrays were produced in TurboCAD Professional 14. Two masks were created, one featuring the multi-array channels and the other featuring the 100-bead arrays. A laser writer system (DWL 66FS; Heidelberg Instruments, Heidelberg, Germany) was used to pattern the designs into 5" x 5" glass substrates pre-coated with chromium (120 nm thick) and positive photoresist (AZ1815, 530 nm thick). The substrate was developed for 45 s in AZ-400K to remove the photoresist and then immersed in chromium

etchant for 3 min to remove the exposed chromium. The remaining photoresist was stripped with acetone and residual resist was removed with Nano-Strip. DI water and nitrogen were used to rinse and dry the masks in between each wet chemistry step.

The photolithography, DRIE, and silanization procedures described in Chapter 2 were used to prepare silicon master wafers for both the multi-array chips and 100-bead chips. The arrays were etched to a depth of approximately 5 μm and the channels were etched to a depth of approximately 20 μm. PDMS chips were fabricated from the master molds, punched and bonded to microscope slides, and loaded with magnetic analyte and control beads.

3.2.3 Fabrication of simple column chips

In Section 3.3.5, chips consisting of straight channels with weirs (referred to as simple column chips) were used to assess assay performance without having to mechanically load the beads into arrays. Beads were pulled into the chips through the inlet via and packed against the weirs. The channels were 70 μm wide, 4.1 cm long, spaced 560 μm apart, and shared common bead/buffer and waste/vacuum vias. A top-down schematic of the chips is shown in Figure 3.2 and a side view schematic is shown in Figure 3.3. An ultraviolet photoexposure system (OAI, San Jose, CA) was used to pattern each quadrant of a 4" x 4" B270 glass substrate coated with chromium and positive photoresist to create a negative master of the chip design. The resist was developed in AZ-400K for 45 s. Exposed chromium was removed with chromium etchant for 3 min and the remaining photoresist was stripped with acetone. The exposed glass was etched to a depth of 6 μm with 10:1 buffered oxide etch. The weir was fabricated by coating the desired location for the weir with S1813 photoresist, then baking the substrate at 95 °C for 30 min. This resist protected the glass underneath from subsequent etching and thus fixed the depth at 6 μm. Etching was resumed until the channels were 9 μm deep. The S1813 was stripped with acetone

and all remaining chromium was stripped with chromium etchant. The substrate was rinsed with DI water and nitrogen between each of the above steps, and its depth was determined with profilometry (P-15; KLA-Tencor, San Jose, CA)

A dicer (Basic Dicer II, Dicing Technologies) was used to dice the 4" x 4" substrate into four 2" x 2" glass masters, each of which contained two 5-channel chips. Prior to dicing, the substrate features were coated with S1813 and baked for 30 min at 95 ºC to protect the channels. The S1813 was stripped with acetone following dicing. The diced masters were treated in an 18-W oxygen plasma for 12 s (PDC-32G; Harrick Plasma) and placed face-up in a vacuum desiccator with 500 µL of octyltrichlorosilane. Vacuum was applied for approximately 3 min to fill it with silane vapor, and then it was sealed and left to react for 30 min. This process covalently coated the masters with the silane and reduced PDMS adhesion to the masters.

Complementary molds were prepared from the masters by placing them face-up in 3" x 3" x 1" rectangular acrylic containers and filling the containers with 10:1 PDMS to a depth of approximately 1 cm. The PDMS in the container was degassed under vacuum for approximately 20 min in a vacuum desiccator, then baked at 95 ºC for 30 min to cure the PDMS. The mold was allowed to cool after curing, and a razor was then used to cut the molds from the containers and the masters from the molds. The razor was used to trim excess PDMS from the edges of the molds as well. The molds were then silanized in the same way as the glass masters.

To fabricate the chips, ~4 mL PDMS was poured over the faces of the molds and degassed under vacuum. The mold faces were sealed with a 2" x 2" glass slide to exclude excess PDMS and ensure uniform chip thickness, then baked at 95 °C for 20 min. The PDMS chips were removed from the molds and excess PDMS was cut from the edges with a razor blade. Reagent/bead inlets and waste outlets were created with a 3-mm biopsy punch (Sklar

Instruments). The prepared PDMS chips were bonded to glass microscope slides after plasma treatment.

3.2.4 Fabrication of stage-weir chips

The chips used in Section 3.3.6 (referred to as stage-weir chips due to their features) are similar to the simple column chips, but feature a shallower zone prior to the weir for imaging the beads in the same focal plane (Figure 3.4). They were fabricated in the same way as the simple column chips with one modification. After the weir was fabricated, chips were etched to either 6.7 µm, 7.25 µm, or 7.8 µm depths. A region immediately before the weir was coated with S1813 and baked to prevent its etching. This formed the viewing stage. After coating the area of the stage with resist, the chips were etched to a 12 µm total depth.

3.2.5 Assay procedures

All experiments in this chapter with array chips followed the long assay protocol described in Chapter 2 unless otherwise noted. Off-chip incubations were conducted by incubating the beads with reagents in 500-µL microcentrifuge tubes (Eppendorf, Hauppauge, New York). An MS3 Basic Mixer (Fisher Scientific) was utilized to suspend the beads in solution at 3000 rpm during each incubation. Incubations were performed at room temperature. 1 µL of a 1:1 mixture of stock VEGF and control beads was incubated in 100 µL of reagent; this amounted to approximately 6,250 of each bead type. Washing in the tubes was performed by using a rare-earth magnet to pull the magnetic beads to the bottom of the tube, removing the supernatant, pipetting in 100 µL of PBS-T, and resuspending the beads via vortex.

PBS-BB (PBS + 1% BSA) was used to passivate chips and prepare assay solutions, except for the samples in the internal standard experiment in Section 3.3.2, which were prepared in ERK buffer. PBS-T (PBS + 0.05% Tween-20) was used to wash the chips in between assay

steps. Unless otherwise specified, the dAb concentration was 3 µg/mL and the SA-PE concentration was 2 µg/mL.

3.2.6 Improved data analysis procedure

All data to this point was analyzed as described in Chapter 2; fluorescence values from the raw data that were not within 2.2 standard deviations of the mean were rejected, and the recalculated mean was used as the fluorescence value for the signal. As extreme outliers can inflate the standard deviation such that other true outliers are not rejected, an improved method of analysis was instituted beginning with the off-chip incubation experiments in Section 3.3.3. Rather than perform a single correction cycle involving the rejection of outliers and recalculation of the mean and standard deviation, multiple correction cycles are performed in which the standard deviation and mean from the previous cycle are used to detect and reject outliers in the next. This process is repeated until no further outliers are removable.[11] This eliminates extreme anomalies and true outliers in order to produce a more accurate estimate of the mean.

3.3 Results and discussion

3.3.1 Assay with multi-array chips

Heterogeneity in flow conditions from chip-to-chip in terms of the flow rate or reagent concentration was the first potential cause of the high variance to be explored. This issue may stem from differential evaporation of reagent droplets during incubations, which would change the reagent concentration differently from chip to chip. Mass transfer is also a major determinant of antibody-antigen binding kinetics[4,5] and heterogeneities here may be the result of differences in sample volume from chip-to-chip. Experiments using the multi-array chips (Figure 3.1) with their symmetrical nature coupled with laminar flow conditions in microfluidic channels ensures that the reagent flux would be identical through each channel and across each array. If the

experimental variance did not improve, fluid flow heterogeneities would be ruled out as a cause of the variance.

VEGF assays were performed with the multi-array chips using samples containing 0, 10, 100, and 1000 pg/mL VEGF in PBS-BB. Results from these chips were inferior to those from single-array chips; the %RSDs were no lower than ~21% and as high as ~45%, and the signal was lower than was usually seen for these concentrations of VEGF. The fact that the assay variance remained high in spite of uniform flow conditions in all the arrays refuted the hypothesis that heterogeneity in fluid flow was a contributor to the high variance problem.

3.3.2 Assay with internal standard

A technique commonly used in chromatography to account for irreproducible injection volumes is the inclusion of an internal standard. An internal standard consists of a known amount of a compound different from the analyte added to a sample. The signal from the analyte (A) is compared to the signal from the standard (S) to adjust for differences in the quantity of solution that are analyzed from experiment to experiment.[8]

$$\frac{Concentration\ ratio\left(\frac{A}{S}\right)\ in\ unknown}{Concentration\ ratio\ in\ standard} = \frac{Signal\ ratio\left(\frac{A}{S}\right)\ in\ unknown}{Signal\ ratio\ in\ standard} \quad (3.1)$$

The possibility of using an internal standard was explored as a way to account for the high variance. For the microbead array experiments, an internal standard could potentially account for differences in the amount of reagent reaching the arrays. For example, in a multiplexed internal standard experiment with both VEGF and ERK1/2 beads, a constant concentration of VEGF would be used along with varying concentrations of ERK1/2 so that the ERK1/2 signal could be normalized to the VEGF signal. If successful, this would be a way of working around the high variance without having to determine the exact cause of the variance. This strategy requires the VEGF assay to be compatible with the ERK1/2 assay in terms of both

multiplexing and buffers. If cross-reaction between antibodies occurs, then a multiplexed assay would not be feasible. The VEGF antibodies must also be compatible with the denaturing ERK buffer. Finally, this strategy requires the VEGF signal to correlate with the ERK1/2 signal in each sample; if it does not, then the ERK1/2 signal cannot be normalized to the VEGF signal.

Sample solutions containing varying concentrations of pERK2 and a constant 1 ng/mL level of VEGF were prepared in ERK buffer. These solutions were assayed in single-array 100-bead chips. The dAb solution contained 3 µg/mL pERK1/2 dAb and 3 µg/mL VEGF dAb. The results (Figure 3.5) depict the pERK2:VEGF signal ratios as a function of the pERK2 concentration. A random scatter of points at each pERK2 concentration is apparent, whereas a plot that satisfied all the conditions for an internal standard assay (including a correlation between the pERK2 and VEGF signals) would be linear. These results indicate that VEGF is not suitable as an internal standard in conjunction with ERK1/2 assays. They also suggest that internal standards in general might be unfeasible for these assays.

3.3.3 Off-chip incubations to isolate error sources

A series of experiments was undertaken designed to isolate each aspect of the assay so its contribution to the variance could be assessed systematically. In these experiments, sample incubations were performed in microcentrifuge tubes to ensure that the beads were exposed to a uniform amount of reagent. The high number of bead-molecule collisions should also led to high amounts of analyte capture.[4,5] Two initial experiments followed the same general format using VEGF and control beads. In the first, the concentration of VEGF was varied at constant concentrations of dAb and SA-PE, while in the second, the concentrations of VEGF and SA-PE were constant while that of the dAb was varied. In both, the sample was incubated for 2 h, the dAb for 45 min, and the beads were washed twice between incubation steps. The 20-min SA-PE

incubation took place after loading the beads into 100-bead array chips filled with PBS-BB. After pulling PBS-BB through the channels via vacuum to remove all SA-PE solution, the arrays were imaged. Four arrays were used per concentration.

The assay %RSDs did not improve for either experiment. In the experiments with varied VEGF concentrations, %RSDs ranged from ~21% to ~117%. The experiments with varied dAb concentrations yielded %RSDs from ~21% to ~57%. As the %RSDs were not affected by performing the sample and dAb incubations off-chip, these were ruled out as sources of the high variance.

3.3.4 Assay with off-chip dye incubation

This left two major candidates as the high variance causes: the dye incubation step and the process of mechanically loading the beads into the arrays. Like the previous experiments with the sample and antibody incubations, the dye incubation was taken off-chip to assess its role. The VEGF and detection antibody incubations were performed as in the previous section with a constant concentration of 500 pg/mL VEGF and 1 µg/mL dAb. SA-PE was incubated for 30 min on the mixer at concentrations ranging up to 2 µg/mL and the beads were washed twice. The beads were imaged after loading them into arrays. While the %RSDs at one concentration was ~6%, all other concentrations had %RSDs ranging from ~17% to ~49%. This ruled out the fluorescent dye incubation as the cause of the variance.

Two subsequent experiments looked at the variance from these fully off-chip experiments on a larger scale by loading the beads into more than the typical 4 arrays. VEGF and control beads (2.5 µL each from bead stock) were incubated in a tube with 500 µL VEGF at 500 pg/mL. dAb and SA-PE concentrations were a constant 1 µg/mL and 0.8 µg/mL, respectively. The beads were incubated in a single tube prior to loading them into arrays for imaging.

In the first of these two experiments, the beads were loaded into twenty 100-bead arrays for imaging. The data showed a high interarray variance of ~67%. The intraarray (bead-to-bead) variance was high as well. This is illustrated in Figure 3.6, where the locations of all the assay beads in an array are circled in red (Figure 3.6A), and in Figure 3.6B, the five brightest beads in that array remain circled in red while the five dimmest are circled in yellow. The figure shows that some beads are very bright, others show almost no fluorescence, and many others contain both bright and dark spots. This suggested that either the bead surface chemistry differs strongly from bead to bead – because given the high reagent concentration, all beads should show similar fluorescence if uniformly coated with antibodies – or some beads are being damaged while others are not.

To examine the intrabead signals on a larger scale than the 100-bead arrays, the experiment was repeated with the beads loaded into eight 1,024-bead arrays for imaging. The interarray fluorescence %RSD was ~48%, and the distribution of bead brightness was also similar, but the large arrays revealed a phenomenon that was hidden in the smaller 100-bead ones: the majority of the bright beads lie in the lower half of the array (Figure 3.7). Because of the array size and the number of beads loaded, it is almost impossible for all the bright beads to selectively load into a single band, especially in eight separate arrays. It was noticed that the beads in the upper half of the arrays tended to load before the beads in the lower half. This suggested that the mechanical loading process was adversely affecting either the beads or the antibodies/complexes on the early loading beads.

These experiments differed from prior ones in that the beads were loaded after reacting with the antigen, dAb, and fluorescent dye, not before. As the capture antibodies are covalently bound to the beads while the antigen-antibody-dye complex is held together through weaker

noncovalent interactions, it is possible that the post-assay bead surfaces are vulnerable to mechanical damage while the pre-assay beads are not. In order to determine whether the mechanical damage hypothesis applies to post-loading, pre-assay beads, a means of loading the beads without using physical force was developed.

3.3.5 Assays with simple column chips

In order to image the beads without their having had physical contact with PDMS, straight-channel chips were fabricated with weirs that are impassible to the beads (Figure 3.3). With this chip design, beads were incubated with sample, antibody, and dye in the mixer and then packed into the chip columns against the weirs and imaged.

VEGF assays were run in tubes with 500 pg/mL VEGF, 1 µg/mL anti-VEGF dAb, and 0.8 µg/mL SA-PE. After the final wash step, the beads were pipetted into the inlet via of the column chips and packed on-chip. They were then imaged. Sample images from one of these chips are shown in Figure 3.8. Not only is the VEGF signal obtained more than threefold higher than it was in array chips for this concentration, but the %RSD in signal from column to column is just ~3.5%. This constitutes strong evidence that the bead immunoassays work well when not mechanically loaded.

3.3.6 Assays with stage-weir chips

An improved type of column chip was fabricated for further studies with non-microwell bead loaded assays. As the channels in the previous chip design are several µm deeper than the bead diameter, some beads pack into the columns out of focus. This can significantly alter their apparent signal. Stage-weir chips (Figure 3.4) were made to eliminate this focus issue. These feature a zone immediately before the weir that is slightly deeper than the diameter of the beads forcing the beads into a monolayer on the same focal plane.

The assay described in the previous section was repeated and the assayed beads were loaded into stage-weir chips. Immediately before introducing the beads to the chips, non-fluorescent, non-magnetic Luminex beads were mixed with the assay beads. These beads served as spacers to spread out the assay beads in the column and help prevent overlap of their signals. Example images from one of these chips are shown in Figure 3.9. At the same time, another set of 6.7-µm chips were pressed several times with the mechanical loading wand to simulate the microarray loading process. The results shown in Figure 3.10 indicate that the vast improvements in signal and variance seen in the simple channel-weir chip were not a fluke; the %RSDs across the three different viewing stage sizes ranged from ~6% to 10.42%, while the chips that were pressed lost almost all their fluorescence. Figure 3.11 shows example fluorescence images comparing the unpressed (Figure 3.11A) and pressed (Figure 3.11B) 6.7-µm stage-weir chips. It is evident that the chips that were pressed with the wand lost almost all their fluorescence. Their signal %RSDs were also over 138%. This corroborates the notion that the loading process is mechanically damaging the bead surfaces.

One final experiment was run with the stage-weir chips to show that the low %RSDs from these chips were reproducible from experiment to experiment. VEGF samples at 500 pg/mL were prepared in four separate tubes from four separate stock solutions and assayed. The beads were loaded into the stage-weir chips with the 7.8-µm stage, as the best results were achieved with them. The results shown in Figure 3.12 show low variance, indicating reproducible results from experiment to experiment. The %RSDs for each sample ranged from less than 1% to just over 5%, and the aggregate %RSD for all samples was ~6%.

3.3.7 Mechanical damage assays

The stage-weir experiments showed that if the beads are mechanically pressed after

sample, detection antibody, and dye incubations, a considerable loss in fluorescence signal is seen. At this point, the bead surfaces are coated with a non-covalent complex in the form of the antibody sandwich and streptavidin-biotin bond between the antibody and dye. This differs from the initial array assays described in Chapter 2 in that the loaded array beads were coated solely with covalently-bound surface antibodies before anything else was introduced to them. Covalent bonds would be harder to disrupt than non-covalent ones. These experiments explored whether this mechanical damage did indeed carry over to the array beads during loading, and if so, whether the damage could be quantified.

Two major types of motions were used when loading chips and are referred to as presses and grinds. Presses involved simple up-and-down motions with a thumb or the bead-loading magnetic wand. Grinds involved pressing on the array with the wand and rotating it. As beads were pulled over the arrays, they were subjected to these motions until 90% or higher bead loading; the number of presses and/or grinds required was not recorded. For the purposes of being quantitative, pressing was defined as strictly up-and-down motions on the arrays, while grinds involved a single press and 90-degree rotation of the wand. Two sets of 1,024-bead array chips were loaded with VEGF and control beads according to these loading definitions, and either pressing or grinding was used to evaluate the effect of each type of loading motion independently. The number of presses or grinds was counted. The chips were filled with PBS-BB, sealed, and left to block for at least 24 h at 4 °C. They were then assayed according to the long format assay from Chapter 2 with 500 pg/mL VEGF as the sample.

The results from the first chip set are shown in Figure 3.13. It is evident that there is an indirect relationship between the number of presses and grinds and the amount of fluorescence obtained from the beads. Grinds also appear to be more damaging than presses, with only 5

grinds being comparable to 30 presses in this regard. The second chip set (Figure 3.14) showed similar results; signal steadily decreased as the number of presses or grinds increased, with 15-20 grinds almost completely eliminating the signal altogether. The %RSDs are high in all cases.

3.4 Conclusions

In this chapter, sources of error leading to unacceptably high assay %RSDs were explored and eventually traced to the process of mechanically loading the beads into the arrays. While the mechanical damage assays showed that loading with very few movements minimized the bead damage, an extremely concentrated bead slurry would be necessary to rapidly load the arrays. This is not practical due to the number of beads lost in this process and the associated costs. Further development of the pERK1/2:ERK1/2 assay could therefore follow two diverging paths. The arrays would either be kept and a gentler means of loading the chips would need to be developed, or an alternate chip design that did not require mechanical loading would be employed.

3.5 Figures

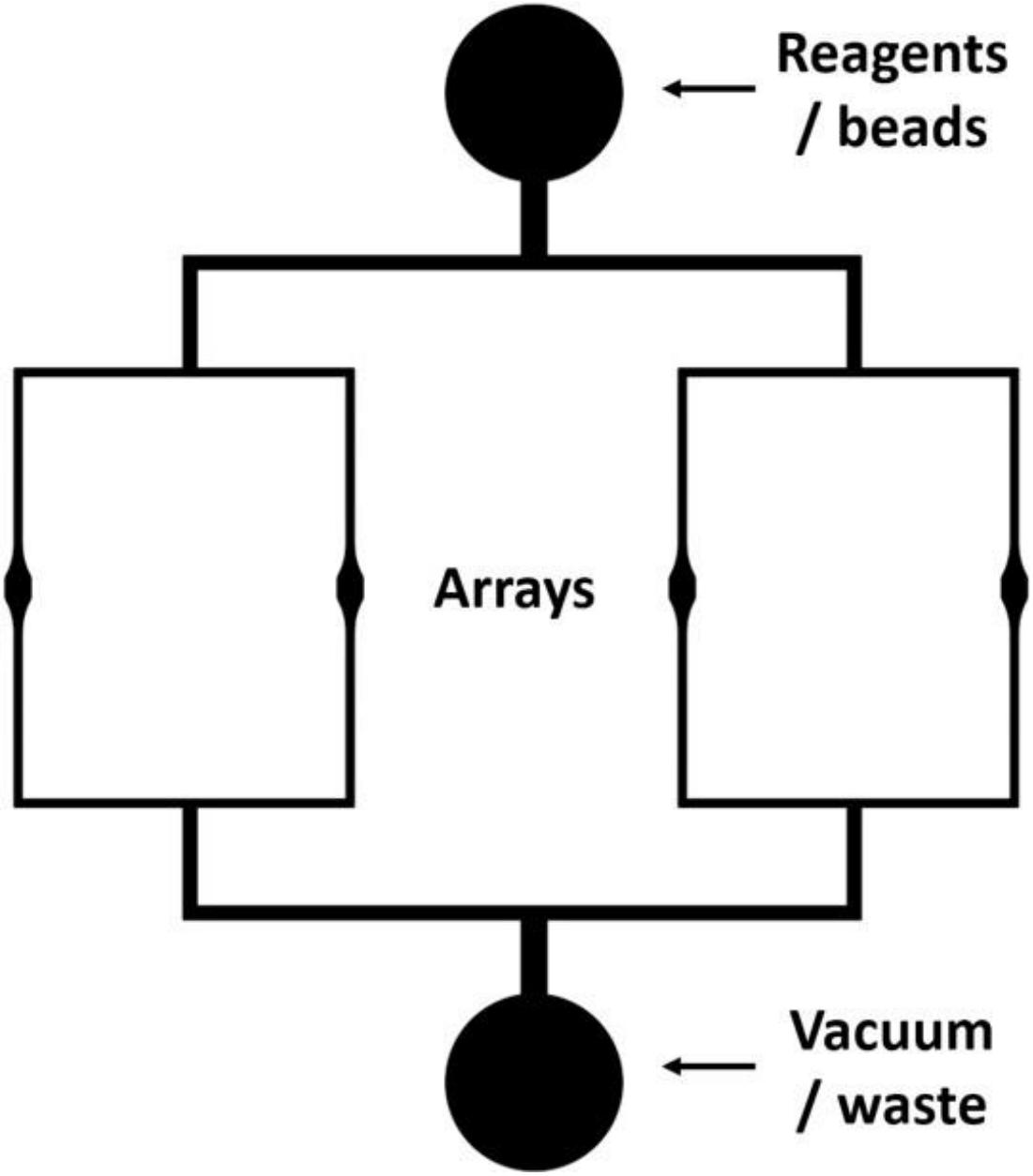

Figure 3.1. Schematic of a multi-array chip. One via is used for reagents and bead delivery, while a second is used for waste and vacuum. Four 1,024-bead arrays are located in the center of the chip.

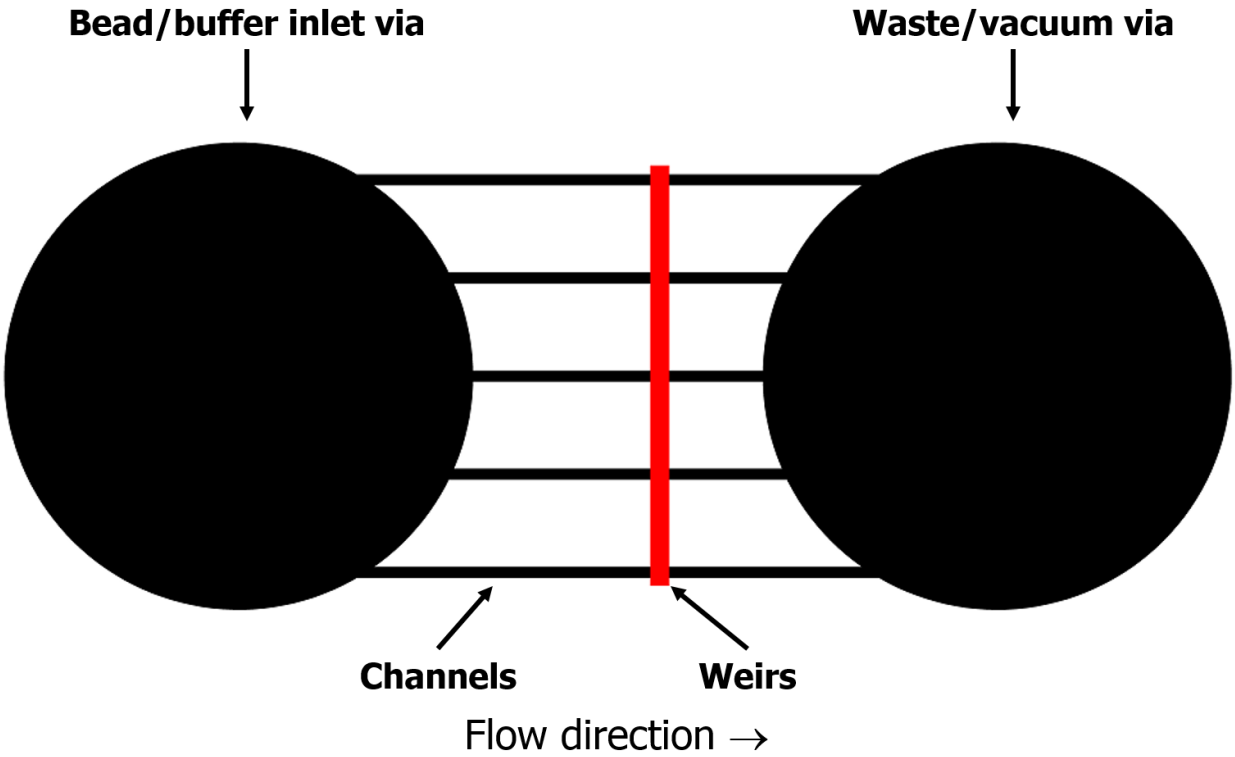

Figure 3.2. Top-down schematic of simple column chip. Five channels share common vias. Beads and buffer are introduced to the chip through the left via. Beads are packed against the weirs by applying vacuum through the right via. The vias (3 mm diameter) and channels (70 µm width, 560 µm spacing, 4.1 cm length) are to scale but the weir locations are approximate.

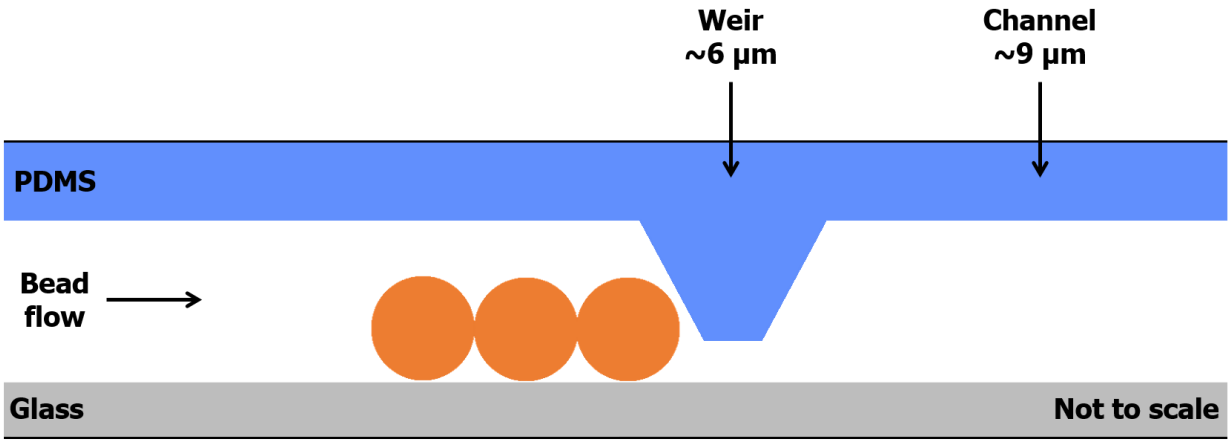

Figure 3.3. Cutaway schematic of a simple column chip. The channels are 9 µm deep. Beads (6.5-µm) are packed against a 6-µm weir. The microscope objective during imaging is located under the beads.

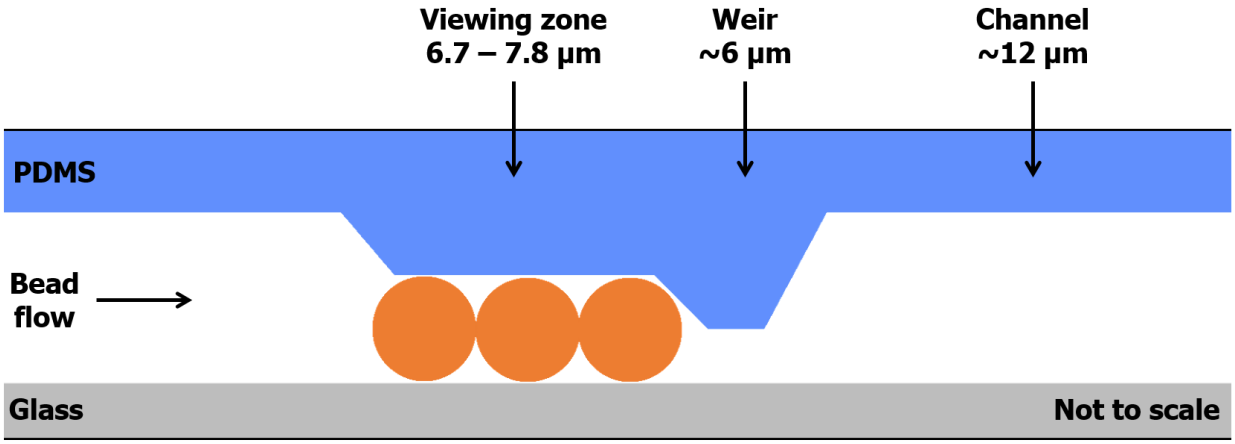

Figure 3.4. Schematic of stage-weir chips showing beads in the viewing zone (either 6.7, 7.2, or 7.8 µm deep) packed against a 6-µm weir. Due to the spatial constraints of the viewing zone, the beads are in more uniform focus than they are in the simple column chips. The channel depth is otherwise 12 µm.

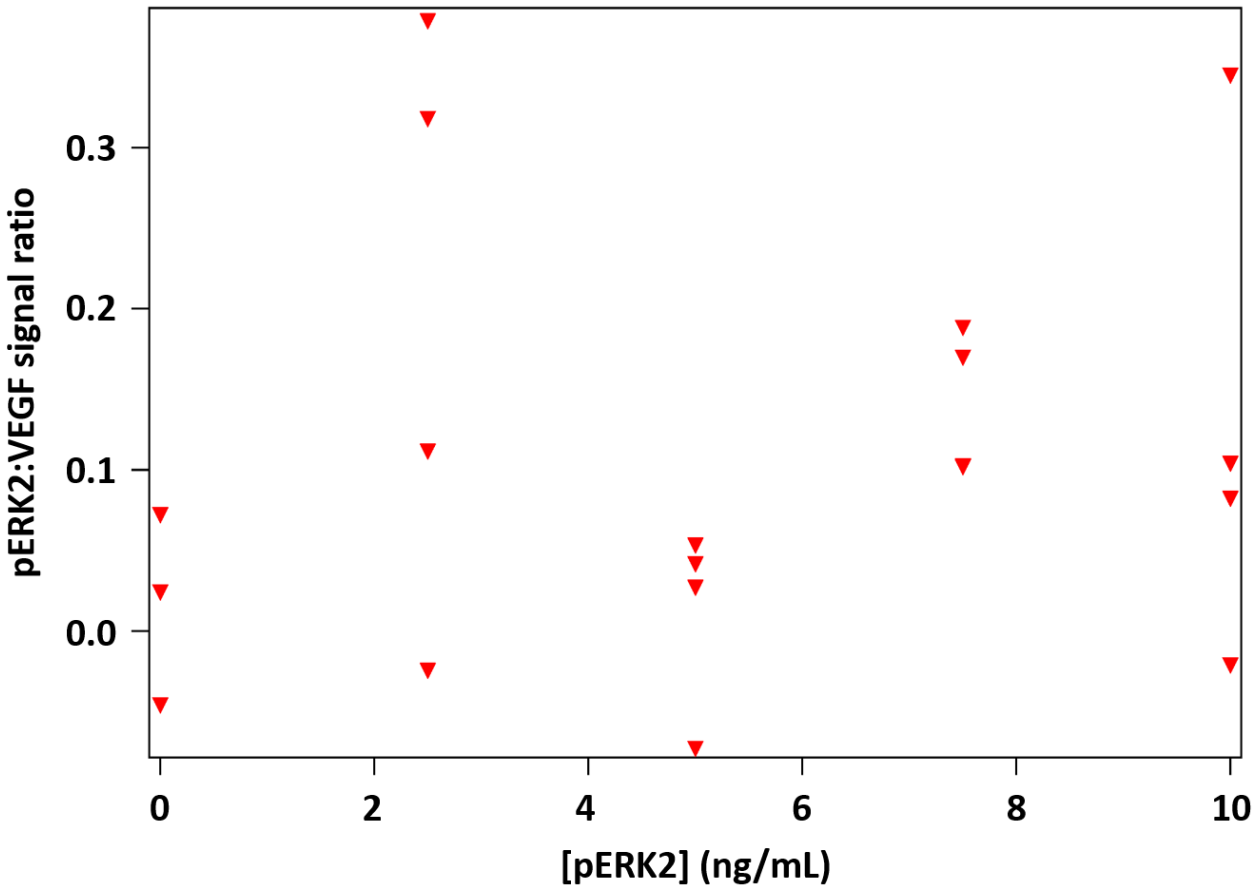

Figure 3.5. pERK2:VEGF signal ratio with pERK2 concentration using VEGF as an internal standard. While VEGF and its antibodies are compatible with the denaturing ERK1/2 buffer, the VEGF signal is not a function of the pERK2 signal at any concentration of pERK2 and thus not suitable as an internal standard.

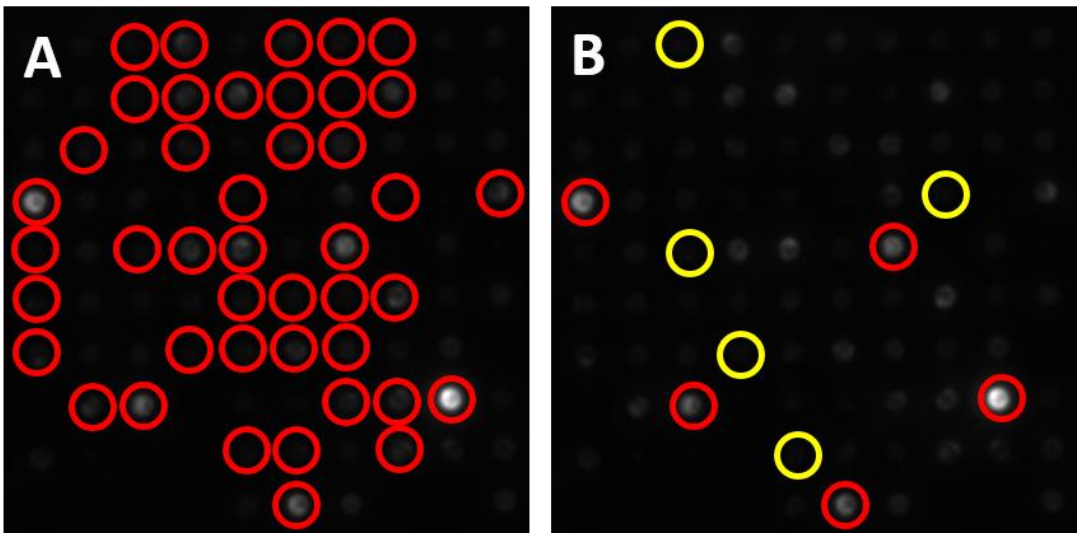

Figure 3.6. Assay images of a 100-bead array from large-scale variance experiment. Both arrays are the same, but the red circles in (A) indicate the location of every VEGF bead in (B). Other locations in the array contain control beads or are unloaded. In (B), the brightest five VEGF beads remain circled in red while five of the dimmest beads are circled in yellow. It can be seen here that some beads are considerably brighter than others, while some show almost no fluorescence whatsoever.

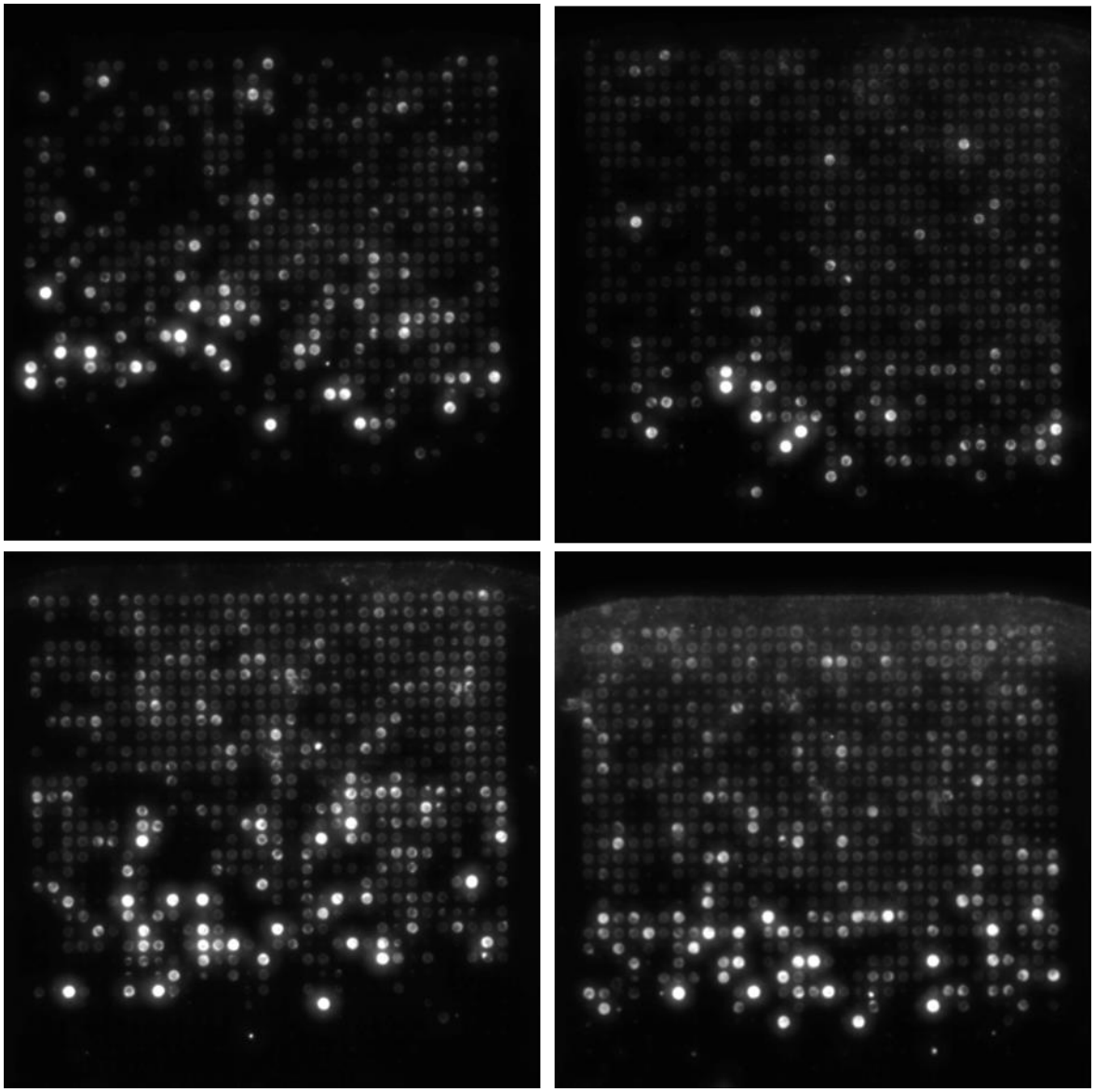

Figure 3.7. Fluorescence images of four 1,024-bead arrays after VEGF sandwich immunoassays showing "bright zones." Almost all of the high-fluorescence beads are located on the bottom half of the array.

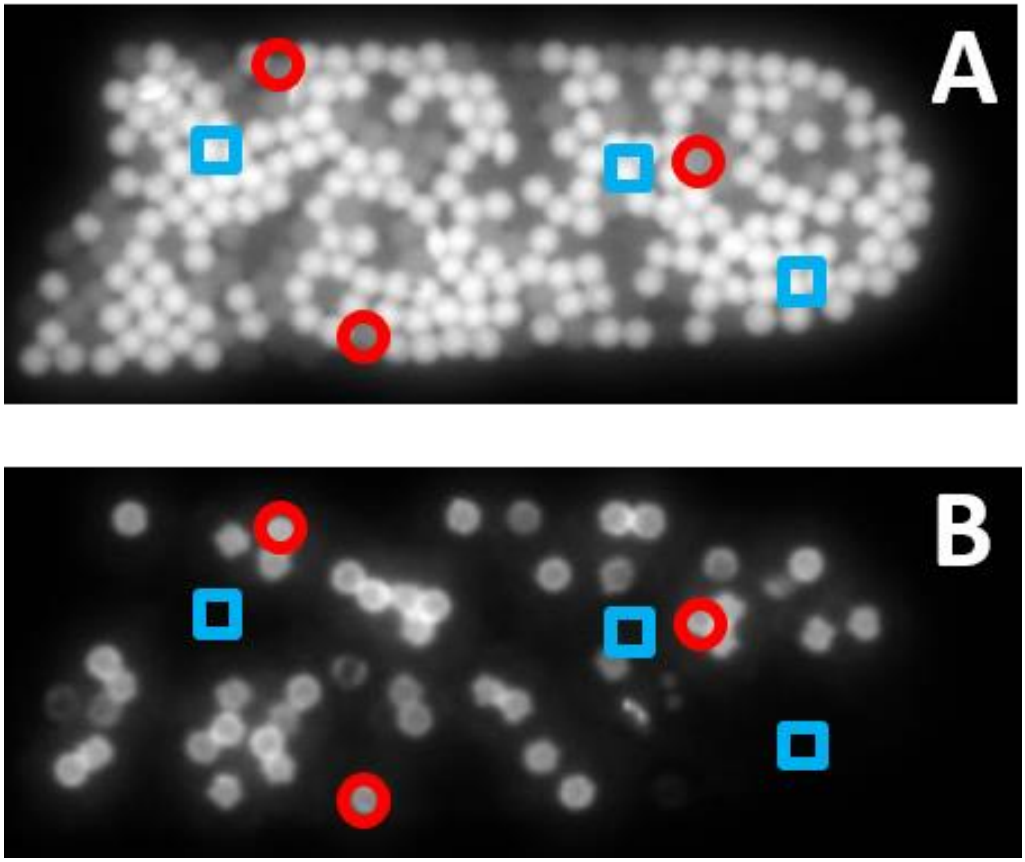

Figure 3.8. (A) Encoding image and (B) fluorescence assay image from simple column chip. The bright beads in the top image are control beads while the dimmer ones are VEGF beads. Three example control beads and VEGF beads are indicated by blue boxes and red circles, respectively, in each image. The weir is located on the right side of the above images.

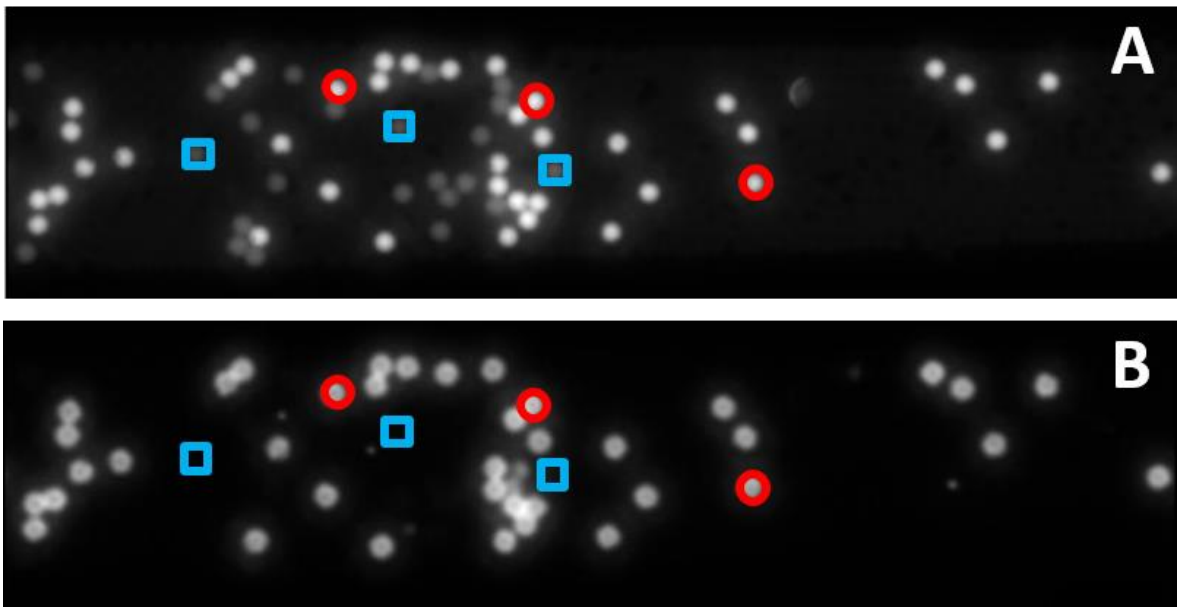

Figure 3.9. (A) Encoding image and (B) fluorescence assay image from stage-weir chip assay. Three control beads are enclosed in blue boxes and three assay beads in red circles for comparison. The beads in the stage-weir chips showed far less variance and far greater signal than those in the array chips. Assay and control beads are spaced apart by non-fluorescent, non-functionalized beads in order to mitigate signal overlap from neighboring beads.

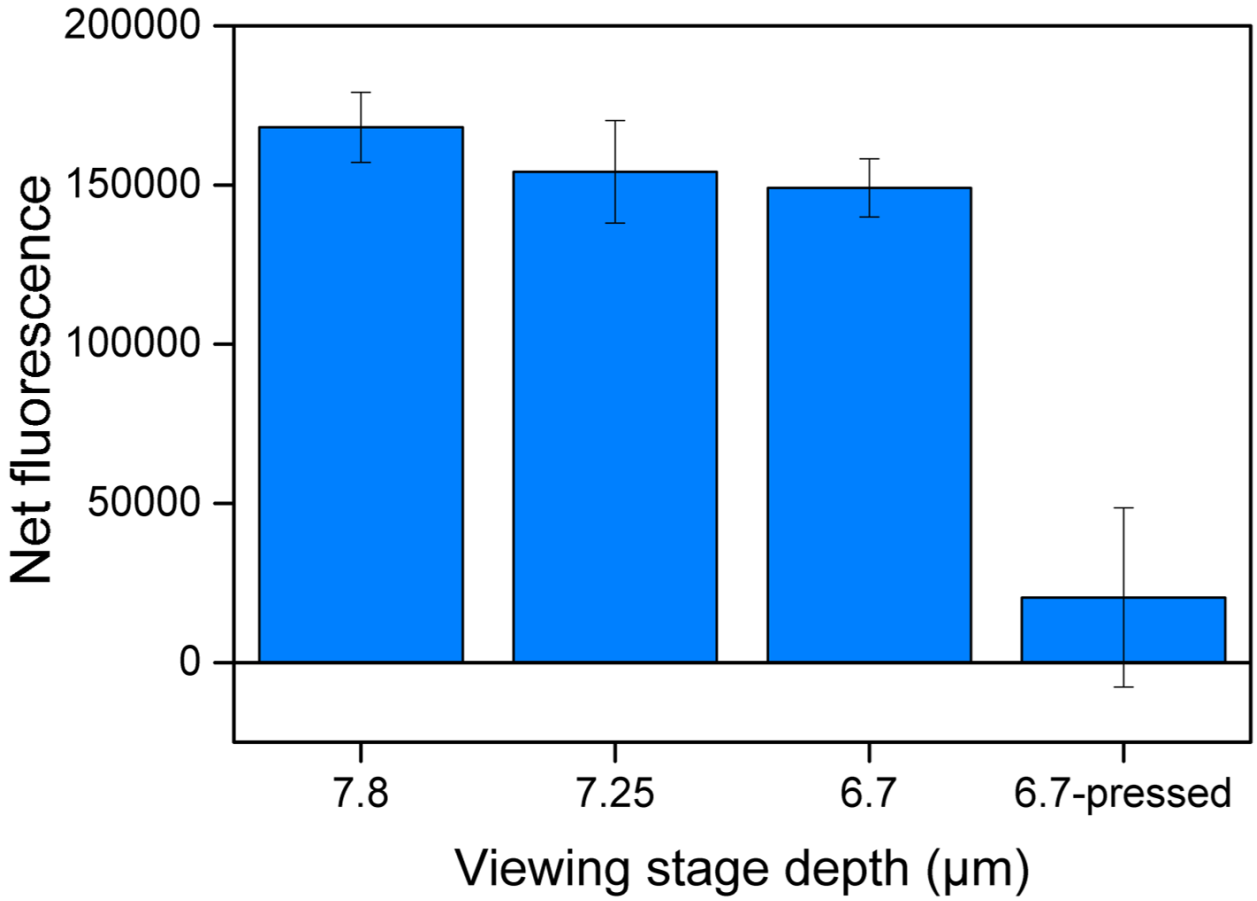

Figure 3.10. Fluorescence signal with viewing stage depths of three stage weir chips, plus one additional 6.7-µm set that had been pressed upon by the wand. The 7.8-µm chips perform best, while almost all fluorescence in the mashed channels was lost. The %RSDs (left to right) were 6.53%, 10.42%, 6.15%, and 137.74%.

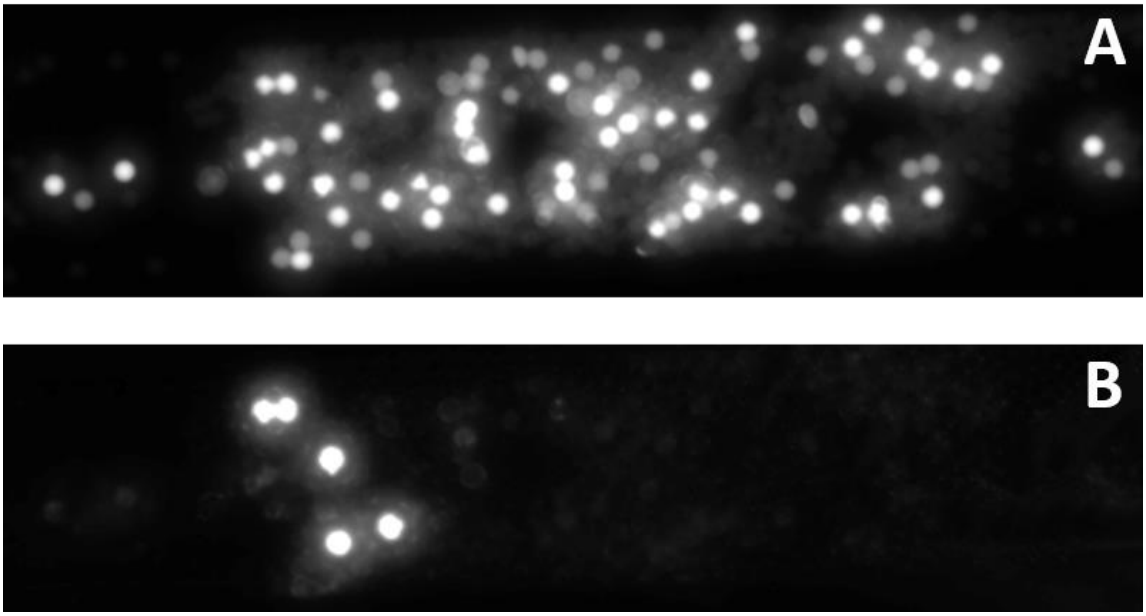

Figure 3.11. (A) Fluorescence assay image from a stage-weir chip and (B) fluorescence assay image from a stage-weir channel in which the bead column was pressed upon by the magnetic loading wand prior to imaging. The number of VEGF beads in (B) is on the order of that in (A), but almost no fluorescent beads can be seen in (B).

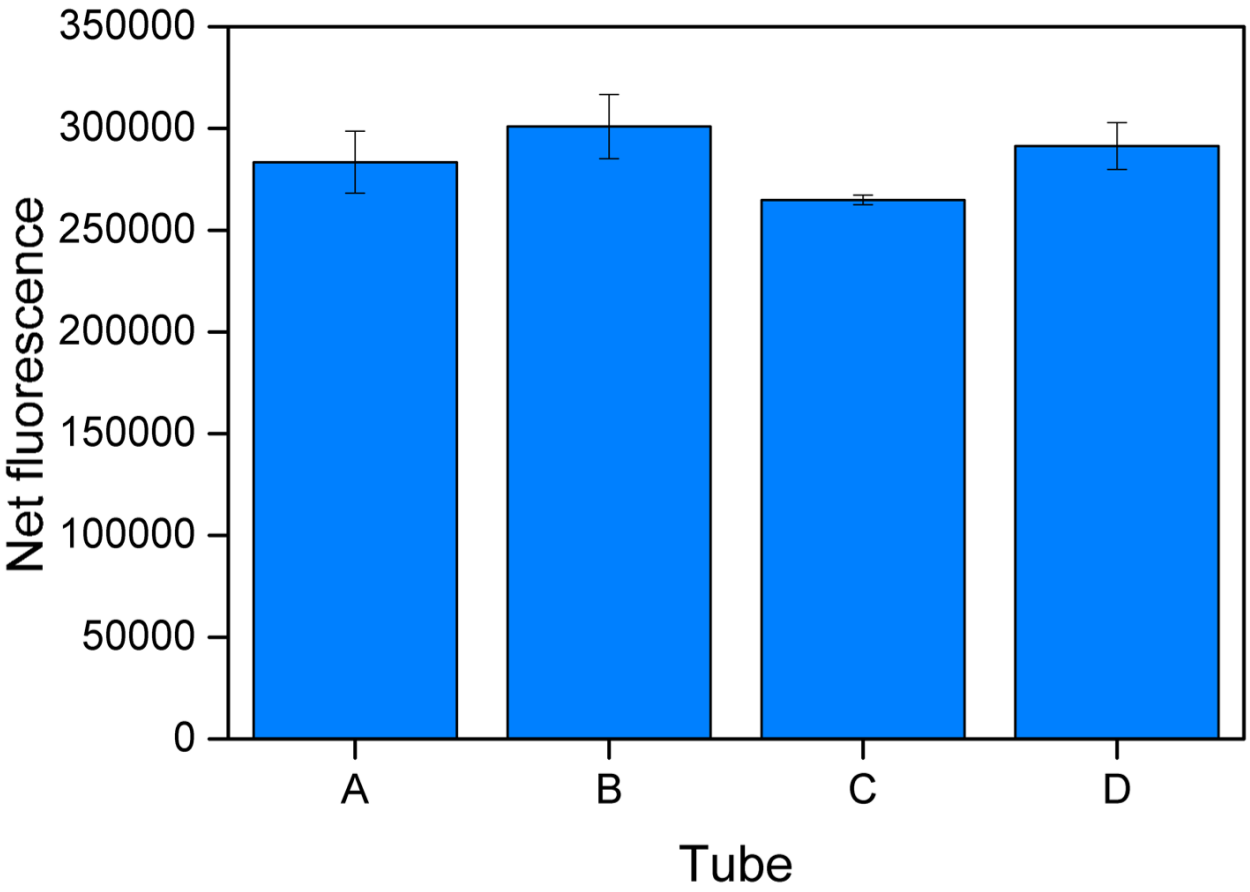

Figure 3.12. Fluorescence assay signal comparing the reproducibility across four separate tubes with identical assay conditions. The %RSDs of the four channels imaged per tube (left to right) were 5.37%, 5.24%, 0.89%, and 3.95%. Each tube shows low variance, and the %RSD across all columns and tubes is 6.06%.

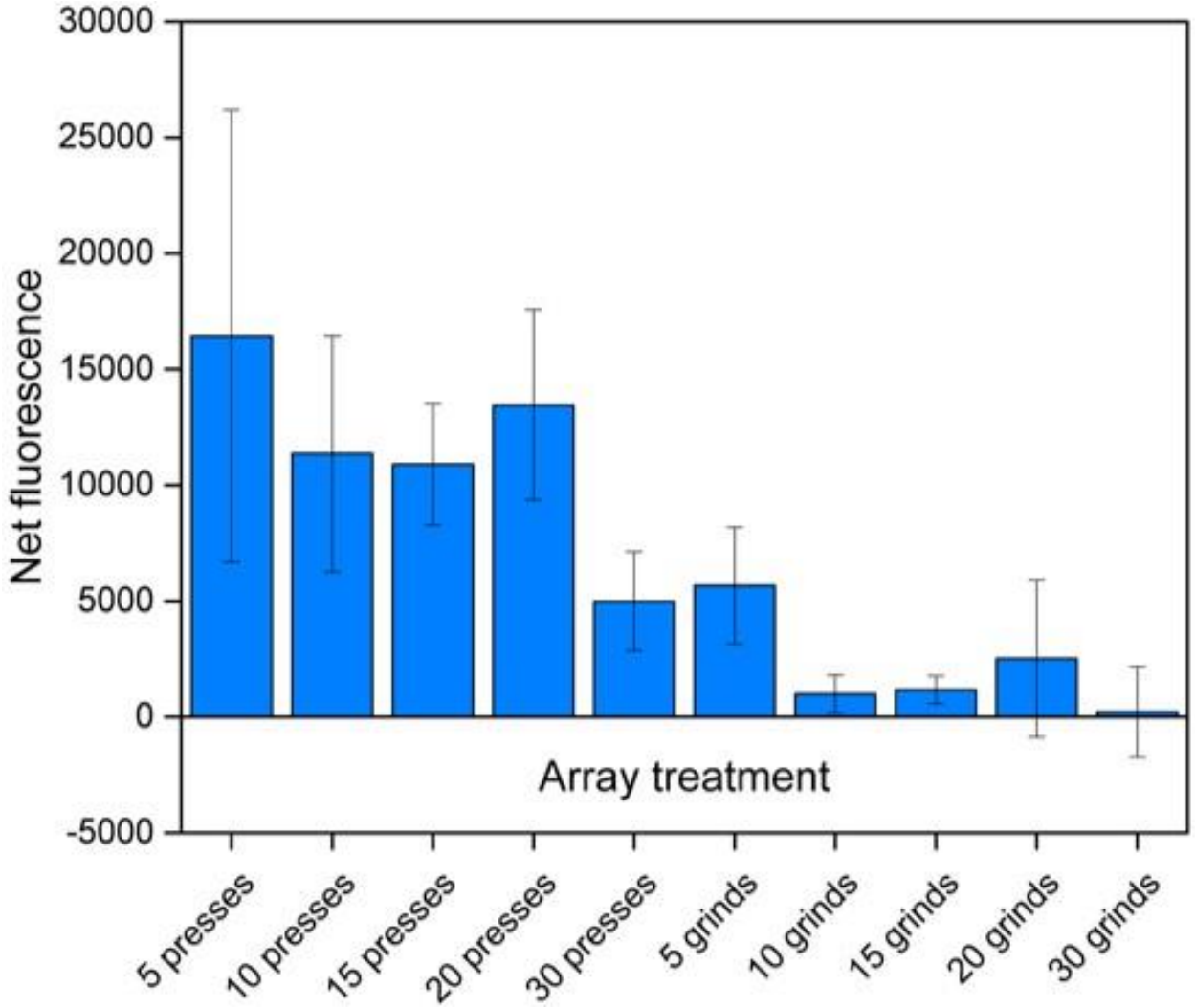

Figure 3.13. Fluorescence signal with the number or presses or grinds used to load beads. The assay appears to perform worse as more presses are performed on each array, and the grinding motion appears to be particularly damaging.

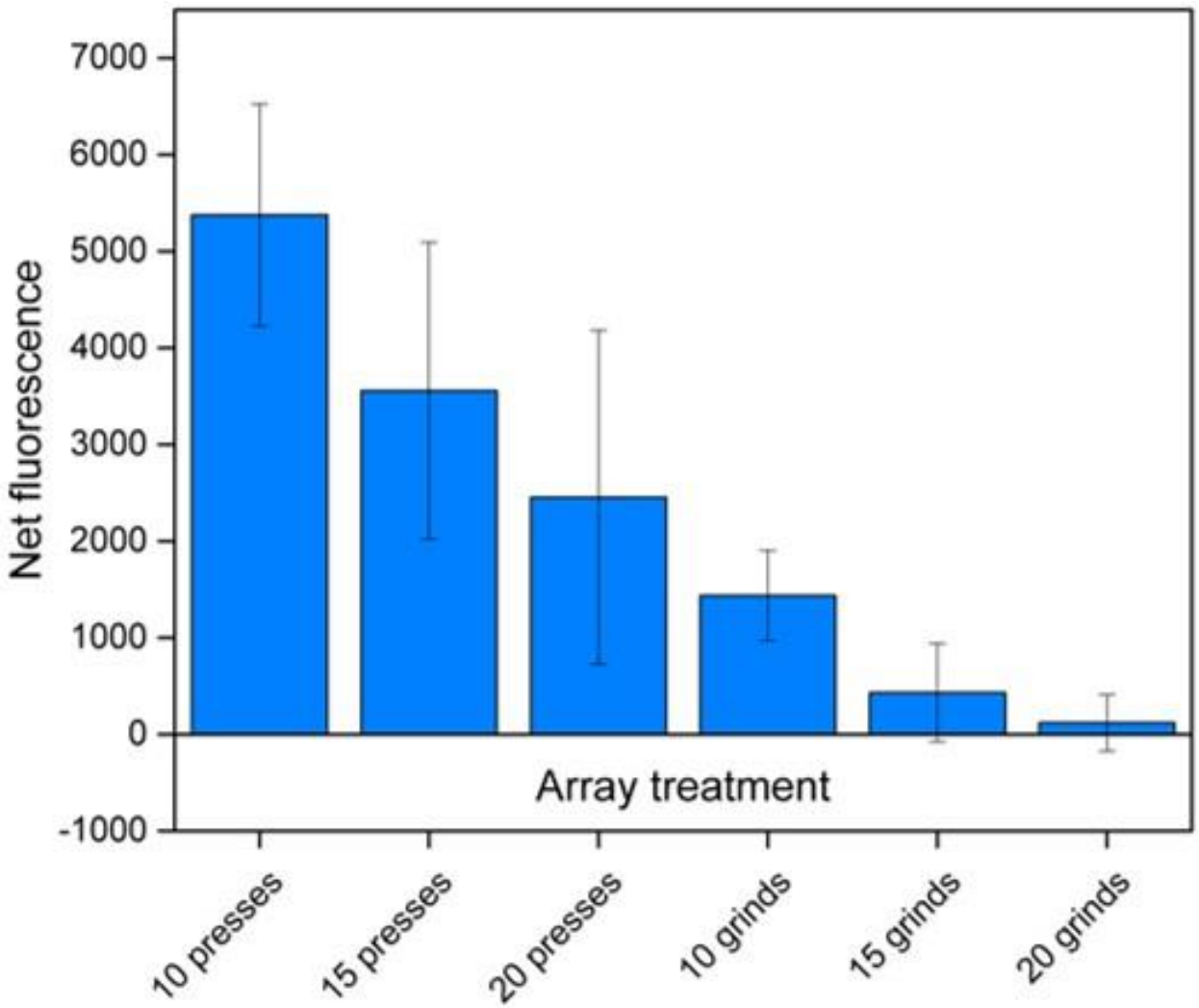

Figure 3.14. Fluorescence signal with number of presses or grinds used to load beads. There is a steady downward trend in signal as the number of presses and grinds increases. Virtually no signal can be seen after 15-20 grinds.

3.6 References

(1) Wians, F. H. Clinical Laboratory Tests: Which, Why, and What Do The Results Mean? *Lab. Med.* **2009**, *40*, 105–113.

(2) Saviranta, P.; Okon, R.; Brinker, A.; Warashina, M.; Eppinger, J.; Geierstanger, B. H. Evaluating Sandwich Immunoassays in Microarray Format in Terms of the Ambient Analyte Regime. *Clin. Chem.* **2004**, *50*, 1907–1920.

(3) Ekins, R.; Chu, F.; Biggart, E. Development of Microspot Multi-Analyte Ratiometric Immunoassay Using Dual Fluorescent-Labelled Antibodies. *Anal. Chim. Acta* **1989**, *227*, 73–96.

(4) Kusnezow, W.; Syagailo, Y. V; Rüffer, S.; Klenin, K.; Sebald, W.; Hoheisel, J. D.; Gauer, C.; Goychuk, I. Kinetics of Antigen Binding to Antibody Microspots: Strong Limitation by Mass Transport to the Surface. *Proteomics* **2006**, *6*, 794–803.

(5) Kusnezow, W.; Syagailo, Y. V; Rüffer, S.; Baudenstiel, N.; Gauer, C.; Hoheisel, J. D.; Wild, D.; Goychuk, I. Optimal Design of Microarray Immunoassays to Compensate for Kinetic Limitations: Theory and Experiment. *Mol. Cell. Proteomics* **2006**, *5*, 1681–1696.

(6) Butler, J. E.; Ni, L.; Nessler, R.; Joshi, K. S.; Suter, M.; Rosenberg, B.; Chang, J.; Brown, W. R.; Cantarero, L. a. The Physical and Functional Behavior of Capture Antibodies Adsorbed on Polystyrene. *J. Immunol. Methods* **1992**, *150*, 77–90.

(7) Butler, J. E.; Ni, L.; Brown, W. R.; Al., E. The Immunochemistry of Sandwich ELISAs - VI. Greater Than 90% of Monoclonal and 75% of Polyclonal Anti-Fluorescyl Capture Antibodies (CAbs) Are Denatured by Passive Adsorption. *Mol. Immunol.* **1993**, *30*, 1165–1175.

(8) Harris, D. C. *Quantitative Chemical Analysis*; 7th ed.; W.H. Freeman and Company: New York, 2007.

(9) Blicharz, T. M.; Siqueira, W. L.; Helmerhorst, E. J.; Oppenheim, F. G.; Wexler, P. J.; Little, F. F.; Walt, D. R. Fiber-Optic Microsphere-Based Antibody Array for the Analysis of Inflammatory Cytokines in Saliva. *Anal. Chem.* **2009**, *81*, 2106–2114.

(10) Rissin, D. M.; Kan, C. W.; Campbell, T. G.; Howes, S. C.; Fournier, D. R.; Song, L.; Piech, T.; Patel, P. P.; Chang, L.; Rivnak, A. J.; et al. Single-Molecule Enzyme-Linked Immunosorbent Assay Detects Serum Proteins at Subfemtomolar Concentrations. *Nat. Biotechnol.* **2010**, *28*, 595–599.

(11) Healy, M. J. Outliers in Clinical Chemistry Quality-Control Schemes. *Clin. Chem.* **1979**, *25*, 675–677.

CHAPTER 4

DEVELOPMENT OF A pERK1/2:ERK1/2 SANDWICH IMMUNOASSAY USING ANTIBODY-BOUND BEADS AND MONOLAYER CHIPS

4.1 Introduction

Based on the assay development work minimizing the variance, it was evident that a device where minimal mechanical contact with the antibody-bound beads was needed. The use of a packed bead bed like those in the stage-weir chips was pursued for several reasons. First, it is easy to prepare the chips; the beads can be packed into beds simply by introducing them to the chip and applying vacuum. The design is also flexible because the beads are no longer fixed in a single position as they are in the loaded array chips. Magnetic beads can be moved through different sections of a chip over the course of an experiment if necessary to perform reagent incubations, wash steps, or mixing.[1–4]

There are also disadvantages with using packed bed chips. Given the close proximity of the beads to one another and the potential for overlapping signals from different analytes, it is more difficult to multiplex with this format. Ideally for this work, one bead type would be used to determine both pERK1/2 and ERK1/2 in two imaging steps; the average fluorescence of the bead bed would be measured and overlapping signals would not pose problems. Since the pERK1/2 beads are compatible with a pERK1/2 dAb and a total ERK2 (tERK2) dAb, this capture Ab-bead assay would be realizable if a compatible total ERK1 (tERK1) dAb were found.

Another potential issue with packed beds is when the channels are significantly deeper than the bead diameter, the beads may pack at different heights on the z-axis relative to the

microscope objective. The 6.5-µm MagPlex beads have shown this phenomenon in some of our microfluidic chips, and this results in beads at different focal planes. The fluorescence photons emitted from out-of-focus beads near in-focus ones are spread over a larger area, lowering their apparent fluorescent signal. The depth of focus for a microscope is described mathematically as follows:[5]

$$d_f = \frac{\lambda n}{NA^2} + \frac{n}{M*NA} e \tag{4.1}$$

where d_f is the depth of field (in µm), λ is the wavelength of illuminating light (in µm), n is the refractive index of the medium, NA is the numerical aperture of the objective, M is the magnification level, and e is the smallest distance the detector can resolve for objects in the image plane (in µm). For 600-nm light being imaged by the 0.5 NA air objective at 30x magnification and EM-CCD camera in our Nikon Ti-U Eclipse Microscope, d_f is approximately 2.4 µm. This is less than half the diameter of the MagPlex beads.

Keeping the beads in the same focal plane places design constraints on the channel dimensions, as the channels should be deep enough for the beads to pack into a monolayer, but not deep enough for them to pack out of focus. Reducing the channel depth from 20 µm (as in the array chips from Chapters 2 and 3) to approximately 7 µm (appropriate for a monolayer with 6.5-µm MagPlex beads) comes with a sharp reduction in flow rate. For a channel of rectangular cross-section like those produced by DRIE fabrication, the hydraulic resistance follows equation 4.2:[6]

$$R_{hyd} = \frac{12\eta L}{1-\frac{0.63h}{w}} \frac{1}{h^3 w} \tag{4.2}$$

where R_{hyd} is the hydraulic resistance (in 10^{15} Pa·s/m^3), η is the viscosity of the fluid (in Pa·s), L is the length of the channel (m), h is the depth of the channel (m), and w is the width of the

channel (m). A 7 μm deep channel will thus have more than 21 times the hydraulic resistance of a 20 μm deep channel. The hydraulic resistance of packed bed chips is further increased by the fact that packed columns of micrometer-scale beads have little interstitial space for fluid flow. This translates to a greatly reduced flow rate, as the flow rate of a fluidic conduit is inversely proportional to its hydraulic resistance.[6] This is problematic in terms of leading to long incubation times and ensuring uniform reagent delivery to all the beads.

The flow-frit chip design was created to address the issue of flow rate with packed bead beds. Like the stage-weir chips, there is a straight 100 μm-wide channel with a punched via at one end for introducing beads and reagents and a second via for vacuum and waste (Figure 4.1A). An individual channel with its frit location indicated is shown in Figure 4.1B. The features distinguishing them from the stage-weir chips are their frit and flow bed. Instead of a weir, these chips feature a frit for trapping the beads (Figure 4.2). The frit consists of 12-μm-wide PDMS pillars that span the channel depth. These pillars are spaced 4 μm apart and trap the 6.5-μm beads to create the packed bed. The frit serves the same function as the weir from previous designs, but unlike the manually-fabricated weir, its fabrication through photolithography is reproducible from chip to chip. The other distinctive feature of the flow-frit chips is the flow bed (shown on the left side of Figure 4.2). The flow bed consists of spaced pillars that populate the entire channel lengthwise (except the frit region). The purpose of the flow bed is to provide additional fluid flow space that is inaccessible to the beads, thus increasing the flow rate throughout the chip. Like the previous column chip designs, the flow-frit chips require no mechanical action in order to load beads; they are simply packed into a monolayer bed via vacuum-driven flow.

In addition to standard solutions, the analysis of pERK1/2 and ERK1/2 in human cell

lysate was undertaken. Assaying cellular proteins with a bead-based immunoassay requires lysing the cells in order to recover the proteins. Numerous methods have been demonstrated for accomplishing on-chip cell lysis. These include disrupting the cell membrane by high-temperature thermal lysis[7] or with a high electric field.[8,9] Thermal lysis, while simple to implement, is not amenable to the needs of this assay because it causes aggregation of the cellular proteins, making protein analyte recovery difficult. Electrical lysis has the disadvantage of requiring areas of high field strength on the chips, which places constraints on the chip design. Cells can also be lysed chemically. Here, a chemical agent is used to disrupt the cell membrane. Triton X-100 is one such agent; it is a nonionic surfactant that incorporates itself into the cell membrane and solubilizes its lipids and proteins, creating pores that eventually produce lysis.[10] At Triton X-100 concentrations in the range of 0.5% - 1%, lysis takes place in seconds. This can be incorporated on-chip and is compatible with the ERK1/2 capture and detection antibodies. An ideal assay would incorporate an on-chip lysis method in a fully-integrated device, but such a device would also possess other factors that were developed in this project instead, including valving and the ability to assay multiple samples on a single chip.

In this chapter, sandwich immunoassays with pERK1/2 beads in packed bed devices instead of an array are investigated. Preliminary experiments are run using stage-weir chips to validate the packed bed format, then an improved chip design incorporating a flow bed and frit is developed. Sample incubations are performed on-chip and the compatibility of the pERK1/2 beads with a total ERK1 detection antibody is established, making it possible to assay all phospho-forms of ERK1 and ERK2 with a single bead type. Finally, the developed assay is used to determine pERK1/2:ERK1/2 in lysate from human Jurkat (acute T-cell leukemia) cells.

4.2 Materials and methods

4.2.1 Materials and reagents

Sylgard 184 PDMS was purchased from Ellsworth Adhesives (Germantown, WI) and was prepared according to the manufacturer's instructions at a 10:1 elastomer/cross-linker ratio. MagPlex Luminex beads were purchased from Bio-Rad Laboratories (Hercules, CA). Purified recombinant human vascular endothelial growth factor (VEGF), phosphorylated and non-phosphorylated extracellular signal-related kinase 2 (pERK2 and nERK2), non-phosphorylated extracellular signal-related kinase 1 (nERK1), biotinylated detection antibodies for VEGF, pERK1/2, ERK1, and ERK2, capture antibodies for pERK1/2, VEGF, and a control capture antibody were purchased from R&D Systems (Minneapolis, MN). All proteins and antibodies were reconstituted according to the manufacturer's instructions. Soda lime glass photolithography substrates (5" x 5") were purchased from Telic (Valencia, CA). Nano-Strip was purchased from KMG Chemicals (Fremont, CA). Octyltrichlorosilane, sodium fluoride, ethylene diamine tetraacetic acid (EDTA), urea, Triton X-100, phorbol 12-myristate 13-acetate (PMA), leupeptin, phenylmethanesulfonyl fluoride (PMSF), aproptinin, sodium pyrophosphate, and sodium orthovanadate were purchased from Sigma-Aldrich (St. Louis, MO). AZ-400K was purchased from AZ Electronic Materials USA (Somerville, NJ). Chromium etchant and 10:1 buffered oxide etch (BOE) were purchased from Transene Corp. (Danvers, MA). Acetone, 10x phosphate-buffered saline (PBS, pH = 7.4), 10% bovine serum albumin (BSA) in PBS, optically clear polypropylene plate-sealing tape (PCR tape), Contrad 70, and microscope slides (75 mm x 25 mm x 0.99 mm) were purchased from Thermo Fisher Scientific (Waltham, MA). KMPR 1010 photoresist and SU-8 thinner were purchased from MicroChem (Newton, MA); the SU-8 thinner was mixed with KMPR 1010 to prepare 35% (w/w) KMPR solutions. MF-319

photoresist developer was purchased from Rohm and Haas Electronic Materials (Marlborough, MA). P-type 6" crystalline Si wafers were purchased from University Wafer (Boston, MA). Streptavidin-B-phycoerythrin (SA-PE), RPMI 1640 media, fetal bovine serum, penicillin, and streptomycin were purchased from Invitrogen (Carlsbad, CA). Human Jurkat T-cells were acquired from American Type Culture Collection (Rockville, MD).

All aqueous solutions were prepared with deionized (DI) water from a NANOpure Diamond system (Barnstead International, Dubuque, IA). Buffer solutions used include PBS-BB (PBS + 1% BSA), cell lysis buffer (PBS + 1 mM EDTA + 0.5% Triton X-100 + 5 mM sodium fluoride + 6 M urea + 10 µg/mL leupeptin + 100 µM PMSF + 3 µg/mL aprotinin + 2.5 mM sodium pyrophosphate + 1 mM activated sodium orthovanadate), ERK buffer (PBS + 5 mM sodium fluoride + 1 mM EDTA + 0.5% Triton X-100 + 1 M urea), and ERK diluent (ERK buffer with no urea).

4.2.2 Design and fabrication of flow-frit chips

Experiments following the pilot stage-weir assays were performed with flow-frit chips (Figure 4.1 and Figure 4.2). Chip designs were created in TurboCAD Professional 14 drafting software and the photolithography mask made with a Heidelberg Instruments DWL66 laser lithography system. The master molds and PDMS/glass chips were fabricated as described in Chapter 2 using photolithography, DRIE on 6" Si wafers, soft lithography, and plasma bonding. In the first photolithography/DRIE step, the flow bed layer was patterned and etched into the wafer molds to a depth of 5 µm. In the second step, the channel layer was patterned and etched to a depth of 7.5 µm, bringing the total channel depth to 12.5 µm. Frit pillars were etched spanning the height of the channel.

As the flow-frit chips contained many high aspect-ratio features, the chips were filled

with PBS-BB immediately after bonding. This was done to take advantage of the temporary hydrophilicity of the activated PDMS,[11] as the chips were easily wettable in this state and air bubbles were not a concern. PBS-BB filled chips were either used after 2 h of passivation at room temperature or sealed with PCR tape and stored at 4 °C for use after 24 h.

4.2.3 Flow-frit chip assay method

Early proof-of-concept assays with the flow-frit chips used off-chip sample incubations in microcentrifuge tubes as described in Chapter 3. This was done to maximize signal while developing assay protocols.

Sample solutions containing ERK1/2 were prepared in ERK buffer. All other solutions were prepared in PBS-BB. Solutions are introduced to the chips by removing the fluid in the chip inlets with vacuum, filling the inlets with 10 µL of new solution, and applying vacuum for 15 s. Washing is performed by filling the chip inlets with PBS-BB and applying vacuum for 1 min in between each incubation step and before imaging steps. Unless otherwise specified, all dAb solutions are at 3 µg/mL, all SA-PE solutions are at 2 µg/mL, and replicates of 5 assays are used for each sample. Encoding and assay images were taken as described in Chapter 2.

4.2.4 Data analysis

The preliminary experiments with stage-weir and flow-frit chips in Sections 4.3.1-4.3.2 used control and VEGF or pERK1/2 beads and were decoded through the manual selection process described in Chapter 2. Control beads were no longer used starting with the on-chip incubations with flow-frit chips in Section 4.3.3 onward. The encoding dye in the beads was used to locate the bead beds, focus the microscope, and provide a fluorescent encoding image (Figure 4.3A). Assay images of the sandwich complex were then taken with the SA-PE filter cube (Figure 4.3B). The bead bed in the encoding image was selected in ImageJ (Figure 4.3C),

the selection was overlaid in the assay image (Figure 4.3D), and the aggregate fluorescence data was exported to Microsoft Excel as a 5000-bin histogram. Formulas for grouped data[12] were used to calculate the mean and standard deviation of the fluorescence:

$$\mu = \frac{\sum xf}{n} \tag{4.3}$$

$$s = \sqrt{\frac{\sum x^2 f - \frac{(\sum xf)^2}{n}}{n-1}} \tag{4.4}$$

where μ represents the mean, x is the fluorescence value of a histogram bin, f is the number of points in the bin, n is the total number of values across all bins, and s is the standard deviation. The iterative correction cycle process described in Chapter 3 was used to remove outliers, and the standard deviation and mean were calculated from the corrected data.

4.2.5 Cell culture

Human Jurkat T-cells were cultured according to the vendor's instructions[13] in RPMI 1640 media containing 10% (v/v) fetal bovine serum, 100 IU/mL penicillin, and 100 µg/mL streptomycin. Cells were incubated at 37 °C and 5% CO_2 and kept at concentrations between 1 x 10^5 and 1 x 10^6 cells/mL.

4.2.6 Cell lysis

The recipe for the lysis buffer was provided by R&D Systems.[14] The cells are chemically lysed with 0.5% Triton X-100, a non-ionic surfactant that breaks down the cell membrane by solubilizing its proteins and lipids.[10] The buffer also contains a cocktail of leupeptin, aprotinin, PMSF, sodium fluoride, sodium pyrophosphate, and activated sodium orthovanadate that preserves ERK1/2 phosphorylation by inhibiting cellular proteases and serine and tyrosine phosphatases.[15] Cell lysate was obtained by first transferring cell aliquots to an Eppendorf Lo-

Bind microcentrifuge tube and washing them twice by centrifuging at 1000 rcf for 3 min, and resuspending in PBS. After the second wash with PBS, the cells were centrifuged at 1000 rcf for 3 min, the supernatant was removed, and the cells were resuspended in lysis buffer at 10^7 cells/mL and incubated for 15 min on ice. The lysed cells were centrifuged at 2000 rcf for 5 min and the supernatant was transferred to a fresh centrifuge tube. It was then diluted six-fold with ERK diluent prior to making further dilutions in ERK buffer for analysis.

4.3 Results and discussion

4.3.1 Preliminary pERK2 and nERK2 assays with stage-weir chips

Preliminary experiments were conducted to evaluate the performance capabilities of bead monolayer chips for assaying pERK2 and nERK2. In each experiment, the parameters for off-chip incubations described in Chapter 3 were used, except the dAb concentration was 1 µg/mL. Stage-weir chips with a 7.8-µm viewing zone were used for imaging the beads.

The first experiment in this series investigated the detection limit of pERK2. Solutions of pERK2 were prepared at concentrations ranging from 250 pg/mL to 5000 pg/mL. As 250 pg/mL (S/N = 137) was easily distinguishable from the blank, the experiment was repeated with the pERK2 concentration ranging from 50 pg/mL to 250 pg/mL. The lowest concentration of pERK2 (S/N = 37) was easily distinguishable from the blank in this experiment as well. Using S/N =3 as the LOD, the limit of detection would be approximately 5 pg/mL. Both sets of data are plotted in Figure 4.4 showing that the fluorescence as a function of the pERK2 concentration is linear ($R^2 = 0.9943$) across the entire range of the curve. The %RSDs are below the targeted 10% limit for each sample as well. The detection of nERK2 was examined next using the same methods and concentrations as the second pERK2 assay (50 to 250 pg/mL) and a tERK2 dAb. The results (Figure 4.5) are comparable to that of the second pERK2 assay in terms of signal

level for each concentration, and the limit of detection is approximately 50 pg/mL. Only two samples have %RSDs above 10%, both because of a single datum that was not sufficiently anomalous to be removed via the q-test at 95% confidence. These results show that with bead monolayer chips, pERK2 and nERK2 are detectable at concentrations (approximately picomolar) well below their physiological concentrations (approximately micromolar)[16,17] with low %RSDs, validating the usefulness of bead monolayer type chips for the pERK1/2:ERK1/2 assays.

After the individual assays for pERK2 and nERK2, a multiplex assay for both analytes was performed. Five samples were prepared with the total concentration of ERK2 held at a constant 250 pg/mL and differing percentages of pERK2 and nERK2. Their sample compositions are noted in Table 4.1 as a representative example of the standards prepared for pERK1/2:ERK1/2 assays in other experiments. Following the sample incubation step, the bead population for each concentration was divided into two microcentrifuge tubes. One was incubated with 3 µg/mL pERK1/2 dAb, while the other was incubated with a 1:1 mix of pERK1/2 dAb and tERK2 dAb (3 µg/mL each). Both bead populations were then incubated with SA-PE, loaded into chips, and imaged. The results in Figure 4.6 show that for samples containing mixed ERK2 phosphorylation states, the fluorescence signal obtained from the pERK1/2 dAb as a function of the sample's %pERK2 increases linearly (red triangles). Compared to the increase in fluorescence from the pERK1/2 dAb as a function of %pERK2, the fluorescence from the mixed dAbs (black circles) is relatively constant, although it still increases by nearly 19% from the 0% pERK to the 100% pERK samples. The curve's slight upward slope as a function of the %pERK thus indicates some cross reactivity of the pERK2 molecules with the pERK1/2 dAb and the total ERK2 dAb. This cross-reactivity is accounted for when the ratio of the two signals is taken when determining the %pERK as shown in Figure 4.7. The

fluorescence ratio increases linearly as a function of the %pERK in the sample.

Although the stage-weir chips produced reproducible results, several drawbacks to the devices are detrimental to their use as potential POC devices. First, the manual fabrication of the weir for creating the packed beds is not reproducible, affecting the uniformity of fluid flow from one device to another. Second, fabricating chips with the PDMS complement mold method is time-consuming, thus increasing fabrication costs. Most importantly, the flow rates in these chips are very low because the packed beds have little interstitial fluidic space. This considerably lengthens the time required for introducing sample and reagents. While this has not been a problem with the stage-weir chips owing to sample incubations being performed off-chip, the goal of the project is to create an on-chip assay, so a chip design using short incubation times and a packed bead bed was developed.

4.3.2 Preliminary flow-frit chip experiments

Flow-frit chips with square pillars in the flow beds featuring sides of 5 µm, 6 µm, 7 µm, or 8 µm, and spacings of either 4 µm or 6 µm were tested using the model analyte VEGF. The purpose was to compare the assay performance of the different flow bed feature size configurations. In the first of these assays, VEGF and control beads were packed into beds by pipetting a 10:1 dilution of stock VEGF and control beads in PBS-BB into the reagent vias and pulling vacuum and incubated for 2 h to passivate them. The chips were then filled with 500 pg/mL VEGF, incubated for 1 h followed by a 1 min wash, filled with anti-VEGF dAb, and incubated for 30 min. The chips were washed again and incubated with SA-PE for 20 min, then washed and imaged.

A fluorescence gradient across the flow bed was seen for these on-chip sample-incubated beads, with the brightest beads being closest to the reagent via and the darkest beads closest to

the frit (Figure 4.8A). As a result, the interchip %RSDs increased to greater than 10% (Figure 4.8B) for all tested devices. It appears that the beads at the head of the packed bed capture more sample molecules. To eliminate this problem, beads should be incubated with sample prior to being packed to ensure uniform sample exposure. In comparison, stage-weir devices used off-chip sample incubation and uniform bead fluorescence across the length of the bed was exhibited. As such, these experiments were repeated with modifications intended to reproduce conditions in the stage-weir assays.

First, the VEGF and control beads were incubated with samples in microcentrifuge tubes off-chip. A vortexer was used to keep the beads in suspension over a 2 h period to ensure uniform exposure to the sample. Second, after washing the sample-incubated beads, non-fluorescent spacer beads were added to the bead solutions. The purpose of the spacer beads was to prevent overlap of fluorescence signals from assay beads. As the spacer beads do not contain fluorescent dyes, they manifest as dark spots in the images of the beds. The bead mixture was packed into flow-frit chips and the assay was completed as in the previous experiment. A representative fluorescence image of one flow bed exhibiting uniform fluorescence levels over the length of the bed is shown in Figure 4.9A. The assay's results in Figure 4.9B show that the flow bed feature sizes (height/spacing) all produce similar results in terms of fluorescence and variance, and so in subsequent experiments, all sizes were used interchangeably. The absence of a fluorescence gradient in any of the bead beds is in spite of both the dAb and SA-PE incubations being done on-chip. This is indicative of the antibody and dye being able to permeate the bed sufficiently to bind to the sandwich complex on the beads' surfaces, with the limiting factor in the beads' fluorescence being the amount of sample captured. This suggests that to achieve consistent results, the sample incubation with the beads should be done outside of a packed bed

with all other incubations and imaging steps done post-packing.

4.3.3 On-chip sample incubation

All experiments up to this point used off-chip sample incubations, but as the goal of the project is an on-chip assay, a method of doing sample incubations on-chip while exposing the beads to a uniform amount of sample was sought. A simple means of accomplishing this was tried by incubating pERK2 samples with pERK1/2 beads in the bead inlet vias. pERK2 samples were prepared at 0, 2.5, 5, 7.5, and 10 ng/mL in ERK buffer and combined with 0.5 µL pERK1/2 beads. Each solution was evenly distributed across five chip reagent vias and incubated for 30 min. The beads were then packed by applying vacuum and the beds were washed for 5 min with PBS-BB. The chips were then incubated with dAb, SA-PE, and imaged. The results are shown in Figure 4.10. All %RSDs are below 5%, and the lowest assayed concentration of 2.5 ng/mL (average S/N = 154) is easily distinguishable from the blank. This concentration of approximately 60 pM is many orders of magnitude below the micromolar concentrations found in cells.[16,17] Although cell lysis results in dilution of the intracellular proteins, the concentration change and thus number of cells required is addressable through future refinements in chip design, particularly of the cell lysis/sample incubation regions. These results show that this facile on-chip incubation method is sufficient for determining ERK2 in cell lysate, so all future flow-frit assays were conducted in this manner.

The packed beds imaged in these and subsequent flow-frit chip experiments typically had between 300-600 beads per bed. Within this range, the signal was not found to be dependent upon the size of the bed. This is likely because these immunoassays are operating in the ambient analyte regime in which <1.5% of molecules are captured from solution.[18] In this regime, molecules in bulk solution are not significantly depleted during incubations and thus the number

of molecules captured per bead is not a function of the number of beads.

4.3.4 Optimization of flow-frit assay steps

Additional experiments were run with VEGF to optimize assay parameters prior to determining pERK1/2:ERK1/2 in cells. The first of these was designed to optimize the incubation time for the dAb. VEGF beads were incubated with 500 pg/mL VEGF. The chips were then filled with anti-VEGF dAb and incubated for 5, 10, 15, 20, 25, and 30 min. An additional chip set was not incubated with any dAb. The chips were imaged after being washed and incubated with SA-PE as usual. Figure 4.11 shows that the assay signal steadily increases up to approximately the 20-min incubation mark, then diminishing returns set in; 30 min of dAb incubation yields approximately 10% more signal than 20 min, while 20-min dAb incubations yield approximately 64% more signal than 10-min incubations. The dAbs were therefore incubated for 20 min in subsequent experiments as the 10-min reduction in incubation time equates to a 20-min reduction over the course of the two dAb incubation steps. All %RSDs are below 5%, except the 25-min incubation

The incubation time for SA-PE was optimized next. Beads were incubated off-chip with 500 pg/mL VEGF, packed into the chips, and incubated with 1 µg/mL anti-VEGF for 20 min. After washing the chips, SA-PE at 2 µg/mL was incubated for 0, 4, 8, 12, 16, and 20 min. The chips were washed for 5 min and imaged. Figure 4.12 shows that a constant signal is seen for all incubation times. This is consistent with the extremely fast binding kinetics between streptavidin and biotin.[19] All %RSDs are below 10%, except the 16-min incubation which is 10.3%. All subsequent experiments used 5 min SA-PE incubation time. The increase from 4 to 5 min was done to make it easier to handle multiple chips simultaneously during experiments.

4.3.5 Detection of total ERK1

At this point, a dAb for total ERK1 was tested for its compatibility with the pERK1/2 capture antibody. Previous ERK1/2 experiments using stock pERK2 and nERK2 proteins did not test this, but the detection of nERK1 is a necessity in a cell assay for pERK1/2:ERK1/2. The pERK1/2 capture antibody has been shown to target a common epitope on nERK1/2 and pERK1/2, but a detection antibody capable of binding to nERK1 captured by the pERK1/2 antibody needed to be identified. Such an antibody was pursued, as a nERK1 dAb compatible with the pERK1/2 capture antibody would facilitate assaying all phosphorylation states of ERK1/2 with a single bead type.

A biotinylated tERK1 dAb and nERK1 standard were obtained from R&D Systems. Samples of nERK1 were prepared at 0, 2.5, and 5 ng/mL. nERK2 samples were prepared at these concentrations as well for comparison. pERK1/2 beads were incubated with each sample and packed into flow-frit chips. The chips containing nERK1-incubated beads were incubated with tERK1 dAb while the nERK2 chips were incubated with tERK2 dAb. The chips were washed and incubated with SA-PE and imaged. The results are shown in Figure 4.13, with the blue bar representing fluorescence from nERK1 and the red bar representing fluorescence from nERK2. For each ERK concentration, signal levels are higher from nERK1 using the tERK1 dAb than from nERK2 using the tERK2 dAb. This shows that the total ERK1 dAb is capable of binding to ERK1 captured by the pERK1/2 beads, and to a greater degree than the tERK2 dAb binding to captured ERK2. This can be caused by the tERK1 dAb having a greater affinity for its epitope than the tERK2 dAb, as well as by the epitope on captured ERK1 being more sterically accessible to the dAb than the corresponding epitope on ERK2. All %RSDs are below 10% except those for the highest ERK1 concentration.

4.3.6 Simultaneous nERK1 and nERK2 detection on-chip

While flow-frit assays successfully detected nERK1 in isolation, the simultaneous detection of nERK1 and nERK2 is required as part of the assay. Samples containing equal parts nERK1 and nERK2 at 0, 5, 10, and 20 ng/mL were prepared and incubated on-chip with pERK1/2 beads. After packing and washing, the chips were incubated with solution containing 1 µg/mL each tERK1 and tERK2 dAb. The chips were finally washed, incubated with SA-PE, and imaged. The results in Figure 4.14 show the successful simultaneous detection of the two unphosphorylated proteins as the fluorescence obtained increases linearly as a function of the total ERK1/2 concentration with all %RSDs below 10%.

4.3.7 Cell lysis assay

At this point, the reproducible detection of pERK1/2, nERK1, and nERK2 has been demonstrated with the flow frit chip. This was followed up with the determination of pERK1/2:ERK1/2 in human cell lysate. This assay followed the dual-dAb, pERK1/2 dAb-first strategy discussed in Chapter 2. Jurkat cell aliquots containing ~1 million cells each were transferred to culture flasks and diluted to 5 mL with culture media with 200 nM phorbol 12-myristate 13-acetate (PMA) added to one. PMA is a tumor promoter that induces ERK1/2 phosphorylation by activating the MAPK signaling cascade upstream at protein kinase C; this in turn activates the Raf $\rightarrow$ MEK1/2 $\rightarrow$ ERK1/2 pathway.[20] The use of PMA creates a high concentration pERK1/2 cell for comparison with an untreated control that should have a lower pERK1/2 concentration. Both PMA-treated and untreated cells were incubated for 30 min, transferred to a microcentrifuge tube, and lysate was prepared as described in Section 4.2.6.

Five calibration standards containing pERK2 and nERK1/2 were prepared at a constant total ERK1/2 concentration of 10 ng/mL. The %pERK in the samples was 0%, 25%, 50%, 75%,

and 100%. A fifth standard containing no ERK1/2 served as a blank. Each standard and lysate sample was incubated on-chip with ERK1/2 beads. After packing the beads, pERK1/2 dAb (3 µg/mL) was incubated. The chips were imaged after the appropriate wash steps and SA-PE incubation. The imaged chips were then incubated with the tERK1 and tERK2 dAbs (3 µg/mL each) and imaged a second time after the final SA-PE incubation and wash step.

Figure 4.7 shows the ratio of the pERK2:ERK2 phosphorylation fluorescence ratio with increasing pERK1/2 percentage in solution. Also shown are the signals from PMA-treated cells and non-PMA treated cells. The fluorescence ratio is linear as a function of the %pERK1/2 for the standards. The pERK2:ERK2 fluorescence ratios for the untreated cells (black square) and PMA treated cells (upright triangle) fall on the standard curve with ratios of ~4% and ~30% respectively. The higher ratio is as predicted because of the activation of the ERK1/2 signaling cascade by PMA. Although this method of increasing ERK1/2 phosphorylation is artificial, in a real-world patient sample, increased ERK1/2 phosphorylation is often seen when upstream mutations occur in the ERK1/2 signaling cascade, as is the case in many cancers.[21,22] Overall, these results show that the assay can determine pERK1/2:ERK1/2 at physiologically relevant concentrations, both in standards as well as human cell lysate. The detection of increased ERK1/2 phosphorylation in the PMA-treated cells also shows that the assay is useful for detecting upstream mutations in the ERK1/2 signaling cascade.

4.4 Conclusions

The flow-frit chip assays were successful in determining pERK1/2:ERK1/2. In order to move the pERK1/2:ERK1/2 assay toward a self-contained, automatable LOC, a chip design with the necessary functional elements such as reagent delivery and valving was explored. Such modifications include the placement of vias for all assay solutions and samples on a single chip –

that is, wash buffer, the pERK1/2 and total ERK1/2 dAbs, the fluorescent SA-PE complex, and the sample/bead incubations themselves. Simultaneous inclusion of all these features on one chip requires a method of controlling which fluid is being delivered to the beads at any given time. Development of a valving method for the pERK1/2:ERK1/2 device is thus the subject of the next chapter.

4.5 Tables and figures

[pERK2] (pg/mL)	[nERK2] (pg/mL)	%pERK2
0	250	0
62.5	187.5	25
125	125	50
187.5	62.5	75
250	0	100

Table 4.1. Sample compositions for preliminary pERK2:ERK2 assay. The total ERK2 concentration is 250 pg/mL in all samples while the pERK2 percentage is varied. [pERK2] and [nERK2] are calculated from stock protein concentrations.

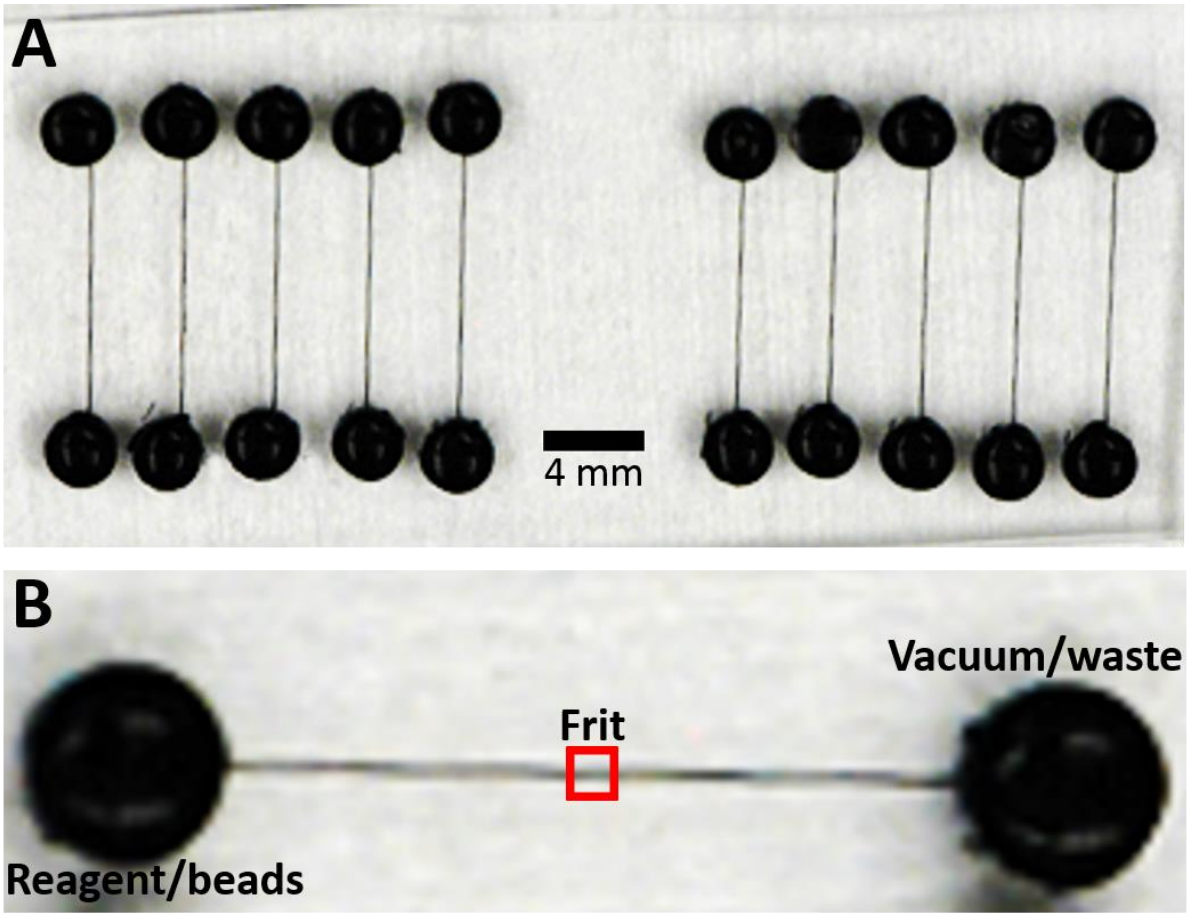

Figure 4.1. Photographs of flow-frit chips filled with ink for visualization. (A) Flow-frit chips with 10 channels. Samples are analyzed in replicates across 5 channels each. (B) Single flow-frit channel showing location of frit and reagent/bead and vacuum/waste vias.

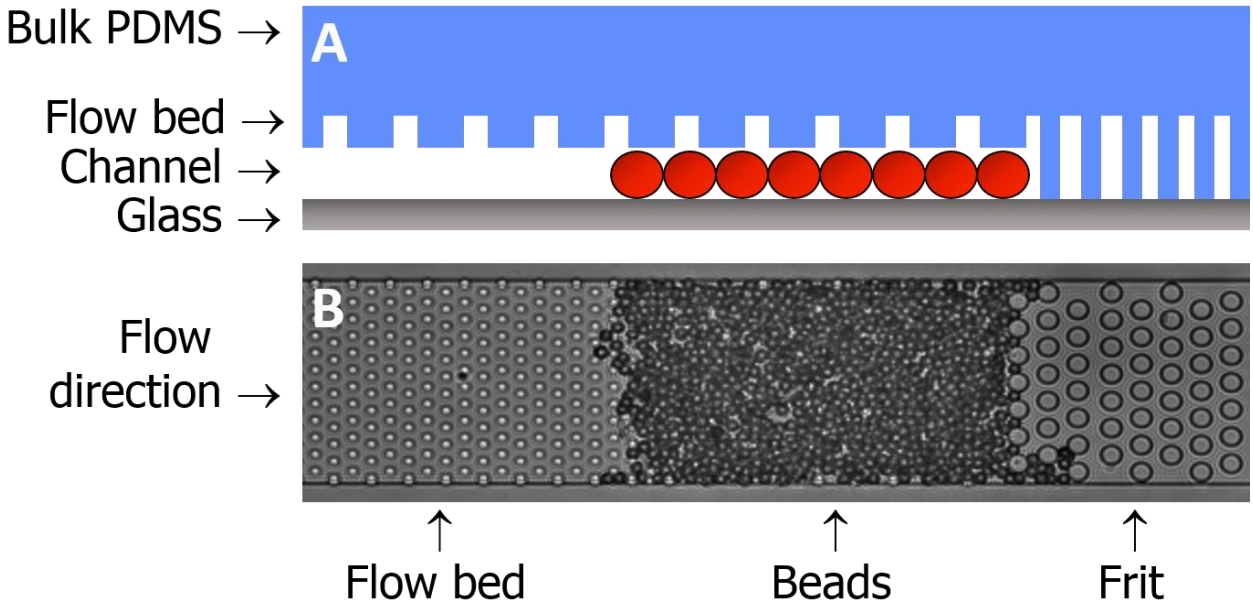

Figure 4.2. Side and bottom views of flow-frit chips. (A) Schematic of flow-frit chip with bead monolayer and (B) white light microscope image of chip with bead bed. The flow bed pillars and channel depth force the beads into a monolayer as they pack against the frit. (A) is not to scale.

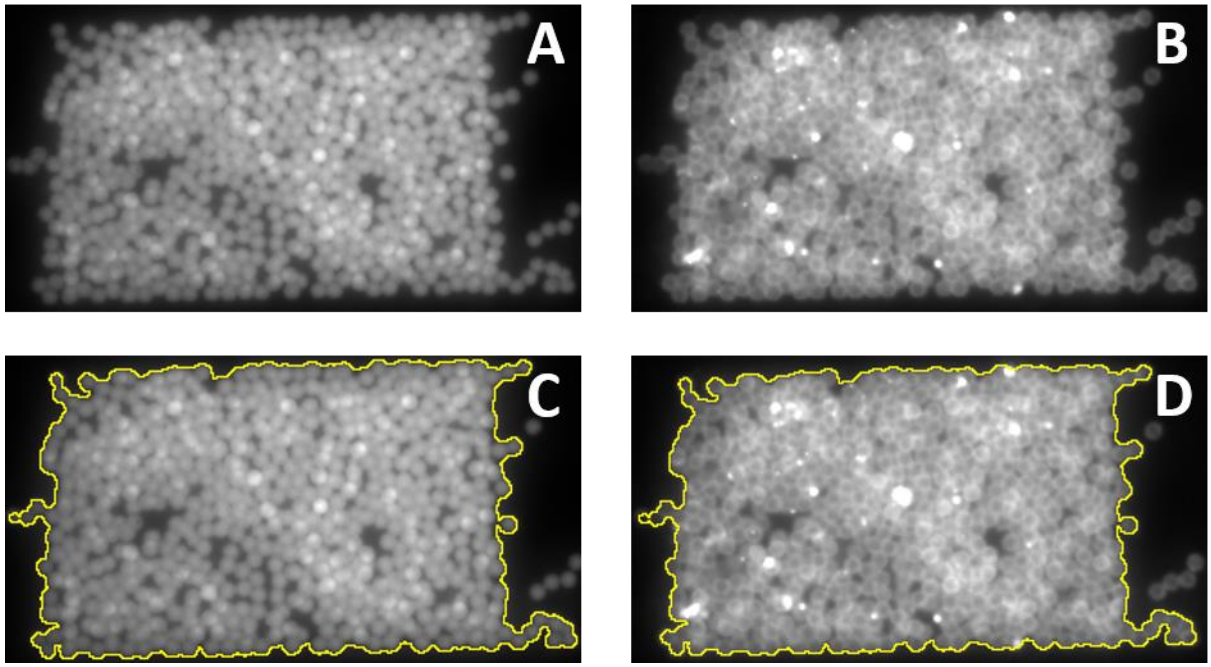

Figure 4.3. Data analysis process for flow-frit chips. (A) Fluorescent encoding image (λ_{ex} = 631 nm) and (B) fluorescent assay image (λ_{ex} = 532 nm). (C) The encoding image is used to focus on the bead bed, select the signal area, and overlay the selection on the fluorescence signal image (D) for analysis. The fluorescence data are exported in the form of a 5000-bin histogram and analyzed.

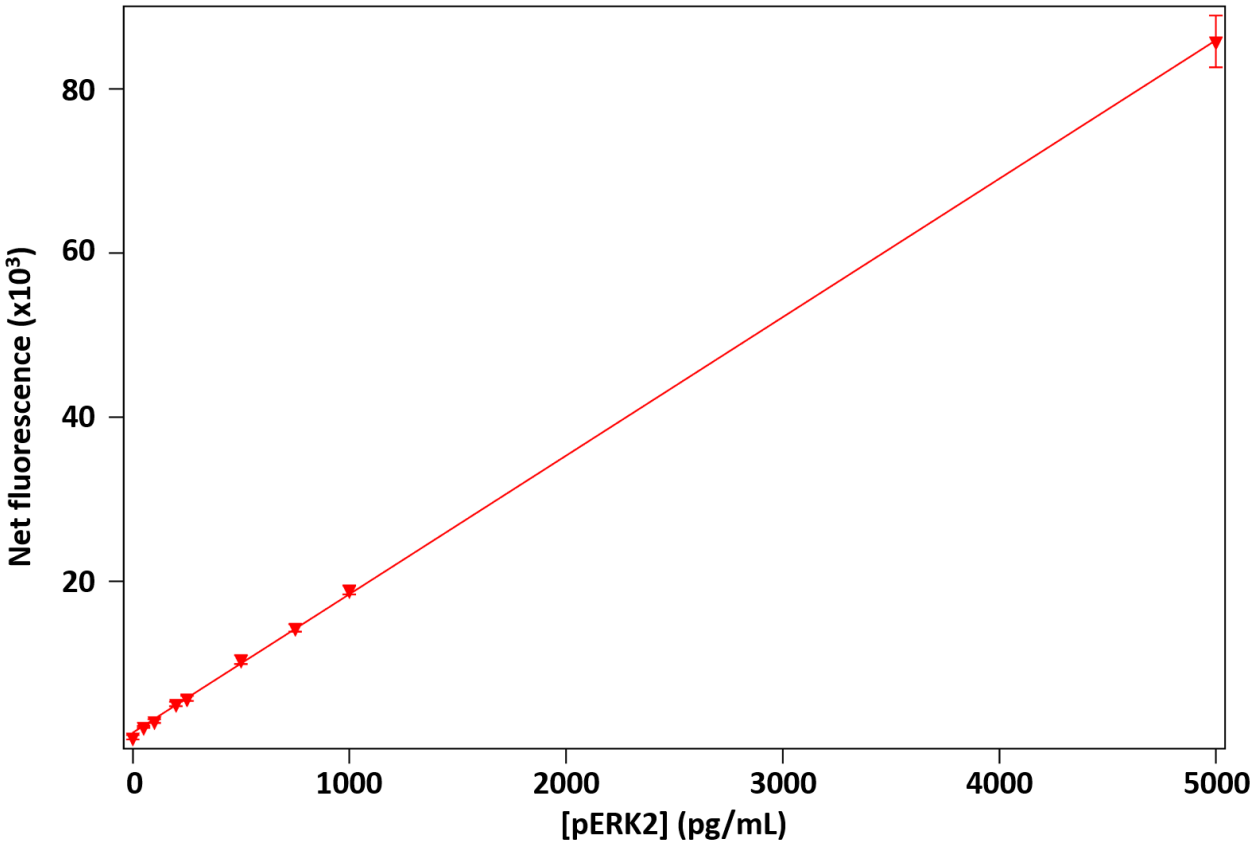

Figure 4.4. Net fluorescence intensity with pERK2 concentration and stage-weir chips. The detection limit is approximately 5 pg/mL (~0.12 pM).

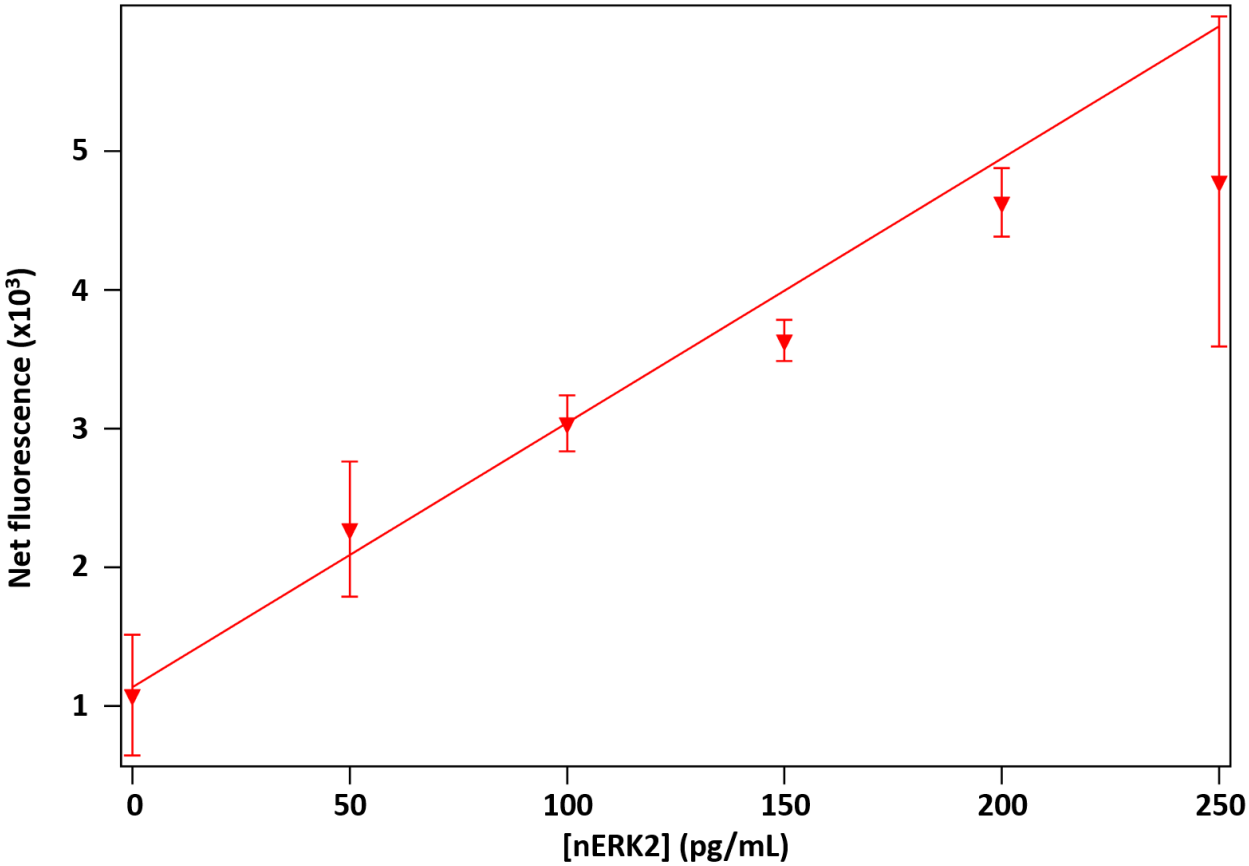

Figure 4.5. Net fluorescence intensity with nERK2 concentration taken with stage-weir chips. The fluorescence and variance results are similar to those for pERK2 detection. All %RSDs are below 10% except those for the 50 pg/mL and 250 pg/mL samples, both of which owe their variance to a single anomalous data point that could not be removed via the q-test.

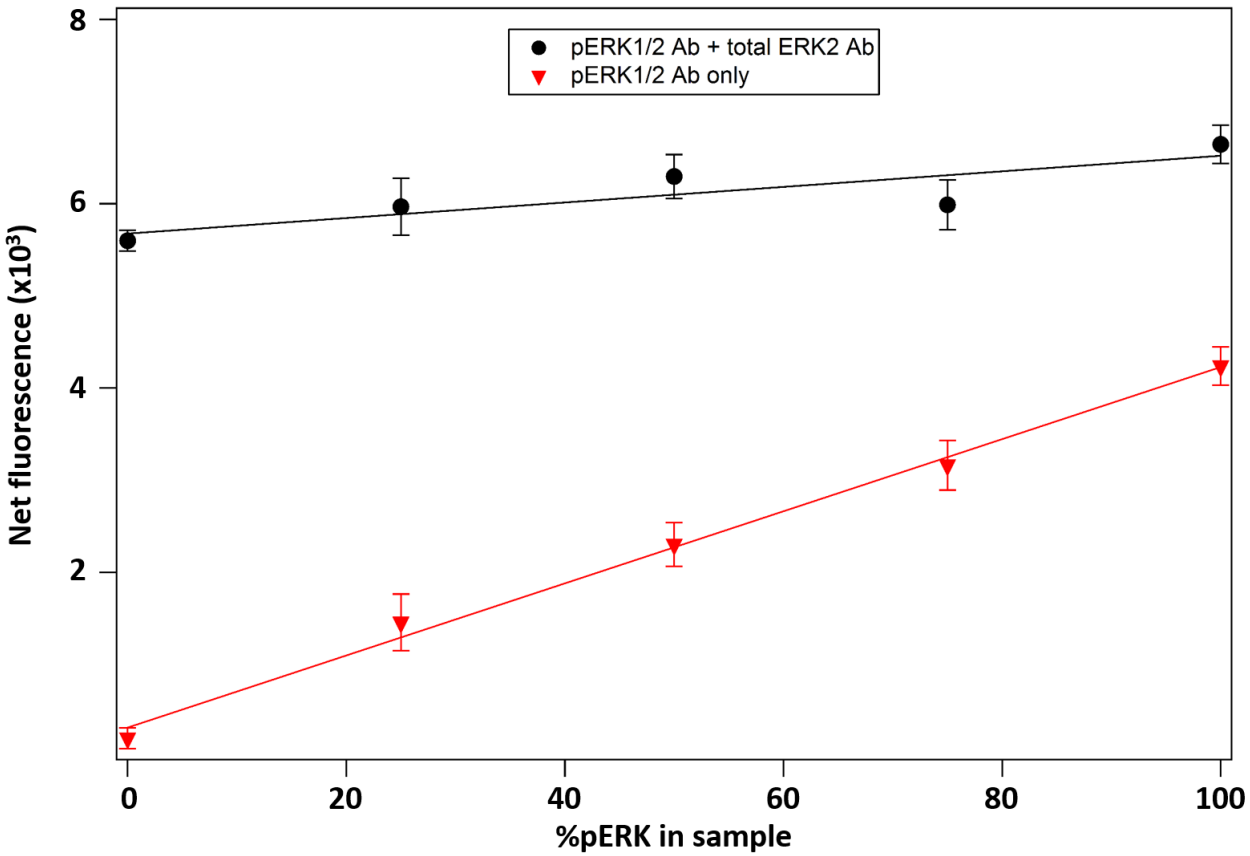

Figure 4.6. Net fluorescence intensity with pERK2:ERK2 ratio taken with stage-weir chips. The fluorescence increase from the pERK1/2 dAb-incubated beads (red triangles) is linear as a function of the percentage of pERK2 in the sample. The fluorescence from the combined pERK1/2 and total ERK2 dAb-incubated beads (black circles) slightly increases as pERK2 increases because some pERK2 molecules bind to both dAbs at the same time.

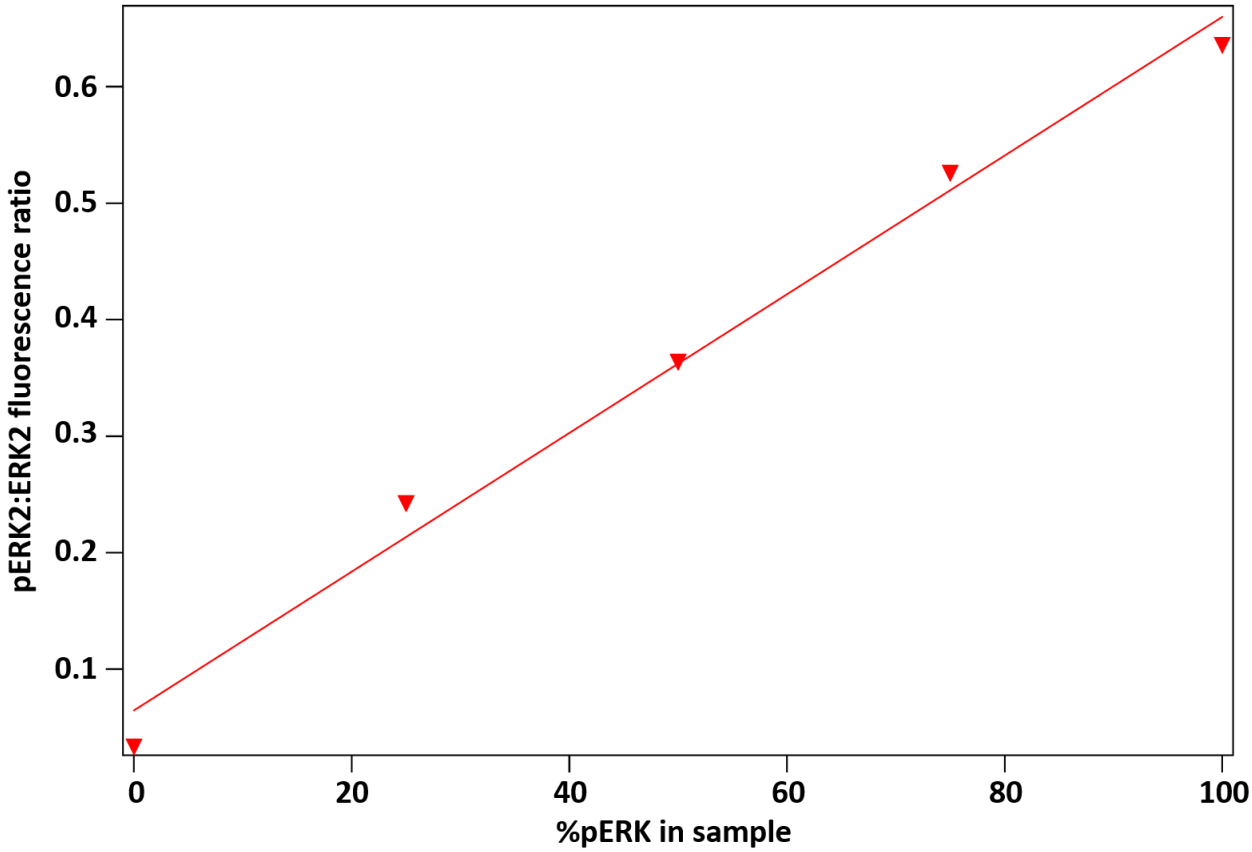

Figure 4.7. pERK2:ERK2 fluorescence ratio with %pERK in the sample using a stage weir device. The left axis reflects the fluorescence from the combined pERK1/2 and total ERK2 antibodies divided by the fluorescence from the pERK1/2 antibody. The result is linear as a function of the %pERK in the sample. In actual clinical samples, the %pERK would be very low in healthy patients. In samples from patients with cancer, the %pERK would generally be higher but would vary considerably depending on the disease and the treatments being received.

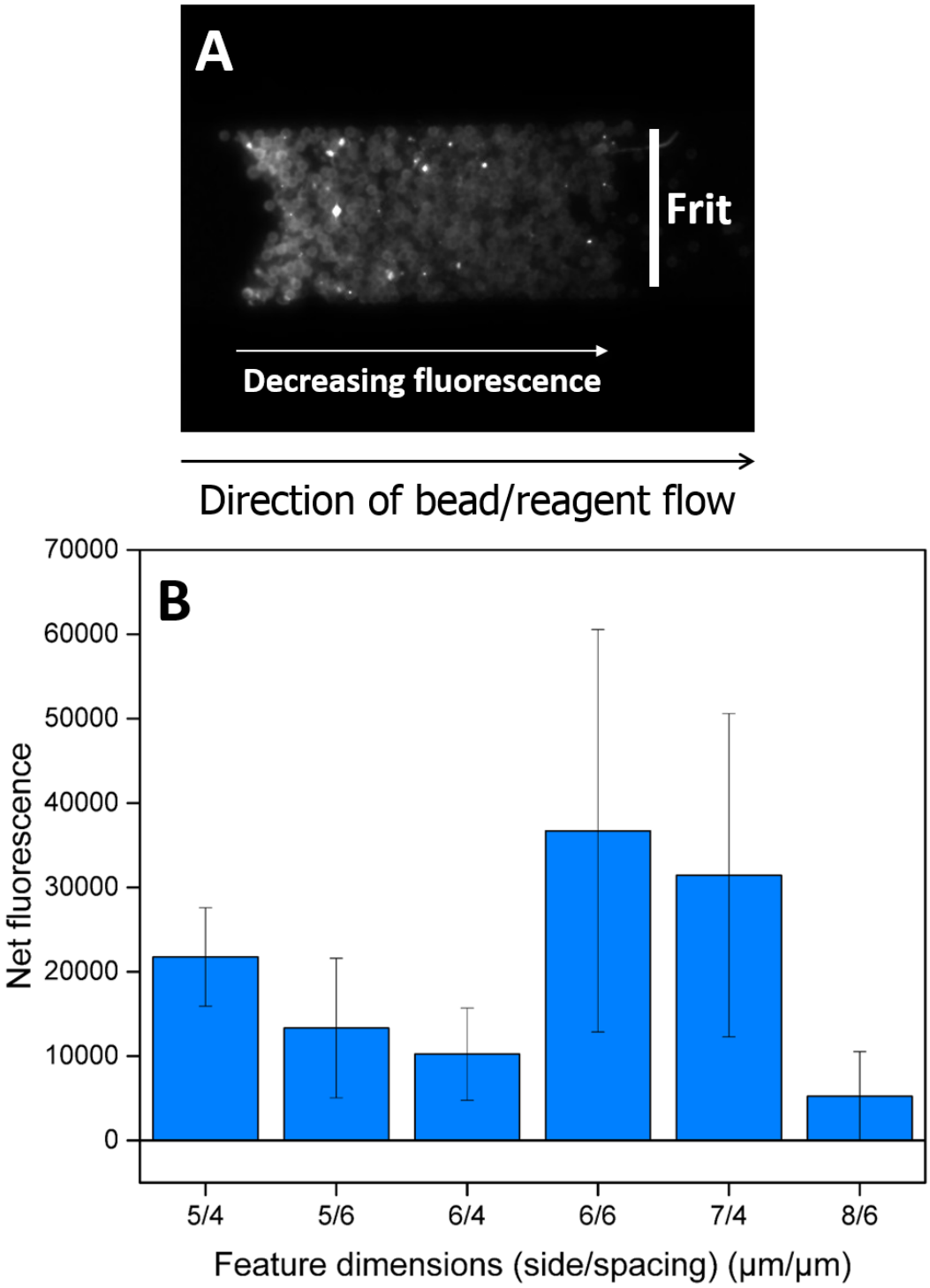

Figure 4.8. Results from initial attempt at on-chip incubation with packed bead bed in flow-frit chips. (A) Fluorescence image of a packed bed with on chip sample incubation. The beads closest to the reagent via are brightest. (B) Assay results showing high variance due to the fluorescence gradient.

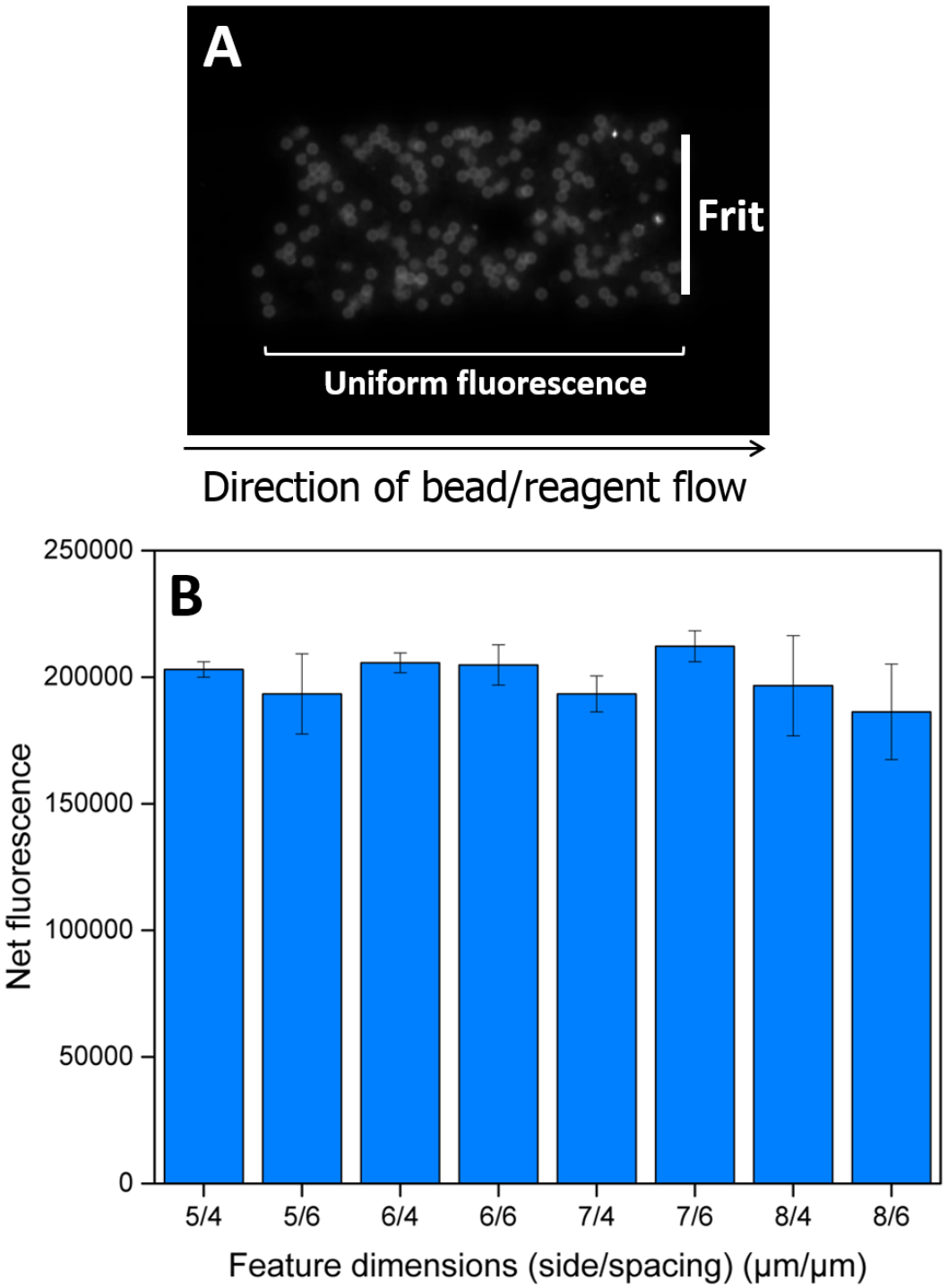

Figure 4.9. Results of experiment evaluating each configuration of flow bed features with off-chip sample incubations. (A) Fluorescence image of flow bed with uniform fluorescence due to off-chip incubations. (B) Assay results showing similar fluorescence and %RSDs for each configuration of flow bed features.

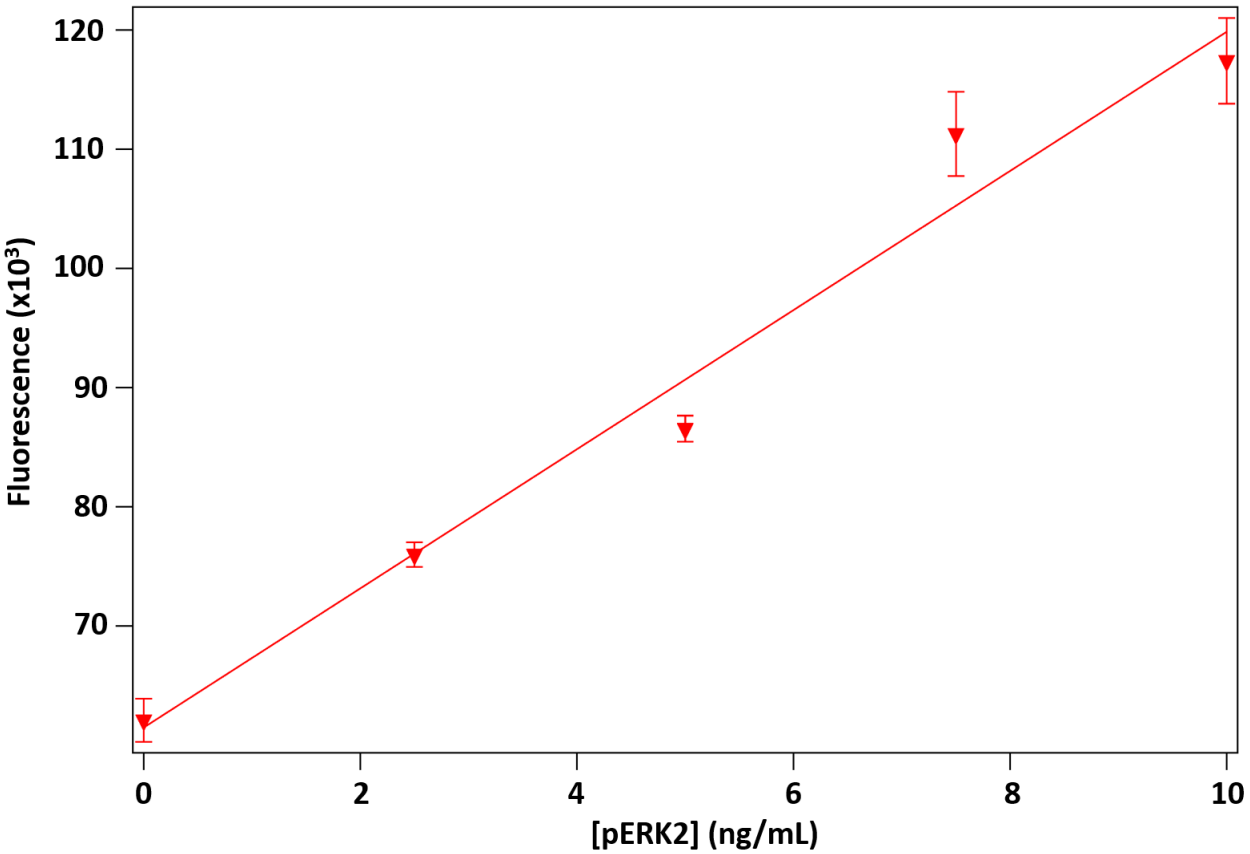

Figure 4.10. Fluorescence response with pERK2 concentration using on-chip sample incubation. The sensitivity is such that various sample concentrations (pM-range) well below physiological concentrations (µM-range) can be distinguished from one another, showing that this assay is suitable for assaying human cell lysate. The exact number of cells required for the assay is something subject to optimization through chip design, since lysing the cells results in dilution of their contents.

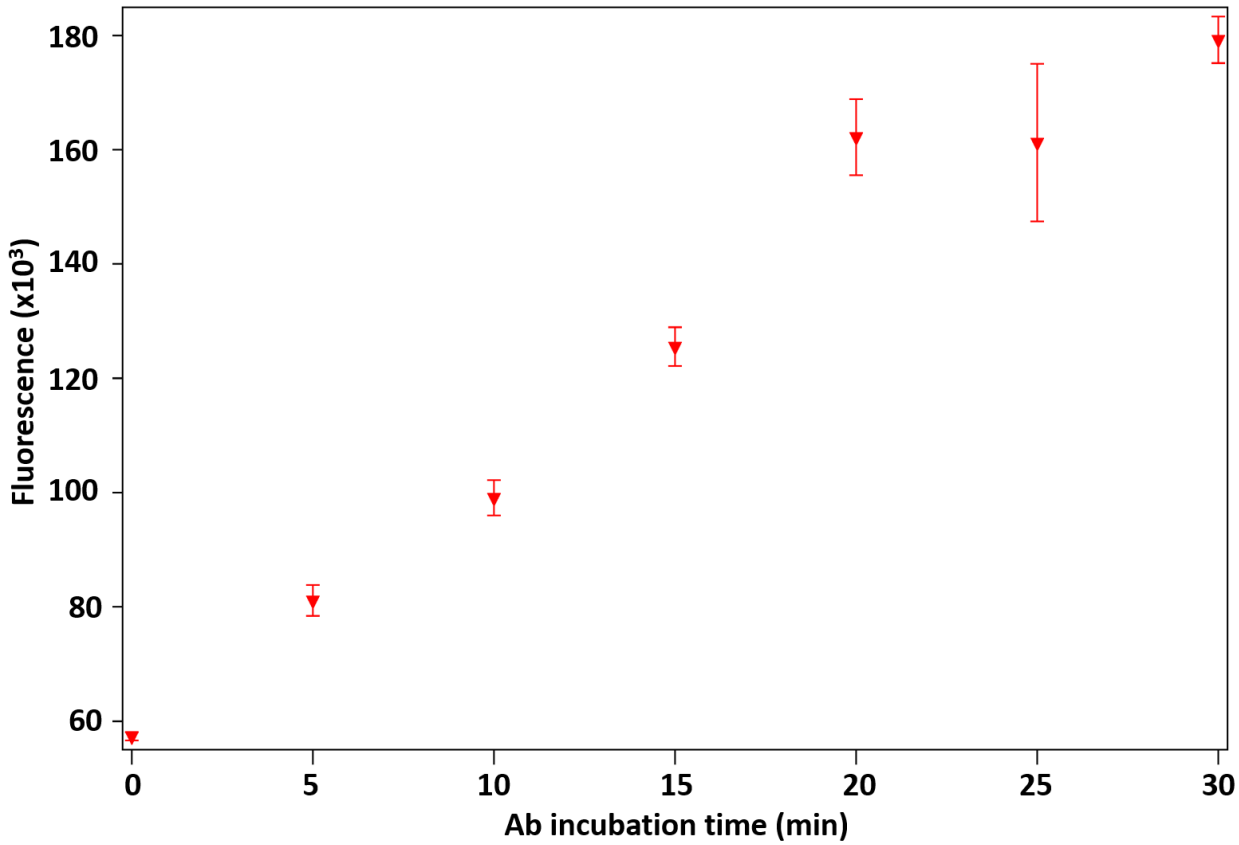

Figure 4.11. Fluorescence signal with dAb incubation time**.** The signal increases steadily until approximately 20 min, then diminishing returns set in. 30 min incubations yield approximately 10% more signal than 20-min incubations, while 20 min incubations yield approximately 64% more signal than 10-min incubations.

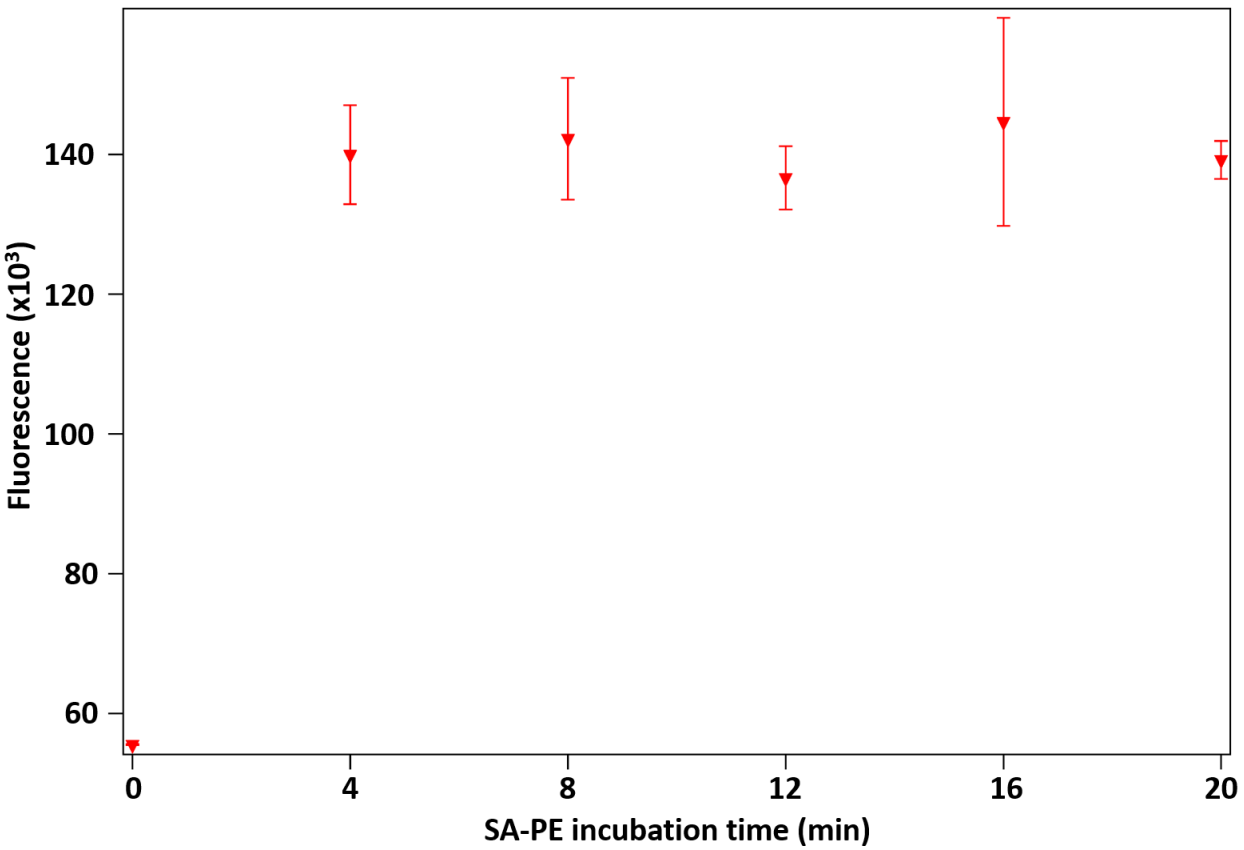

Figure 4.12. Fluorescence signal with increasing SA-PE incubation time. After 4 min, no further increase in the signal was seen. 5 min was used as the SA-PE incubation time in subsequent experiments.

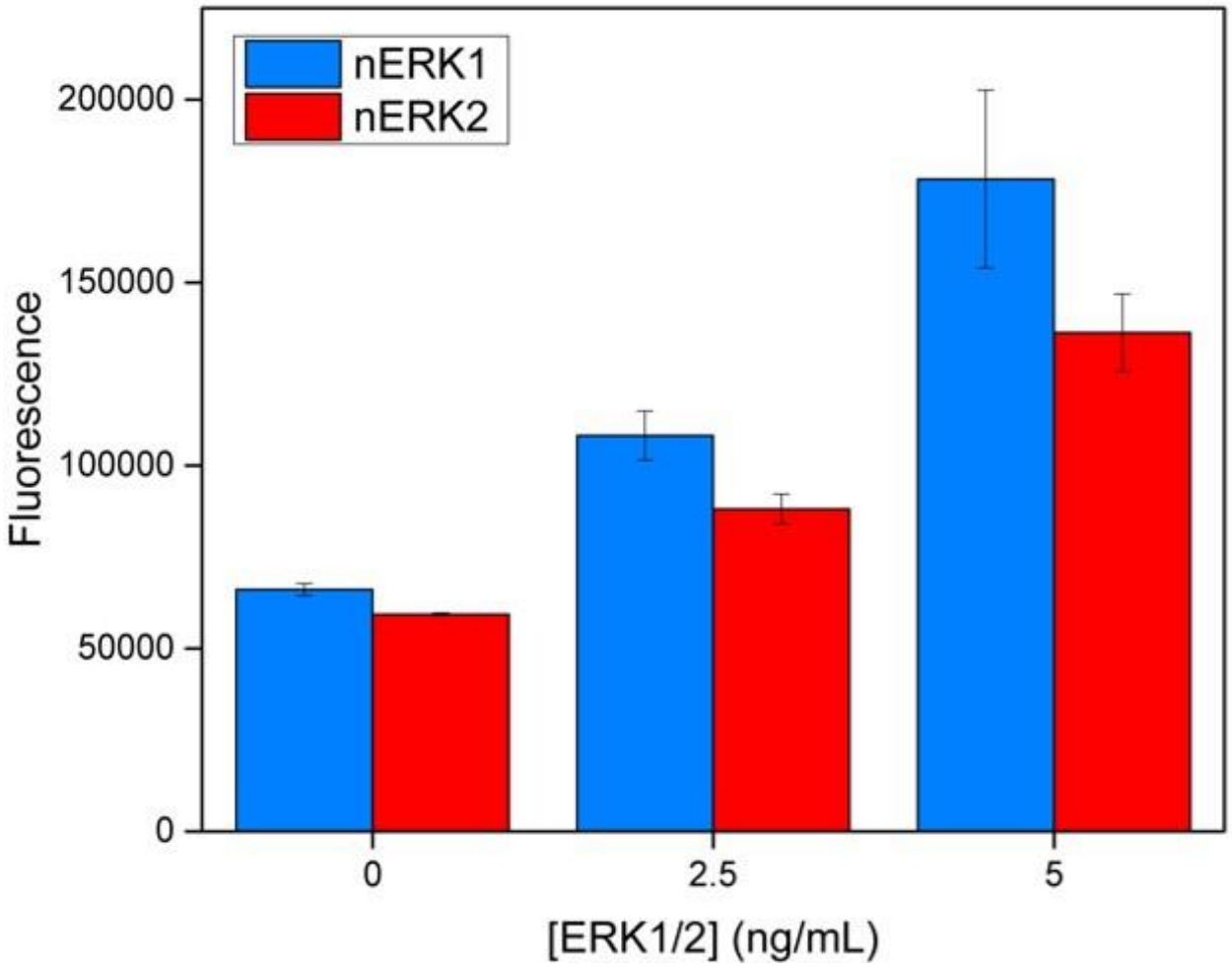

Figure 4.13. Fluorescence signal comparison between nERK1 and nERK2 at varying concentrations. The signal obtained from the total ERK1 dAb shows that it is capable of binding to nERK1 captured by pERK1/2 beads. It also produces somewhat more signal than the total ERK2 dAb.

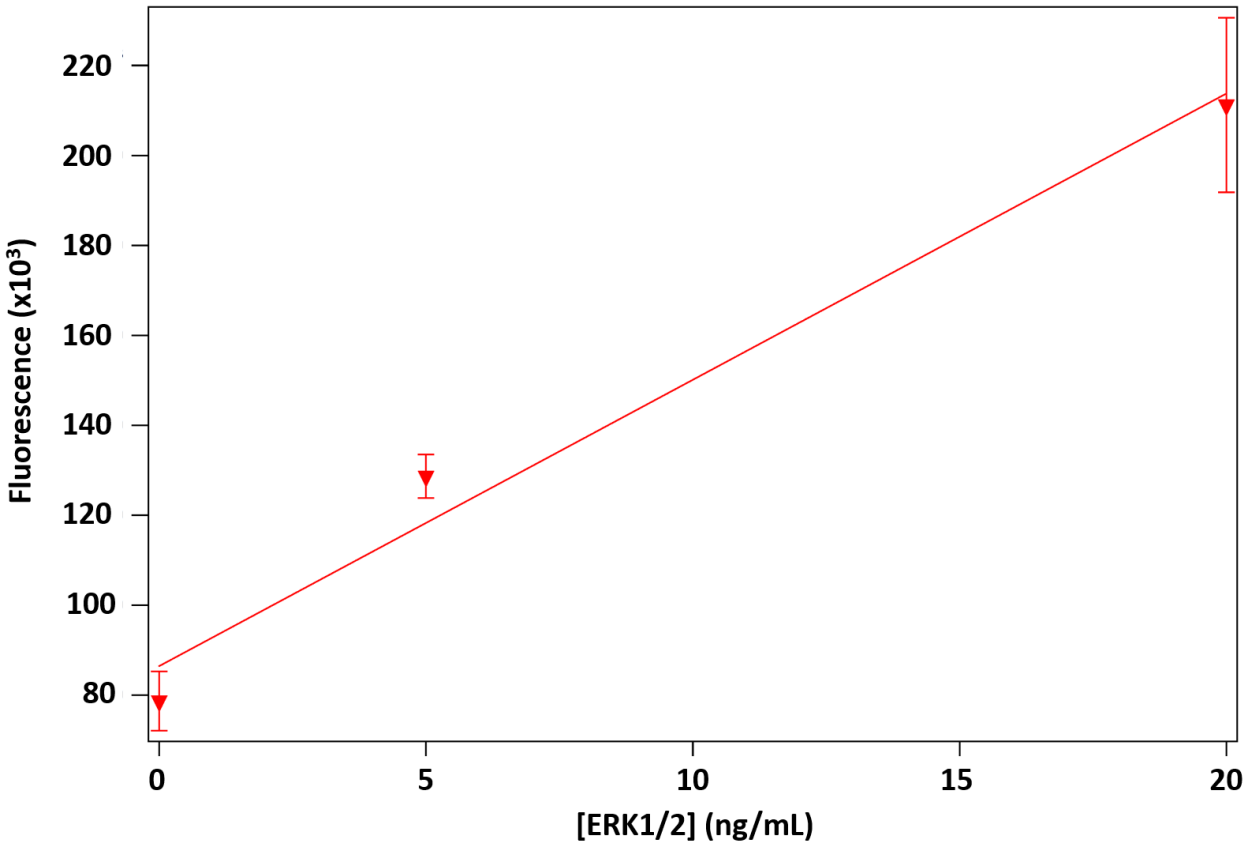

Figure 4.14. Fluorescence signal from the simultaneous detection of nERK1 and nERK2 at varying concentrations. Samples contained equal concentrations of both analytes and the dAb solution contained equal concentrations of both total ERK dAbs. Both analytes are detectable in a single imaging step.

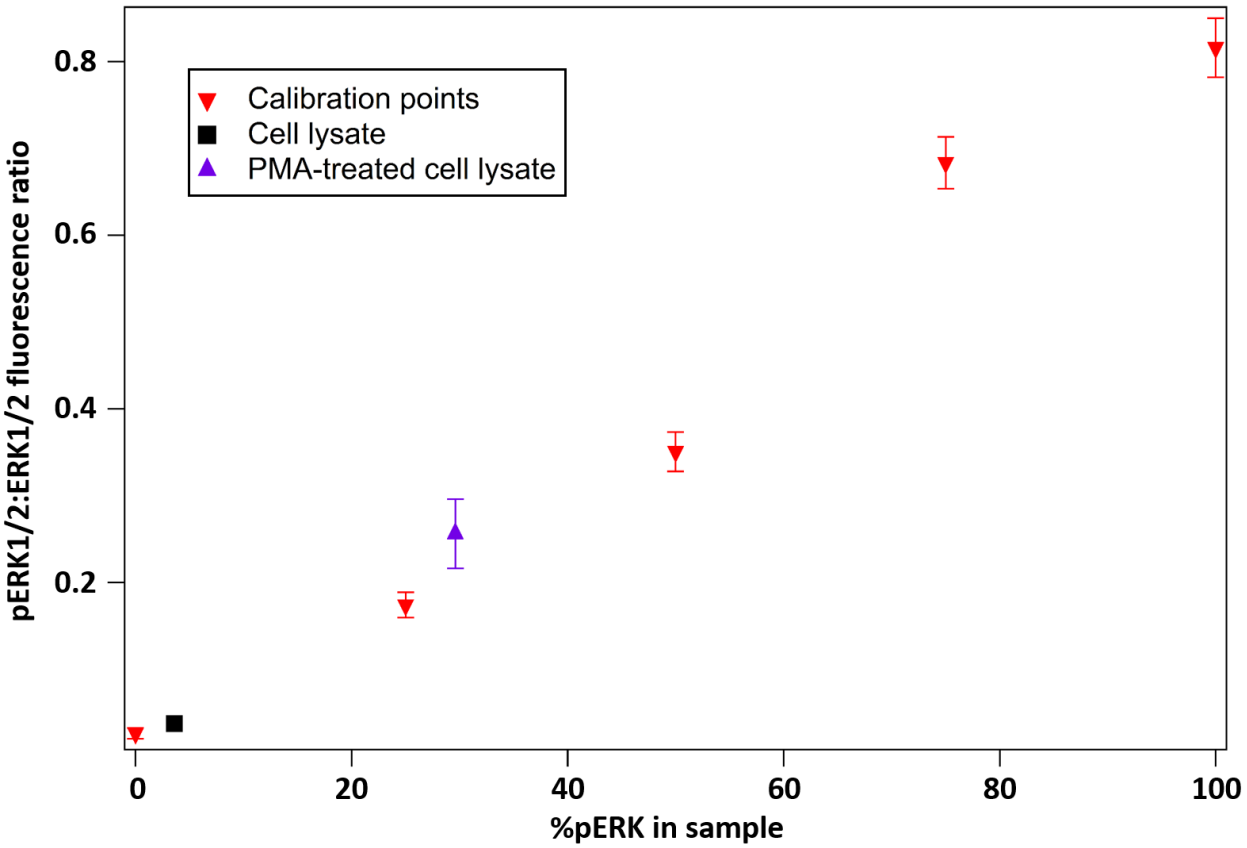

Figure 4.15. pERK1/2:ERK1/2 fluorescence ratio with increasing %pERK in standards and cell lysate samples. The points from standard solutions are displayed as red inverted triangles and are linear as a function of the %pERK. The untreated cell lysate (~3.6% phosphorylation) is shown as a black square. The PMA-treated cell lysate is shown as a blue upright triangle (~30% phosphorylation). The increased phosphorylation in the PMA-treated samples was a result of upstream activation of the MAPK signaling cascade, showing the utility of the assay for detecting mutations in the cascade that lead to increased ERK1/2 activation.

4.6 References

(1) Chen, H.; Abolmatty, A.; Faghri, M. Microfluidic Inverse Phase ELISA via Manipulation of Magnetic Beads. *Microfluid. Nanofluidics* **2010**, *10*, 593–605.

(2) Otieno, B. A.; Krause, C. E.; Latus, A.; Chikkaveeraiah, B. V; Faria, R. C.; Rusling, J. F. On-Line Protein Capture on Magnetic Beads for Ultrasensitive Microfluidic Immunoassays of Cancer Biomarkers. *Biosens. Bioelectron.* **2014**, *53*, 268–274.

(3) Gottheil, R.; Baur, N.; Becker, H.; Link, G.; Maier, D.; Schneiderhan-Marra, N.; Stelzle, M. Moving the Solid Phase: A Platform Technology for Cartridge Based Sandwich Immunoassays. *Biomed. Microdevices* **2014**, *16*, 163–172.

(4) Yu, X.; Xia, H.-S.; Sun, Z.-D.; Lin, Y.; Wang, K.; Yu, J.; Tang, H.; Pang, D.-W.; Zhang, Z.-L. On-Chip Dual Detection of Cancer Biomarkers Directly in Serum Based on Self-Assembled Magnetic Bead Patterns and Quantum Dots. *Biosens. Bioelectron.* **2013**, *41*, 129–136.

(5) Spring, K. R.; Davidson, M. W. Depth of Field and Depth of Focus http://www.microscopyu.com/articles/formulas/formulasfielddepth.html.

(6) Bruus, H. *Theoretical Microfluidics*; Oxford University Press Inc.: New York, 2008; pp. 71–74.

(7) Kim, J.; Johnson, M.; Hill, P.; Gale, B. K. Microfluidic Sample Preparation: Cell Lysis and Nucleic Acid Purification. *Integr. Biol. (Camb).* **2009**, *1*, 574–586.

(8) McClain, M. A.; Culbertson, C. T.; Jacobson, S. C.; Allbritton, N. L.; Sims, C. E.; Ramsey, J. M. Microfluidic Devices for the High-Throughput Chemical Analysis of Cells. *Anal. Chem.* **2003**, *75*, 5646–5655.

(9) Hargis, A. D.; Alarie, J. P.; Ramsey, J. M. Characterization of Cell Lysis Events on a Microfluidic Device for High-Throughput Single Cell Analysis. *Electrophoresis* **2011**, *32*, 3172–3179.

(10) Brown, R. B.; Audet, J. Current Techniques for Single-Cell Lysis. *J. R. Soc. Interface* **2008**, *5 Suppl 2*, S131–8.

(11) Zhou, J.; Ellis, A. V.; Voelcker, N. H. Recent Developments in PDMS Surface Modification for Microfluidic Devices. *Electrophoresis* **2010**, *31*, 2–16.

(12) Green, L. μ and σ for Grouped Data http://www.ltcconline.net/greenl/courses/201/descstat/meanSDgrouped.htm.

(13) ATCC. Jurkat, Clone E6-1 Culture Method http://www.atcc.org/products/all/TIB-152.aspx#culturemethod.

(14) Phospho-ERK1 (T202/Y204)/ERK2 (T185/Y187) DuoSet IC http://www.rndsystems.com/pdf/DYC1018B.pdf.

(15) Deutscher, M. P. Maintaining Protein Stability. *Methods Enzymol.* **1990**, *182*, 83–89.

(16) Fujioka, A.; Terai, K.; Itoh, R.; Aoki, K.; Nakamura, T.; Kuroda, S.; Nishida, E.; Matsuda, M. Dynamics of the Ras/ERK MAPK Cascade as Monitored by Fluorescent Probes. *J. Biol. Chem.* **2006**, *281*, 8917–8926.

(17) Bhalla, U. S. Signaling in Small Subcellular Volumes. II. Stochastic and Diffusion Effects on Synaptic Network Properties. *Biophys. J.* **2004**, *87*, 745–753.

(18) Saviranta, P.; Okon, R.; Brinker, A.; Warashina, M.; Eppinger, J.; Geierstanger, B. H. Evaluating Sandwich Immunoassays in Microarray Format in Terms of the Ambient Analyte Regime. *Clin. Chem.* **2004**, *50*, 1907–1920.

(19) Srisa-Art, M.; Dyson, E. C.; deMello, A. J.; Edel, J. B. Monitoring of Real-Time Streptavidin-Biotin Binding Kinetics Using Droplet Microfluidics. *Anal. Chem.* **2008**, *80*, 7063–7067.

(20) Seger, R.; Krebs, E. The MAPK Signaling Cascade. *FASEB J.* **1995**, *9*, 726–735.

(21) Balmanno, K.; Cook, S. J. Tumour Cell Survival Signalling by the ERK1/2 Pathway. *Cell Death Differ.* **2009**, *16*, 368–377.

(22) Kohno, M.; Pouyssegur, J. Targeting the ERK Signaling Pathway in Cancer Therapy. *Ann. Med.* **2006**, *38*, 200–211.

CHAPTER 5

DEVELOPMENT OF A FREEZE-THAW VALVING SYSTEM FOR MICROFLUIDIC DEVICES

5.1 Introduction

In microfluidic devices that use multiple reagent and sample solutions, valves are necessary to control and direct the fluid flow. They serve purposes such as modulating which samples are being assayed at a given time or which reagents are flowing through the chips. Many valving strategies are possible depending upon the chip design. Devices fabricated from the elastic material PDMS can be valved by using mechanical pressure to pinch the channel shut. The Whitesides group has demonstrated numerous designs for the purpose, including screw valves that are manually opened and closed and solenoid valves that use a magnetically-driven rod to pinch the channel shut.[1] Another major class of valves for PDMS devices comes from the Quake group. These use pneumatic pressure in multilayer devices to pinch shut default-open channels or push open default-closed channels.[2,3] These designs all have the disadvantages of either requiring the fabrication of complicated chips, or in the case of the manual valves, of not being automatable. For our purposes, the desired valves would be pre-fabricated and reusable, used with a simple single-layer device, and would require minimal alignment. The Ramsey and Walt groups have demonstrated such a device, wherein an aligned PDMS/glass chip is locked into place underneath mechanically-actuated, computer-controlled pinch valves.[4] That system used chips made from PDMS, but a valving system usable with solid materials such as glass or plastic would have broader applications.

One possible valving method that meets our requirements is the freeze-thaw valve (FTV). For FTVs, the fluid in the channel is cooled until it freezes with the frozen plug preventing fluid flow. In microfluidic devices fabricated from smooth materials like PDMS and glass, there are few nucleation sites for ice crystals to form so supercooling the liquid in order to freeze it may be necessary;[5,6] small volumes (<1 µL) of pure water may require a temperature as low as -35 °C to freeze,[5] while another study observed water freezing at -17 ºC.[7] The frozen channel is opened by thawing, either through the application of heat or the removal of the cooling source. While some early demonstrations of FTVs used cold fluids such as liquid nitrogen[8] or carbon dioxide[9,10] to accomplish the freezing, it is also possible to utilize Peltier devices to freeze and thaw channels.[6,11]

Peltiers consist of a layer of alternating semiconductors sandwiched between two parallel insulators. The material used to make the semiconductors is thermoelectric and can carry heat in addition to electrons.[12] Through the application of voltage, heat is pumped across the device and a temperature differential is created between the two insulating layers. By stacking several Peltiers of successively smaller size, a cascading temperature differential can be created from tier to tier with the net effect of producing much colder temperatures than are possible with a single Peltier. Temperatures sufficient to freeze supercooled water can be generated this way. The use of multi-Peltier tiers also makes it possible to hold the first tier close to the supercooling temperature so that freezing may be rapidly effected by the second tier when desired.[6] Figure 5.1 shows one such 2-tier Peltier configuration that could be used as a FTV. A constant-temperature water block is used as a heat sink for the base Peltier (BP). It also functions as a constant hot-side reference temperature for the base Peltier, which is critical for ensuring the stability and reproducibility of the Peltier's cold-side temperatures.[6] In a freeze cycle, the cold-side

temperature of the base Peltier, T_{BP}, sets the hot-side temperature for the valve Peltier (VP). T_{VP}, the cold-side temperature of the valve, is thus colder than T_{BP}. Examples for T_{BP} and T_{VP} are -16 °C and -40 °C, respectively. Reversing the voltage polarity switches the hot side and cold side of a Peltier to induce thawing. In this case, T_{BP} sets the cold-side temperature for the valve, and T_{VP} can easily reach +50 °C or more. A major advantage of Peltier-based FTVs is that cooling and heating are actuated by simple low voltage control. Multiple Peltier devices can be simultaneously used as valves with a single base Peltier to remove heat.

One disadvantage of the FTVs is that their response times are generally slower than other valves.[6] Depending on the configuration of the system, opening and closing the valves can take seconds to tens of seconds, so they are not suitable for applications that demand immediate actuation. The pERK1/2:ERK1/2 immunoassay developed to this point does not require rapid on/off valving action, so FTVs are acceptable as the valving mechanism.

In this chapter, a Peltier-based freeze-thaw microfluidic valving system under computer control is built and characterized. A thermal camera is used to monitor the system for hot spots. Mixing tee chips for imaging the valving action are designed, fabricated, and employed to demonstrate the efficacy of the valves. Ultimately, it is shown that freezing and thawing of a given valve is repeatable over many cycles with reproducible timescales suitable for the needs of the pERK1/2:ERK1/2 immunoassay.

5.2 Materials and methods

5.2.1 Materials and reagents

Sylgard 184 PDMS was purchased from Ellsworth Adhesives (Germantown, WI) and was prepared according to the manufacturer's instructions at a 10:1 elastomer/cross-linker ratio. Tween-20 was purchased from BioRad Laboratories (Hercules, CA). Glass photolithography

substrates (5” x 5” soda lime) were purchased from Nanofilm (WestLake Village, CA). Nano-Strip 2X was purchased from KMG Chemicals (Fremont, CA). AZ-400K was purchased from AZ Electronic Materials USA (Somerville, NJ). Chromium etchant and 10:1 buffered oxide etch (BOE) were purchased from Transene Corp. (Danvers, MA). SU-8 2050 photoresist and SU-8 developer was purchased from MicroChem (Newton, MA). MF-319 photoresist developer was purchased from Rohm and Haas Electronic Materials (Marlborough, MA). P-type 6” crystalline Si wafers were purchased from University Wafer (Boston, MA). D263 glass was purchased from S.I. Howard Glass Company (Worcester, MA). Octyltrichlorosilane was purchased from Sigma-Aldrich (St. Louis, MO). Contrad 70 detergent, 10x phosphate-buffered saline (PBS, pH = 7.4), 10% bovine serum albumin (BSA) in PBS, acetone, 200 proof ethanol, fluorescein, and polystyrene Petri dishes were purchased from Thermo Fisher Scientific (Waltham, MA).

The base Peltier (TE-63-1.4-1.15) was purchased from Thermoelectric Technology (Traverse City, MI). The valve Peltiers (C2-04-0102) were purchased from Tellurex (Traverse City, MI). Pyrolytic graphite (17 μm thick), thermally conductive silver epoxy, adjustable 10-Ω power resistors, and an Arduino UNO R3 were purchased from Digi-Key (Thief River Falls, MN). Thermally conductive double-sided tape was purchased from Thor Labs (Newton, NJ). DP-805 waterproof acrylic adhesive was purchased from 3M (St. Paul, MN). Power supplies were purchased from BK Precision (Yorba Linda, CA). NPT-27 brass elbow fittings were purchased from Swagelok (Solon, OH). A 4-channel motor controller was purchased from Jameco Electronics (Belmont, CA). Tygon tubing was purchased from McMaster-Carr (Elmhurst, IL).

All aqueous solutions were prepared with deionized (DI) water from a NANOpure Diamond system (Barnstead International, Dubuque, IA), including PBS-BT (PBS + 1% BSA +

0.05% Tween-20) and PBS-BTF (PBS-BT + 5 μM fluorescein). PBS-BT is referred to as "buffer" and PBS-BTF as "dye" throughout the text.

5.2.2 Mixing tee chip design and fabrication

The chips used to study the freeze-thaw valves featured a mixing tee where the flow from two channels could be imaged. The chips consisted of two sample inlets (buffer and dye) with serpentine valving regions that converge to form a tee-intersection or mixing tee. A schematic of the chip is shown in Figure 5.2. The channels are 40 μm deep and 100 μm wide. The channels in the serpentine regions are 60 μm wide to increase the density of channels over the Peltiers. The mixing tee is circled in red. Following initial studies with the 2-valve single mixing tee chips, a second generation chip was designed for studying four valves at once. It features 4 inlet vias and 4 valving regions and thus three mixing tees. A schematic of the chip is shown in Figure 5.3. The mixing tees are again circled in red. Switchbacks from the dye channels that equalize the volume between the dye/buffer channels are boxed in blue. Channel dimensions are the same as the 2-valve single mixing tee chip.

Designs for the mixing tee chips were created in TurboCAD Professional 14. Mixing tee designs were written into a 5" x 5" soda lime glass substrate coated with chromium and positive photoresist using a Heidelberg Instruments DWL66 laser lithography system. The photoresist was developed for 45 s with AZ-400k and the exposed chromium was removed with chromium etchant. The remaining bulk photoresist was stripped with acetone and residual resist was removed with 70% Contrad. This substrate was then used as a mask to pattern designs into negative resist on a 6" silicon wafer. To promote adhesion of the negative resist, the native oxide layer was removed from the wafer by immersing the wafer in the 10:1 BOE for 30 s prior to the photolithography steps.

SU-8 2050 was then spun at 3200 rpm for 30 s and baked at 95 ºC for 10 min to produce a 40-µm thick layer of SU-8. This wafer was exposed to UV light for 15 s in a mask aligner (approximately 160 mJ/cm^2 radiation dose) and post-exposure baked at 95 °C for 6 min. Development was performed in SU-8 developer for 5 min. The wafer was finally hard-baked at 160 °C for 30 min and silanized with octyltrichlorosilane in a vacuum oven (Thermo Fisher Scientific) at 115 °C for 1 h. PDMS/glass chips were fabricated from the wafer molds as described in Chapter 2, except 2" x 3" x 0.0082" D263 glass was used instead of microscope slides.

5.2.3 Valve construction

To dissipate the heat generated by the Peltiers, the base Peltier is mounted on a custom water block constructed from a block of brass (2.6" x 1.8" x 1"). Serpentine water channels were machined in its underside and sealed with a Lexan cover, screws, and waterproof acrylic adhesive (DP805; 3M, St. Paul, MN). A refrigerated bath circulator (4100R20; Thermo Fisher Scientific) operated with 15 °C water was attached to the water block. Screw holes were drilled into the top of the water block to secure the block to a custom-made acrylic stage. A side view of the water block with its water tubing and stage attached is shown in Figure 5.4A. The stage sits above the block and is designed to fit on the stage of a Nikon Ti-U Eclipse microscope. Figure 5.4B shows a top-down view of the stage and block with a 20 mm x 40 mm Peltier (referred to as the base Peltier) mounted on the block. Thermally-conductive silver epoxy (Resin Technology Group LLC, South Easton, MA) was used to permanently bond the hot side of the base Peltier to the water block.

The valves operate well below the dew point, so the Peltiers were sealed in PDMS to protect their internal semiconductors from water condensation. This was accomplished by

submerging the Peltiers into uncured PDMS, degassing the PDMS, and curing overnight at 65 °C. After curing, excess PDMS was cut away from the Peltiers' surfaces and sides such that the only remaining PDMS was encasing the internal semiconductors.

A 2-tier, 5-Peltier setup forms the core of the freeze-thaw valve system. The first tier consists of the base Peltier with a sheet of pyrolytic graphite (17 μm thick) attached to the cold (upper) side. Pyrolytic graphite has extremely high lateral thermal conductivity,[13] and is used to spread out the heat pumped by the valve Peltiers (4.3 mm x 4.3 mm), four of which are mounted on the graphite with thermally conductive double-sided tape. A photo of the system is shown in Figure 5.5. A chip is affixed to the stage with rare-earth magnets and one of its mixing tees (boxed in red) is directly over the microscope objective. The valves and valving regions are circled in white. The surface of the base Peltier surrounding the valve Peltiers is insulated by styrofoam pellets embedded in PDMS to prevent condensation buildup.

5.2.4 Peltier control electronics

Two power supplies (9110; BK Precision, Yorba Linda, CA) are used to power the Peltiers and freeze-thaw electronics. The base Peltier is run at a constant DC current of 5.1 A. A second power supply is set to a constant voltage of 4.5 V with a maximum current of 3.9 A and provides power for the four valve Peltiers via the electronics used to modulate their temperatures. This supply is connected to a motor controller (RS011MC; Jameco Electronics, Belmont, CA) with 4 output channels. Each channel consists of an H-bridge that is used to power one valve Peltier. While the voltage applied by these H-bridges is constant, the motor controller includes logic circuitry that modulates each channel's polarity and duty cycle. Changing the duty cycle of a channel alters its current output by setting the percentage of time the Peltier is actively pumping heat and thus drawing power. Also, as the motor controller's

outputs have a minimum voltage that exceeds the valve Peltiers' maximum operating voltage, a 2.8-Ω power resistor (Vishay Huntington Electric, Malvern, PA) is wired in series between the positive leads of each channel and its corresponding Peltier in order to serve as a voltage divider. An Arduino UNO R3 (SmartProjects, Ivrea, Italy) microcontroller board is used to control the logic on the motor controller. A 5-Volt Vcc pin provides the power for the motor controller's logic circuitry. Digital output pins regulate the polarity of each channel by applying either +5 V for freeze mode or 0 V for thaw mode, and pulse-width modulation (PWM) pins set the channels' duty cycles in increments of approximately 0.392%.

The Arduino is powered and controlled by a USB connection to a PC. Custom software for controlling the freeze-thaw valves was written in LabVIEW (National Instruments, Austin, TX). National Instruments' LabVIEW Interface for Arduino Toolkit was utilized to connect LabVIEW and the Arduino microcontroller.

5.2.5 Image collection

The complete imaging setup is shown in Figure 5.6. Chips were placed atop the valves and custom stage on a Nikon Ti-U Eclipse inverted fluorescence microscope. A Nikon B-2E/C optical filter cube was used to select excitation/emission wavelengths for imaging the fluorescein in the channels. Fluorescence videos of the microchannels were recorded with an ExwaveHAD Color Video Camera (Sony Corporation of America, New York, NY) using GrabBee software (VideoHome Technology Corp., New Taipei City, Taiwan). An A35sc infrared camera (FLIR Systems, Wilsonville, OR) was mounted above the chips and used to take thermal images of the valves. Thermal pictures and videos were recorded with FLIR Tools+ software (FLIR Systems).

5.3 Results and discussion

The valves are based on a 2-tier Peltier configuration that creates a cascaded temperature

differential where the top valve Peltier can reach temperatures suitable for freezing and thawing aqueous solutions in microfluidic channels. Four valves are needed for the pERK1/2:ERK1/2 assay to control the flow of wash buffer, pERK1/2 dAb, tERK1/2 dAb, and SA-PE. The valve Peltiers were spaced evenly on a base Peltier to prevent or minimize the overlap of heat from their hot sides. Though initial testing placed all four valves at the base Peltier's edge closest to the microscope objective, two were moved backwards to take advantage of colder surface temperatures on the base (Section 5.3.2). The unused topside of the base Peltier is insulated with PDMS and styrofoam, and the Peltier pumps the system's heat into a chilled water block. The system is affixed to a custom stage and mounted inside an inverted microscope for imaging the chips. The completed system is shown in Figure 5.5 and is characterized here.

5.3.1 Temperature characterization of valving system

In order to produce valve temperatures suitable for freezing and thawing, each component of the freeze-thaw block was characterized during its construction to determine which parameters produce the coldest temperatures. The temperature of the water in the block was set to 15 °C. Lower temperatures were initially tried, but condensation buildup near the system's electronics proved to be problematic as there was no straightforward way of insulating the water block. The 15 °C water was not cold enough to produce condensation and proved effective for generating sufficiently cold temperatures for valve freezing.

The base Peltier was characterized first. Early in the construction process, the topside of the base Peltier was imaged with the FLIR A35sc infrared camera with and without pyrolytic graphite in place. The thermal images showed a nonuniform surface temperature of the base Peltier with some areas significantly warmer than others. These are shown in Figure 5.7. Figure 5.7A depicts the base Peltier near the microscope objective and is shown to provide a reference

orientation for the images. The warm spots (boxed in white) were present at currents >0.4 A for the base Peltier. This is shown in Figure 5.7B-G, with B-D showing thermal images of the base Peltier with graphite and E-G showing images without it. These hot spots likely arise because their locations are farthest from the cooling channel in the water block as well as from the center of the base Peltier, and thus they do not dissipate heat as efficiently as the rest of the base Peltier. While this study was qualitative and measurements of the base Peltier's temperature were not determined, the warm regions were insufficiently cold to freeze water. Due to the temperature heterogeneity across the base Peltier and the regions not suitable for valving, the temperature across the base Peltier was measured to locate potential sites for the FTVs.

To find colder regions suitable for mounting the valve Peltiers, the base Peltier was further characterized by directly measuring the temperature at various points along its surface using a Barnstead-Thermolyne pyrometer (Thermo Fisher Scientific) and thermocouple probe (Omega Engineering, Stamford, CT). The thermocouple's tip was sandwiched between the Peltier and a thick piece of styrofoam to ensure that the thermocouple would only be measuring the Peltier's temperature. These measurements located four cold regions (white squares in Figure 5.8) that were suitable for mounting the valve Peltiers, both in terms of their temperatures (-14 °C, -17 °C, -14 °C, and -7 °C for valves 1-4, respectively) and the spatial orientation of the valved regions on the intended assay chip design. This study further revealed that the base Peltier as a whole was coldest (average temperature of approximately -16 °C) at a current of 5.1 A.

Finally, styrofoam pellets embedded in PDMS were used to insulate the exposed surface of the base Peltier. This prevented frost buildup and minimized condensation deposits on the base Peltier. Also, as chips do not occupy the region of the base Peltier behind the valve Peltiers,

the styrofoam layer was made considerably thicker there in order to further reduce the amount of heat the Peltier would pump from the air. Ultimately, valve Peltiers could reach temperatures several °C colder with an insulated base Peltier than with a non-insulated base Peltier.

5.3.2 Temperature and thermal characterization of valve Peltier

Over the course of building the FTV system, its performance – namely, the temperatures produced by the Peltiers at various parameters – needed to be characterized. This was necessary to establish that the Peltiers could produce temperatures appropriate for freezing and thawing on command. It was also a means of determining the stability and reproducibility of temperatures produced by the system, i.e., whether a desired temperature could be reliably produced at any time with given settings, and whether that temperature would remain stable.

Peltiers have a voltage (V_{max}) at which they produce their maximum temperature differential, and thus coldest cold-side temperature (T_{BP}, T_{VP}). Applying voltages beyond this point will not reduce either T_{BP} or T_{VP}; their temperatures will instead increase due to the Peltiers' ability to dissipate its waste heat being exceeded.[12] To overcome this limitation, the best strategy is to use pulse-width modulation (PWM) to apply the Peltier's V_{max} at varying duty cycles. In this strategy, the Peltier is either off where no current is generated or at V_{max}. The current, and thus temperature, is varied according to the fraction of time that the Peltier spends at V_{max}.[12] At 100% duty cycle with V_{max}, the current through a Peltier will be its I_{max}. V_{max} is a function of the hot-side temperature and was determined for each Peltier by increasing the applied voltage until the Peltier's cold-side temperature no longer decreased with additional voltage.

The temperatures of the valve Peltiers were measured with a thermocouple in the same manner as the base Peltier. The base Peltier was allowed to equilibrate for approximately 5 min

prior to measuring the valve temperatures. The valve temperatures were calibrated by varying the PWM (at ~V_{max}) on the Arduino between 0 (0% duty cycle) and 255 (100% duty cycle) by increments of 5. Temperatures were measured first in closed (freeze) mode, then the voltage polarity was switched to set the valves to open (thaw) mode and the temperatures were measured again. This process was repeated for all 4 valves. Figure 5.9 shows the results, with valve 1 represented by black circles, valve 2 by blue circles, valve 3 by red diamonds, and valve 4 by purple inverted triangles. The lowest temperatures achieved were -38.5 °C for valve 1, -43.1 °C for valve 2, -38.6 °C for valve 3, and -31.3 °C for valve 4. The open mode temperatures of the valves were not determined past +50 °C as temperatures beyond this are unneeded. After the valves were characterized, temperatures were periodically monitored on random days to confirm the accuracy and reproducibility of the temperatures produced. Measured temperatures were found to deviate from recorded temperatures by no more than a few tenths of 1 °C.

During this process, only the valve being measured was powered on; all others were off. This mimics assay conditions, as the valves will only be active when freezing or thawing. When powered off, they are cold enough to maintain the default frozen or closed state because the top surface of the valve Peltier will equilibrate to a temperature close to that of the base Peltier underneath. This temperature is well below the freezing point of water.

5.3.3 Freeze/thaw valve efficacy with single mixing tee chips

The first generation of chips designed to study and demonstrate the efficacy of the freeze-thaw valves featured a single mixing tee (Figure 5.2). Prior to experimentation, bonded chips were filled with 200 proof ethanol to wet their channels and ensure the removal of air bubbles. The sample vias were then vacuumed empty, one was filled with 10 µL PBS-BT (buffer solution), the other with PBS-BTF (dye solution), and vacuum was applied to the waste

via for 30 s to replace the ethanol. The prepared chip was placed atop the freeze-thaw block with the serpentine valving regions sitting over the two valve Peltiers (Figure 5.5). A vacuum line with a 25-gauge needle was placed in the chip's vacuum via as shown in Figure 5.6. This line was controlled with a remote valve so that fluid flow could be turned on and off without disturbing the chip.

The serpentine valving regions of the channels pass over separate valve Peltiers. The serpentines add to the channel length providing more potential nucleation sites for freezing and increasing the fluid/valve contact time. Four potential valving scenarios are possible: dye valve open:buffer valve open (DO:BO, Figure 5.10A), dye valve open:buffer valve closed (DO:BC, Figure 5.10B), dye valve closed:buffer valve open (DC:BO, Figure 5.10C) and both valves closed (DC:BC, not shown). The fluid flow directions for each case are shown in Figure 5.10A-C. As the two channels leading to the mixing tee are identical in length and volume, and as the flow rate from each side of the tee is identical, fluorescence images of the mixing tee will appear half fluorescent and half dark for the DO:BO case (Figure 5.10A), completely fluorescent for the DO:BC case (Figure 5.10B), and completely dark for the DC:BO (Figure 5.10C). Arrows indicate direction of flow, and the arrow size indicates relative flow rate. The complete fluorescence in the DO:BC case and complete darkness in the DC:BO case is due to the open-valve's reagent diffusing into the closed-valve reagent's side of the tee.

The mixing tee was monitored for the duration of every experiment, beginning with both valves in the open state (DO:BO) (shown in Figure 5.11A) where there is a 50/50 flow from the dye and buffer channels into the tee. Valves were closed by setting them to their lowest possible temperature. Thawing was induced by setting them to 25 °C. When a valve closed, a pulse of fluid is generated that penetrates into the opposite channel (Figure 5.11B). This is due to the

increased volume from the ice formation in the serpentine channels. Likewise, when a valve is re-opened, the slightly reduced volume in the valve region from the thawing ice manifests as a retreat of fluid in the tee (Figure 5.12A-C) followed by the tee returning to its DO:BO state (Figure 5.12D). Neither the freeze pulse nor the thaw retreat significantly affect the downstream bead regions in assay chips.

Figure 5.13 shows a time series of a freeze/thaw cycle (taken from a fluorescence video). Inset in each fluorescence image is a thermal image of the two valves, the locations of which are highlighted in white. The thermal images were taken simultaneously with the fluorescence images. The initial state of the system with both valves open (DO:BO) is shown in Figure 5.13A. In Figure 5.13B, a pulse from closing the buffer valve (DO:BC) is seen by the concave deflection of the dye solution back into the dye channel. Closing of the buffer valve is shown by the increase in the depth of blue in the thermal image with the Peltier at its coldest temperature. In Figure 5.13C, the dye diffuses into the buffer channel while flowing down the tee channel. Figure 5.13D shows the beginning of the thaw process for DO:BO (orange area in thermal image) with the buffer valve set to room temperature. In Figure 5.13E, thinning of the dye on the buffer side of the tee is evident as non-fluorescent buffer returns to the tee, and in Figure 5.13F, the fluid flow is back to its initial state with the 50:50 mix flowing down the tee channel.

5.3.4 Double mixing tee chips and reproducibility of valve times

The first generation of mixing tee chips featured only two valving regions. This was suitable for establishing proof-of-concept for the FTVs, but for studying four valves simultaneously, a 4-valve chip was designed (Figure 5.3). This was used to study the reproducibility of open/close times of 4 valves over the course of three experiments. In all experiments, the time between setting the close temperature (-43 °C) and the appearance of the

freeze pulse (Figure 5.11) was used as the close actuation time, while the time between setting the open temperature (+25 °C) and the appearance of the reverse thaw pulse (Figure 5.12) was used as the open actuation time.

In the first experiment, the system was cycled between opening (+25 °C) and closing (-43 °C). Figure 5.14 shows that while the close time (represented by blue inverted triangles) trends slightly downward over time, the open time (red boxes) trends slightly upward. The freeze/thaw times are reproducible within several seconds; the average close time was 37.1 s with a standard deviation of 4 s, while the average open time was 13.4 s with a standard deviation of 2 s. Over the course of 9 freeze/thaw cycles, no valve closing took longer than 44 seconds and no valve opening took longer than 16 seconds.

In an actual assay, the valves cycling between the open and closed states in such a rapid fashion is not required. Once closed, the valve Peltier can either be set to an intermediate temperature not conducive to initiate thawing, or shut off altogether. This reduces the valve opening time and prevents excessive frost/condensation buildup. If shut off, the valve would equilibrate to the base Peltier temperature; this varies from -8.3 °C to -16.7 °C depending on the valve. This temperature variance between valves is a function of their proximity to the cooling block's water channels and the base Peltier's center (in both cases, closer sites are colder).

The performance of the freeze/thaw valves was next tested under assay-like conditions. In the first experiment, the valve Peltier was held at -2.5 °C for 20 s between each open and close event. The results are shown in Figure 5.15, where the average close time was 31.8 s with a standard deviation of 6.7 s and the average open time was 7.3 s with a standard deviation of 3 s. These times are as expected when compared to the first experiment; close times were shorter as the Peltier was cooling down from -2.5 °C rather than room temperature, and open times were

shorter as the Peltier was warming up from -2.5 °C rather than -43 °C. In the second, the valve Peltier was shut off and the base Peltier set to -16.7 °C for 20 seconds between each freeze/thaw. The results in Figure 5.16 show an average close time of 25.8 s with a standard deviation of 5.5 s and an average open time of 10.7 s with a standard deviation of 3.9 s. These times are also as expected when compared to the previous experiments; compared to the -2.5 °C-equilibration experiment, the close time is shorter because the Peltier is starting from -16.7 °C, while the open time is longer. The same slight upward trend in opening time with successive events is evident in both, as is an upward trend in the closing times, although this did not continue indefinitely; subsequent tests found that in all cases, freezing was effected in less than 45 s and thawing in less than 20 s. All data presented here are from a single valve but are representative of all valve operations. Vacuum was not applied to the chips during these three experiments, but in others, vacuum did not appear to affect open/close times.

Based on these results, a time buffer for each valve open/close sequence was incorporated. For closing, a 50 s time frame was used while a 20 s time frame was used for opening. This extra time ensures that the valve is in the desired state, but does not significantly impact the overall assay time.

5.3.5 Verification of sustained valve closure over time

All valve tests so far examined valving with short-term closure (~20 s). However, assays will require closure times approaching an hour. To ensure there is no leakage through the valve for the required times under assay-like conditions, a valve leading to a mixing tee was closed (Figure 5.17A-B) and temperature set to -2.5 °C and left to sit for an hour. The mixing tee was monitored for the entirety of this period for fluorescence dye leaking through the tee. Vacuum was applied periodically to mimic assay conditions and in case of a leak, to pull the dye to the tee

intersection. No fluorescent dye was seen at the tee once the valve was closed with Figure 5.17C showing a representative image of this time frame. Once the valve was re-opened, fluorescent buffer flow with the 50/50 mix in the tee channel is present (Figure 5.17D).

5.4 Conclusions

In this chapter, a simple Peltier-based freeze-thaw valve for microfluidic devices was developed. A custom heat sink and stage were made for mounting the valves and chips. It was found that casting the Peltiers with a layer of PDMS and styrofoam was an effective means of thermally insulating them and protecting them from condensation. The electronics for the Peltiers were assembled and a custom LabVIEW program for controlling them was written. Following characterization of the Peltiers with a thermocouple and infrared camera, mixing tee chips for visualizing the valving were designed and fabricated. Experiments with the mixing tee chips found that the valves behave reproducibly and open/close at timescales suitable for the needs of the pERK1/2:ERK1/2 assay device. Once closed, they remain stable in that state as long as the Peltiers controlling them are held at a temperature slightly below the freezing point of water.

5.5 Figures

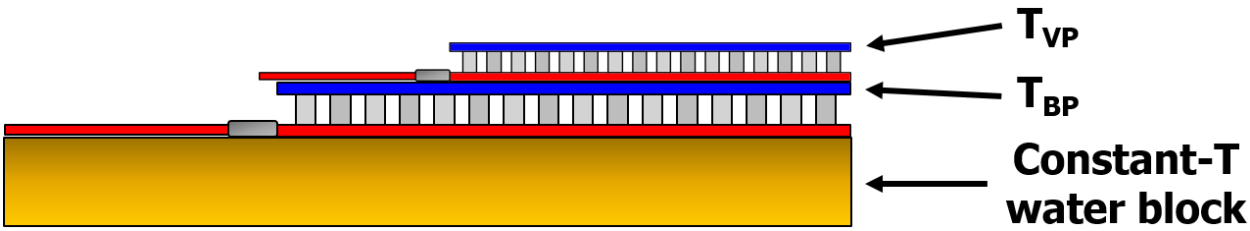

Figure 5.1. Schematic of a 2-tier cascaded Peltier setup. The cold and hot sides of the Peltiers are shown in blue and red, respectively. A constant-temperature water block is used as a heat sink and a reference temperature for the base Peltier's hot side, which keeps its cold side temperatures stable. The cold side of the larger Peltier removes heat from and is used as a hot-side reference temperature (T_{BP}) for the smaller Peltier, whose cold side (T_{VP}) can then become much colder than if the Peltier were used as a single unit. In our setup, example temperatures are 15 °C for the water block, -16 °C for T_{BP}, and -40 °C for T_{VP}. If the polarity of the top valve Peltier is reversed, it is capable of generating temperatures well over 50 ºC for opening valves.

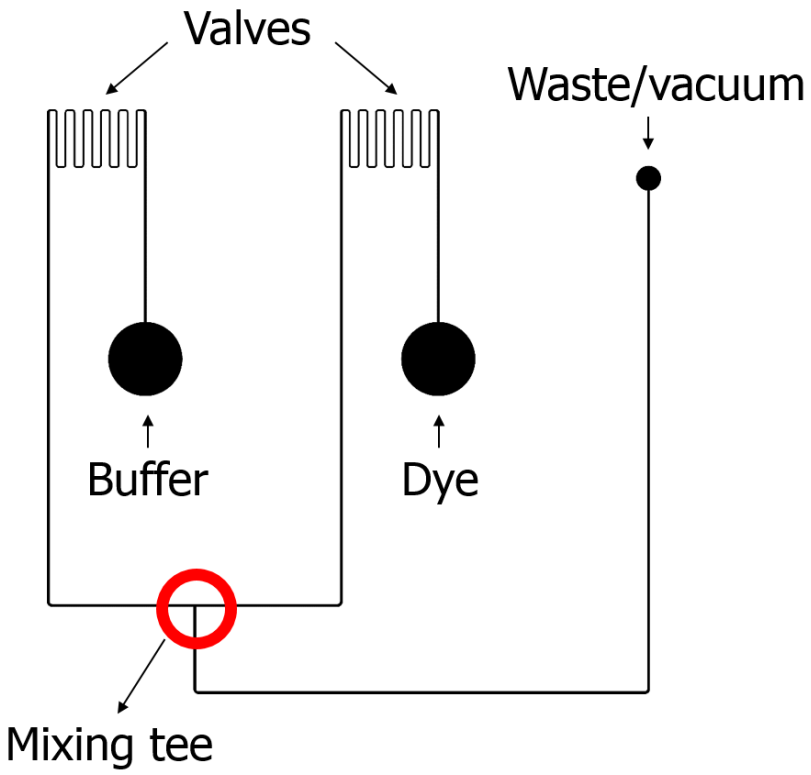

Figure 5.2. Schematic of mixing tee chip used for valve development. The main channels are 40 µm deep and 100 µm wide. The serpentine regions increase the fluidic space across the Peltiers and provide more potential nucleation sites, and the channels here are 60 µm wide to allow more channel lengths to occupy the same area. Dye and buffer channels converge in the mixing tee (circled in red) and are used to visualize the valving.

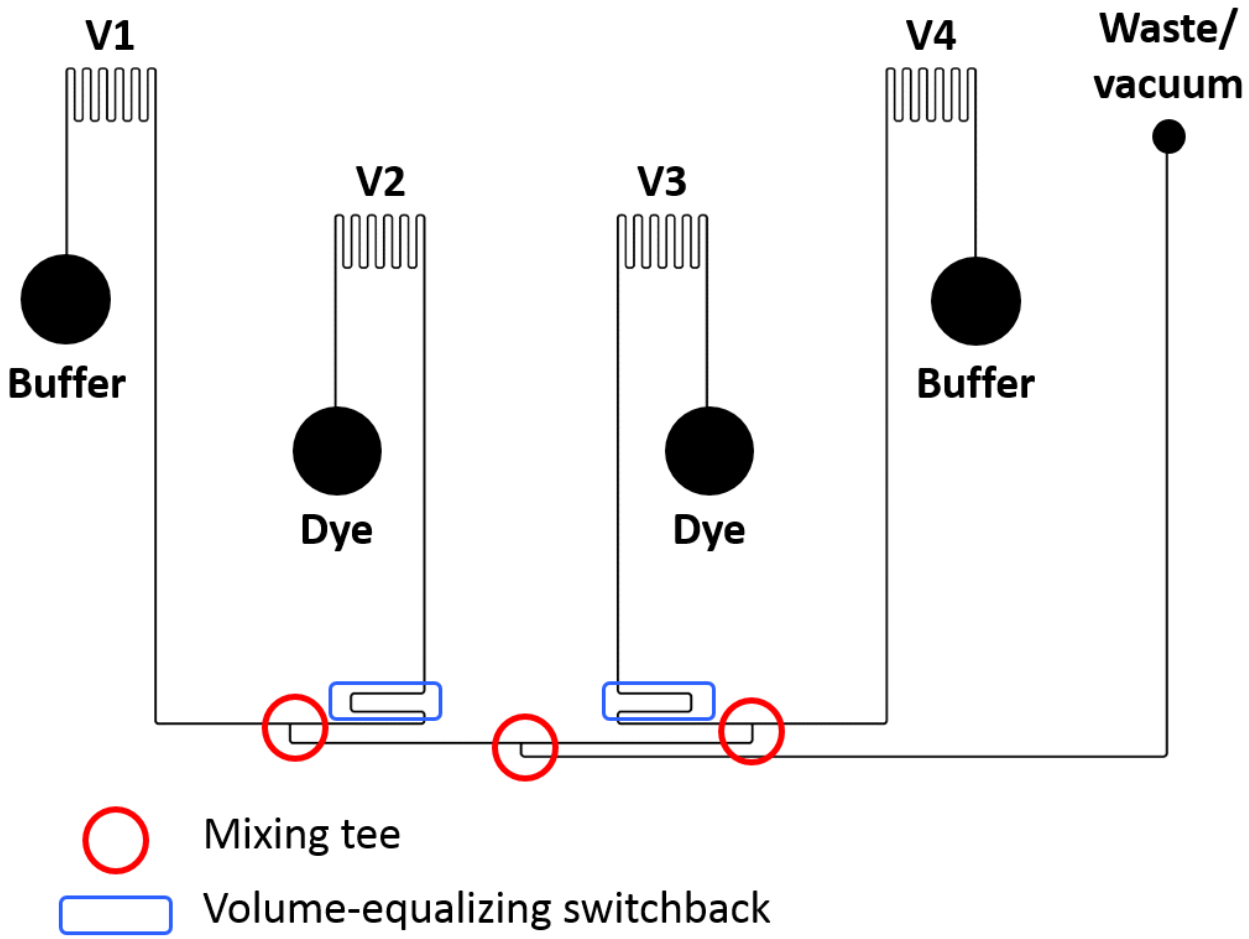

Figure 5.3. Schematic of triple mixing tee chip used to study all four valves. This chip possesses four FTVs (V1-V4). Tees are circled in red. The switchbacks (highlighted in blue boxes) in the two dye channels equalize the channel lengths to ensure equal fluid flow between buffer and dye channels.

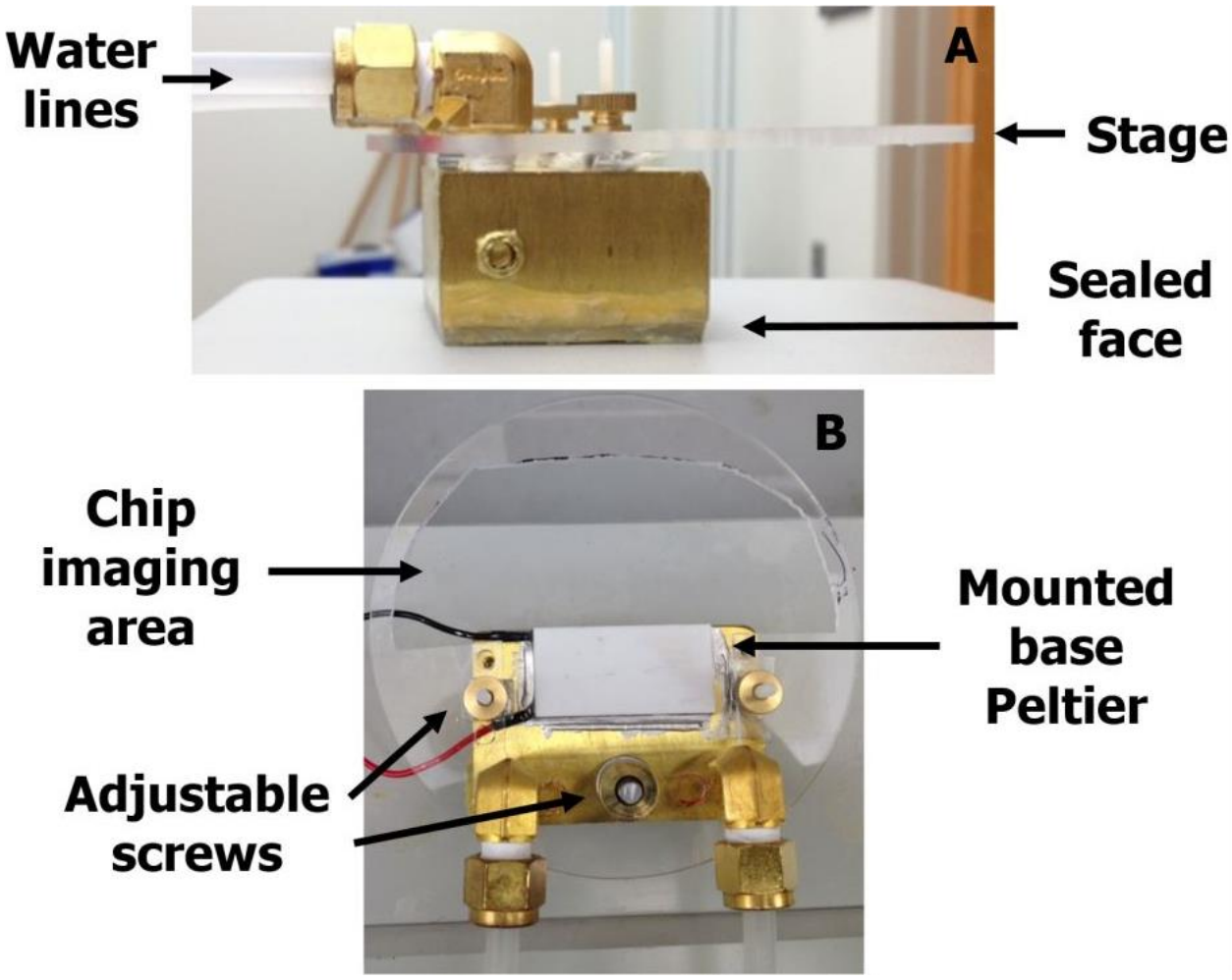

Figure 5.4. Photographs of water block with mounted base Peltier. (A) Side view of water block with water lines, base Peltier and attached stage. (B) Top view of water block with stage and mounted base Peltier.

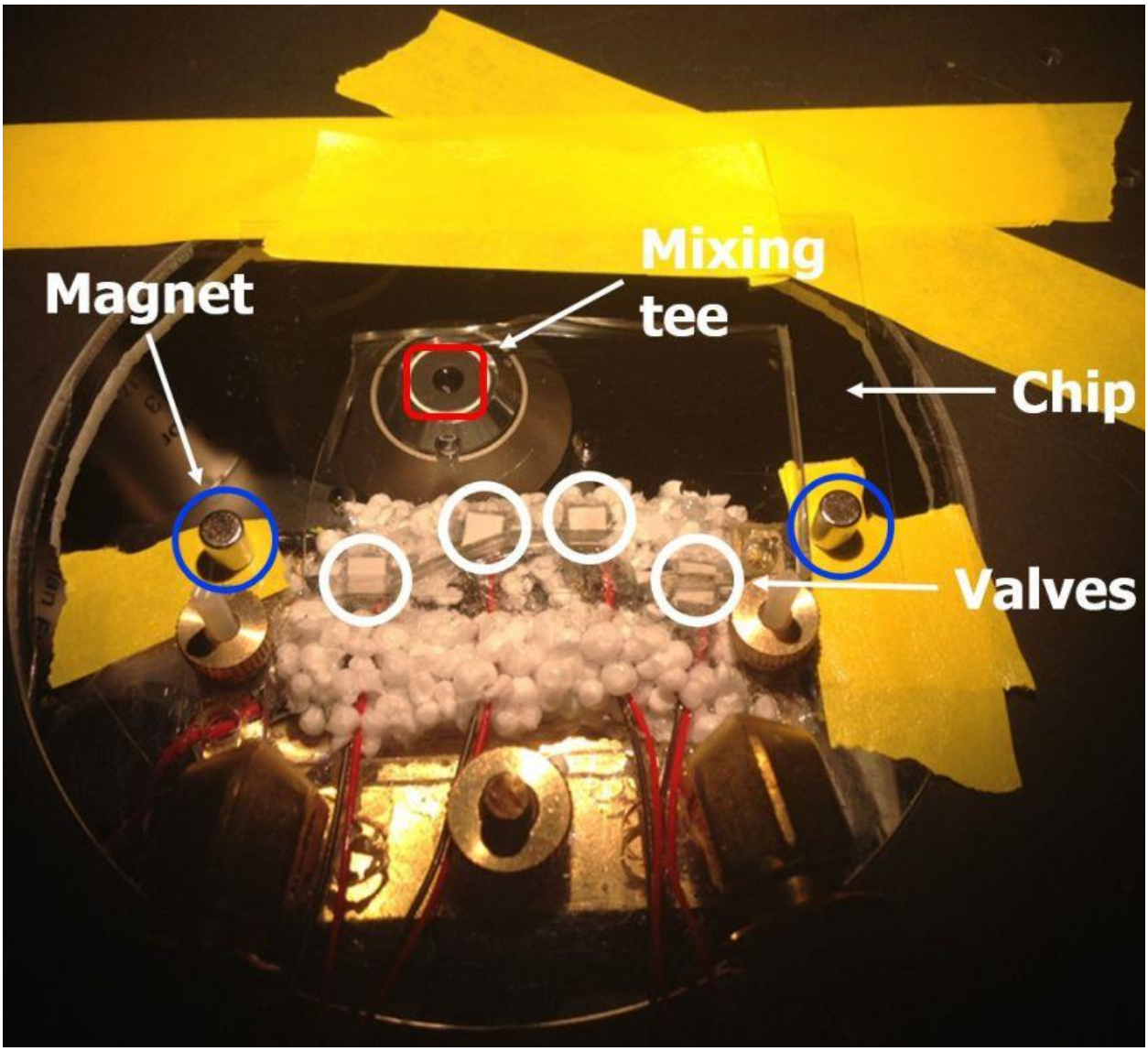

Figure 5.5. Triple mixing tee chip placed on freeze-thaw valve platform. The valving regions of the chip (circled in white) sit atop the valves (4.3 mm x 4.3 mm), which are mounted on the 20 mm x 40 mm base Peltier and the water block. One of the chip's mixing tees (boxed in red) is located over the microscope objective. Thin pieces of metal covered in yellow tape are attached to the stage (circled in blue) and are used to secure the chip with magnets.

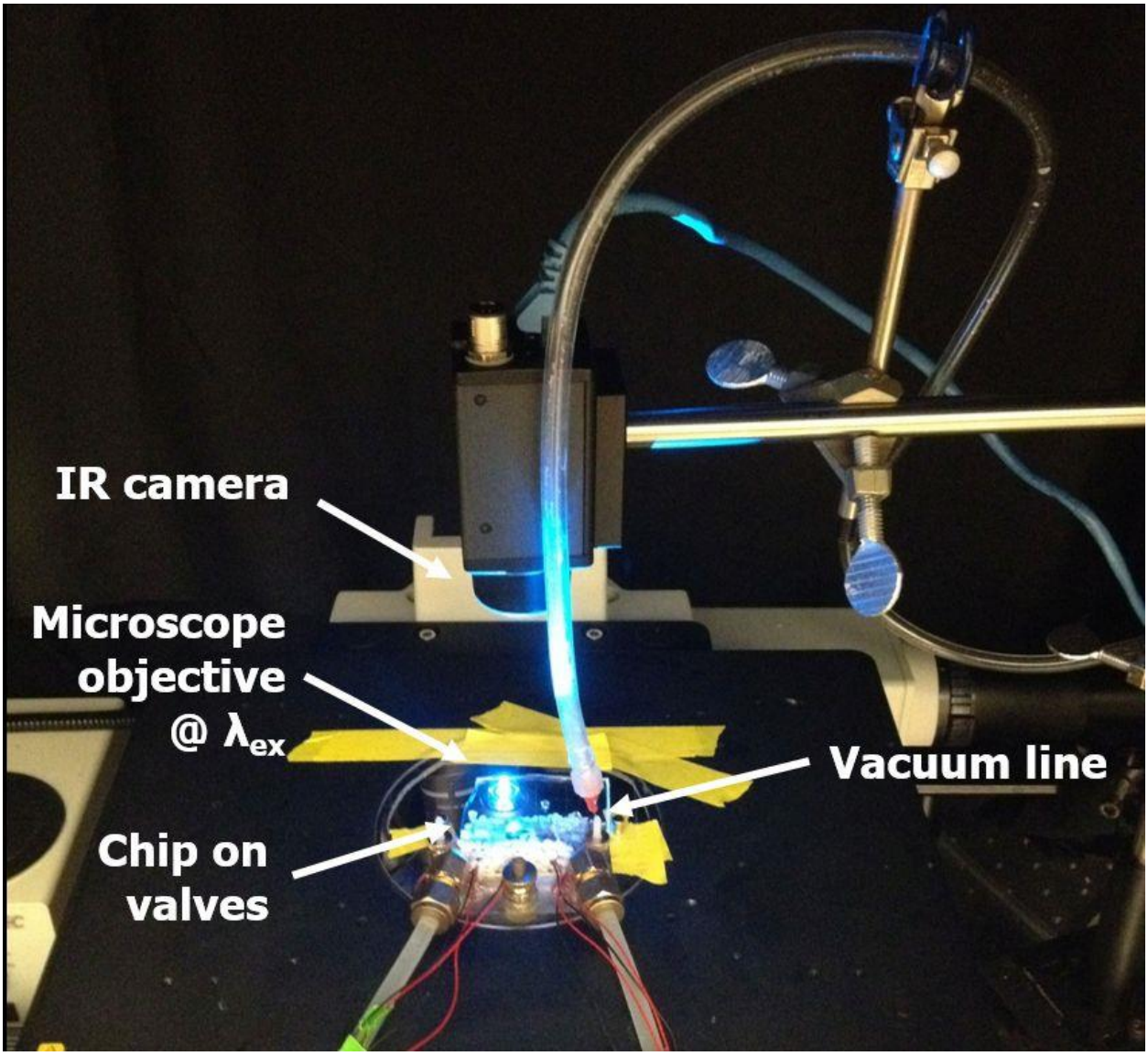

Figure 5.6. Imaging setup for simultaneous fluorescence/thermal studies. The chip sits atop the valves and the channels imaged with the inverted fluorescence microscope (shown emitting λ_{ex} for fluorescein). An infrared camera images the valves from above. A vacuum line is secured in place and is manipulated remotely to control flow without disturbing the chip.

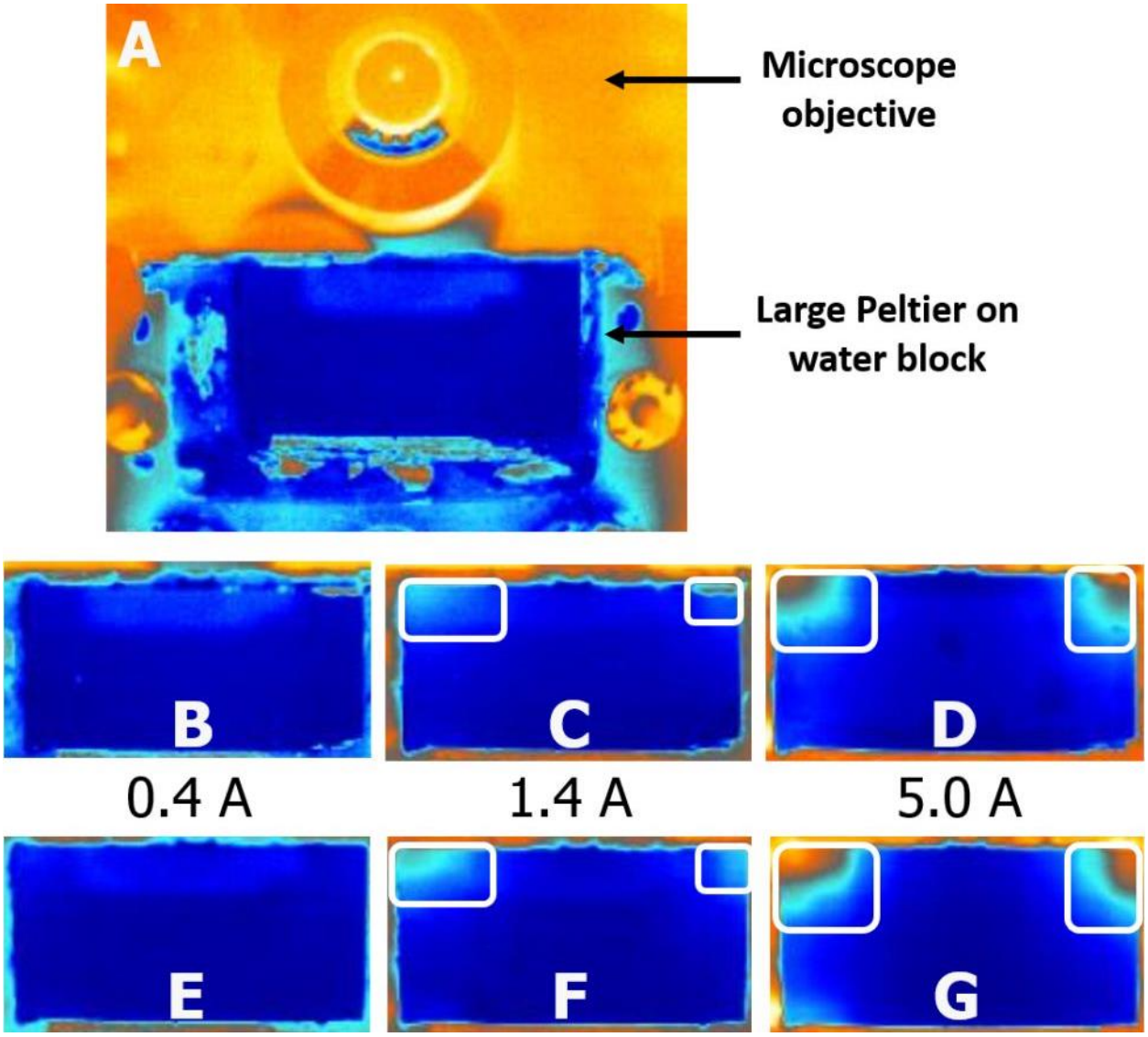

Figure 5.7. Schematic for thermal camera study of base Peltier at various currents. The color-based temperature scale is precise but not accurate and exact temperatures were not measured in this study. (A) Thermal image of microscope objective and base Peltier. The valve Peltiers have been removed. This image illustrates the viewing perspective for the subsequent images as the base Peltier's orientation is the same in all of them. (B) – (D) Thermal images of base Peltier with pyrolytic graphite at the indicated current levels. (E) – (G) Thermal images of base Peltier at indicated current levels with the pyrolytic graphite stripped. Note the presence of warmer areas in the upper corners in (D) and (G). These begin to appear in (C) and (F) as well. These regions are warmer than the freezing point of water.

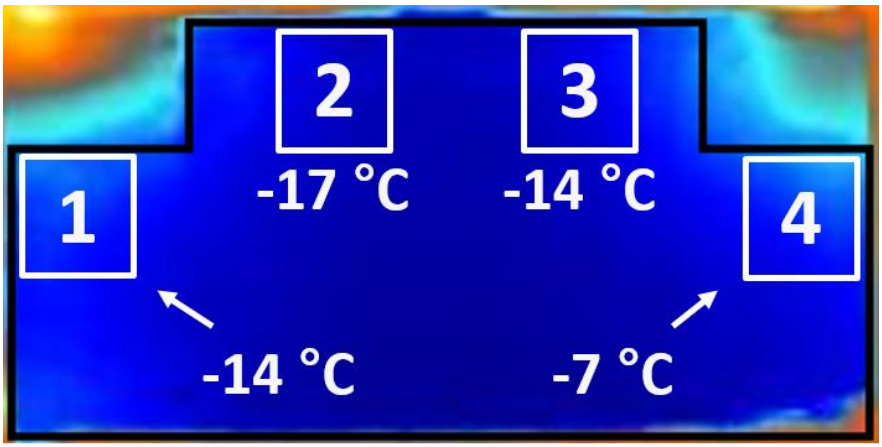

Figure 5.8. Thermal images of base Peltier at 5.1 A showing new mounting locations for the valves (outlined in white). The temperature of the base Peltier at each mounting location is noted. The region outlined in black is covered with pyrolytic graphite.

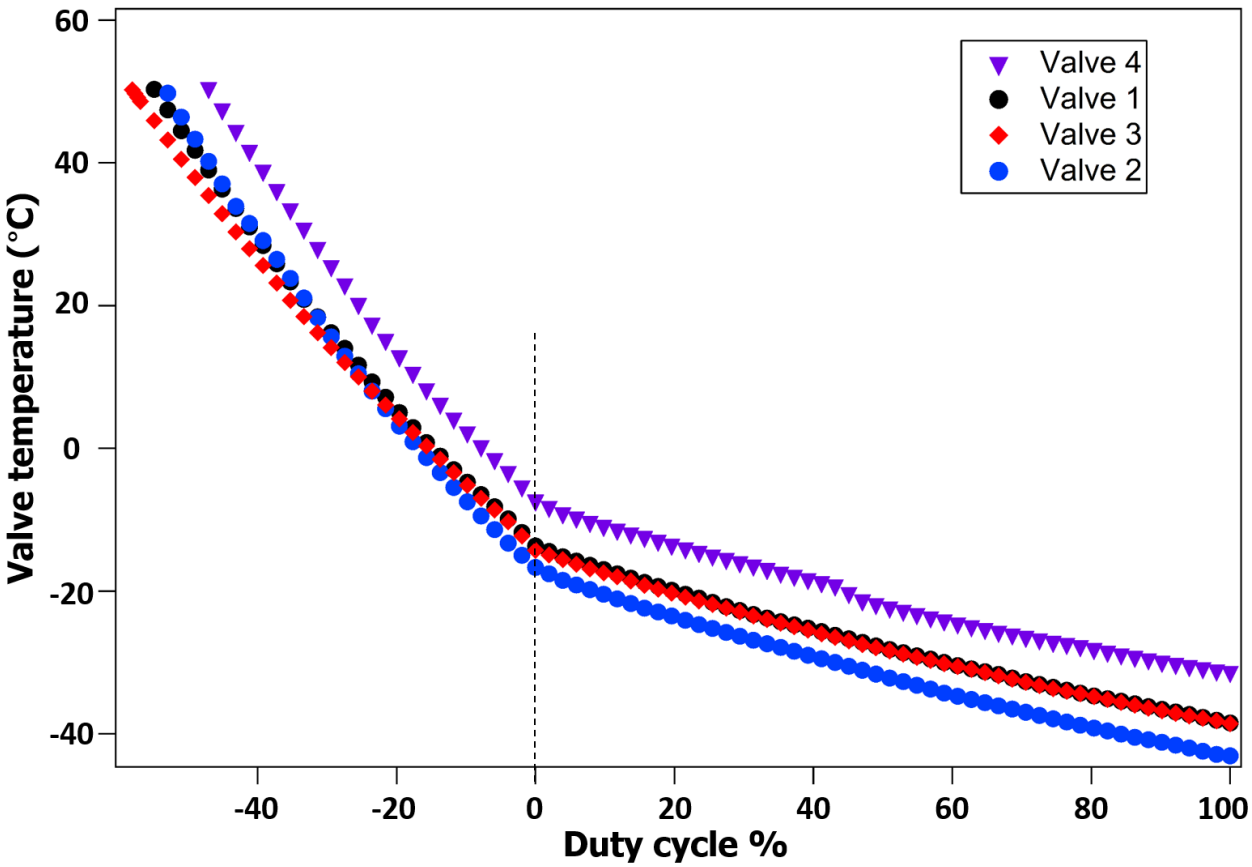

Figure 5.9. Valve temperatures as a function of their duty cycle and polarity. Positive duty cycles are closed valves while negative duty cycles are open valves. Valve #1 is represented by black circles, valve #2 is represented by blue circles, valve #3 is represented by red diamonds, and valve #4 is represented by purple inverted triangles. Their maximally cold temperatures vary (-38.5 °C for valve 1, -43.1 °C for valve 2, -38.6 °C for valve 3, and -31.3 °C for valve 4), but all are cold enough to rapidly freeze microfluidic channels.

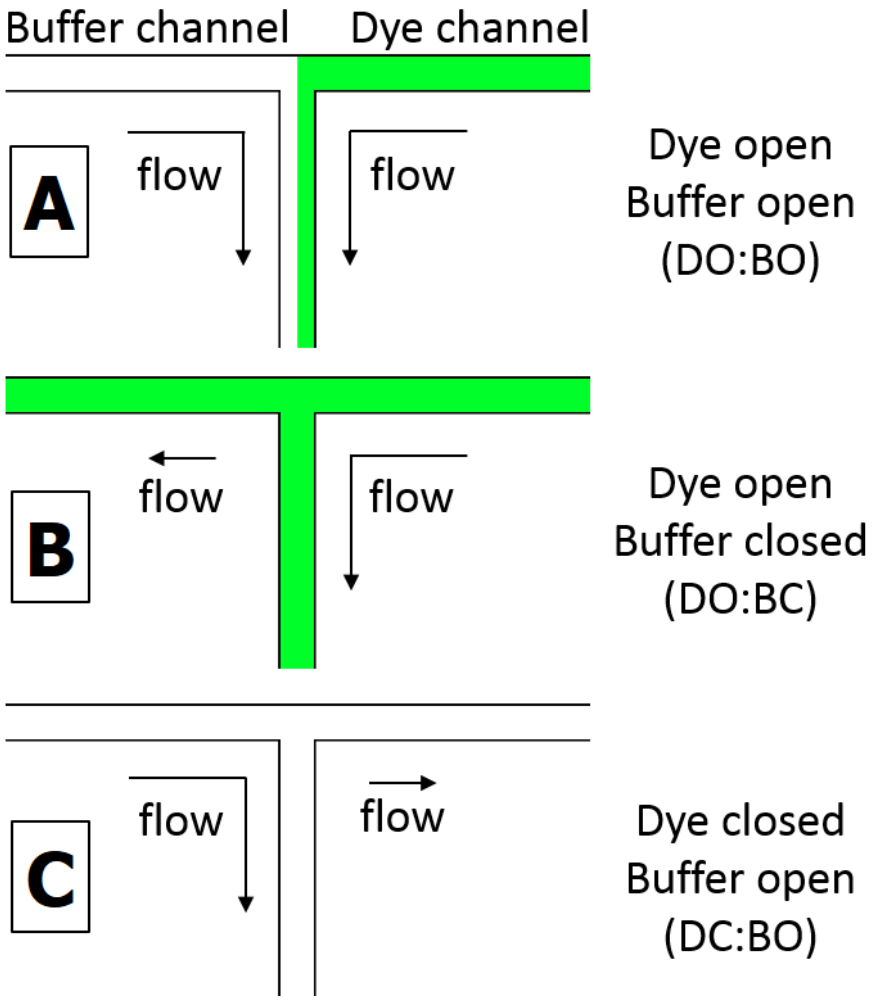

Figure 5.10. Visualization schematic for valve states in mixing tee. Arrows indicate direction of flow, and relative size of the arrows indicates relative flow rate. (A) Both the dye and buffer valves are open (DO:BO) and are flowing in equal quantities into the tee. The channel appears half fluorescent and half dark. (B) The tee appears completely fluorescent after the buffer valve's closure (DO:BC) due to the dye flowing into both sides of the channel. (C) The tee appears completely dark after the dye valve's closure (DC:BO).

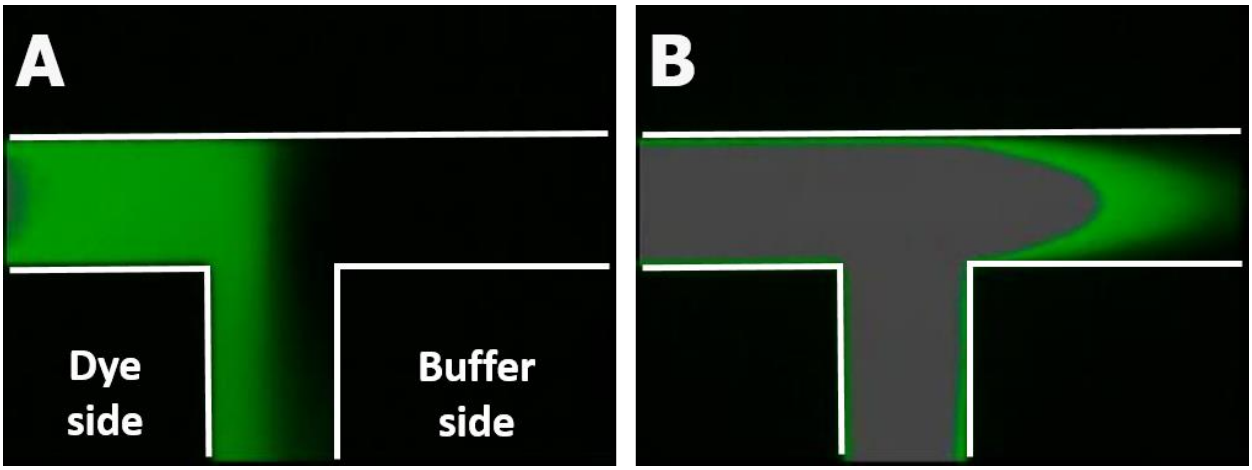

Figure 5.11. Fluorescence images of freeze event. The tee is outlined in white. (A) Mixing tee with both valves open (DO:BO) showing equal fluid flow from the dye and buffer channels. (B) Mixing tee immediately after closing the dye channel valve (DC:BO) showing a pulse of dye extending into the buffer channel from the dye's valve region freezing and expanding.

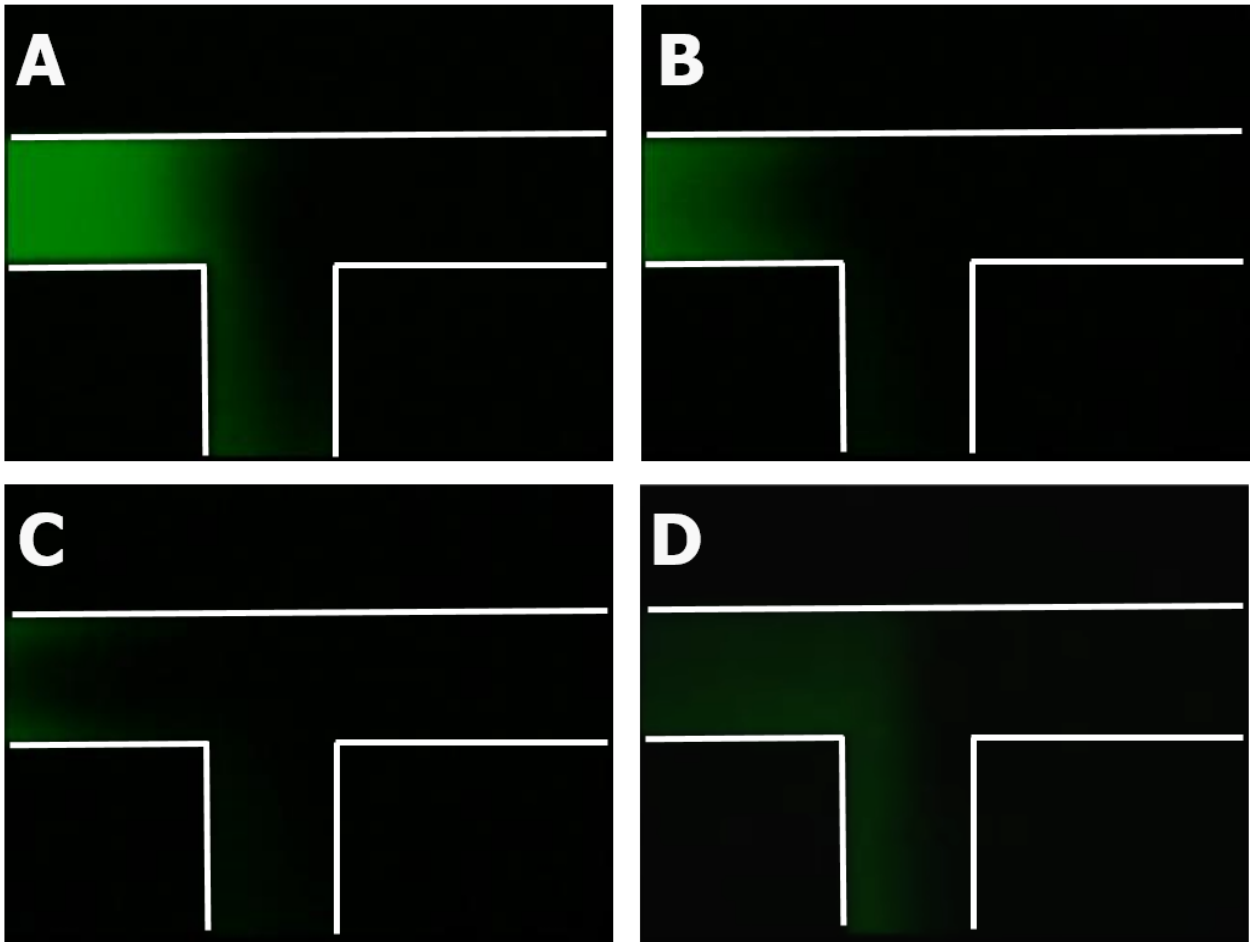

Figure 5.12. Fluorescence images showing thaw event. (A) Mixing tee just as dye valve is opened (DC:BO to DO:BO). (B) Mixing tee as the dye initially retreats back into the channel, and (C) further retreat of the dye. The dye retreats back as the fluid contraction in the valve as its contents thaw. The total timescale of these events is approximately 4 seconds. (D) The fluid flow on either side of the tee has equalized after approximately 18 seconds.

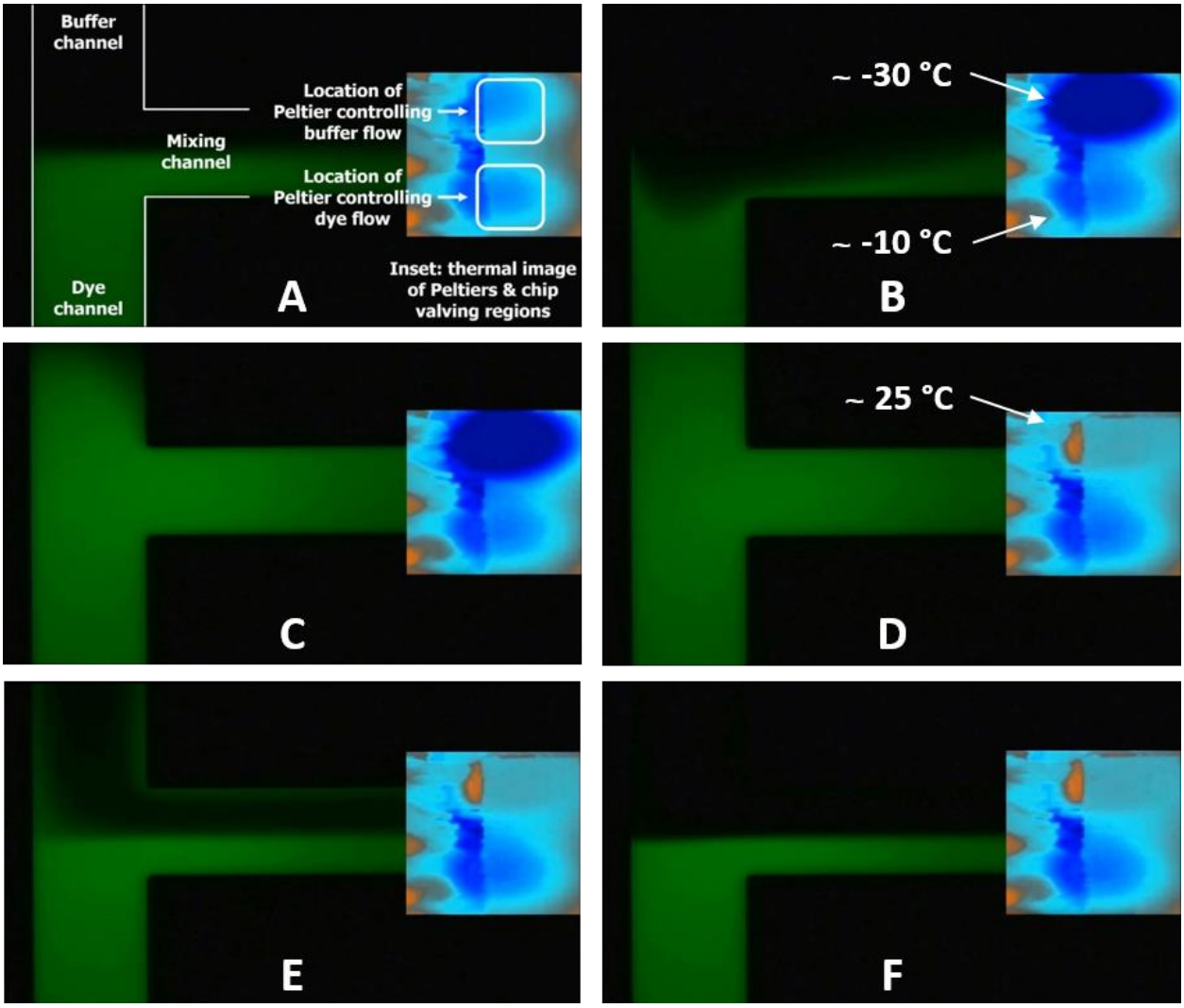

Figure 5.13. Time series of freezing and thawing with inset from thermal camera. (A) Fluorescence image of mixing tee with both valves open. The locations of the buffer channel, dye channel, and mixing channel are indicated. Inset: thermal image (simultaneous with fluorescence image) of the two Peltiers controlling the valves for the buffer and dye. The locations of the Peltiers themselves are boxed in white. (B) Freeze pulse from buffer channel into dye channel. The buffer's Peltier appears deep blue in the thermal image because it is at its maximally cold temperature. (C) Dye has taken over the buffer side of the tee due to diffusion following the buffer valve closure. (D) The buffer's Peltier is set to room temperature. It now appears orange in the thermal image. (E) Buffer is beginning to flow back into the tee following the thawing of its valving region. Note the dimmer fluorescence on the buffer side of the tee. (F) The buffer's flow is back to normal after its valve was opened.

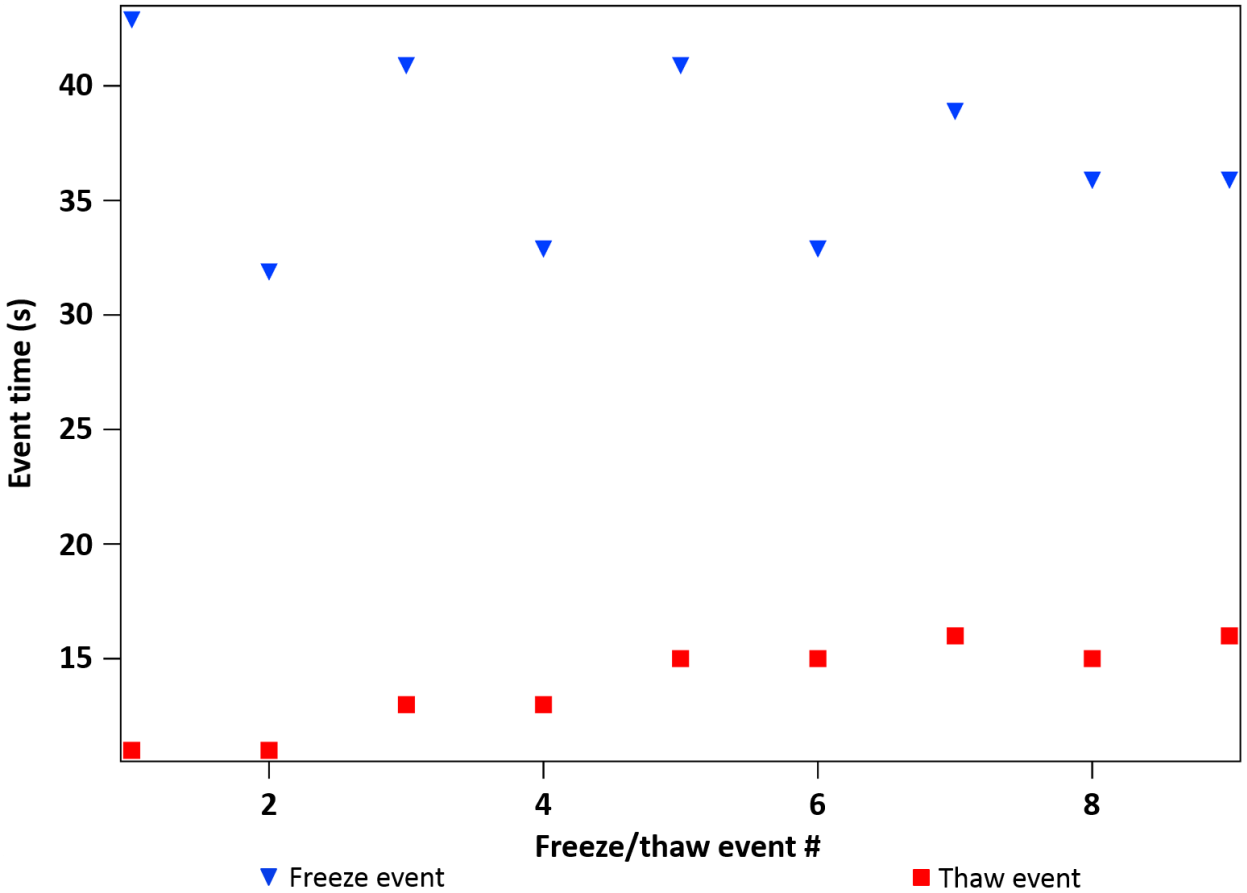

Figure 5.14. Event times for multiple freeze/thaw cycles of the same valve. Freeze events are indicated with blue inverted triangles and thaw events with red boxes. The valve Peltier was switched directly between -43 °C and 25 °C to induce freezing and thawing, and the event times were determined based on the appearance of the freeze pulse shown in Figure 5.11B and the thaw retreat shown in Figure 5.12A. The average freeze time was 37.1 s with a standard deviation of 4 s. The average thaw time was 13.4 s with a standard deviation of 2 s.

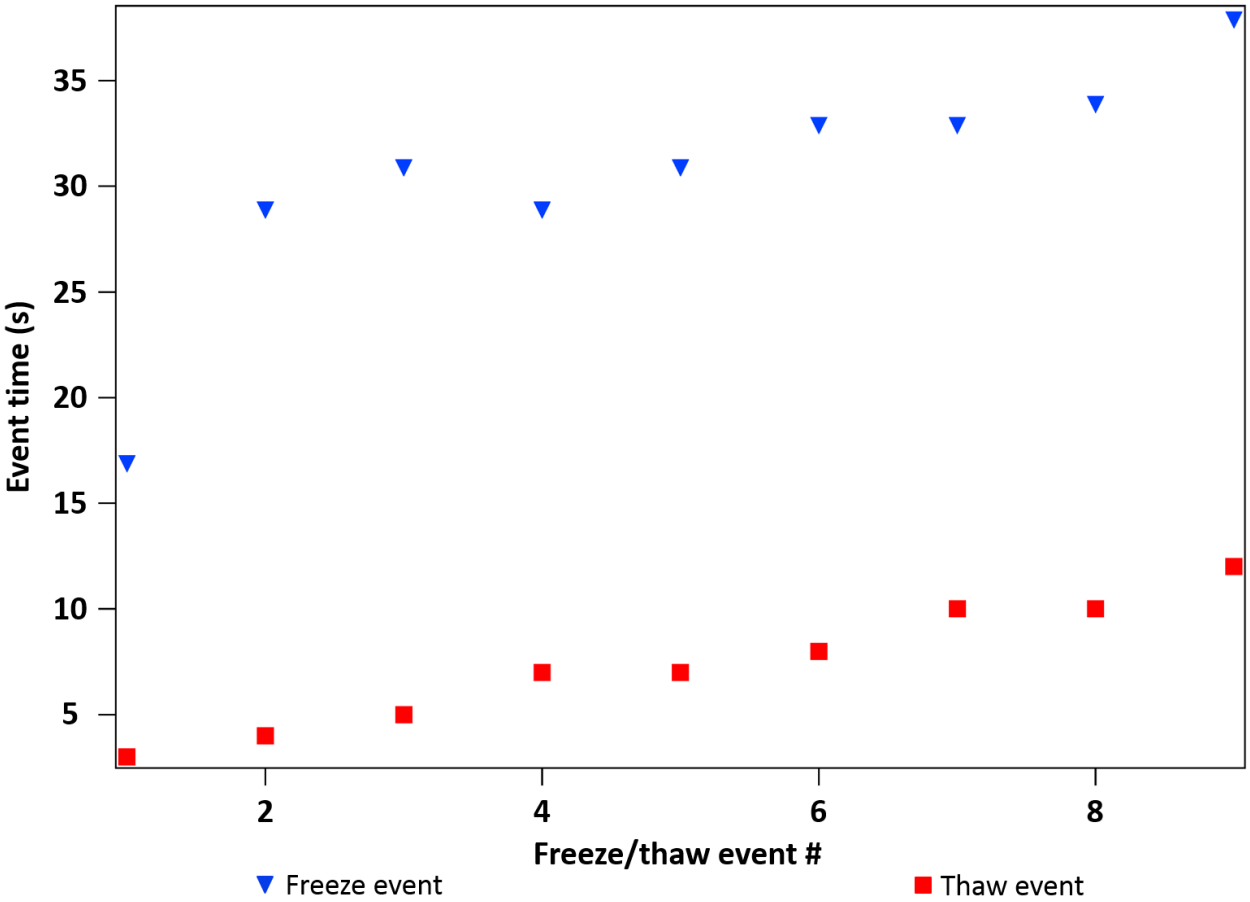

Figure 5.15. Event times for multiple freeze/thaw cycles in which the system was held at -2.5 °C for 20 s between each event. The average freeze time was 31.8 s with a standard deviation of 6.7 s. The average thaw time was 7.3 s with a standard deviation of 3 s.

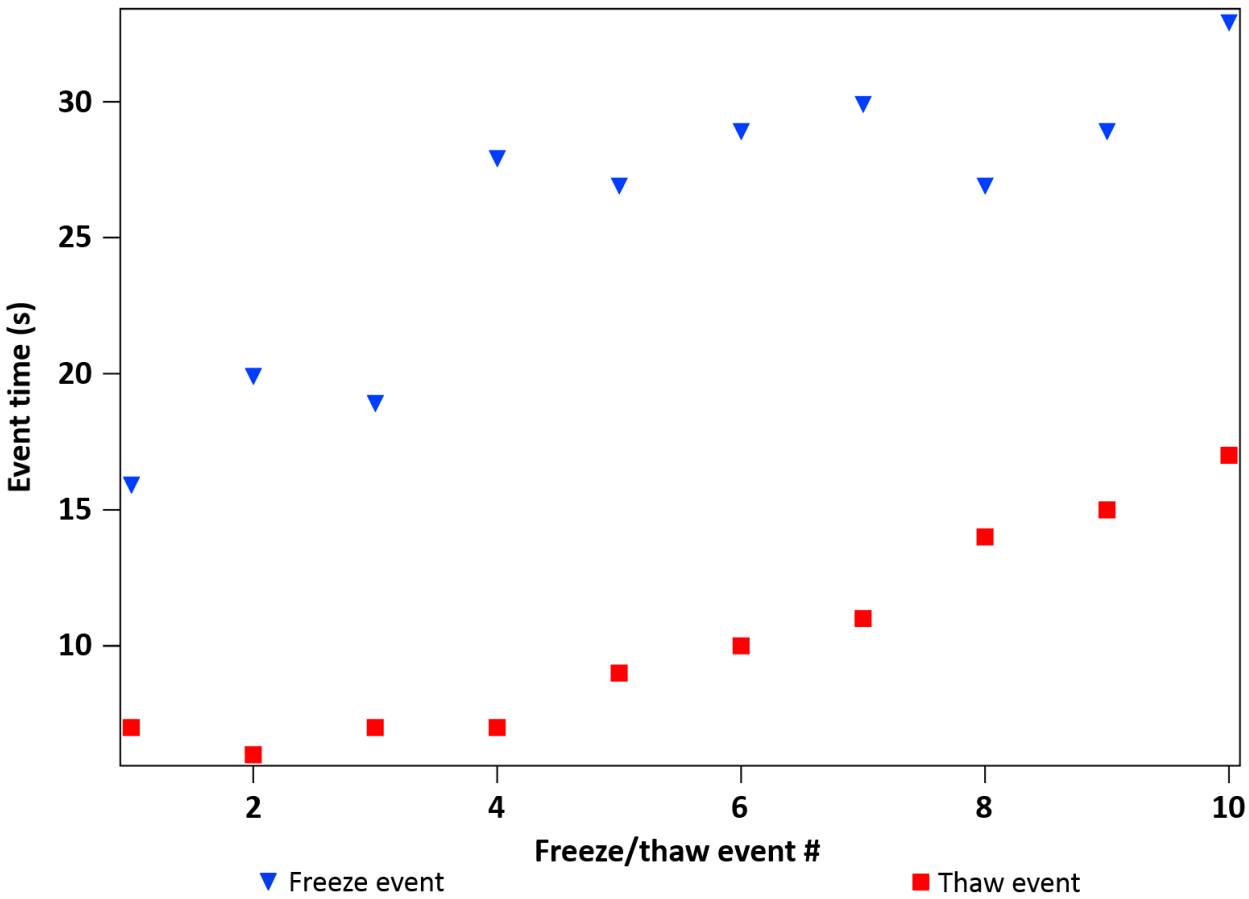

Figure 5.16. Event times for multiple freeze/thaw cycles in which the system was shut off for 20 s between each event. The average freeze time was 25.8 s with a standard deviation of 5.5 s. The average thaw time was 10.7 s with a 3.9 s standard deviation.

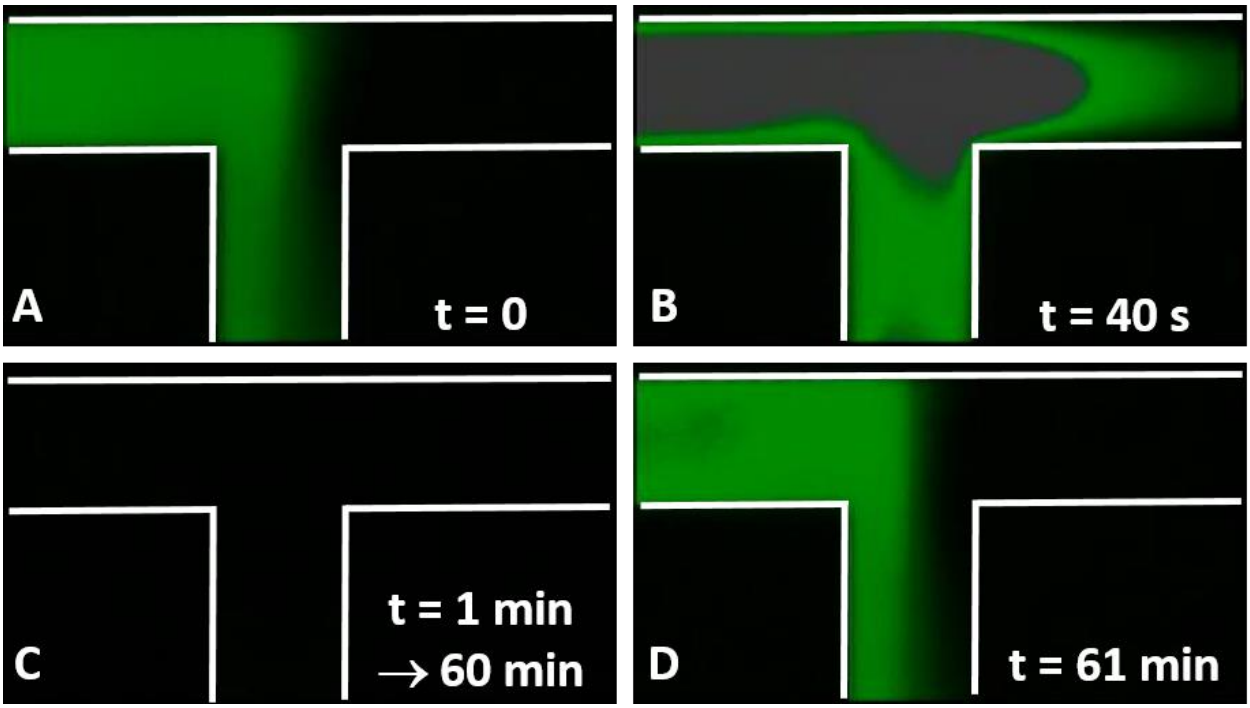

Figure 5.17. Time series of sustained valve closure experiment. Channel walls are outlined in white. (A) Mixing tee prior to valve closure (BO:DO). (B) Freeze pulse as the dye valve closes (BO:DC). The tee was video recorded continuously for an hour to confirm sustained closure of the dye valve. (C) Representative image of tee from t = 1 min to t = 60 min. (D) Final image of tee 1 minute after re-opening of dye valve (BO:DO). It has returned to its t = 0 state.

5.6 References

(1) Hulme, S. E.; Shevkoplyas, S. S.; Whitesides, G. M. Incorporation of Prefabricated Screw, Pneumatic, and Solenoid Valves into Microfluidic Devices. *Lab Chip* **2009**, *9*, 79–86.

(2) Studer, V.; Hang, G.; Pandolfi, A.; Ortiz, M.; Anderson, W. F.; Quake, S. R. Scaling Properties of a Low-Actuation Pressure Microfluidic Valve. *J. Appl. Phys.* **2004**, *95*, 393–398.

(3) Unger, M. A.; Chou, H.-P.; Thorsen, T.; Scherer, A.; Quake, S. R. Monolithic Microfabricated Valves and Pumps by Multilayer Soft Lithography. *Science (80-.).* **2000**, *288*, 113–116.

(4) Nie, S.; Henley, W. H.; Miller, S. E.; Zhang, H.; Mayer, K. M.; Dennis, P. J.; Oblath, E. A.; Alarie, J. P.; Wu, Y.; Oppenheim, F. G.; et al. An Automated Integrated Platform for Rapid and Sensitive Multiplexed Protein Profiling Using Human Saliva Samples. *Lab Chip* **2014**, *14*, 1087–1098.

(5) Stan, C. A.; Schneider, G. F.; Shevkoplyas, S. S.; Hashimoto, M.; Ibanescu, M.; Wiley, B. J.; Whitesides, G. M. A Microfluidic Apparatus for the Study of Ice Nucleation in Supercooled Water Drops. *Lab Chip* **2009**, *9*, 2293–2305.

(6) Gui, L.; Yu, B. Y.; Ren, C. L.; Huissoon, J. P. Microfluidic Phase Change Valve with a Two-Level Cooling/heating System. *Microfluid. Nanofluidics* **2011**, *10*, 435–445.

(7) Chen, Z.; Wang, J.; Qian, S.; Bau, H. H. Thermally-Actuated, Phase Change Flow Control for Microfluidic Systems. *Lab Chip* **2005**, *5*, 1277–1285.

(8) Tan, H.; Yeung, E. S. Automation and Integration of Multiplexed On-Line Sample Preparation with Capillary Electrophoresis for High-Throughput DNA Sequencing. **1998**, *70*, 4044–4053.

(9) Bevan, C. D.; Mutton, I. M. Use of Freeze-Thaw Flow Management for Controlling and Switching Fluid Flow in Capillary Tubes. *Anal. Chem.* **1995**, *67*, 1470–1473.

(10) Bevan, C. D.; Mutton, I. M. Freeze-Thaw Flow Management: A Novel Concept for High-Performance Liquid Chromatography, Capillary Electrophoresis, Electrochromatography and Associated Techniques. *J. Chromatogr. A* **1995**, *697*, 541–548.

(11) He, Y.; Zhang, Y. H.; Yeung, E. S. Capillary-Based Fully Integrated and Automated System for Nanoliter Polymerase Chain Reaction Analysis Directly from Cheek Cells. *J. Chromatogr. A* **2001**, *924*, 271–284.

(12) Tellurex. Frequently Asked Questions About Our Cooling And Heating Technology http://tellurex.com/wp-content/uploads/2014/04/peltier-faq.pdf.

(13) Pyrolytic Graphite Sheet Brochure
http://www.panasonic.com/industrial/includes/pdf/PGS_Brochure.pdf.

CHAPTER 6

ASSAYS WITH MULTI-SAMPLE CHIPS AND FREEZE-THAW VALVES AND FUTURE DIRECTIONS

6.1 Introduction

The project discussed in this dissertation aimed to develop an automated microfluidic device for determining pERK1/2:ERK1/2 in a sample. Early immunoassay development experiments focused on the testing of various reagents, buffers, and assay protocols using a simplified single-channel, single-array chip and the model antigen VEGF. In testing detection fluorophore labels, approximately 10 times more signal was obtained from B-phycoerythrin than from the label previously used, AlexaFluor 488. Longer incubation times (1 h for sample, 30 min for dAb, 20 min for SA-PE) at room temperature were shown to yield 3 times more signal than shorter incubation times (30 min sample, 20 min dAb, 10 min SA-PE) at 37 °C. A preliminary protocol for determining pERK2:ERK2 in a sample was developed that involved incubating a dAb for pERK1/2 before a dAb for total ERK2. Upon discovery that the process of mechanically loading the beads into the PDMS arrays induced a large variance, a new chip without the need for harsh loading conditions was design and fabricated.

The new "flow-frit" chips featured flow beds, a continuous pattern of spaced pillars designed to focus beads into a monolayer while providing additional fluidic space for reagents. A frit consisting of pillars spanning the channel height traps the beads, forming a detection zone. These chips were found to perform well in terms of signal and experimental variance, although on-chip bead-sample incubations performed in the packed beds led to a fluorescence gradient

across the bed. Incubating beads with samples in sample vias prior to forming the packed bed solved the problem.

The flow-frit chips required extensive user interaction to perform assays. Solutions were manually removed from and pipetted onto the chips before each incubation step with manually applied vacuum and imaging steps as well. The development of freeze/thaw valves for automating the reagent delivery was then undertaken. A chip featuring serpentine channel valving regions was developed that utilized the flow-frit pack bed design. The FTV system was found capable of opening and closing microfluidic channels on timescales suitable for the pERK1/2:ERK1/2 assay's needs. It did so under computer control, making that component of the system readily automatable.

Having developed a workable valving system, the next step was to develop an assay chip incorporating the valving system and addressing additional assay needs. In addition to possessing four valves for four reagents (buffer, the pERK1/2 dAb, the tERK1/2 dAbs, and SA-PE), a chip capable of analyzing multiple simultaneous samples would be desirable. Examples of microfluidic immunoassay devices capable of handling multiple simultaneous samples are abundant in the literature.[1–5] In contrast to the single-channel, single-array chips, with which replicate measurements required multiple devices, these are capable of taking replicate measurements with a single device. This potentially reduces the time and material requirements for device fabrication, and thus, the overall cost of the device. Taking replicate measurements on a single device also has the potential for minimizing the experiment's variance since samples on a chip will experience the same experimental conditions. It is also possible to use a multi-sample device to generate a calibration curve for each experiment while concurrently measuring unknown samples. Coupled with the fact that many of the extant devices are automated through

the use of computer-controlled valving and imaging, it is thus possible to make quantitative determinations of many samples with a single self-contained device that does not require user intervention once the experiment has begun.

In this chapter, a chip that couples the developed pERK1/2:ERK1/2 assay with the freeze-thaw valves is developed and tested. The chip features 4 reagent valves for modulating the flow of buffer, pERK1/2 dAb, tERK1/2 dAb, and SA-PE. The chip also features 8 flow-frit sample regions so that pERK1/2:ERK1/2 can be determined simultaneously in both calibration solutions and cell lysate samples. Assays with these sample types are demonstrated and the sensitivity of the assay with the current system is determined. This device represents a significant step toward fully automating the assay and, with different beads and detection antibodies, it can be used to determine other analytes as well. Finally, various avenues for improving the assay are suggested as directions for future research.

6.2 Materials and methods

6.2.1 Materials and reagents

Sylgard 184 PDMS was purchased from Dow Corning (Midland, MI) and was prepared according to the manufacturer's instructions at a 10:1 elastomer/cross-linker ratio. MagPlex Luminex beads were purchased from Bio-Rad Laboratories (Hercules, CA). Purified phosphorylated and non-phosphorylated extracellular signal-related kinase 2 (pERK2 and nERK2), phosphorylated and non-phosphorylated extracellular signal-related kinase 1 (pERK1 and nERK1), biotinylated detection antibodies for pERK1/2, ERK1, and ERK2, and capture antibodies for pERK1/2 were purchased from R&D Systems (Minneapolis, MN). All proteins and antibodies were reconstituted according to the manufacturer's instructions. Soda lime glass photolithography substrates (5" x 5") were purchased from Nanofilm (WestLake Village, CA).

Nano-Strip was purchased from KMG Chemicals (Fremont, CA). Pluronic F-127 (PF-127), sodium chloride, octyltrichlorosilane, sodium fluoride, ethylene diamine tetraacetic acid (EDTA), urea, Triton X-100, phorbol 12-myristate 13-acetate (PMA), leupeptin, phenylmethanesulfonyl fluoride (PMSF), aproptinin, sodium pyrophosphate, and sodium orthovanadate were purchased from Sigma-Aldrich (St. Louis, MO). AZ-400K was purchased from AZ Electronic Materials USA (Somerville, NJ). Chromium etchant and 10:1 buffered oxide etch (BOE) were purchased from Transene (Danvers, MA). Acetone, 10x phosphate-buffered saline (PBS, pH = 7.4), 10% bovine serum albumin (BSA) in PBS, 200 proof ethanol, optically clear polypropylene plate-sealing tape (PCR tape), and microscope slides (75 mm x 25 mm x 0.99 mm) were purchased from Thermo Fisher Scientific (Waltham, MA). Contrad detergent was purchased from Decon Labs (King of Prussia, PA). KMPR 1010 photoresist and SU-8 thinner was purchased from MicroChem (Newton, MA); the SU-8 thinner was mixed with KMPR 1010 to prepare 35% (w/w) KMPR solutions. MF-319 photoresist developer was purchased from Rohm and Haas Electronic Materials (Marlborough, MA). P-type 6" crystalline Si wafers were purchased from University Wafer (Boston, MA). D263 glass was purchased from S.I. Howard Glass Company (Worcester, MA). Streptavidin-B-phycoerythrin (SA-PE), RPMI 1640 media, fetal bovine serum, penicillin, and streptomycin were purchased from Invitrogen (Carlsbad, CA). Human Jurkat T-cells were acquired from American Type Culture Collection (Rockville, MD).

All aqueous solutions were prepared with deionized (DI) water from a NANOpure Diamond system (Barnstead International, Dubuque, IA). Buffer solutions used include PBS-BT (PBS + 1% BSA + 0.05% Tween-20), cell lysis buffer (PBS + 1 mM EDTA + 0.5% Triton X-100 + 5 mM sodium fluoride + 6 M urea + 10 µg/mL leupeptin + 100 µM PMSF + 3 µg/mL

aprotinin + 2.5 mM sodium pyrophosphate + 1 mM activated sodium orthovanadate), ERK buffer (PBS + 5 mM sodium fluoride + 1 mM EDTA + 0.5% Triton X-100 + 1 M urea), and ERK diluent (ERK buffer with no urea).

6.2.2 Design & fabrication of freeze-thaw chips

The chips designed for running the pERK1/2:ERK1/2 assays with FTVs (Figure 6.1) feature 4 valved reagent vias for introducing buffer, pERK1/2 dAb, tERK1/2 dAb, and SA-PE solutions. The reagent channels distribute their contents across channels for 8 different samples, and the sample vias are spaced 9 mm apart so that all can be loaded simultaneously with an 8-channel pipette. The regions in which the beads are incubated and packed into beds have flow-frit features. The flow bed pillars are 7 µm x 7 µm, the frit pillars are 12 µm in diameter, and all are spaced 4 µm apart edge-to-edge.

The wafer molds for the FTV chips were fabricated in the same way as the flow-frit chips from Chapter 4 with one exception. Following the first photolithography/DRIE step in which the flow bed, frit, and channels were etched to a depth of approximately 22 µm, the first photoresist layer was not removed as it was in previous fabrication procedures. This was done to keep resist on the high aspect-ratio flow bed/frit features. While they were coated with an additional layer of resist in the next photolithography step, keeping the first layer of resist on circumvented any errors associated with alignment during the second exposure. In the second photolithography/DRIE step, the channel layer of the chips was etched an additional 8 µm for a total depth of approximately 30 µm.

The soft lithography procedure for the PDMS chips did not utilize spin coating as in previous chapters. Aluminum foil was wrapped around the wafer to seal off the unused regions, and degassed PDMS was poured over the chip features to a thickness of approximately 3 mm.

The mold was degassed under vacuum and cured for 10 minutes on a 150 °C hotplate. The PDMS was removed from the wafer, the vias were created with a biopsy punch, and the individual chips were cut out of the bulk PDMS with a razor. They were then plasma-treated along with Contrad-cleaned D263 glass (2" x 3" x 0.0082") and bonded together. These chips were left at room temperature for at least 24 h to stabilize; more rapid stabilization through heating was not done as that caused the thick PDMS to warp upwards in the middle of the chip.

Variants of the full chip were used in early experiments for optimization and testing. These were prepared by fabricating the full chips in PDMS, using a razor to cut off the unused regions, creating vias with a biopsy punch, and bonding the PDMS to microscope slides. Stray channels leading to removed portions of the chip were sealed by placing the bonded chip on a 150 °C hot plate, applying uncured 10:1 PDMS to the unneeded channels, and allowing the PDMS to cure. These optimization chips are shown in Figure 6.2. All have had the valving regions removed and a single via is used to manually introduce reagents and buffer to the chips. The optimization chip in Figure 6.2A does not have sample vias and was used to demonstrate consistency in fluid flow between chips and between different beds on the same chip. The optimization chip in Figure 6.2B adds sample vias to the first optimization chip and was used to develop the freeze-thaw assay manually, as the experimental throughput was much higher with that design and multiple chips could be run simultaneously. Finally, the full chip from Figure 6.1 was subdivided into two chips (Figure 6.2C), one possessing sample vias while the other does not. This chip was used to demonstrate that the method to seal the sample vias post-sample incubation did not interfere with the assay in any way.

6.2.3 Assay procedures with optimization chips

Assays with the freeze-thaw valves used the chip layout shown in Figure 6.1. Valves were closed by setting them to their maximally cold temperature (between approximately -31 °C and -43 °C depending on the valve) for 50 s to rapidly effect freezing, then setting them to -3 °C to maintain the closure. Valves were opened by setting them to +25 °C and were kept at that temperature until closed. Valves were only opened once all other valves were closed.

Sample solutions containing ERK1/2 were prepared in ERK buffer. All other reagents were prepared in PBS-BT. Prior to assays, the chips were passivated with PBS-BT for 2 h at room temperature, and the frits in chips were plugged with 10-µm nonfluorescent beads to enable the ERK1/2 beads to form packed beds. Samples were incubated in their vias for 30 min. Vacuum was applied to the chips for 10 min to pack the beads into beds. The buffer valve was open during this time. After packing the beads, vacuum was used to remove remaining sample solution from each sample via, and the vias were sealed by filling them with a solution of 25% Pluronic F-127 (w/v) + 3.5% sodium chloride (w/v). Each valved reagent via contained 20 µL of solution. Reagent incubations were performed by opening the corresponding valve and applying vacuum for 30 s. The valve was left open for the duration of the incubation. Washes were performed by opening the buffer valve and applying vacuum for 30 s. Incubation times were 20 min for the dAb, and 10 min for SA-PE. Unless otherwise specified, all dAb solutions are at 1 µg/mL and all SA-PE solutions are at 2 µg/mL. Encoding and assay images were taken as described in Chapter 2.

For acquiring cell lysate samples, human Jurkat T-cells were cultured and lysed as described in Chapter 4, both with and without PMA stimulation.

6.2.4 Data analysis

Assays in this chapter were decoded with a WEKA algorithm in ImageJ. The WEKA plugin[6] can be trained to distinguish beads from background, as well as in-focus beads from out-of-focus ones (Figure 6.3A-B). The algorithm is applied to an encoding image (Figure 6.3C) to select all the in-focus beads (Figure 6.3D) and its selection is overlaid on the assay image (Figure 6.3EF). The fluorescence data from the selected beads is then exported to Excel and analyzed as in Chapter 4. The use of WEKA as opposed to manual bead selection allows a consistent standard to be applied to all data.

6.3 Results and discussion

6.3.1 Automated chip design and the use of plug beads

In order to automate the assay, a new chip design with 4 reagent reservoirs and 8 sample vias was developed. Each reagent channel incorporated the serpentine channels for the FTVs (Figure 6.1) for controlling the delivery of wash buffer, pERK1/2 dAb, tERK1/2 dAb, and SA-PE. Instead of a single sample via, a total of eight sample vias were incorporated. These could be used to assay either multiple samples or to produce a calibration curve for single-sample use. The eight sample vias are spaced in increments of 9 mm so that all can be filled using an 8-channel pipette. Sample channels from the sample vias feed into bead regions with the flow-frit design from Chapter 4. Their location on the chip was set according to the distance from the FTVs to the microscope objective's viewing space. All eight sample regions feed into a common outlet via for waste/vacuum which should ensure identical fluid flow. While the single-channel flow-frit chips worked well at a depth of 12.5 μm, the large footprint of these 8 sample devices required deeper channels to maintain an adequate flow rate in light of their significantly higher hydraulic resistance due to the increase in the number of channels and channel lengths.

Initially, multiple chips with varying depths were fabricated and a preliminary qualitative experiment examined the flow rate of the chips. Only a single reagent via was created to simulate a three valves closed + one valve open configuration. The via was filled with 10 µL of buffer and vacuum was applied to the chip. The 30-µm deep devices (flow bed depth ~9 µm), like the first-generation flow-frit chips, required approximately 5 min to fully deplete the sample via and so were used in future experiments. An unexpected outcome, however, was the MagPlex beads did not pack into beds against the frits. Visually monitoring the chips showed the beads passed under the frits as the pillars turned out to be too short to block the bead flow. This is likely because of the high aspect ratio of the frit features with the deeper chips. The frits are pillars in the PDMS chips, so in the corresponding master mold, they are trenches. While they were nominally etched to the same depth as the channels during the DRIE process and thus should have been tall enough to occlude bead flow, in many DRIE recipes, aspect ratio and relative depth change the uniformity of mass transfer of ions and etchant gases, slowing the etch rate of the deeper features.[7] It was thus hypothesized that the frit trenches did not etch to the same depth as the channels. This was corroborated by environmental scanning electron micrographs taken of the chips, showing that the frit pillars were not as tall as the channel walls in the PDMS chips.

Instead of further developing the DRIE recipe, which would have been time-consuming and expensive, this issue was addressed by simply using 10-µm polystyrene beads as plug beads. These nonfluorescent beads pack against the frits acting as a stop for the antibody-based beads. They are stored in PBS-BT to passivate them prior to use in assays. Initially (in the consistency of fluid flow experiment in Section 6.3.2 and the initial assay with PF-127 sealed chips in Section 6.3.4), plug beads were mixed with ERK1/2 beads in a 1:100 (plug:ERK) ratio prior to

packing the beads. Packed beds of ERK1/2 beads did result, but the stochastic mixing with plug beads resulted in many of the ERK1/2 beads packing out of focus. A different protocol was developed in which the plug beads were packed prior to the assay through the sample vias and stored in PBS-BT until used. This resulted in the ERK1/2 beads packing in the same focal plane and was used in every experiment following the initial assays with on-chip sample incubations (Section 6.3.5 onward).

6.3.2 Consistency of fluid flow from chip to chip

The 8-sample chips use a symmetrical design relative to the bead regions such that the fluidic resistance, and thus the flow rate, should be identical across the bead beds. This would be ideal for ensuring the identical delivery of reagents to the bead beds and maintain reproducibility of results within chips and between chips. As sample incubations take place inside the sample vias and not in the bead beds, the consistency of fluid flow was of concern with respect to the dAb and SA-PE incubations as well as the wash steps. To evaluate the consistency from bed to bed and chip to chip, ERK1/2 beads were incubated with samples (pERK2 at 0, 10, and 20 ng/mL) off-chip at 1000 rpm for 30 min. This was to maximize signal as well as ensure that the beads being assayed were exposed to the same sample amount. The beads were mixed with spacer beads and packed into beds using the single-via chips in Figure 6.2A. These chips do not have sample vias and rely on the symmetrical design to deliver equal number of beads to the 8 bed regions from the sample/reagent via. The chips were then filled with pERK1/2 dAb and incubated for 20 min, washed for 1 min, incubated with SA-PE for 10 min, washed for 1 min, and imaged. A single concentration was used per 8-channel chip to evaluate the signal across each chip. Three chips were used for the 10 ng/mL samples and two chips for the 20 ng/mL samples to evaluate the chip-to-chip variance.

The results in Figure 6.4 show that the fluorescence is consistent between measurements. The aggregate %RSD for all measurements at 10 ng/mL (N=19 beds) was 8.14%, while it was 6.25% for the 20 ng/mL chips (N=14 beds). The intrachip (bed-to-bed on the same chip) %RSDs are 7.02% or below in all cases. As both the interchip and intrachip %RSDs were below 10%, the reproducibility of the fluorescence in these results was judged to be sufficient to justify the use of the 8-sample chips in the pERK1/2:ERK1/2 assays.

6.3.3 Sample channel sealing with Pluronic F-127

After packing the beads, it is necessary to close the sample vias so no additional fluid flow from the vias occurs. This prevents any reagent dilution and eliminates the need to keep fluid in the vias. Sealing the eight sample vias also greatly reduces the pressure drop across the sample regions and increases the flow rate from the reagent vias. In an automated version of this device, FTVs could be used to seal the sample channels following sample incubation and packing the beads into beds. Small (~1-2 mm square) Peltiers may be able to accomplish this without any modifications to the chip design by placing one under each sample via. However, due to spatial constraints with the inverted microscope, the addition of FTVs on the sample channel was not feasible. An alternative method of sealing the channels was pursued. Efforts were undertaken to use a sealant that would block the channel when added to the sample via. The sealant itself should not have adverse effects on the assay (in the event of its leaking into the bead beds), and it should be capable of indefinitely preventing flow into or out of the sample incubation regions. This is necessary not only to stop the channels influencing the assay once they are no longer being used, but additionally, eight unsealed samples vias create a sufficient pressure drop to prevent applied vacuum from drawing fluid from the reagent vias into the chip.

PF-127 is a tri-block copolymer of poly(ethylene oxide) and poly(propylene oxide). When solutions containing approximately 20% (w/v) or greater in water are heated above approximately 15 °C, its viscosity increases dramatically, forming a gel.[8] This is due to the formation of micelles approximately 17-19 nm in diameter[9] that swell and desolvate upon heating, causing their hydroxyl groups to undergo hydrogen bonding.[8] The viscosity increase is tunable as a function of both the concentration[8] of PF-127 and the ionic strength[10] of its solution; adding 5% (w/v) sodium chloride to a 30% (w/v) PF-127 solution increases its viscosity approximately tenfold. This is likely the result of the electrolyte solvating water, thus further desolvating PF-127 and enabling the formation of more hydrogen bonds between hydroxyl groups on the micelles. As the viscosity of the PF-127 gel is potentially enough to seal a microfluidic channel, it was hypothesized that the addition of chilled PF-127 to the sample via would seal the channel as the PF-127 warmed to room temperature and its viscosity increased.

To test this hypothesis, solutions of 25% (w/v) PF-127 were prepared containing NaCl in concentrations from 2.5% to 5% (w/v). The solutions were chilled during mixing to keep them in the liquid phase. The 8-sample chip shown in Figure 6.2B with a single reagent reservoir and 8 sample vias was filled with black ink for ease of visualization. The ink was then removed from the sample vias by vacuum and replaced with a PF-127/NaCl solution (Figure 6.5A). The reagent via was then filled with buffer and vacuum was applied. If the PF-127 solution gelled sufficiently, the ink should be removed from all channels except the sample channels. The image in Figure 6.5B clearly shows that all channels were flushed clear by the buffer but the sample channels remained filled with ink, indicating no fluid flow or successfully sealed channels by the gel. The vacuum was shut off following this and the chips were left to sit, with vacuum reapplied every 30 minutes for 20 seconds. Visual inspection of the chips sealed by PF-

127 solutions containing 3.0% - 3.5% NaCl found the seals to hold for at least 4 h. Times longer than that were not tested as they are beyond the timescale of the assay. Lower NaCl concentrations were insufficiently viscous to seal the channels, while higher concentrations were found to be more difficult to work with due to their higher viscosity.

6.3.4 Initial assays with Pluronic F127-sealed chips

Following the successful sealing of sample channels with PF-127 gel, the next step was determining whether the gel would interfere with the assay. While pressure-driven flow from the channel was prevented by the seal, solvated PF-127 could potentially diffuse toward the bead beds. PF-127 is biocompatible with immunoassays and is usable as a reagent for reducing an assay's non-specific binding,[11] but assay-compatible reagents can still cause changes in the assay's signal, so this issue was explored by comparing assays run with PF-127 and without.

The hybrid valveless chips shown in Figure 6.2C were used for this assay. The right half of the chip features sample inlet vias that will be sealed by PF-127. The left half introduces beads and reagents through the via at the top of the chip. To test the effects of PF-127 on the assay, ERK1/2 beads were incubated with pERK2 samples at 0, 5, 10, and 20 ng/mL off-chip on the vortexer for 30 min. They were then mixed with spacer beads and packed into beds in each of the detection regions. Once the bead beds were packed, the chips with sample vias were sealed with PF-127. The assay was then completed with a pERK1/2 dAb incubation, a wash, an SA-PE incubation step, a final wash, and an imaging step.

The results for this experiment are shown in Figure 6.6. The signals from the beads incubated with PF-127 seals (red inverted triangles) are indistinguishable from the beads incubated without PF-127 (black squares). These results show that using PF-127 to seal the

sample channels is viable in conjunction with assays as the results from both methods are effectively identical.

6.3.5 On-chip incubations

Following the successful demonstration of closing the sample via after bead packing, experiments were done to show the efficacy of incubating the sample on-chip. Figure 6.7 shows the 3 steps to prepare the chip for incubation with the assay reagents. In step 1, the samples are incubated with the beads directly in the sample vias (Figure 6.7A) and packed into beds by applying vacuum in step 2 (Figure 6.7B). The sample channels would then be sealed with PF-127 following bed formation (Figure 6.7C) in step 3. While this bears many similarities to the on-chip sample incubations that were performed with the flow-frit chips from Chapter 4, a major difference is that the flow-frit chips featured only one sample per chip, while these feature eight samples per chip. Beyond determining if the sample can be incubated in the sample vias with beads, these experiment can evaluate whether any cross-talk occurs between sample beds. This cross-talk could potentially occur during the sample incubations as the sample vias are directly connecting during the sample incubation. Due to the length of channels (9 mm) between sample vias, no cross-reactivity was expected. Validating the chips in this manner represents the final hurdle before running assays with the FTVs.

Four 8-sample valveless chips shown in Figure 6.7A were used to test the on-chip sample incubations. ERK1/2 samples were prepared with 0%, 5%, 10%, 25%, 33%, 40%, 66%, and 100% pERK at a constant total ERK1/2 of 10 ng/mL. The samples were mixed with ERK1/2 beads and an 8-channel pipet was used to fill the sample vias with all eight samples simultaneously. After incubating for 30 min, vacuum was applied to pack the beads. The sample vias were sealed with PF-127 and the assay was completed with incubations of pERK1/2

dAb, total ERK1/2 dAb, SA-PE, 30-s washes, and two imaging steps. Figure 6.8 shows no adverse effects with on-chip incubations, as the resultant calibration curve has an R^2=0.999 and the %RSDs are all below 10%. Cross-talk between detection regions does not appear to be a significant factor. This is consistent with the fact that sample vias all contain the same volume and thus any flow that does occur between them should be a result of diffusion alone. It is also consistent with the rate of diffusion for a protein across the dimensions of the chip. The time *t* (s) required for a molecule with diffusion coefficient *D* (cm^2/s) to diffuse distance *x* (cm) is governed by Equation 6.1:[12]

$$t = \frac{x^2}{2D} \tag{6.1}$$

The diffusion coefficient in water for a protein similar in size to ERK1/2 would be[13] approximately 7.5 x 10^{-7} cm^2/s and the distance from one sample via to another along the length of the channels is approximately 1.8 cm. It would therefore take approximately 2,100,000 s (or ~24 days) for the protein to traverse that distance through diffusion alone. This is the fastest possible diffusion time under the most favorable circumstances for diffusion to occur; the presence of other proteins in the buffer further slows the diffusion rate. Also, the fluid levels in each sample via are the same, so there is not likely to be any migration from via to via due to misleveling of the reagent droplets.

The final experiment run using an optimization chip tested the inclusion of pERK1 in the standard calibration matrix. Previous experiments in both this chapter and Chapter 4 utilized only pERK2, nERK1, and nERK2, but cell lysate would also contain pERK1. Further, the pERK1/2 dAb recognizes both pERK2 and pERK1, separate dAbs for total ERK1 and total ERK2 are used and may not have the same affinity for their epitopes on their respective targets. Omitting pERK1 from the standards thus gives the total ERK1 dAb progressively fewer

molecules to bind to as a function of the %pERK in the solution (since ERK1 is only present as nERK1). pERK1 should thus be included in the standards in order to generate an accurate calibration curve.

A pERK1/2:ERK1/2 assay was run with samples containing 0%, 33%, 66%, and 100% pERK1/2 at a constant total ERK1/2 = 10 ng/mL. The pERK1/2 and nERK1/2 samples contained equal amounts of ERK1. The samples were mixed with ERK1/2 beads, pipetted into sample vias to begin the first incubation, and assayed as with previous pERK1/2:ERK1/2 experiments. The results in Figure 6.9 show a well-defined fit (R^2=0.9996) and low %RSDs with relative fluorescence ratios similar to the previous on-chip assay. Based on these results, the assay format was ready for implementation on the full freeze-thaw valve chip.

6.3.6 pERK1/2:ERK1/2 assay with full freeze-thaw valve chip and automated fluid delivery

Following the proof-of-concept work with the optimization chips, the 8-sample chips with the serpentine valve regions (Figure 6.1) were used to determine pERK1/2:ERK1/2 in both standard solutions and lysate from Jurkat cells. The 4 assay reagents are loaded in their respective vias and their delivery to the packed bead bed controlled by automated opening/closing of the appropriate valve. Five calibration samples were prepared consisting of a blank (beads in ERK buffer only) and 10 ng/mL total ERK1/2 at 0%, 25%, 50%, 75%, and 100% pERK1/2. Two cell lysate samples were acquired from Jurkat cells, one of which was treated with 200 nM PMA for 30 min to induce ERK1/2 phosphorylation. The lysate in each via came from approximately 20,000 cells. The freeze-thaw platform assays a single chip at a time and the data acquired represent three chips assayed in one day.

The results in Figure 6.10 show the pERK1/2:ERK1/2 fluorescence ratio in the cell lysate (black square) along with the ratio in the PMA-treated lysate (blue triangle) and the calibration

standards (red inverted triangles). The calibration points fit strongly (R^2 =0.992) to a sigmoid curve, showing that the pERK1/2:ERK1/2 fluorescence ratio increases predictably as a function of the %pERK in the sample. As in the previous pERK1/2:ERK1/2 determination from cell lysate, the PMA-treated Jurkat cells showed a higher phosphorylation ratio (~67%) than their untreated counterparts (~2%). One major difference between the results in Figure 6.10 and the previous cell lysis assay from Chapter 4 is the degree of phosphorylation of the PMA-treated cells. While both experiments showed low-single-digit pERK1/2:ERK1/2 ratios in the untreated cells (~4% in Chapter 4 and ~2% in this experiment), in the previous experiment the PMA-treated cells showed approximately 30% phosphorylation while here they are approximately 67% phosphorylated. This difference may be the result that two different cell populations were used for the experiments. Though nominally from the same line, the cells that exhibited 30% phosphorylation post-PMA were cultured and passed dozens of times prior to use in the experiment, while the cells used in this experiment had been passed fewer than 10 times. The cells in the first line thus had much more time to mutate, potentially affecting their susceptibility to PMA.

Regardless of the cause of the phosphorylation differences, this assay, like its predecessor in the flow-frit chips, successfully measured pERK1/2:ERK1/2 in standard calibration solutions (at physiologically relevant concentrations) as well as in cell lysate samples. The demonstration of this assay on the 8-sample freeze-thaw valve chips represents a significant step toward automating the assay and the concomitant reduction in user error.

6.4 Conclusions and future directions

An automated microfluidic device for the measurement of pERK1/2:ERK1/2 was developed using freeze/thaw valves. Chips were developed for 8 samples and 4 reagents so that

either multiple real-world samples could be assayed at once, or a combination of samples and standards could be analyzed on the same chip. Initial experiments showed reproducible fluid flow between chips and between bead regions (%RSDs <10%). It was also shown that despite the frits being unable to pack the 6.5-µm ERK1/2 to into beds, the frits could be plugged with nonfluorescent 10-µm beads prior to generating a bed with the assay beads. Following that, it was shown that the beads could be incubated with sample directly on-chip without cross-reactivity between samples and that the sample vias could be sealed with PF-127 gel after the beads were pulled into packed beds. No interference was seen with using the PF-127 gel to seal the sample vias, and thus pERK1/2:ERK1/2 assays with on-chip sample incubations were demonstrated. Finally, the determination of pERK1/2:ERK1/2 in standards and cell lysates using automated reagent delivery was demonstrated on chips actuated by the freeze-thaw valves. The assay's sensitivity was comparable or superior to previous efforts with the flow-frit chips and the efforts in this chapter represented a major step toward automating the device.

Overall, the assay developed takes less than two hours to complete and is significantly faster than methods that require several multi-hour or even overnight incubations (e.g. plate ELISAs and Western blots). The assay performed its analysis on approximately 20,000 cells, while some methods require up to millions of cells. It is semi-automated and is ready for full automation, which would significantly reduce labor requirements over methods that require extensive user manipulation of their systems.

To fully automate the assay with the 8-sample chips, several additional steps are needed. The first and simplest to implement would be the automation of vacuum steps, as a solenoid-driven vacuum line could be attached to the chips and controlled by computer software. Automating the imaging step would be possible through use of a computer-controlled stepper

motor that translates the stage from bead region to bead region. Imaging step automation would also require a means of automatically focusing the microscope at each individual bead bed or of ensuring that the chip is sufficiently level to be in the same focal plane throughout the experiment. The use of a different magnification level might facilitate this (and render unnecessary the use of an autofocus system), as its depth of field would be greater than that of the 30x magnification used here. These additional steps do add complexity to the system and not all would be necessary to automate a single-sample device, but the benefits of the 8-sample chip outweigh the drawbacks. Namely, the ability to generate a calibration curve on the same device as the sample analysis, or to perform simultaneous replicate measurements of the same sample.

Another important step in automating the assay would involve an elimination of the manual PF-127 sample channel sealing. Freeze-thaw valves for actuating the sample channels would be one method of accomplishing this. This strategy was not possible with the inverted microscope setup due to space constraints imposed by the microscope objective turret. Using a custom detection with a top-down optical imaging system would open more space for valve placement, would allow the sample and bead regions to sit atop the valves and water block, and would thus enable the integration of sample valves. The LabVIEW program for valve control could be updated to include the sample channel valves, open/close the valves according to preset timers and drive the vacuum line and stepper motor for translating the chip into the optical pathway. At this point, the assay would be fully automated following the addition of reagents and samples to the chip. The assay can be further simplified by removing the need for plug beads as well. This can be done by optimizing the DRIE fabrication procedure for the wafer molds so that the 6.5-μm beads can pack against the frits, or by coupling capture antibodies to suitable ~10-μm beads, as these do not pass through the current frits.

Additional improvements to the assay beyond full automation are also possible. Switching to the top-down optical setup would allow Peltiers to be placed directly under the sample and bead regions to heat the beads during incubation steps. This strategy was shown to be effective during early assay development in the Ramsey group as diffusion is a limiting step for most immunoassays[14] and the diffusion rate is directly proportional to temperature.[12] Heating the beads to physiological temperature (37 °C) during incubations while keeping the incubation times the same should therefore increase the sensitivity. The incubation times could also potentially be lengthened in conjunction with the use of the higher temperature. These steps may improve the sensitivity of the assay and would enable it to determine pERK1/2:ERK1/2 in samples with fewer cells.

6.5 Figures

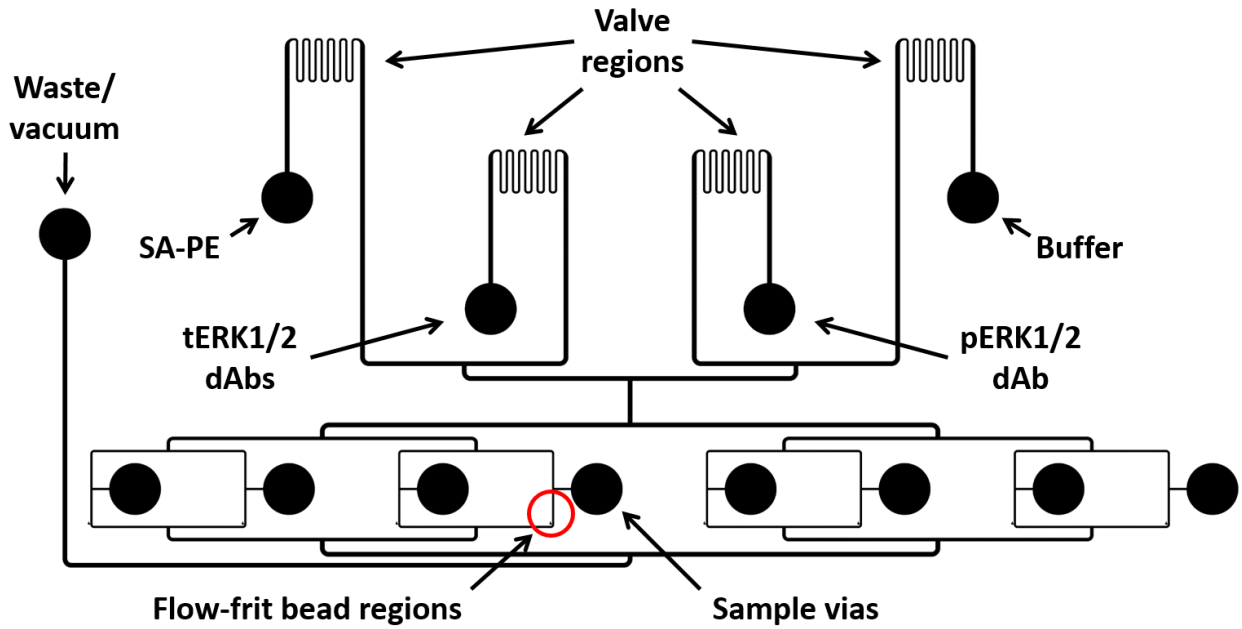

Figure 6.1. Diagram of 8-sample chip. Four vias for reagents (SA-PE, tERK1/2 dAbs, pERK1/2 dAb, wash buffer) feed through four serpentine valve regions before reaching the bead regions of the chip. Sample vias are spaced 9 mm apart so that all can be loaded simultaneously with an 8-channel pipette. The bead channels use the flow-frit design with 7 µm x 7 µm pillars spaced 4 µm edge-to-edge.

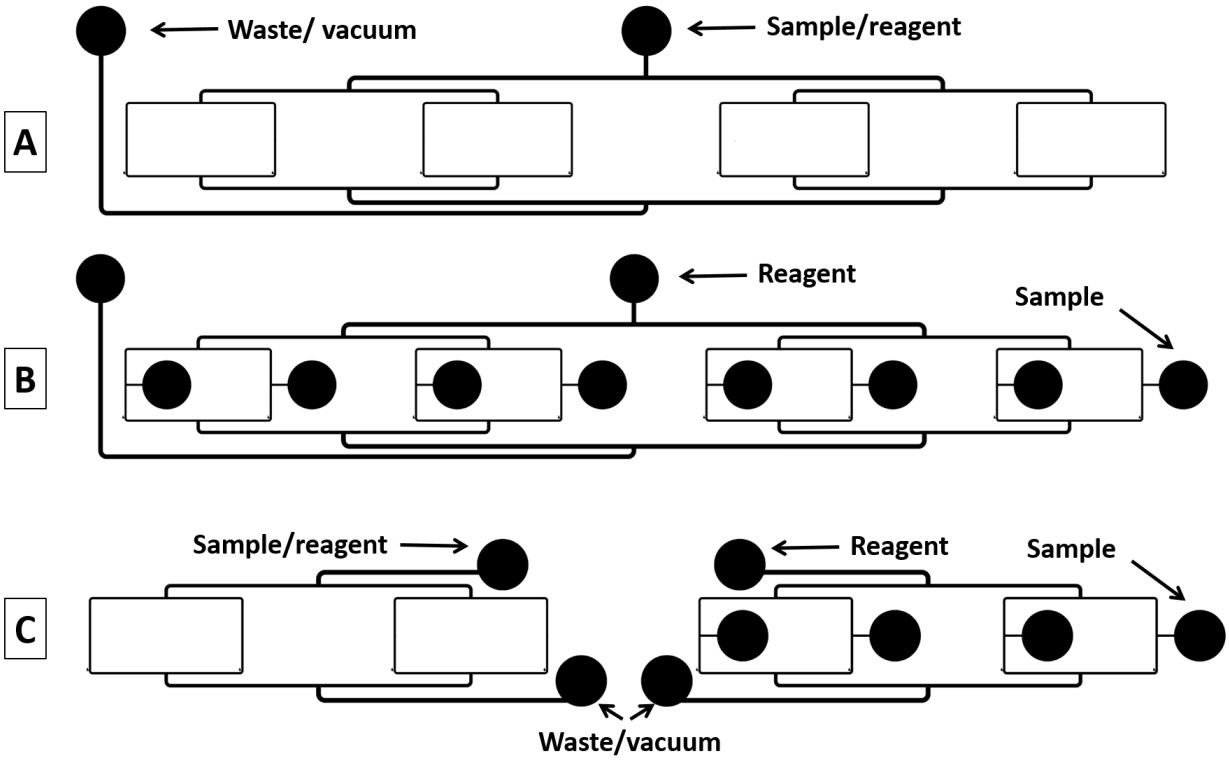

Figure 6.2. Three variations on the multi-sample chip design used for assay development and optimization. The four reagent vias and valves have been removed from all three and replaced with a single via for reagent and/or sample. (A) Chip used to assess the reproducibility of fluid flow across and between chips. The sample channels leading to the bead regions are not used. (B) Chip used to develop pERK1/2:ERK1/2 assay. This most closely resembles the full freeze-thaw chip. (C) Chip used to test the effect of sealing the sample channels with PF-127 by direct comparison with a chip that had no sample vias and thus required no sealing.

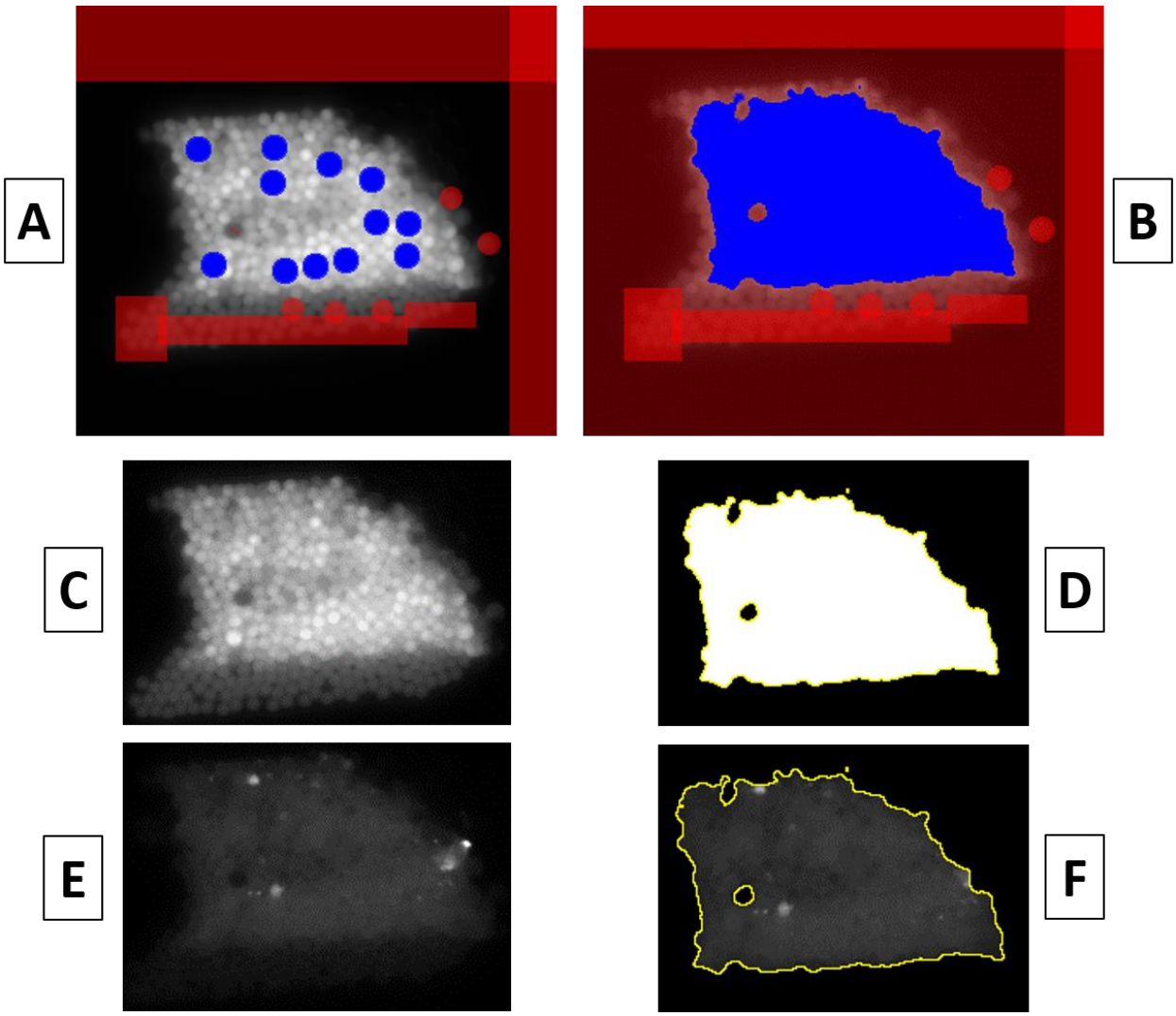

Figure 6.3. Diagram of WEKA analysis. (A) The program is trained to distinguish in-focus beads (blue circles) from out-of-focus beads/background (red). (B) The program generates a selection of the in-focus beads (blue) and excludes everything else (red). (C) Encoding image of bead bed from which (D) a selection mask is created by the WEKA algorithm. This is applied to the assay image (E) for that bead bed and (F) the in-focus beads are selected. Their fluorescence is exported to Excel in the form of a 5000-bin histogram and the mean/standard deviation determined following outlier removal.

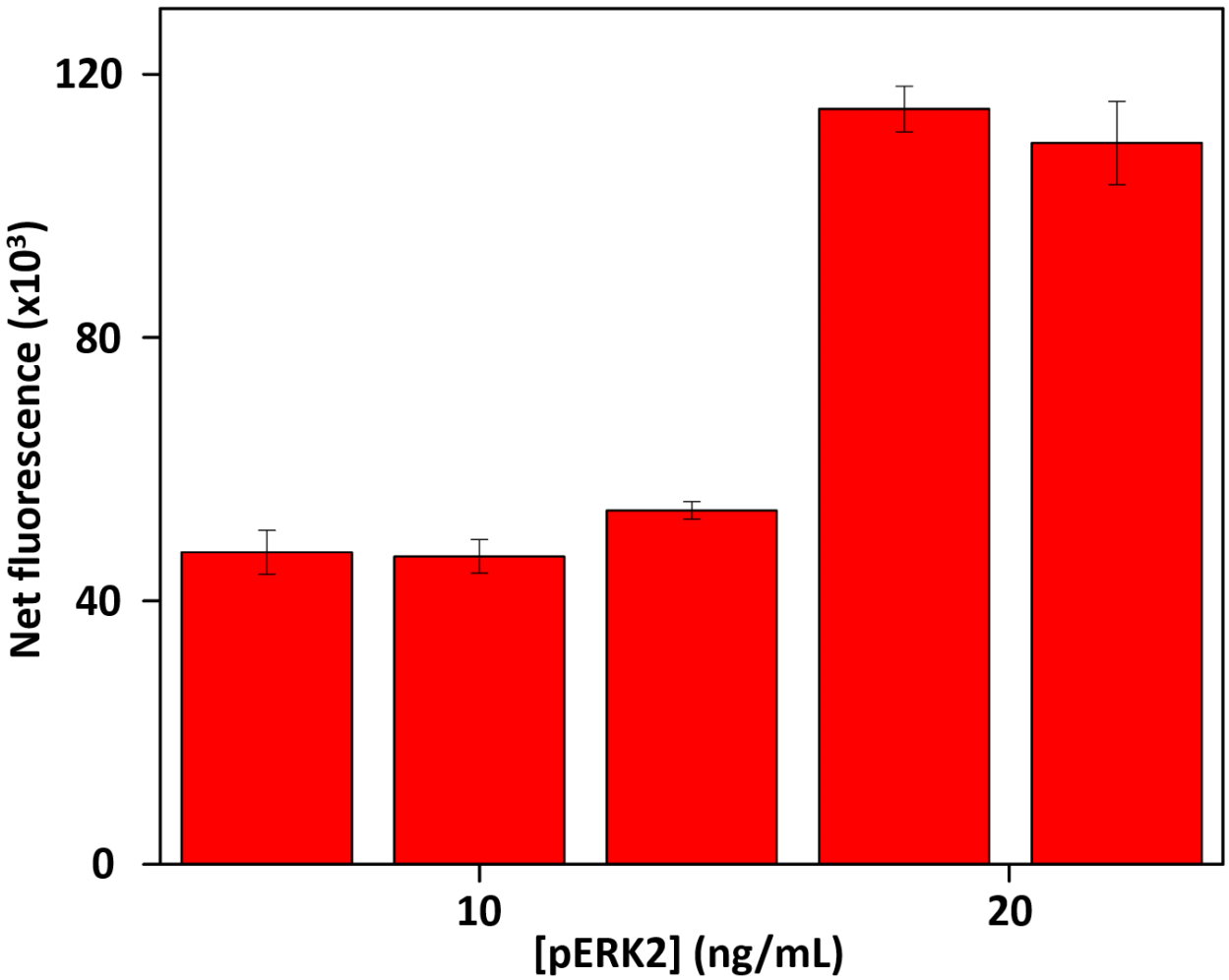

Figure 6.4. Net fluorescence signal with [pERK2] from experiments examining the consistency of fluid flow from chip to chip. The %RSDs for the samples (left to right) are 7.02%, 5.45%, 2.46%, 3.02%, and 5.77%. The aggregate %RSD for the 10 ng/mL samples (N=19) was 8.14% and was 6.25% (N=14) for the 20 ng/mL samples.

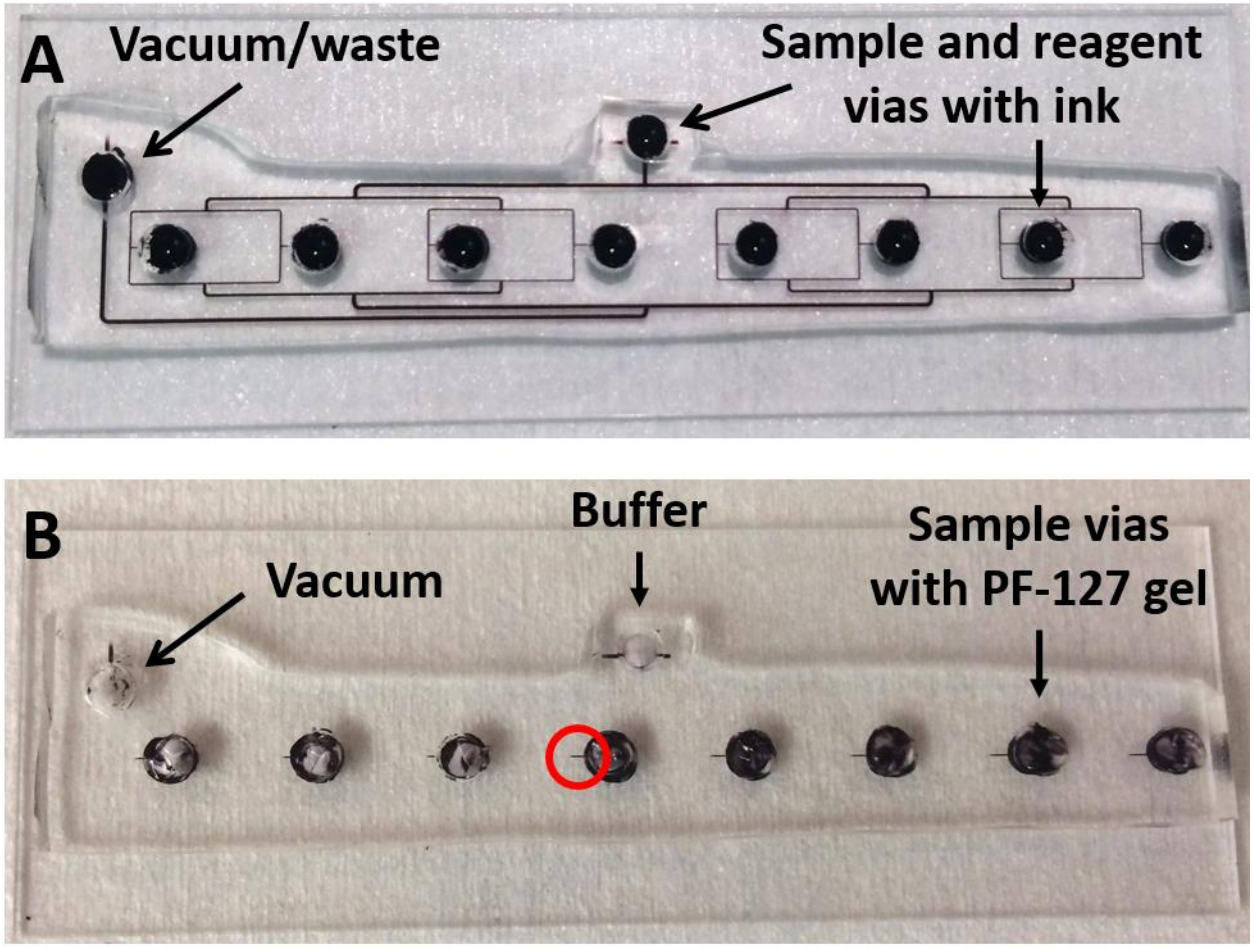

Figure 6.5. Optimization chip before and after Pluronic F-127 sealing of sample channels. (A) Optimization chip with sample vias filled with ink for visualization. (B) Optimization chip after sealing sample vias with PF-127 and the reagent inlet filled with buffer and vacuum applied. This washed the ink from the chip, except in the sample channels (circled in red) which were sealed by the gel.

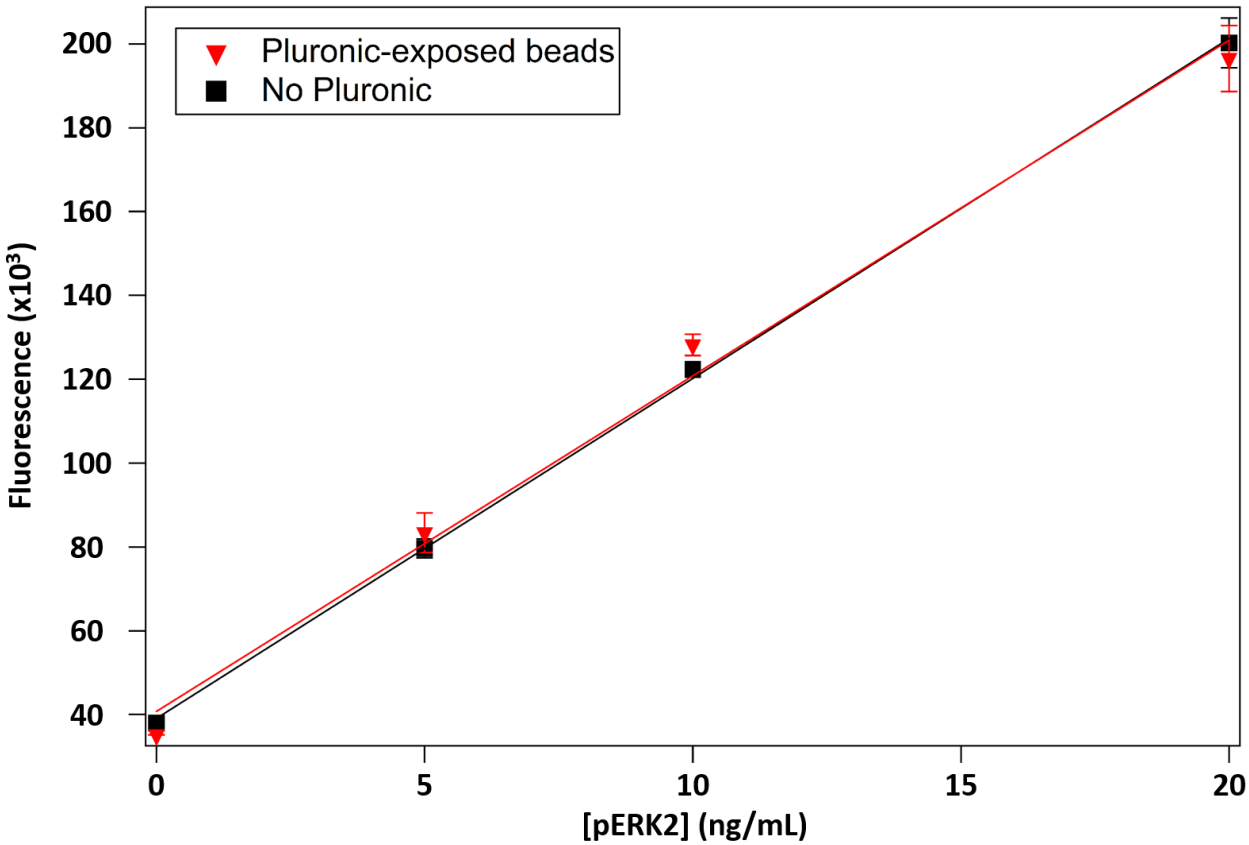

Figure 6.6. Fluorescence signal with [pERK2] with linear fits from experiments comparing fluorescence from chips with and without PF-127 sealed sample channels. Data from the PF-127 sealed channels are represented by the red inverted triangles while those without PF-127 are denoted by the black squares. The curves are effectively identical and indicate that PF-127 sealing does not interfere with the assay.

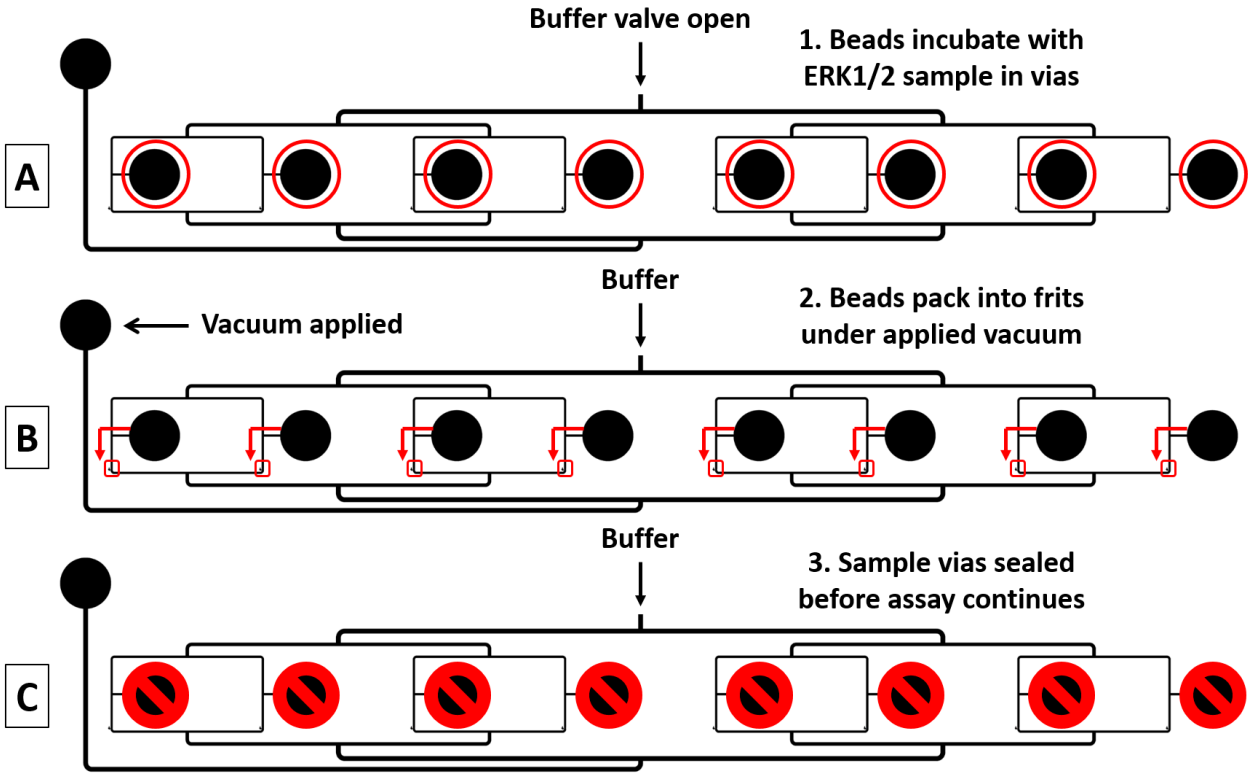

Figure 6.7. The three steps involved in preparing a chip for incubation with the assay reagents. (A) Step 1: Samples are incubated with beads in the sample vias (red circles). (B) Step 2: Vacuum is applied to pack the beads against the frits (red arrows leading to red boxes). (C) Step 3: sample vias are filled with PF-127, effectively closing the channel to fluid flow. Reagents are introduced through the buffer via located at the top of the chip.

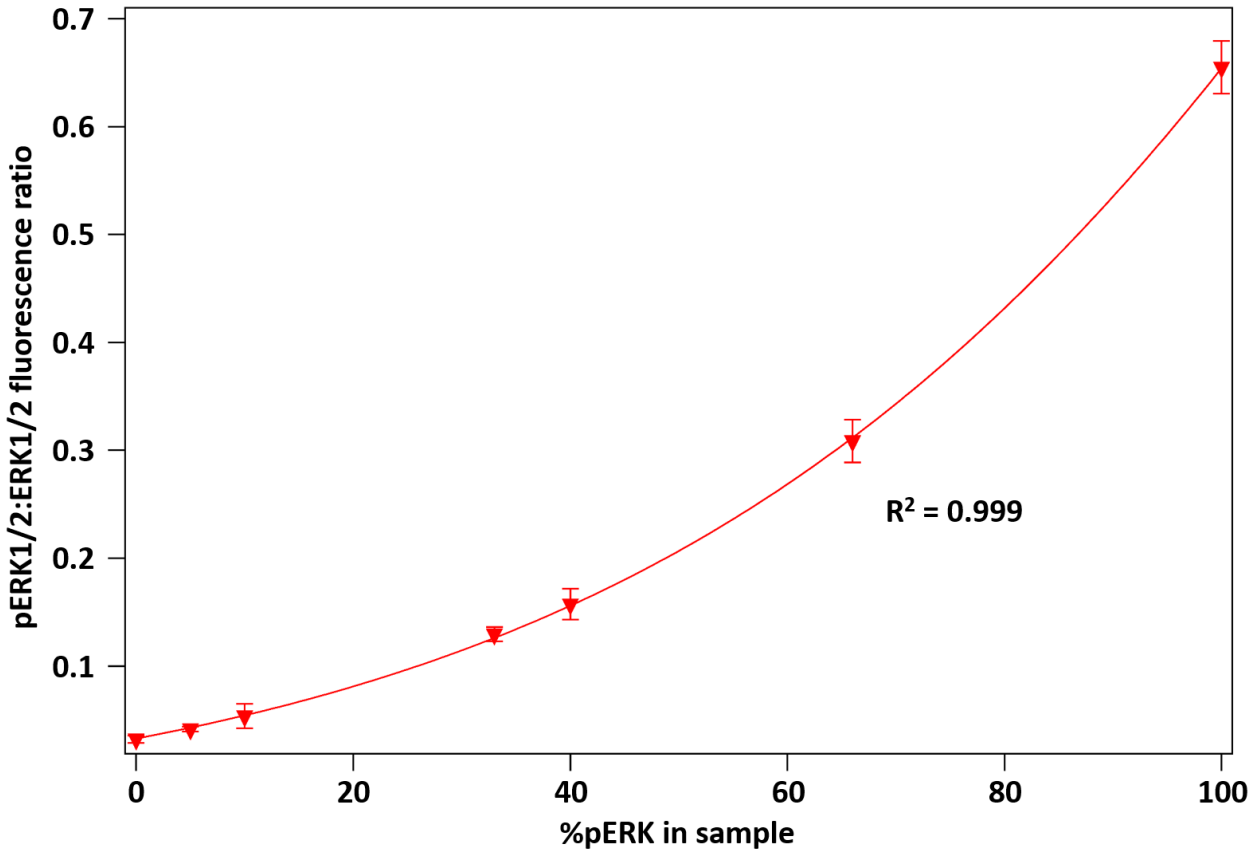

Figure 6.8. pERK1/2:ERK1/2 fluorescence ratio with %pERK with on-chip sample incubations. The calibration curve follows a well-defined (R^2 = 0.999) sigmoidal fit.

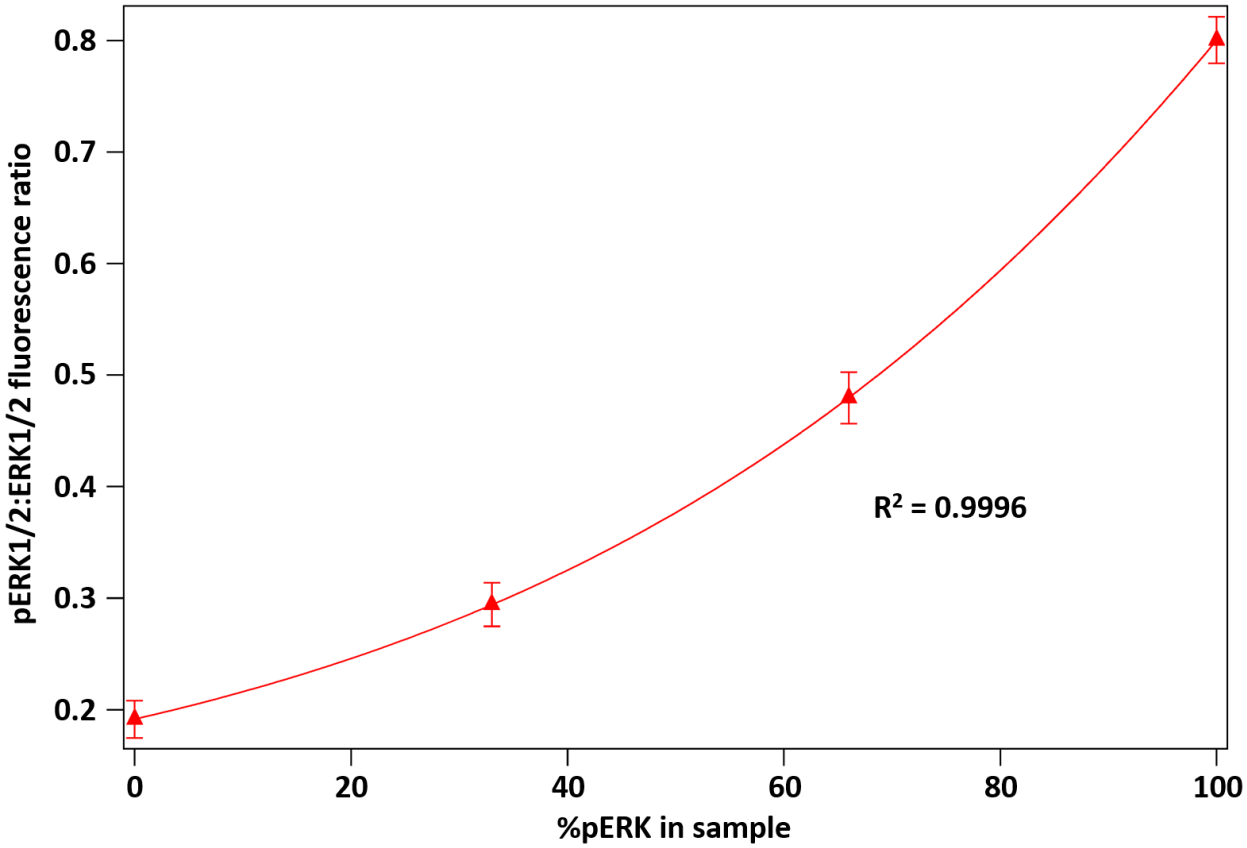

Figure 6.9. pERK1/2:ERK1/2 fluorescence ratio with %pERK after inclusion of pERK1 in the calibration standards. The curve also follows a well-defined sigmoid fit.

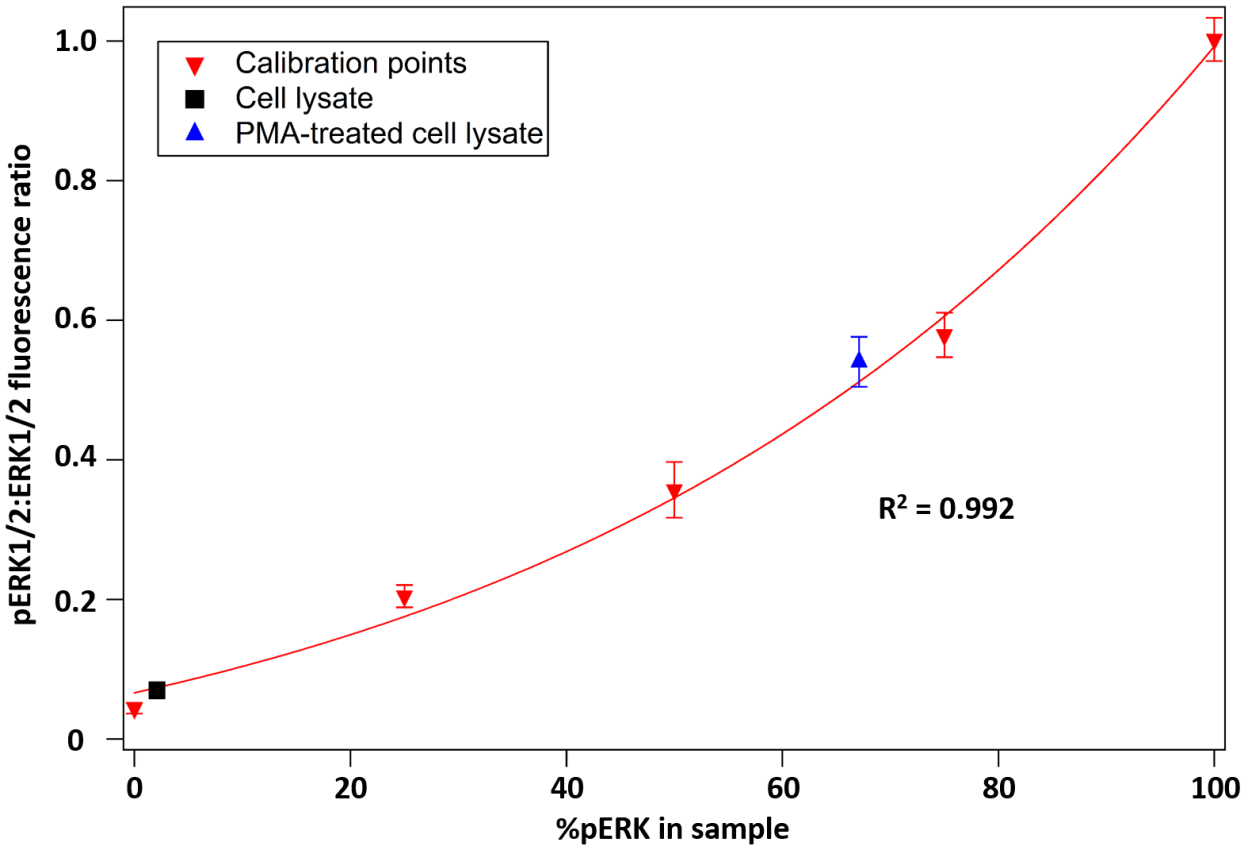

Figure 6.10. pERK1/2:ERK1/2 fluorescence ratio with %pERK using the 8-sample microfluidic chip, freeze-thaw valves, and cell lysate. The calibration standards are represented by red inverted triangles, the cell lysate sample by the black square, and the PMA-treated cell lysate by the blue triangle. The red line is a sigmoidal fit to the standards. The PMA-treated cells show over 30x the phosphorylation of the untreated cells. Approximately 100,000 cells were used to produce each lysate sample.

6.6 References

(1) Barbee, K. D.; Hsiao, A. P.; Roller, E. E.; Huang, X. Multiplexed Protein Detection Using Antibody-Conjugated Microbead Arrays in a Microfabricated Electrophoretic Device. *Lab Chip* **2010**, *10*, 3084–3093.

(2) Diercks, A. H.; Ozinsky, A.; Hansen, C. L.; Spotts, J. M.; Rodriguez, D. J.; Aderem, A. A Microfluidic Device for Multiplexed Protein Detection in Nano-Liter Volumes. *Anal. Biochem.* **2009**, *386*, 30–35.

(3) Bange, A.; Halsall, H. B.; Heineman, W. R. Microfluidic Immunosensor Systems. *Biosens. Bioelectron.* **2005**, *20*, 2488–2503.

(4) Henares, T. G.; Mizutani, F.; Hisamoto, H. Current Development in Microfluidic Immunosensing Chip. *Anal. Chim. Acta* **2008**, *611*, 17–30.

(5) Yu, X.; Xia, H.-S.; Sun, Z.-D.; Lin, Y.; Wang, K.; Yu, J.; Tang, H.; Pang, D.-W.; Zhang, Z.-L. On-Chip Dual Detection of Cancer Biomarkers Directly in Serum Based on Self-Assembled Magnetic Bead Patterns and Quantum Dots. *Biosens. Bioelectron.* **2013**, *41*, 129–136.

(6) Arganda-Carreras, I.; Cardona, A.; Kaynig, V.; Schindelin, J. Trainable Weka Segmentation http://fiji.sc/Trainable_Weka_Segmentation#.

(7) Rangelow, I. W. Critical Tasks in High Aspect Ratio Silicon Dry Etching for Microelectromechanical Systems. *J. Vac. Sci. Technol. A Vacuum, Surfaces, Film.* **2003**, *21*, 1550.

(8) Lenaerts, V.; Triqueneaux, C.; Quarton, M.; Rieg-Falson, F.; Couvreur, P. Temperature-Dependent Rheological Behavior of Pluronic F-127 Aqueous Solutions. *Int. J. Pharm.* **1987**, *39*, 121–127.

(9) Kuroda, D.; Zhang, Y.; Wang, J.; Kaji, N.; Tokeshi, M.; Baba, Y. A Viscosity-Tunable Polymer for DNA Separation by Microchip Electrophoresis. *Anal. Bioanal. Chem.* **2008**, *391*, 2543–2549.

(10) Schmolka, I. R. Artificial Skin I. Preparation and Properties of Pluronic F-127 Gels for Treatment of Burns. *J. Biomed. Mater. Res.* **1972**, *6*, 571–582.

(11) Miller, E. M.; Ng, A. H. C.; Uddayasankar, U.; Wheeler, A. R. A Digital Microfluidic Approach to Heterogeneous Immunoassays. *Anal. Bioanal. Chem.* **2011**, *399*, 337–345.

(12) Berg, O.; Hippel, P. von. Diffusion-Controlled Macromolecular Interactions. *Annu. Rev. Biophys. Biophys. Chem.* **1985**, *14*, 131–158.

(13) Ferrage, F.; Zoonens, M. Slow Diffusion of Macromolecular Assemblies by a New Pulsed Field Gradient NMR Method. *J. Am. Chem. Soc.* **2003**, *125*, 2541–2545.

(14) Kusnezow, W.; Syagailo, Y. V; Rüffer, S.; Baudenstiel, N.; Gauer, C.; Hoheisel, J. D.; Wild, D.; Goychuk, I. Optimal Design of Microarray Immunoassays to Compensate for Kinetic Limitations: Theory and Experiment. *Mol. Cell. Proteomics* **2006**, *5*, 1681–1696.